UNIVERSIDADE D
COIMBRA

Márcio Duarte Albino dos Santos

MODULAR ARCHITECTURE OF STEADY-STATE SIMULATION OF RANKINE BASED MICRO COMBINED HEAT AND POWER SYSTEMS

Doctoral Thesis in Mechanical Engineering, specialization in Energy Materials and Energy Conversion Systems, supervised by Professor Doctor Jorge Campos da Silva André e Professor Doctor José Manuel Baranda Moreira da Silva Ribeiro, submitted to the Department of Mechanical Engineering, Faculty of Sciences and Technology of the University of Coimbra

October 2020

Faculty of Sciences and Technology
of the University of Coimbra

Modular architecture of steady-state simulation of Rankine based micro combined heat and power systems

Márcio Duarte Albino dos Santos

Doctoral Thesis in Mechanical Engineering, specialization in Energy Materials and Energy Conversion Systems, supervised by Professor Doctor Jorge Campos da Silva André e Professor Doctor José Manuel Baranda Moreira da Silva Ribeiro, submitted to the Department of Mechanical Engineering, Faculty of Sciences and Technology of the University of Coimbra

July 2020

UNIVERSIDADE D
COIMBRA

Acknowledgements

Firstly, I want to express my deepest gratitude to my supervisors, Professor Jorge Campos da Silva André and Professor José Manuel Baranda Ribeiro, for their guidance and belief throughout my work. Their enthusiastic encouragement, valuable insights, important discussions, readiness and friendship greatly contributed to the accomplishment of this thesis.

To the members of the examination committee, I thank you all for the time and the energy you devoted to read this thesis and to objectively evaluate my work.

I am also grateful for the support of the research unit where this was conducted, ADAI - Associação para o Desenvolvimento da Aerodinâmica Industrial (LAETA - Associated Laboratory for Energy, Transports and Aeronautics). My sincere thanks to all my colleagues of the Sciven Lda company (past and present) for the encouragement, good mood and friendship. I am very grateful for the brotherhood and friendship of Eduardo Costa, João Pedro Pereira and Professor Ricardo Mendes who during this period have always supported and encouraged me.

Asides of my teammates, I would like to address my acknowledge to my friends and roommates for their support all along this 6-year PhD journey.

To publishers, copyright holders and scientific journals editors, my acknowledgement for providing the licences allowing the print and electronic reuse of the papers published under the scope of this research.

Finally, I wish to thank my family, specially my parents and my sister, for their unconditional support, patience, encouragement and presence all along this journey.

Abstract

The ultimate goal of this thesis is to assist the thermodynamic project and development of a micro Combined Heat-and-Power (CHP) system based in the Organic Rankine Cycle (ORC). A micro CHP solution that produces hot water for both sanitary use and central heating system, able to replace the common wall-hung domestic boilers, is a major solution. The ability to produce a share of electricity together with the hot water allows the user a significantly reduction in the total (e.g., gas plus electricity) energy bill, so more as his annual thermal needs are higher. Among the available technologies for micro-CHP for the former application, the ORC is probably the most profitable. But the proper understanding and characterization of the ORC behaviour is critical to achieve this objective. The work reported in this thesis is part of a bigger R&D Project named HEBE that intends to make the proof-of-concept of such a system (here-to-fore named Hebe) and ultimately achieve a ready to market solution of this technology.

This work begins with the early design project of Hebe. With that purpose, the market and engineering pre-specifications of Hebe are stated, a simplified thermodynamic steady-state model is developed, and an optimization problem is formulated and implemented in an algorithm/software, to find the best design options, in this case, that maximize the thermodynamic efficiency of the micro-CHP. This allowed to select the working fluid and the main components of Hebe, and to identify the ranges of the measure and control instruments of Hebe's test rig for the proof-of-concept.

Following the design stage, a powerful modular modelling architecture with an open library of sub models for potential Hebe's components is conceived. The aim is to easily create a fully steady-state predictive model for the evolving prototypes of Hebe, detailed and realistic, requiring only truly accessible inputs describing Hebe's boundary (nominal or off-design) and control conditions. Such model is a network of sub models duly interconnected. The software implementing the modelling architecture has a powerful numerical solver for the resulting system of non-linear equations of the model. A particular model is developed, calibrated and preliminary validated for Hebe's proof-of-concept prototype.

Finally, this model is applied to thoroughly understand the steady-state behaviour of Hebe, and conceive its optimal control strategy. The former quasi-stationary control strategy is further complemented with a dynamic component to guide the system through a quick and safe operation path during start-ups and user demands transition towards the best performance steady-state. This dynamic control is based on three independent PIDs, is purely empirical and still needs some refinements.

During the three stages of this work, experiments were conducted to validate the early design procedure, calibrate and validate the fully-predictive model and develop the empirical dynamic control algorithm.

Keywords: micro-CHP, ORC, modelling, steady-state, off-design, charge-sensitive, design, control

Resumo

O principal objetivo desta Tese é auxiliar o projeto termodinâmico e o desenvolvimento de um sistema de micro cogeração (CHP). Um sistema de produção combinada de calor e eletricidade que produz água quente para uso sanitário e aquecimento central, é uma ótima solução para substituir as caldeiras domésticas comuns de parede. A capacidade de produzir uma parcela de eletricidade juntamente com a água quente que a casa necessita permite uma redução significativa na conta total de energia (tipicamente, gás mais eletricidade), tanto maior quanto maiores forem as necessidades térmicas anuais da casa. Entre as tecnologias disponíveis para micro cogeração, a baseada no ORC (ciclo de Rankine orgânico) é provavelmente a mais rentável. Para tal, o entendimento e a caracterização adequados do comportamento do ORC são críticos para alcançar este objetivo. O trabalho reportado nesta tese é parte de um projeto mais abrangente de I&D denominado HEBE, que pretende fazer a prova-de-conceito de um tal sistema (daqui em diante chamado Hebe), e alcançar, por fim, um produto pronto a ser lançado no mercado.

Este trabalho começa com o anteprojeto da Hebe. Para atingir este objetivo, as pré-especificações de mercado e de engenharia da Hebe são enunciadas, e um modelo termodinâmico simplificado estacionário e um problema de otimização são desenvolvidos, formulados e implementados num algoritmo/software, para encontrar as melhores opções de projeto. Neste caso, trata-se de maximizar a eficiência termodinâmica do sistema de micro cogeração. Foi assim possível selecionar o fluido de trabalho e os principais componentes da Hebe, além de identificar as gamas operacionais dos instrumentos de medição e controle da bancada de testes da Hebe para a prova-de-conceito.

Após a fase de projeto e construção, é criada uma potente arquitetura modular para a construção de modelos de micro-CHP baseados no ORC, com uma biblioteca aberta de submodelos dos seus componentes potenciais. O objetivo desta ferramenta é permitir criar facilmente um modelo realista detalhado de comportamento estacionário dos protótipos evolutivos da Hebe, que seja totalmente preditivo ou completo, i.e., que requeira apenas informação de entrada verdadeiramente acessível, relativa às condições de controle e fronteira da Hebe (nominais ou não-nominais). Um tal modelo é constituído por submodelos devidamente interconectados. O software que implementa a arquitetura de modelação possui um poderoso algoritmo de resolução numérica do sistema de equações não-lineares do modelo. Concretamente, um modelo específico foi desenvolvido, calibrado e validado preliminarmente para o protótipo laboratorial da Hebe.

Finalmente, o modelo é aplicado para compreender em profundidade o comportamento estacionário da Hebe e conceber a sua estratégia de controle ótima. A estratégia quási-estacionária anterior é depois complementada com uma componente empírica de controle dinâmico para guiar o sistema de forma rápida e segura durante o arranque e transições no pedido do cliente, até ao correspondente ponto ótimo de funcionamento estacionário.

Durante as três etapas do trabalho, foram realizados testes experimentais para validar o procedimento de anteprojeto, calibrar e validar o modelo completo e desenvolver o algoritmo de controlo estacionário e dinâmico.

Palavras-chave: micro cogeração, Ciclo Orgânico de Rankine, Modelação, Estado estacionário, *off-design*, balanço de massa, anteprojeto, controlo.

Contents

List of Figures

List of Tables

List of Acronyms

CAGR	Compound Annual Growth Rate
CHE	Condenser Heat Exchanger
COP	Coefficient of Performance
CHP	Combined Heat-and-Power
DHW	Domestic Hot Water
EES	Engineering Equation Solver™
EHE	Evaporator Heat Exchanger
EU	European Union
FC	Fuel Cell
FVM	Finite Volume Model
GA	Genetic Algorithm
GWP	Global Warming Potential
HPR	Heat-to-Power Ratio
ICE	Internal Combustion Engine
IEA	International Energy Agency
LCOE	Levelized Cost Of Electricity
LHV	Low Heat Value
LMTD	Logarithmic Mean Temperature Difference
LPG	Liquefied Petroleum Gas
MBM	Moving Boundary Model
MGT	Micro Gas Turbine
NPV	Net Present Value
ODP	Ozone Depletion Potential
ORC	Organic Rankine Cycle
PBI	Polybenzimidazole
PBP	Payback Period
PEMFC	Polymer Electrolyte Membrane Fuel Cell
PV/ST	Photo-Voltaic / Solar Thermal
R&D	Research and Development
SA	Specific Area
SE	Stirling Engine
SIC	Specific Investment Cost
SH	Space Heating
SOFC	Solid Oxide Fuel Cell
TCC	Total main Components Cost

UK	United Kingdom
US	United States
USD	United States Dollar
WHR	Waste Heat Recovery

List of Symbols

Symbol	Description	Units
A	Area	m^2
Bo	Boiling number	-
C	Cost	€
d	Diameter	m
h	Specific enthalpy	$kJ\ kg^{-1}$
L	Length	m
M	Mass	kg
$\dot{m}$	Mass flow rate	$kg\ s^{-1}$
N	Rotational speed	$rpm\ or\ rad \cdot s^{-1}$
Nu	Nusselt number	-
P	Pressure	$kPa\ or\ bar$
Pr	Prandtl number	-
$\dot{Q}$	Heat power	kW
q_{c0}	Low heat value	$kJ \cdot kg^{-1}$
R	Cash flow	$€ \cdot year^{-1}$
Re	Reynolds number	-
r_p	Pressure ratio	-
r_v	Volume ratio	-
s	Specific entropy	$kJ\ kg^{-1}K^{-1}$
t	time	$year$
T	Temperature	$K\ or$ ℃
U	Global Heat transfer coefficient	$W\ m^{-2}K^{-1}$
V	Velocity	$m\ s^{-1}$
$\dot{V}$	Volume flow rate	$m^3\ s^{-1}$
x	Quality	-
$\dot{W}$	Mechanical power	kW
We	Weber number	-
α	Void fraction	-
β	Chevron angle	°
Δ	Differential	-
ε	Effectiveness	-
ϕ	Enlargement factor	-

η	Efficiency	-
θ	Complementary to the Chevron angle	°
ρ	Density	$kg\ m^{-3}$

List of Subscripts

c	Combustion
$cond$	Condensation
$crit$	critical
e	Electrical
em	Electro-mechanic
$evap$	Evaporation
ex	Exergy
exp	Expander
f	Working fluid
fg	Flue gases
gen	Generator
H	Heat source
i	Isentropic
in	Input
inv	Investment
L	Heat sink
lam	Laminar
liq	Liquid
$motor$	Motor
net	Net
out	Output
$pinch$	Pinch point
$pipe$	Pipe
$pump$	Pump
$shaft$	Shaft
su	Supply
sub	Subcooling
sup	Superheating
t	Thermodynamic
th	Thermal
tot	Total
$turb$	Turbulent
vap	Vapour
w	Water

Chapter 1

General Introduction

In the first place, this chapter concerns the motivation for investigating the topics addressed in the thesis. The key objectives and achievements mainly around the development of a complete steady-state off-design charge-sensitive model of a combined heat and power organic Rankine cycle are highlighted next, and the outline of the whole text is finally presented.

General Introduction

1.1 Motivation

The continuous increase in global primary energy consumption over the past decades and environmental concerns regarding carbon emissions press the research to improve and develop new more energy-efficient technologies. According to the IEA, there is a lot of scopes to increase energy savings and reduce the residential sector's primary energy consumption. Heat energy is commonly provided to residential buildings by natural gas, biomass or electric boilers for space heating and hot water supply, and represents a significant energy consumption in residential buildings. For instance, in the UK, the electrical energy consumed in the domestic sector is 45% of the total electrical energy consumption [1]. In this context, Combined Heat and Power (CHP) generation is recognized as one of the technically and economically viable strategies to face the rising trend of primary energy consumption [2]. Moreover, CHP has been considered, worldwide, as the main alternative to traditional systems in terms of energy savings and environmental conservation and represents a sustainable path towards reducing Green House Gas emissions [3].

Although this concept is already well known and applied in the medium-high power range (>100kW_e), small and, particularly, micro size systems are not so diffused yet. Recognising its vast market and potential benefits, micro-CHP systems have still not reached a sufficient state of maturity to be considered an actual valid alternative to the standard domestic heating systems [4]. Among the several alternatives for CHP technologies, the Organic Rankine Cycle (ORC) stands as one of the most promising due to its high overall efficiency, high availability and versatility (namely, regarding the nature and grade of the heat source), and low maintenance costs. However, the downsizing of this technology poses challenges that make small-scale ORC still unattractive on economic grounds [5]: their specific cost (€/kW_e) is still too high to guarantee a reasonable return on investment. In fact, the existent micro-CHP boilers in the market for residential applications, of whatever technology, exhibit such high prices that the payback period makes them unattractive.

This is an extremely interesting opportunity because, according to Alane and Saari [6], the most promising market for the micro-CHP systems lies in the residential sector. In fact, for these authors, the expected worldwide sales for residential micro-CHP (~1 kW_e) in the years 2020 and 2030 are 52 and 2900 thousand units, respectively. The expected stock in 2040 is circa 30.5 million units which evidences the enormous potential market of these systems.

To the moment, the only ORC-based micro-CHP system for the residential sector was brought by FlowEnergy Company in 2015 but, nowadays, has been discontinued and unavailable. The

FlowEnergy system produced up to 1 kW_e of electrical power, using a scroll expander connected to a generator, and a thermal power output ranging from 7.4 to 14.1 kW_t [7]. It is a wall-mounted system that can be retrofittable with combi-boilers despite needing to integrate an auxiliary hot water tank. However, the price and efficiency did not allow it to stand out in the market. In this micro-scale, some companies develop ORC modules that are not true autonomous CHP, but basically waste heat recovery units that need to be coupled to an external heat source previously available, usually by means of an intermediate circuit of thermal oil or hot water. It is the case of the Spanish Rank [8], the Italian Kaymacor [9], and the French Enogia [10].

Numerical simulations play a vital role in the ORC systems' design and analysis for stable, safe and economical operation, because of the variety of boundary conditions that occur in evaluating the economic potential of real applications. The ORC system simulation is often performed using simplified models based on integral conservation equations in steady-state conditions and characterizing the components solely through nominal yields (lumped-parameters approach). However, they are not accurate, can only get a first approximation of the ORC behaviour because the components do not behave the same way in design and off-design conditions. In fact, the components will never work simultaneously in design conditions except, possibly, in a tiny region of the space of domestic user demands.

One step further, detailed ORC modelling includes separate sub-models for each component using semi-empirical or purely empirical models or performance maps (characteristic curves) that describe their behaviour truthfully in given boundary conditions. The overall cycle model is obtained interconnecting the components sub-models. However, most of these models still require the previous specification of some constant thermodynamic properties, such as, the working fluid liquid subcooling degree at condenser exit or vapour superheat degree at evaporator exit, which deprives them of full predictability. A way to overcome this is to incorporate further the conservation equation of the working fluid charge in the system that plays a vital role in the off-design performance and has, itself, a non-negligible cost. Although the fluid charge is a well-known parameter in vapour compression systems, it is almost unexplored in the ORC systems modelling.

1.2 Objectives and Achievements

This thesis aims to assist in the thermodynamic project and development of a micro-CHP (Combined Heat and Power) gas boiler based on Rankine technology that satisfies the hot waters and central heating domestic needs, thus replacing current boilers, and further producing electricity. For simplicity, here-to-fore this micro-CHP is called Hebe, after the acronym of the market focused

R&D Project HEBE within and for which most of the work of the thesis was developed. Although Hebe consumes slightly more gas than a comparable state-of-the-art condensing boiler, as gas is usually much cheaper than electricity, the annual saving in the energy bill is supposed to pay back the extra investment in a reasonable time. The ultimate goal of the thesis is to produce a fully predictive and accurate model capable of characterizing the behaviour of Hebe under off-design conditions in order to support the experimental tests, establish the system control and forecast the performance.

In pursuit of this objective, a bottom-up approach is followed, from simple thermodynamic models, evolving to more sophisticated component sub models and complex global ORC model.

In the first stage, a simplified thermodynamic steady-state model for the early project of Hebe considering its market and engineering pre-specifications is proposed. The model describes with sufficient detail and precision the steady-state near nominal conditions of operation of Hebe embedded in its test rig, based on plausible simplifying hypotheses. Then, an optimization problem and algorithm are formulated and implemented to find the design options and parameters that maximize the thermodynamic efficiency of the micro-CHP, subject to the imposed constraints, throughout the complete range of the desired user conditions. These first stage tools allowed to select the working fluid, the main components and to identify the ranges of the measure and control instruments.

In the second stage, with Hebe's design mainly defined, a more detailed, precise and fully predictive model is constructed to describe the system steady-state off-design behaviour. In fact, more than a single model of this kind, it was conceived a modular modelling architecture with an open library of sub models for a variety of possible components of the evolving prototype of Hebe. A particular model, such as the one constructed for the first prototype of Hebe, is a network of sub models duly interconnected. The software implementing the architecture has a powerful numerical solver for the resulting system of non-linear equations of any model that can be generated. The overall model of the system has truly accessible inputs, based only on its boundary and control conditions, without any assumptions. Such a fully predictive model is practically absent in the literature. The empirical parts of the component's sub models and the overall model are calibrated with experimental measurements of Hebe in the test rig. The overall calibrated model of the micro-CHP achieves a good fit between experimental and predicted results and affords a rich characterization of its off-design steady behaviour.

In the third and final stage, the former complete model is applied to thoroughly understand the steady-state behaviour of Hebe, and devise a safe and optimal strategy of (steady-state) control for it. This control strategy is complemented with a preliminary proposal of an empirical dynamic control component based on PIDs to guide the system through a quick and safe operation path during start-ups and user demands transition towards the best performance steady-state previously identified.

During the three stages of this work, three major experimental campaigns were carried out. A set of preliminary experimental tests were conducted to assess Hebe's performance, determine the influence of the basic control variables on the system behaviour and validate the early design procedure. An extensive campaign with around 50 steady-state test points covering a broad range of Hebe's operating space was performed to calibrate and validate the second model. The last experimental tests were performed to develop the empirical dynamic control algorithm.
Along the thesis, the contribution of the author for the various works reported is clearly discriminated from the one of other members of the research team of Project HEBE.

Most of the research in this PhD thesis is based on the following core articles published or under review in ISI-indexed journals

Santos M, André J, Costa E, Mendes R, Ribeiro J (2020) Design strategy for component and working fluid selection in a domestic micro-CHP ORC boiler, *Applied Thermal Engineering* 129, 848 - 867.
doi: 10.1016/j.egypro.2017.09.143. JCR Impact Factor® (2020): 4.725; Citation: 2

Santos M, André J, Francisco S, Mendes R, Ribeiro J (2018) Off-design modelling of an organic Rankine cycle micro-CHP: Modular framework, calibration and validation, *Applied Thermal Engineering* 137, 848 - 867.
doi: 10.1016/j.applthermaleng.2018.04.009. JCR Impact Factor® (2018): 4.550; Citation: 11

Santos M, André J, Augusto C, Costa E, Mendes R, Ribeiro J (2020) Quasi-steady state behavior and control of an Organic Rankine Cycle-based micro combined heat-and-power system (submitted)

1.3 Thesis Outline

This thesis is composed of seven chapters, including this introductory chapter, and is structured as follows:

Chapter 1: Introduction

The first chapter introduces the motivation for carrying out this work. The interest in micro-CHP systems won a renewed and growing interest with the continued increase in the consumption of petroleum products and electricity. At the moment, no economically viable micro-CHP replacement for standard domestic boilers appears in the market. Proper development of an ORC based micro-CHP system – in particular, the one which design and control is assisted along the thesis is designated as Hebe – requires a thermodynamic project that uses a fully predictive model to characterize its behaviour. This thesis aims to answer the mentioned problematic.

Chapter 2: Micro-CHP market

First of all, the practical importance of the work must be highlighted by a proper micro-CHP market analysis in order to demonstrate the benefits regarding energy savings for the user and thus the potential market of these systems. Therefore, the second chapter presents the micro-CHP systems, their advantages over existing systems and the different micro-CHP developed technologies. Furthermore, a detailed description of the prime movers and competitors of Hebe is disclosed. Finally, a comprehensive business opportunity and economic assessment are performed for Hebe. If its foreseen technical performance and costs are achieved, Hebe is positioned ahead of the competitors and can obtain a high share in the domestic gas boilers market.

Chapter 3 ORC modelling

Before any novel modelling attempt can be done, a proper understanding of the system physical principles and possible modelling approaches for ORC simulations must previously be attained. Chapter 3 reviews the literature firstly about the general organic Rankine cycle and then focused on the specific modelling strategies that have been applied for the system behaviour comprehension. Simplified thermodynamic models are widespread and commonly used to select main components, choose the appropriate working fluid, perform a techno-economic analysis and some system optimization, and, as such, are surveyed in the first place. In the second place, the off-design models are revised with an emphasis on the review of the few existing charge-sensitive models, where the mass balance of working fluid distributed throughout the ORC circuit is taken into account in order to turn them fully predictive.

Chapter 4 ORC design and construction

Chapter 4 (first paper published of a trilogy) presents the initial stage towards the main objective of developing the proof-of-concept prototype of Hebe, a new micro-CHP gas boiler. In that sense, a strategy for early design is proposed from the very initial problem formulation to the construction and assessment of the experimental test-rig. The basic design, demands and pre-specifications of the micro-CHP system are initially stated. Afterwards, a simplified model of the micro-CHP, that given the pre-specified inputs, describes as detailed and realistically as possible its steady-state

operation condition, is developed. Following, an optimization problem and a numerical algorithm to solve it are formulated and implemented, that lead to the best selection/dimensioning of the working fluid and the main components, i.e., the early design of Hebe and its test rig. Finally, a preliminary experimental campaign was conducted to assess design procedure suitability.

Chapter 5 Charge-sensitive model development

The fifth chapter (second paper published of a trilogy) is the most original and valuable core of the thesis, where the physical and mathematical framework of the most sophisticated developed model is described. The chapter provides a modelling tool for predicting the steady-state ORC performance in any off-design condition considering the working fluid charge, user demand conditions and control strategy. Consequently, this model is assumption-free, takes just the known boundary conditions as inputs and, for that reason, is fully predictive. The model has a modular architecture implemented in Fortran interconnecting the various components' sub-models. In particular, purely empirical models encompassing the manufacturer's characteristic curves were proposed for the turbine/expander and for the pump. A medium level semi-empirical model using a one-dimensional moving-boundary method was applied to the condenser. In contrast, a more complex semi-empirical model finite volume method was developed for the evaporator, including the boiler's combustion chamber. Finally, an extensive experimental campaign was conducted in order to calibrate and validate each sub-model and the overall model.

Chapter 6 Quasi-steady behaviour and control

The sixth chapter (third paper of the trilogy submitted for publication) analyzes Hebe's behaviour in the experimental test-rig and develops a control strategy using as tool the off-design model presented in the former chapter. Stationary off-design models have been used for performance evaluation in real operating conditions but were very rarely employed to develop an optimal steady-state control strategy for the ORC. In the first and most important part of the chapter, the aforementioned model is employed to characterize the exhaustive steady-state behaviour of the micro-CHP, identify the stable operation regions, generate the complete control maps for the system and, as a final result, establish its full steady-state control strategy. In the second part of the chapter, an empirical dynamic control strategy based on PIDs is preliminary proposed to guide the system through a quick and safe operation path during start-ups and user demands transitions towards the best performance steady-state identified with the control strategy presented in the first part.

Chapter 7 Conclusions and perspectives

To conclude, the last chapter summarises the main findings and results of this work. Perspective themes and improvements for future work are also revealed.

Chapter 2

Micro-CHP

This chapter provides an overview of the literature on micro combined heat-and-power technologies as replacements of conventional boilers, with a particular focus on the potential market share of the ORC technology. In the first subchapter, a brief introduction to the micro-CHP technologies development is performed. The description of micro-CHP prime movers and the market competitors are presented in the second and third subchapters, respectively. Finally, the business opportunity foreseen for Hebe, the new micro-CHP ORC combi-boiler to which development this thesis contributed, and the correspondent potential market analysis are described in the fourth subchapter.

2.1 Introduction

Fossil energy was a fundamental driver of the Industrial Revolution in the 19th century, playing a dominant role in technological, social and economic development which has followed. As a result, fossil fuels are still at present the main source of primary energy for most domestic and industrial needs leading to exhaustion of oil reserves and extensive greenhouse gas emissions. Figure 2.1 exhibits the broad diversification of fossil energy consumption in the 20th century, especially due to the transports and heating sectors [11].

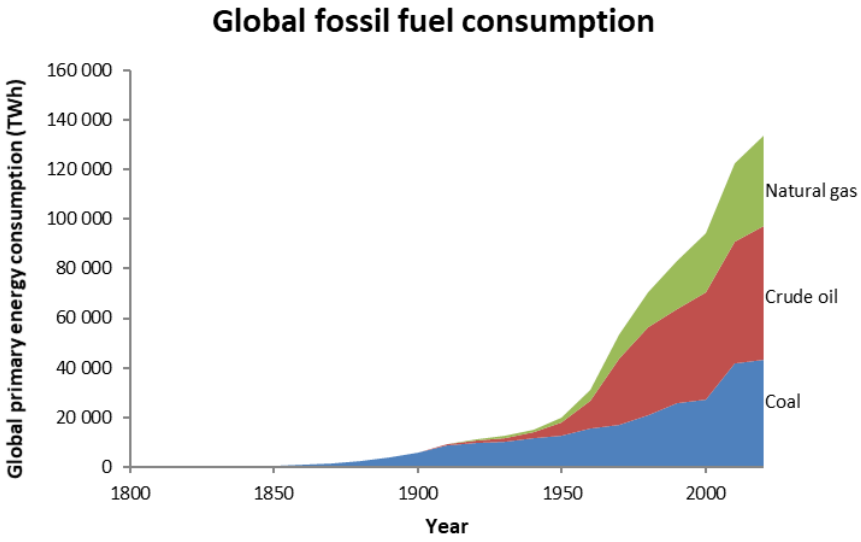

Figure 2.1 - Global primary energy consumption by fossil fuel source [11].

According to EIA, the world energy consumption will grow by nearly 50 percent between 2018 and 2050 and most of the anticipated growth will come from developing nations, particularly in Asia [12]. The EIA also predicts that electricity consumption will be 79 percent higher in the buildings sector, both residential and commercial, and should see a 65 percent rise in overall consumption over the next 30 years. For instance, in the UK, the total energy consumption in the domestic sector is 45% of the total electrical energy consumption [13]. Hence, energy consumption in residential buildings is significant. Therefore, the continuous increase in energy demand is posing challenges to the academy and industry on how the network of energy production should

evolve in future years. In that sense, distributed micro combined heat and power systems can contribute to reducing the total primary energy consumption.

Generally, electricity is supplied through a centralized distribution energy network to the residential sector to meet the demand for lighting, home appliances, air conditioning, entertainment devices, among others. In developed countries, the heat energy for space heating and hot water supply is provided by biomass and electric boilers, but more often by natural gas boilers. Furthermore, environmental and sustainability concerns are continuously increasing, leading to, among other measures, constant improvements in the traditional methods of energy conversion.

The Combined Heat and Power (CHP or cogeneration) systems produce useful heat and electricity simultaneously. Consequently, they increase overall efficiency, save primary energy and promote environmental preservation, reasons enough for CHP to have been considered as the major alternative to traditional systems [3]. Moreover, distributed CHP can be integrated into the public power network and offer a tremendous increase in revenue to declining fossil-fuelled emissions while saving operational costs for power generation [14]. Figure 2.2 depicts the differences between separated and cogeneration productions of electrical and thermal energies for a given generic process. As micro-CHP exhibit higher overall efficiency than traditional boilers and also produce a share of electricity, a reduction of the primary energy input to fulfil the user needs is achieved.

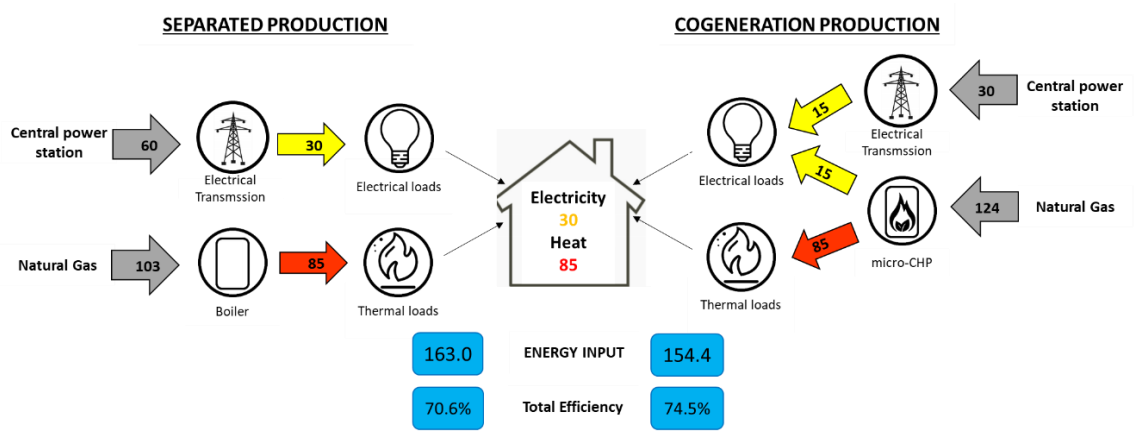

Figure 2.2 - Differences on primary energy consumption and total energy efficiency between cogeneration production and separated production [14].

Historically, cogeneration is as old as electricity generation itself. District heating systems were popular in the late 1800s and district electrification starts with Thomas Edison's plants in New York. The two were rapidly combined until the development of large centralized power units which produced cheaper electricity. CHP regains interest during the energy crisis in the early 1970s and since the 1990s micro-CHP have been proposed as a possible alternative to gas-fired boilers for households [15]. In 2008, IEA listed several country policies in order to promote CHP and some countries pointed out that incentive policies can have significant effect on CHP development and spread [12]. Public departments at national and international level were specifically created to

identify the CHP potentials, promote policy measures and develop CHP technology. From these departments appears the European Directive 2012/27/EU that incentives European countries to develop CHP systems and to increase the use of cogeneration in order to save non-renewable primary energies [14]. According to the previous directive, CHP systems can be classified in three categories depending on the electrical capacity, namely, "micro-CHP" if fewer than 50 kW_e, "small-scale CHP" if ranging from 50 kW_e to 1 MW_e and simply "CHP" if higher than 1 MW_e [16]. Cogeneration systems are a mature technology with a fairly widespread use but specifically micro-scale systems are still very limited, specially due to the downsizing problems of the main components [17]. Nevertheless, if the domestic hot waters for space heating and direct use are considered, the potential market for CHP systems in this scale is huge [4]. In particular, the availability of natural gas supply networks in most buildings invites the appearance of micro-CHP for easy replacement of existing gas-fired boilers, providing power in addition to heat [18]. According to Alane and Saari, the most promising market for micro-CHP relies on the residential sector of developed cold countries as United Kingdom, Ireland, Belgium, Netherlands, Germany or Denmark in Europe [6].

The current estimations of the annual sales and stocks of the European residential boiler market are 8 and 100 million, respectively. An increasing share of this giant market is expected to be fulfilled by micro-CHP, replacing the existent residential boilers that only supply hot water, in the following years [19].

2.2 Micro-CHP technologies

To start with, the available technologies for micro-CHP can be separated and distinguished in technologies based and not based on thermodynamic cycles. The first group can be further subdivided into internal combustion (Internal Combustion Engines, ICE) and external or no combustion technologies (Stirling Engines [SE], Micro Gas Turbines [MGT] and Organic Rankine CycleORC). Within the latter subgroup, the Rankine cycle (ORC) is the most common. The second group mainly concerns Fuel Cells (FC) and Solar Thermal Photovoltaic hybrid technologies (ST/ PV).

This subsection presents the potential prime movers of micro-CHP systems for residential applications already available in the market and in development stage. For a better understanding of the comparison among different technologies, common performance indicators will be described next.

The standard thermodynamic efficiency η_t is given by:

$$\eta_t = \left(\dot{W}_{out} - \dot{W}_{in}\right)/\dot{Q}_{in} \quad (2.1)$$

where $\dot{W}_{out}$ and $\dot{W}_{in}$ are the mechanical power delivered and consumed by the system, respectively, and $\dot{Q}_{in}$ is the heat power input to the system. The thermal efficiency is the ratio between the output ($\dot{Q}_{out}$) and input heat powers:

$$\eta_{th} = \dot{Q}_{out}/\dot{Q}_{in} = 1 - \eta_t \quad (2.2)$$

The Heat-to-Power Ratio (HPR) is commonly used by the industry to compare the thermal and electrical deliveries of a CHP:

$$HPR = \dot{Q}_{out}/P_{e,out} \quad (2.3)$$

where $P_{e,out}$ is the electrical power output of the CHP. The electrical efficiency is given by:

$$\eta_e = P_{e,out}/\dot{Q}_{in} = \eta_{th}/HPR \quad (2.4)$$

Finally, the global or total CHP efficiency is the ratio between the total energy output of the CHP (heat plus electricity) and heat input of the CHP. Basically, it is the sum of the electrical and thermal efficiencies:

$$\eta_{CHP} = \left(\dot{Q}_{out} + P_{e,out}\right)/\dot{Q}_{in} = \eta_e + \eta_{th} \quad (2.5)$$

Internal Combustion Engines (ICE)

Internal combustion engines (ICE) are widely accepted and the most well-established technology for small and micro CHP applications. Basically, it is a heat engine that produces heat and power directly from the combustion of a fuel and an oxidizer that takes place in a combustion chamber with movable walls. There are two basic ICE technologies: the "Otto engine" or spark-ignition engine, and the "Diesel engine" also called compression ignition engine. The ICE rotating shaft drives an electric generator when operating in CHP systems while the heat released both through its hot exhaust gases and jacket water is used to produce steam or heat water for space heating and/or direct use. Despite most of the engines use natural gas as an energy source, liquefied petroleum gas (LPG), gasoline and diesel are still used, and alternative fuels, such as syngas from biomass, have also been considered. The ICE has been successfully commercialized for emergency generators of all sizes and for small- and large-scale CHP systems, ranging in size from a few hundred kilowatts to several megawatts in electrical capacity. They are majorly employed in the services and industry sectors; however, they are increasingly used in the residential sector. For applications that suit domestic installations, an electric efficiency ranging from 20% to 26% and a total CHP efficiency up to 90% has been reported [4].

Although ICE-based micro-CHP have been readily available in the market, some of the issues yet to be solved are: (i) achieving low emissions from the engines; (ii) improving power density per kW_e; (iii) introducing renewable fuels not compromising a successful operation; and (iv) increasing the durability of the engine in line with the longevity of the dwellings or large apartments [13].

Stirling Engines (SE)

The Stirling technology came shortly afterwards the ICE based CHP. The Stirling engine is an external combustion engine which operates on a closed regenerative thermodynamic cycle with expansion and compression of the working gas fluid at different temperature levels. The mechanical and ultimately electrical power is generated by the pressure forces exerted by the gas on the two sides of a linearly alternating piston, and the heat source input is partly used to maintain the gas in one chamber of the cylinder at high temperature and partly delivered to the water that cools the gas in the other chamber of the cylinder [20]. The crank-driven and free piston are the two basic Stirling technologies available for micro-cogeneration, the latter of which can immediately produce grid compatible AC electricity with a linear generator [13]

Stirling engine based micro-CHP systems exhibit high thermodynamic efficiency and high fuel flexibility, which has made them to be considered for many years the most promising technology for micro-CHP, as stated by Harrison and On [21]. Moreover, for the low level of noise and the long maintenance interval, SE seems better suited for residential applications than ICE [22]. Despite the many advantages, sealing, need of an external combustion heat addition and dynamic balancing of the unit leads to higher cost than ICE. Also, heavy and complex units are major issues with the Stirling engine based micro-CHP [13].

Micro Gas Turbines (MGT)

Simple micro gas turbines consist of a compressor, combustor, turbine and generator. Air is conveyed and pressurized through the compressor and mixed with fuel in the combustion chamber. Then, the combustion products are expanded through the turbine/diffuser producing rotation on the rotor assembly and generating electricity through the alternator [23]. The compressor and turbine have typically radial-flow designs, similar to those of automotive engine turbochargers. The air admitted in the combustion chamber can be preheated by the exhaust gases forming a regenerated cycle allowing to practically double the thermodynamic efficiency. However, this also reduces the amount of recoverable heat from the system, which can be undesirable for some CHP applications [24].

According to Murugan and Horák, micro gas turbine systems are scaled down versions of gas turbines that provide reasonable electrical efficiency of about 30%, multi-fuel capability, low emission levels, and high heat recovery potential, and need minimal maintenance. For cogeneration applications, an overall efficiency above 80% can be achieved [13]. The major issues that challenge the development of micro gas turbines are related to costs and small-scale effects causing large fluid dynamic heat and mechanical losses [25]. The lower global efficiency than ICE or SE, the efficiency decrease for partial loads and the high rotating speed are current technical barriers to the wide spreading of this technology [24].

Fuel Cells (FC)

Fuel cells are electrochemical energy devices, similar to primary batteries, that rely on the chemical reaction of hydrogen with oxygen to produce water and electricity. In this reaction, a fraction of the energy produced becomes available as heat. Two technologies are majorly applied in CHP applications: the low-temperature polymer electrolyte membrane fuel cells (PEMFC) which operate around 80ºC and high-temperature solid oxide fuel cells (SOFC) working at about 800-1000ºC.

PEMs use a proton exchange membrane sandwiched between two electrodes that form the cell. The PEMFC has high power density, low emissions and a quick start-up which makes it a promising technology for adoption as a prime mover for micro-CHP [26]. However, water management is problematic for Naflon-based PEMFC because the membrane should be slightly hydrated but the catalyst is frequently flooded by excessive liquid water from the reaction products. For this reason, Polybenzimidazole (PBI)-based PEMFC has been developed that operates with lower hydrogen quality and at slightly higher temperature (140-180ºC). This capability allows a more straightforward configuration of the fuel processor and a more compact unit which is desirable for domestic applications [27].

Solid-oxide fuel cells (SOFC) use the oxidation of hydrocarbons (e.g., natural gas) to produce hydrogen and then electricity. The major merits of this technology are the high electric efficiency, high-grade waste heat, low emissions, fuel flexibility and power scalability. However, a key disadvantage of early SOFCs systems was an extremely long time for a cold start-up (~10h). Therefore, a trend to lower the operating temperature to an intermediate temperature range (500-750ºC) arises in order to minimize this problem at the cost of decreasing the electrical and thermodynamic efficiencies [28].

In comparison to heat engine-based micro-CHP systems, fuel-cell based systems offer higher overall efficiency, lower heat-to-power ratio HPR, quieter operation, simpler maintenance requirements and more efficient part-load performance [29]. In fuel cell-based systems, the electrical efficiency can reach 35-45 % instead of the 10-25 % of the former [30]. On the other hand, for domestic systems, the heat delivered may be insufficient to the needs due to the low HPR of the fuel cell CHP. Consequently, both PEMFC and SOFC are usually complemented with auxiliary boilers, which allied to the already high price of the primary system turns out in overall prohibitive costs [31].

Organic Rankine Cycle (ORC)

The classic steam Rankine Cycle is a thermodynamic cycle based on the vaporization of high-pressure liquid water which expands to a lower pressure steam, while producing mechanical work, that later can generate electricity. The main components are the evaporator, the expander, the condenser and the pump. The Organic Rankine cycle (ORC) uses the same principles of the steam Rankine cycle but replaces the water as a working fluid for an organic fluid. The great advantage

is not requiring a superheating degree of the vapour at the expander inlet if the saturated vapour-line of the fluid is vertical or has even a positive slope in the *T-s* thermodynamic diagram, leading to an expansion that ends in the superheated vapour zone instead of the liquid-vapour zone, as it would happen if water was used. An important outcome of this feature is the relatively low system operating temperature and pressure that increases the range of possible applications and decreases the manufacturing compliance and security issues. According to Maghanki et al. [4], the use of ORC based solutions for micro-CHP systems represents a good alternative to household boilers with electrical efficiency ranging from 6% to 19% and a potential overall CHP efficiency always higher than 90% for an electric power size of 1–10 kW_e and a corresponding thermal power size of 8−44 kW_t meeting the typical residential water heating needs.

At the moment, there are many different proposals for ORCs ranging from large to small-scale and for different applications. However, for micro-scale, only a limited number of units have been produced so far, because, until now, they are not able to reach economic competitiveness. In fact, the simple downsizing of ORC technology results in too high specific costs to make micro ORC units attractive on commercial grounds.

Global Overview

To conclude, some reviews and techno-economic assessments of the developed micro-CHP technologies over the years are present in the scientific literature, such as Bianchi et al., that analysed several market CHP units and obtained their rated electrical and thermal efficiencies, which are displayed in Figure 2.3 [17]. It is interesting to observe that all present CHP technologies exhibit values of overall efficiency η_{CHP} over 75%. In particular, the ORC micro-CHP presents the lowest values of electrical efficiency but the highest of thermal efficiency.

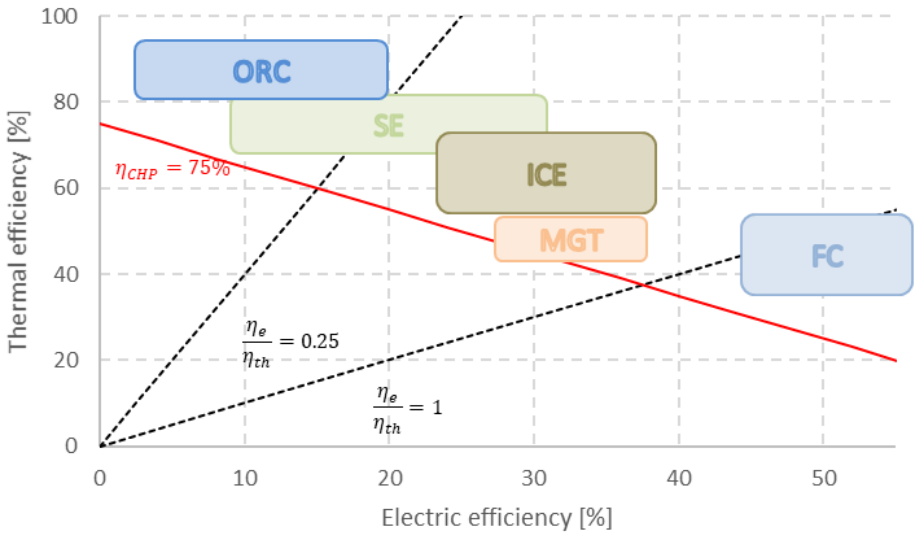

Figure 2.3 - Representative areas of various micro-CHP technologies in the plane (η_e-η_{th}) [17]

At the moment, micro-cogenerators based on internal combustion engines, Stirling engines and fuel cells are already available in the market while several R&D groups aim at producing commercially available units based on micro gas turbines and Organic Rankine Cycle. An outlook of the market available products is displayed in the next section.

2.3 Market Competitors

Simon Pezuto et al. collected and analysed data from multiple sources, including large data sets available online and scientific papers, to assess the space heating (SH) and domestic hot water (DHW) market in Europe [32]. The authors found that a variety of equipments are used for SH and DHW that they divided into the following categories: boilers, stoves, electric radiators, heat pumps, solar thermal systems, CHP and district heating. Moreover, in the EU28, the traditional boilers (non-condensing) have the greatest diffusion with over 80 million units while condensing boilers and heat pumps have a bit more than 10 million and internal combustion CHP only have 50 thousand installed units, as shown in Table 2.1. However, the average capacity (i.e., nominal heat power $\dot{Q}_{out_n}$ delivered for SH and DHW) and equivalent full-load hours of yearly operation in the last referred equipment are the highest. For comparison purposes, the "Efficiency" in Table 2.1 is always the ratio between the output power (heat power delivered to SH or DHW) and the input power of the equipment. For boilers, the input power is the combustion heat power based on the low heat value of the gas. For heat pumps, the input power is the power (ultimately electric) consumed by the compressor, and as the authors characterized the heat pumps by a COP coefficient (see eq. 2.6) with an average value of 3.5, this results in a "350% efficiency". For CHP-ICE, the "efficiency" coincides with the thermal efficiency which is quite lower than the global efficiency.

$$COP = \dot{Q}_{out}/\dot{W}_{in} \tag{2.6}$$

Table 2.1 - Assessment of the space heating (SH) and domestic hot water (DHW) market in Europe [32].

	Operative Units (million)	**Average capacity [kW_t]**	**Efficiency [%]**	**Full-load hours [h]**
traditional boilers	82	22	85	1000
condensing boilers	13	22	100	1000
heat pumps	11	6	350	700
CHP-ICE	0.05	190	58	1900

Finally, using the data of Table 2.1, it is possible to plot the results in terms of energy consumption per equipment type. As depicted in Figure 2.4, the largest share belongs to non-condensing boilers, followed by condensing boilers and two small parts account for heat pumps and CHP systems.

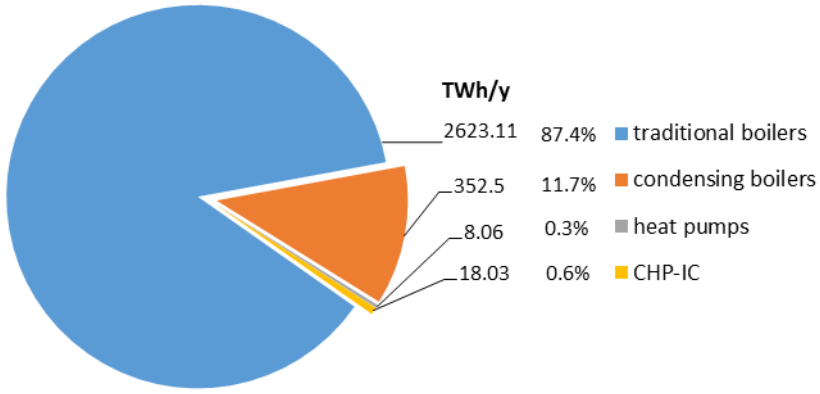

Figure 2.4 - Energy consumption and share of the SH and DHW equipments in Europe.

The competitors for a new micro-CHP gas boiler (i.e., for replacement of present domestic boilers) based on Rankine technology can now be divided into the following classes:

i. Classic direct competitors: present domestic gas boilers, both traditional and condensing.
ii. Emerging close and direct competitors: other micro-CHP gas boilers based on different technologies (e.g., Stirling, micro gas turbines, internal combustion engines and fuel cells) and even on the same technology (Rankine).

i) Traditional and Condensing Boilers

In the 2016 report on Boiler Market, by Global Market Insights Inc., a market size of 10 billion euros (b€) has been declared and an annual installation of over 6 million units by 2024 is expected, just in Europe [33]. The same report announces a USD 50 billion global boiler market size in 2017 and anticipates an annual installation exceeding 13 million units by 2024. A very large share of these boilers corresponds to the residential wall-hung boilers. As stated above, there are two main types of residential boilers: the traditional and the condensing boilers. The main difference between the two systems is the ability of the latter to condense the water existent in the flue gases, as long as the cold source (water) is cold enough, leading to a higher exploitation of the hot source, in this case the combustion gases of the natural gas. Because of that, condensing boilers have efficiency above 95% while non-condensing boilers can only slightly overpass 80% efficiency, both efficiencies based on the low heat value of the gas [34].

Over the past years, the European Union (EU) introduced rigorous energy efficiency norms which have led to the widespread replacement of traditional heating units. For instance, the Ecodesign Directive aims to minimize the ecological effects of energy related products while promoting the

adoption of energy efficient heating technologies [35]. In the US, the Federal Energy Management program has set a minimum efficiency of 95% for gas fired residential and commerce boilers with a capacity between 88 and 733 kW [33]. The BSRIA report mentions a Compound Annual Growth Rate (CAGR) of 8.5% in the sales of condensing boiler units from 2013 to 2017 and a - 7.5% CAGR on the sales of non-condensing units for the same period worldwide [36]. An interesting fact is that it occurs essentially in Europe, the US and Japan, largely because of the adoption of the described measures, while it remains almost constant in other regions.

The domestic boilers industry (namely, of wall hung boilers) is dominated by some nine major companies (e.g.: Bosch, Vaillant and Viessmann [Germany]; Ariston [Italy]; BDR Thermea [UK/Netherlands]; Rinnai [Japan]; Kyungdong [South-Korea]), each one, in general, close (at least in the same continent) to the markets in which one or more of its brands have a significant share. Moreover, all of them hold important market shares in China; the European Baxi (now BDR Group) sells also in Canada; and the German Bosch Thermotechnology Group has a truly worldwide distribution network.

Table 2.2 compares the current commercial prices for various models of traditional and condensing gas boilers available in the market with a nominal thermal output power of 24 kW_t, the standard for the residential sector. A price slightly lower than 1.000€ for traditional boilers and ranging from 1.500-2.000€ for condensing boilers can be observed.

Table 2.2 - Example of traditional and condensing boilers with the largest shares in the residential market, of some manufacturers [37].

Type	Manufacturer	Model	Price [€]
Traditional	Baxi	Victoria plus	899
	Vulcano	Life2	999
	Ariston	Clas X	875
	Cerapur	ZWBC	875
Condensing	Baxi	Platinum	1.849
	Vulcano	Aquastar	2.049
	Ariston	Clas One	1.650

Comparing the two gas boiler types along their life-span, condensing boilers have a higher initial cost but they will be more cost efficient in the long-run. Also, condensing boilers significantly reduce carbon emissions, saving up to 1200 kg of carbon a year per unit [34]. Nevertheless, the system can shut down in very cold weather because the external pipe is susceptible to freezing and can start to become corroded by the acid condensate. Additionally, condensing boilers are more expensive to maintain due to their complexity, while non-condensing boilers are cheaper to fix.

ii) Prime mover technologies (CHP)

Micro Combined Heat and Power Market size exceeded USD 1 billion in 2019 and is projected to exceed the annual installation power capacity of 895 MW_e by 2026. Micro CHP Market size is expected to surpass USD 3 Billion by 2026, as reported in the latest study by Global Market Insights, Inc [38]. Table 2.3 presents the installed capacity and market value in 2016 for three ranges of micro-CHP systems. Although micro-CHP with power capacity less than 2 kW_e has the lowest installed capacity, it is predicted that will dominate through large scale residential deployments. Growing demand for energy efficient, reliable, and non-intermittent energy supply to provide space heating, hot water and electricity for the residential sector has increased the product penetration.

Table 2.3 - Global market in 2016, by power capacity, volume and revenue [33]

Unit Capacity [kW_e]	Installed capacity [MW_e]	Value [USD Million]
0 − 2	11.42 (7.3%)	229.17 (31.9%)
2 − 10	47.56 (30.3%)	208.67 (29.1%)
10 − 50	97.88 (62.4%)	280.48 (39.0%)
Total	**156.86 (100.0%)**	**718.32 (100.0%)**

A simple calculus of the ratio between the value and the installed capacity of the different ranges of micro-CHP allows to conclude that the specific cost decreases with the capacity, as expected. Moreover, the specific cost for the <2 kW_e range exceeds 20.000 USD/kW_e which demonstrates the economic unfeasibility of the residential micro-CHP until now. Circa 80% of these residential systems are in the Asia Pacific area, mostly in Japan, and circa 20% in Europe.

Five main technologies of micro-CHP applied to domestic boilers have been tested until now, based on the following engines or thermodynamic cycles: I) internal combustion, burning gas or oil; II) Stirling; III) Micro gas turbines; IV) Fuel Cells; and V) Rankine. From the technology/industry and market points of view, the five should be considered as emergent technologies, though with a decreasing degree of maturity from I) to V). In consequence, they justify a detailed case-by-case market and industry analysis at the onset, before the competitive analysis with Hebe, the micro-CHP proposed.

Several fuels or primary energies can be used in CHP systems. Natural gas held a dominant market share in 2016 with 67.3% and will continue to witness robust growth on account of its cost-effectiveness, improved efficiency, “eco-friendly” and non-corrosive features. Coal, renewable sources, oil and other fuels complete the list with a share ranging between 5-8% each. Regarding the different prime movers, the internal combustion engines lead the installed capacity but the major share of the global market revenue belongs to fuel cells, as depicted in Table 2.4.

Table 2.4 - Global market by prime mover in 2016 [38]

Prime mover	Installed capacity [MW_e]	Value [USD Million]
Stirling Engine	33.33 (21.2%)	132.24 (18.40%)
Internal Combustion Engine	70.81 (45.1%)	254.49 (35.40%)
Fuel Cell	48.57 (30.9%)	327.65 (45.60%)
Others	4.15 (2.7%)	3.94 (0.56%)
Total	**156.86 (100.0%)**	**718.32 (100.00%)**

A general observation, only with mild differences among the technologies, is that micro-CHP boilers still have residual shares of the boilers' market and low growth rates of sales when compared with their believed potential. This is due marginally to the fact that they have only recently reached the market and the industry capacity is also still low. Mostly, the circumstances that led to the low widespread are: (1) they are still significantly more expensive than simple boilers and (2) have still not had the market time to prove that they have similar technological reliability (e.g., maintenance cost and lifetime) [39].

I) Internal Combustion Engines

The following companies were the first to reach the market in the internal combustion technology segment, with the products which main characteristics are displayed in Table 2.5. Notice that the thermal efficiency is based on the low heat value of the fuel, which may cause the overall efficiency to overpass 100%. A second important remark is that, for all products, the thermal power capacity is clearly below the domestic needs for SH and DHW, which means that they require a backup boiler.

- Honda began selling Ecowill in Japan, a 1 kW_e unit designed for single-family dwellings with an overall energy efficiency of 85%. According with Schweitzer and Formanski (2008) [40], sold 65 000 units until 2008 [41]. They were released in some countries of Europe five years later, via Vaillant ecoPower 1.0 with a price rounding 14.000 €, including installation [42].
- In February 2002, Tokyo Gas and Aisin launched in Japan a micro-CHP, available also in the European market since 2006. The model supplies an electric output of 6.0 kW_e with a total efficiency at full load equal to 85% [42].
- The consortium BDR Thermea – Senertec sold 20 000 units of Dachs G/F 5.5 to the European market in the period 1996-2008 [43].
- Founded in 2008 in Saterland (Germany), RMB/ENERGIE GmbH was later acquired by the globally operating Yanmar Group to develop cogeneration units with Yanmar engines and increase the market share in the micro-CHP sector. In 2016, the first cogeneration unit for family homes, the neoTower LIVING, was released [44].

- Marathon Ecopower proposes a micro-CHP fuelled by natural gas or propane, able to modulate the electric power between 2.0 kW_e (for 6.0 kW_t of thermal power) and 4.7 kW_e (for 12.5 kW_t), with an overall energy efficiency at full load equal to 93% [45].
- EC POWER was established in 1996 and is one of the major European producers of CHP plants with electric power capacity ranging from 6 to 80 kW_e. EC Power reported that over 10 000 XRGI systems have already been sold in more than 27 European countries. The XRGI 6, the smallest model of the product range has condensing technology, produces up to 6 kW_e and has an overall energy efficiency of 92.4% [46].

Table 2.5 - Leading ICE micro-CHP manufacturers and important characteristics.

Company	Model	P_e (kW_e)	$\dot{Q}$ (kW_t)	η_e (%)	η_{th} (%)	Weight (kg)	Condensing
Honda	EcoWill [41]	1	2.5	22.5	65	83	No
Aisin	GECC 60 A2 [47]	4.6	11.0	25	60	465	No
Senertec	Dachs 5.5 [48]	5.5	14.8	25.6	68.4	580	Yes
Yanmar	Living [49]	2/3.3/4	5.2/8.2/8.8	28	72	-	Yes
	5.0-7.2 [49]	5/7.2	12/18.1	31	77	410	Yes
Marathon	Ecopower [45]	4.4	12.3	25	68	390	Yes
EC Power	XRGI 6 [46]	6	12.4	30.1	62.3	440	Yes

II) Stirling Engines

A number of companies have brought Stirling engine technology to a commercial stage but today only a few companies are building and selling Stirling engines. The biggest volume of engines sold can be found in the residential co-generation market. Table 2.6 (see the remarks made to Table 2.5) shows the main features of the market available products.

- Whisper Tech was born in 1987 from a R&D project of the University of Canterbury (New-Zealand). Around 3000 units were produced over 15 years, with large trials in New Zealand and UK leading to plans for mass production in Spain. By the end of 2012, the manufacturer EHE went bankrupt and the Whispergen is no longer available [42].
- The Baxi Group was created in 2000 and teamed with De Dietrich Remeha Group in 2009 forming the BDR Thermea. Among the various technologies mastered by the group, Stirling engine technology is BDR Thermea's choice for micro-CHP for domestic applications, typically serving single and two-family homes. From 2010 they offer two wall-hung solutions for replacing boilers in existing homes that share the same specifications: Remeha Evita and Baxi Ecogen, but sales data are not forthcoming [42].
- In 2005, a consortium among the boilers' manufacturers Rinnai (Japan)/ Bosch (Germany)/ Ariston (Italy) and ENATEC (Netherlands)/ Infinia (USA) was formed. As a result, they released the Greenstar CDi DualGen, a micro-CHP boiler powered by a Stirling engine in

2012. In 2013, Infinia was acquired by Qnergy, an Israeli company best known for its cryogenic Stirling as well as solar conversion technologies [50].

- In 1992, Sigma Elektroteknisl (Norway) was formed to develop its own Stirling micro-CHP boiler, starting from a patent bought to the University of Luan. The unit has a kinematic design originated in the Swedish TEM SCP Stirling engine which was subsequently developed by Sigma Elektroteknisk AS in Norway, before being taken up by Disenco in the UK. In early 2010, Disenco was placed in receivership and the design was taken over by Inspirit Energy [51].

Table 2.6 - Leading SE micro-CHP manufacturers and important characteristics [52].

Company	Model	P_e (kW_e)	$\dot{Q}$ (kW_t)	η_e (%)	η_{th} (%)	Weight (kg)	Working Fluid	Price (€)
Whisper Tech	Whispergen [53]	1	8.3	12	68	120	Nitrogen	7.000 - 9.000
Remeha	eVita [54]	1	5	15	80	110	-	10.260
Viessman	Vitotwin 300 [55]	1	5.3	15	80	125	Helium	13.500
Qnergy	PowerGen [50]	1.2	3.6	-	-	110	Helium	n.a.
Inspirit Energy	Charger [51]	6.4	15	27	63	350	Helium	n.a.

III) Micro Gas Turbines

Leading manufacturers of small-gas turbines, such as Elliot Energy System [56], Capstone [57] or ABB [58], report an electrical efficiency of 28-33% for system's power range from 25 to 100 kW_e, a range suitable to meet the thermal and electrical requirements of multi-family residential, commercial or institutional buildings. Micro Turbine Technology MTT B.V. (Netherlands) developed the only commercially available system for residential μCHP systems (<10 kW_e), the Enertwin Heat and Power [59]. A net electrical power and thermal power of 3.2 kW_e and 15.6 kW_t are announced together with an electrical efficiency of 16% and total efficiency over 94%. The microturbine operates at 24 000 rpm in nominal conditions and the market cost of the Enertwin system is around 13.000 € [60].

IV) Fuel Cells

Fuel cell products include a range of technologies and system sizes, provided mainly by ten different manufacturers (Ballard, Bosch, Ceres Power, Elcore, Hexis, RBZ, SenerTec, SOLIDpower, Vaillant, Viessmann). The development and widespread of these systems have benefited of the several EU public programs created to promote fuel cell technology. The ENEFIELD Program allowed to install more than 1 000 fuel cell micro-cogeneration units throughout Europe, and its successor, the PACE Program, aims at bringing costs further down,

although manufacturers and users say that the technology is already market-ready. This program shared between European industry and European Comission aims to bring unit costs down sufficiently to mainstream the technology and establish Europe as a global leader in fuel cell micro-cogeneration. By 2021, PACE aims at installing at least 2 500 units in Europe, manufactured by the program partners BDR Thermea, Bosch, SOLIDPower and Viessman. Japan's ENEFARM Program, in which government and manufacturers joined forces to increase production volumes and subsequently lower costs, saw the installation of 200 000 units by the end of 2016, and the Japanese government is aiming at 5.3 million units by 2030. In 2009 the cost per unit was around 24.000€, while in 2015 it had decreased to approximately 10.000€ [61].

- Since 2009 Japan has installed over 300 000 Enefarm units, most of them in the less than 1 kW_e output power range. The journey to this point has been difficult, with subsidies dropping away gradually each year as part of the program and only one company remains in each of the technology categories PEMFC and SOFC. Panasonic is selling now a PEMFC fuel cell without no subsidies at all, while Aisin-Seiki remain selling a higher priced solid-oxide residential unit that has a small subsidy of less than a 1.000$ [62].
- BDR Thermea group has two branches that develop the same product for different markets. Senertec is the company that produces the Dachs 0.8 for the European market while Remeha produces the eLecta 300 for the Asian market [54].
- Bosch group developed initially Logapower FC10 and Cerapower FC10 with the Buderos and Junkers brands, respectively. However, due to the highly integrated system, the flexibility for installation was limited. The new model consists of a Buderus GCB with high electrical efficiency and a storage tank to buffer the heat from the fuel cell.
- SOLIDpower company was founded in 2006 in Italy as SOFCpower S.R.L. and rebranded in 2014. The first micro-CHP system based on SOFCpower's fuel cell technology was achieved in 2009 in a prototype phase but the Bluegen system was delivered to end-customers in Europe only in early 2016. In 2018, the company was acquired by the Bosch group and a 1 000 installed units milestone has been reached [63].
- Viessman Vitovalor is a PEMFC micro CHP unit which has integrated the Panasonic fuel cell module, a gas condensing boiler, a DHW cylinder and a control unit [64].
- Sunfire company was founded in 2010 and is the smallest one of the listed. However, they report over 250 installed systems based on Sunfire fuel cells [65].

Table 2.7 reveals the electric and thermal power and efficiencies of the products developed by the above companies. The same remarks made to Tables 2.5 and 2.6 apply also here. In fact, these micro-CHP have heat power capacities so low that they should be envisaged more as electrical generators than as true CHP.

Table 2.7 - Leading FC micro-CHP manufacturers and important characteristics [66].

Company	Model	P_e (kW_e)	$\dot{Q}$ (kW_t)	η_e (%)	η_{th} (%)	FC Type	Price (€)
SolidPower	Bluegen	1.5	0.85	57	33	SOFC	25.000
Panasonic	Enefarm	1		35		PEMFC	10.000
Buderus	Logapower FC10	0.7	0.6	45	40	SOFC	26.500
Buderus	GCB	1.5	0.6	60	28	SOFC	-
Senertec	Dachs 0.8	0.75	1.1	38	54	PEMFC	-
Viessman	Vitovalor PT2	0.75	1.1	37	55	PEMFC	>12.500
Sunfire	Home 750	0.75	1.25	38	40	SOFC	-

V) Organic Rankine Cycle

At present, ORC is a mature technology in the MW power range with 3 major companies (Ormat [67], Turboden[68] and Exergy[69]) covering most of the ORC applications worldwide. However, the ORC micro-CHP market is still a niche market. Besides, the downsizing of this technology poses challenges that make small-scale ORC still unattractive at the commercial level. In fact, the plant specific cost (€/kW_e) for small-scale applications is still too high to guarantee a reasonable return on investment. To date, the above three major companies have not been trying to expand their business towards the small-scale market. This constitutes an additional proof that scaling down this technology is not straight forward.

The ORC market share in the range of 10–100 kW_e is small, with an overall installed capacity worldwide of 4.95 MW_e [70]. Despite the relatively large number of companies that already have developed systems at this scale, which is outlined in Table 2.8, most of these systems are developing prototypes or are still in an initial sales stage. They are characterized by electrical power and thermal power size ranges of 1−10 kW_e and 8−44 kW_t, respectively. In fact, Rankine technology was the latest to be developed (as applied to domestic boilers) and is coming now to market, as explained below.

- In 1997, Energetix Group (UK) was founded and later become FlowEnergy Limited, a UK based company that launched in January of 2015 a natural-gas fuelled micro-CHP boiler. The system is composed of a wall-mounted boiler, an exterior storage tank and an intermediate water-steam circuit to transfer heat to the working fluid, which makes it hardly considered as retrofittable with combi-boilers. A helical-coil heat exchanger is employed to heat and vaporize water with the hot gases of the natural gas combustion, and the steam thus generated will then vaporize the working fluid in a plates type heat exchanger [7].
- Kaymacor is an Italian company that initiated its activity in 2014 developing ORC systems in the 2−24 kW_e power range, using different energy sources for diverse applications, including the domestic CHP [9]. The system uses an in-company developed scroll

expander, a positive displacement gear pump and plates-type heat exchangers for the condenser and evaporator. An interesting feature of the Kaymacor systems is the use of multiple expanders in parallel for scalable solutions, instead of an increase of the power output of the developed expander.

- Rank is a Spanish company that develops mainly three ORC modules ranging from 20 to 100 kW_e of power, for low, medium and high temperature heat sources [8]. The ORC has a regenerative configuration, a screw-type expander and brazed plates-type heat exchangers as evaporator and condenser. In 2019, the "Rank Micro" has been released, a module that generates electricity at powers up to 2.5 kW_e and heats water at rates up to 50 kW_t, but requires an external heat source.
- Viking Development Group, a Norwegian company, developed a system named Craftengine with a power size suitable to domestic-CHP applications [71]. The system possesses an electrical power output of 2−12 kW_e and thermal power outputs from 25 to 140 kW_t. This solution uses a reciprocating engine from the automotive industry, as expander, and plates heat exchangers for the evaporator and condenser. Unfortunately, an external heat source must be supplied to the system.
- Since 2009, ENOGIA has developed a range of ORC products for waste heat recovery, especially for stationary engines. The company, based in France, offers four products with electrical outputs power ranging from 10 to 100 kW_e. To date, ENOGIA has sold more than 40 ORC units around the world, a number of them being small units producing between 5 and 10 kW_e of power [10].

Table 2.8 - Leading ORC micro-CHP manufacturers and important characteristics.

Company	**Model**	P_e **(kW_e)**	$\dot{Q}$ **(kW_t)**	η_e **(%)**	η_{th} **(%)**	**Working Fluid**	**Price (€)**
FlowEnergy	Genlec [7]	1	7.4-14	-	-	Pentane	7.000
Kaymacor	Morgana [9]	2/4/8	15/30/60	10	75	R245fa	n.a.
Rank	Micro [8]	1-2.5	20-45	6	80	R1233zd	4.500/kW_e
Viking	Craftengine [71]	2-12	~25-140	-	-	-	20.000
Enogia	10-LT [10]	10	~50-145	7	92	R1233zd	45.000

From the mentioned ORC micro-CHP manufacturers, the model produced by Flowenergy is the only comparable to Hebe, our micro-CHP boiler, since the others are essentially ORC modules reported as able to be used as CHP units. They are not ready to use as replacement of domestic gas boilers as they require an external heat source to couple to the evaporator. However, even the Flowenergy unit is no longer produced because the branch of the company that produces it went bankrupt and changed the main line of business.

2.4 Business Opportunity

The world population growth leads to a straight increase of the global energy consumption. In 2015, EU's primary energy consumption accounted for about 1600 Mtoe/y, which approximately half, 800 Mtoe/y, is due to heating and cooling applications (including industrial heat), followed by transport and electricity (about 490 Mtoe/y and 310 Mtoe/y, respectively). Pezzuto et al. investigated the European space heating (SH) and domestic hot water (DHW) market in Europe and estimate that SH and DHW account for over 20% of the total EU energy utilization, almost 3900 TWh/year. At the same time, the authors report that district heating systems are growing and the replacement of the traditional boilers occurs at a slow pace [32].

A micro-CHP solution that produces hot water for both sanitary use and central heating system, able to replace the common wall-hung domestic boilers, is a major solution for a family householder with energy bill concerns. For instance, a three-bed semi-detached house, typical of the UK, the largest market in Europe for domestic boilers, has a medium thermal demand within the range of 15 000 to 24 000 kWh/year [72]. In 2019, the overall annual heating cost (including the fixed costs, gas consumption, circulating pump costs and maintenance) may range from 890€/year for a condensing boiler burning natural gas, to 2.200€/year for a whole electric solution with a significant fraction during the peak electricity period [72].

Generally, a major catalyst for micro-CHP technology widespread is the cost of electricity and a more attractive payback period can be achieved for countries with higher electricity cost. Over the past decade a clear growth in the electricity price and a less perceivable increase in the natural gas price can be observed in Figure 2.5, in Portugal and EU27.

The benefit to the user is a significant reduction in the energy bill by acquiring a micro-CHP boiler relative to present boilers, so more as his annual thermal needs are higher. In fact, as gas energy is usually much cheaper than electricity (typically a 1:3 ratio), the decrease of the electricity bill allowed by the micro-CHP more than compensates the associated increase of the gas consumption. This solution remains attractive even in a self-consumption mode where the produced electricity is locally consumed by the user, without subsidies of the authorities, such as feed-in tariffs. As shown in Figure 2.5, the household average cost of electricity and natural gas is relatively near in Portugal and in European Union. To the following analysis on the business opportunity, an average cost of 0.215€/kWh and 0.072€/kWh is assumed as input data on markets for electricity and natural gas, respectively.

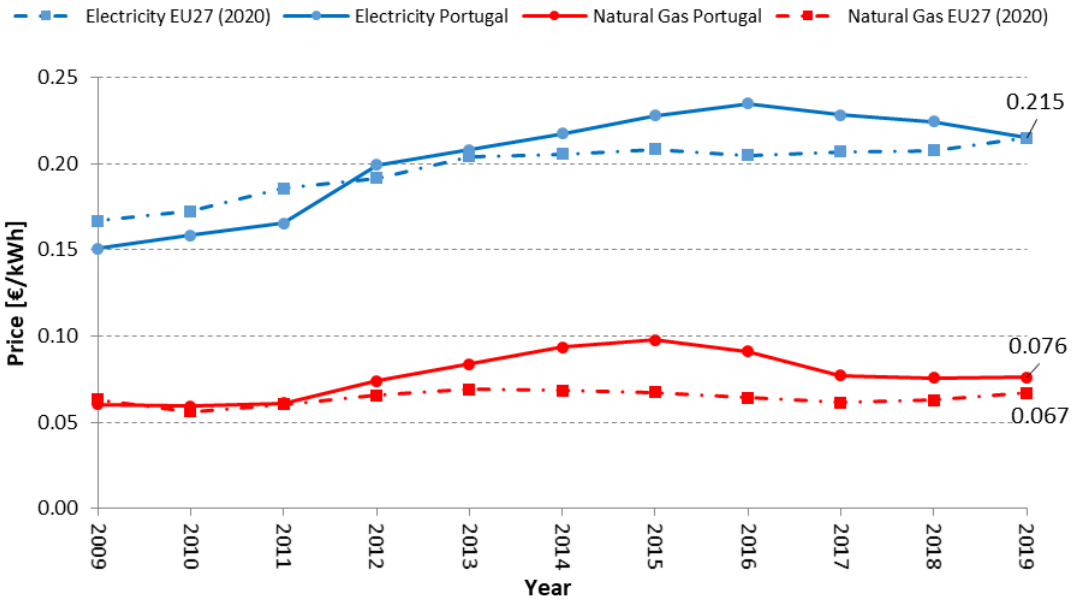

Figure 2.5 - Evolution of electricity and natural gas prices for household consumers in Portugal and EU27 (2020). Source: PORDATA [73]

The techno-economic analysis proposed in this subchapter relies on the following hypotheses:

H1 transients following on/off operations are neglected; and

H2 for any instantaneous heat request $\dot{Q}_{out}$[kW$_t$], the equipment is supposed to function in physically similar nominal conditions, namely, with the same efficiencies.

These hypotheses give some (unfair) advantage to micro-CHP boilers in a competitive analysis with simple boilers. The combustion efficiency is defined for simple or micro-CHP boilers, respectively, as:

$$\eta_C = \left(\dot{Q}_{out} \; or \; \dot{Q}_{in}\right)/\dot{Q}_C \tag{2.7}$$

with

$$\dot{Q}_C = q_{c0} \cdot \dot{m}_{ng} \tag{2.8}$$

where: $\dot{Q}_{out}$ is the heating rate of the domestic water and $\dot{Q}_{in}$ is the heat rate supplied to the power circuit of the micro-CHP (at the evaporator), $\dot{m}_{ng}$ is the mass flow rate of natural gas consumption and q_{c0} is the natural gas low heat value. For any micro-CHP, the thermal and electrical efficiencies are given, by the Equations 2.2 and 2.4, respectively. In this analysis, the electrical power $P_{e,in}$ consumed by the micro-CHP was neglected due to its low value compared to the generated power $P_{e,out}$. A general electro-mechanical efficiency of the Generator/Converter group of 0.85 was assumed, and defined by:

$$\eta_{em} = P_{e,out}/\dot{W}_{out} \approx 0.85 \tag{2.9}$$

This value is typical of simple/good joint designs of coupled turbine/generator/converter.

Table 2.9 provides the features and prices of conventional and condensing boilers, Hebe (conservative/target values), and a micro-CHP boiler best-selling competitor of each technology (with power output comparable to Hebe), used in the comparative analysis.

The combustion efficiency of a conventional boiler is few dependent on the operating conditions, which is not the case of a condensing boiler. Typical efficiency values of condensing boilers operating in optimum conditions can attain η_C=1.07 (based on the gas low heat value) but, according to Cooke et al., a more realistic season-average of η_C=0.98 should be considered [74]. The combustion efficiency of Hebe is equal to the one of condensing boilers and the electric efficiency corresponds to values of micro-scale ORC experimental tests reported in the literature [75]. Hebe's thermal efficiency is obtained indirectly from the former efficiencies. The figures for electric and thermal efficiency and Heat-to-Power ratio of all micro-CHP, when the manufacturer does not directly give them, are computed from the known data using Equations 2.1-2.6, with no significant extra assumptions.

Table 2.9 - Technical efficiencies, capacities and prices of conventional and condensing boilers, Hebe, and other competing micro-CHP boilers.

Equipment	η_c[%]	η_{th}[%]	η_e[%]	**HPR**[−]	$\dot{Q}_{out}$ [kW$_t$]	$P_{e,out}$ [kW$_e$]	**Price [€]**
Conventional Boiler	92		-		24.0	-	900
Condensing boiler					24.0	-	1.750
Hebe (conservative)	98	90	7.0	12.82	24.0	1.9	5.000
Hebe (target)		86	10	8.62	24.0	2.7	2.750
ICE Ecowill	85	50	30	1.66	2.5	1.0	14.000
SE Evita	90	72	15	4.82	5.0	1.0	10.260
ORC FlowEnergy	88	79	8.0	9.82	7.4-14	1.0	7.000
FC Vitavalor	87	50	37	1.35	1.1+19	0.75	12.500

Figure 2.6 shows the curves of payback period [years] versus user annual thermal needs [kW$_t$h/year], of substituting a conventional gas boiler for a condensing boiler, Hebe, or each one of the various micro-CHP competitors already in the market. No feed-in tariffs are taken into consideration for the exported electricity price. As seen in Figure 2.6, if a user has a yearly thermal need of 13 000 or 24 000 kWh, the lower and upper limits of the medium range in the UK, the payback period of target Hebe system is 7.4 and 4.0 years, respectively.

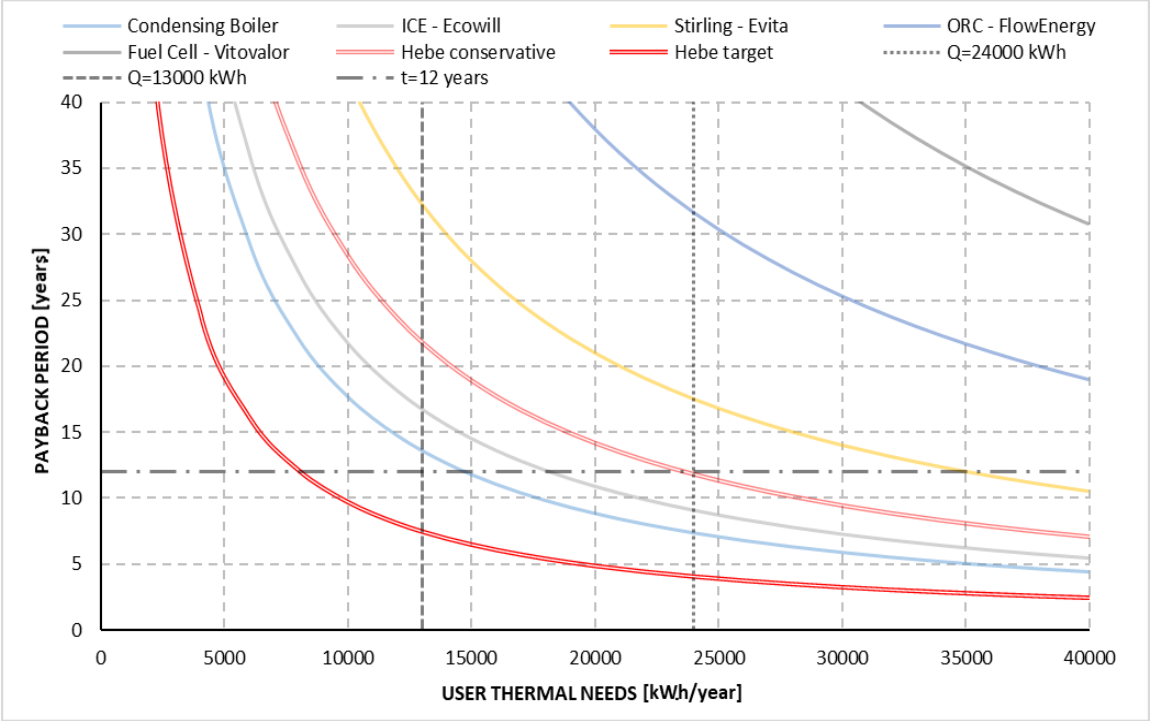

Figure 2.6 - Payback period of substituting a traditional gas boiler for a condensing boiler, Hebe or other micro-CHP competitors, as a function of the user's thermal needs.

The relatively low payback time of Hebe can be justified by the good electric and thermal efficiencies and, above all, by the very competitive price. Another form to present the advantage of Hebe (target) relative to a traditional boiler, for the user, is to say that it reduces the specific cost of thermal heat from 0,0735€/kWh to 0,0591€/kWh.

Notice that, to be able to replace domestic boilers in thermal needs, ICE Ecowill and SE Evita require both a supplementary boiler or thermal inertia tank, which further increases their payback time. The FlowEnergy boiler compensates the deficiency of thermal power in peak demands with an inertia tank already included in the base price. Analogously, the fuel cell equipment Vitovalor already has an auxiliary boiler of 19 kW_t to fulfil the user thermal demand.

Gas boilers are known to have a lifetime of 12-16 years [76]. Regarding the lifetime expectancy of Hebe, its critical component is the micro vapour turbine/expander. Some authors consider possible for a scroll expander to function 30 000 hours in continuous, without the need to substitute any of its main parts [77]. In consequence, for Hebe's lifetime to be similar to the one of a simple boiler, the turbine should function for less than 1 875-2 500 h/year or a fraction of 0.21-0.29 of the year, which is adequate for the water heating needs of most dwellings. Assuming the lowest lifetime of the system (12 years), a yearly thermal need of just 8 000 kWh is needed to pay Hebe (target) during its lifetime.

This analysis also allows realizing most systems are not economically viable since the payback period is above the system lifetime, unless the user has extremely high heating needs that are rare in the domestic sector. In fact, if the chart area is cropped by the 12 years and the maximum thermal

needs of 24 000 kWh/year, just the target Hebe, the condensing boiler, the ICE - Ecowill (which can't substitute domestic boilers) and the conservative Hebe would be seen in it, in this order of appearance. A huge difference between the target and conservative Hebe can be noted, which turns crucial to obtain a reduced price and a high electrical efficiency.

A nice thing for Hebe's sales widespread is that society is interested in supporting it (e.g., through feed-in electricity tariffs as in the UK) because it reduces the consumption of non-renewable primary energy sources. Additionally, the CO_2 emissions required to produce electricity available at home are lower for Hebe than for the network of power plants and distribution lines of the public electric grid of most countries. In that sense, the incentives allow diminishing the payback period of replacing a common boiler for Hebe and increasing its share in the residential boiler market. However, one should always keep in mind that state helps are temporary and don't assure the business sustainability in the long term, and for that reason were not accounted for in the analysis above.

Market Cost of Hebe

In the business opportunity analysis performed above, an ultimate target price for Hebe of 2.750 € was considered, 1.000€ above the price of condensing gas boilers. In order to estimate the cost of Hebe and compare it with its target price, the work of some authors that perform thermo-economic optimizations of ORCs for specific applications will be used. Quoilin et al. estimate the cost of the expander based on the cost of compressors with the same swept volume multiplied by a factor of 1.5 to take into account the lower maturity of the expander technology. It has indeed been showed in the literature that turning volumetric compressors (such as scroll compressors) into expanders is feasible with a reasonable efficiency [78][79]. The pump cost correlation proposed by Bejan is an exponential expression that depends on the nominal power as single input [80]. The condenser (a compact plates heat exchanger), piping, control system, miscellaneous hardware and labour have cost functions devised by Quoilin et al [81]. A "direct evaporator" exchanging heat from the combustion gases directly to the working fluid should be developed disregarding an intermediate oil circuit which allows increasing the overall efficiency, simplifying the system and sparing costs. For this reason, the Amicabile et al. cost correlation for a carbon steel heat exchanger was chosen instead of the plates heat exchanger' correlation applied to the condenser [82]. The working fluid cost was derived from current prices of the Portuguese market for R245fa (sold at 40-45€/kg, while its market succedaneum, R1233zd, that satisfies all environmental requirements, is sold at 20-30€/kg). This is indeed the most widely used fluid in the literature and compatible with the most common ORC construction materials [83]. Table 2.10 details the Hebe cost estimation process. Further explanations follow below.

Table 2.10 - Costs of the various parts and labour of Hebe.

Component	Input Variables		Cost function [€]	Cost [€]
	Description	Value		
Expander	Volume flow rate $\dot{V}_{exp}$	0.014 m^3/s	$1.5(225 + 170\dot{V}_{exp})$	338
Pump	Nominal Power $\dot{W}_{pump}$	0.1543 kW	$900\left(\frac{\dot{W}_{pump}}{300}\right)^{0.25}$	136
Electric Generator/Inverter	-	-		200
Evaporator	Heat transfer area A Maximum pressure P_2	2.08 m^2 15 bar	$383.5A^{0.65}(2.2 + FC(P_2))$	1.420
Condenser	Heat transfer area A	0.94 m^2	$297A$	279
Working fluid	Mass M	3 kg	$47M$	141
Piping	Pipe diameter d_{pipe} Pipe length L_{pipe}	0.024 m 10 m	$(0.89 + 21d_{pipe})L_{pipe}$	14
Control system	-			500
Miscellaneous hardware	-			300
Labour	Total main Component Costs TCC[€]	2372 €	$0.25\,TCC$	593
HEBE				**3.920**

To estimate the values of the input variables of the cost functions for Hebe, a simple calculation of the thermodynamic states of the working fluid at the main points of the ORC cycle of Hebe depicted in Figure 2.7 is made, based on the following assumptions:

- The output heat delivered to the domestic water is $\dot{Q}_{out}$ =24 kW;
- The cycle high pressure is P_2 =15 bar;
- The vapour superheating at the expander inlet is ΔT_{sup} =5 ºC;
- The liquid subcooling at the condenser exit is ΔT_{sub} =5 ºC;
- The pressure ratio at the expander is r_p =4;
- The isentropic efficiency of the expander is $\eta_{i,exp}$ =80%; and
- The isentropic efficiency of the pump is $\eta_{i,pump}$ =70%.

Recall the definitions of pressure ratio (Eq. 2.10), and isentropic efficiencies of the expander (Eq. 2.11) and pump (Eq. 2.12):

$$r_p = P_2/P_3 \tag{2.10}$$

$$\eta_{i,exp} = \frac{h_2 - h_3}{h_2 - h_{3i}} \tag{2.11}$$

$$\eta_{i,pump} = \frac{h_{1i} - h_4}{h_1 - h_4} \tag{2.12}$$

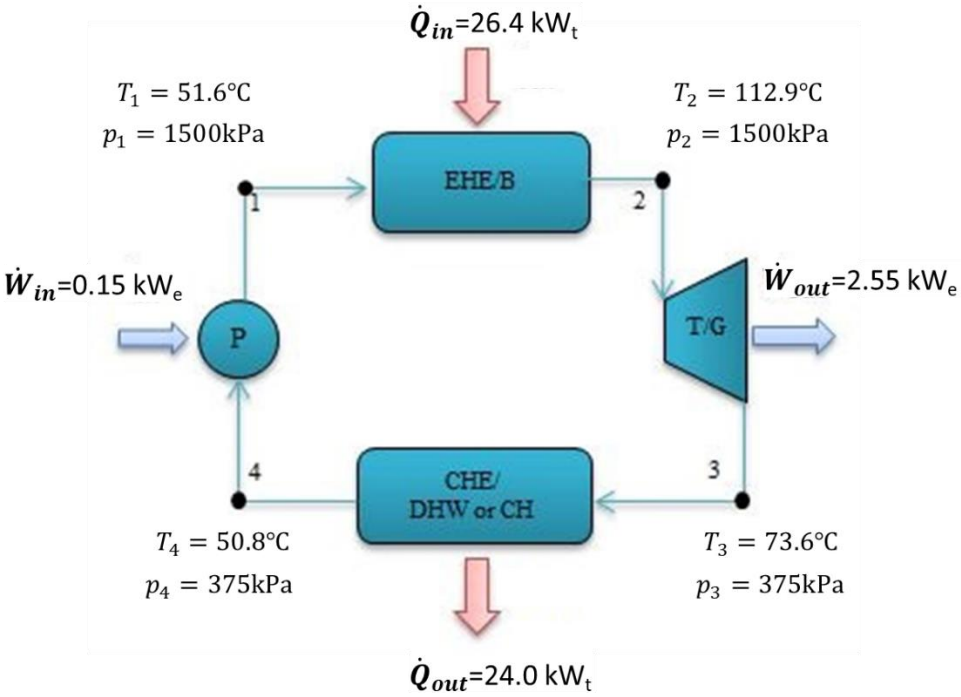

Figure 2.7 - Thermodynamic states of the fluid across Hebe (pump P, gas boiler and evaporator heat exchanger EHE/B, turbine and generator T/G, condenser heat exchanger to domestic hot waters or central heating CHE/DHW or CH) used to estimate its cost.

Starting from the top of Table 2.10, the flow rate through the expander is given by:

$$\dot{V}_{exp} = \dot{m}_f / \rho_2(p_2, T_2) \tag{2.13}$$

where the mass flow rate $\dot{m}_f$ can be roughly projected through the heat delivered by the working fluid to the water, in the condenser:

$$\dot{Q}_{out} = \dot{m}_f [h_3(p_3, T_3) - h_4(p_4, T_4)] \tag{2.14}$$

The mechanical power delivered to the fluid by the pump, which is the input of the pump cost function, is given by:

$$\dot{W}_{out} = \dot{m}_f [h_1(p_1, T_1) - h_4(p_4, T_4)] \tag{2.15}$$

The total area of the heat exchangers is obtained by means of the Logarithmic Mean Temperature Difference (LMTD) method for counter-flow heat exchangers. For the condenser, it can be written in the following way:

$$\dot{Q}_{out} = \dot{m}_f [h_3 - h_4] = \dot{m}_w \left[h_{w,out} - h_{w,in}\right] = U_{CHE} \cdot A_{CHE} \cdot LMTD_{CHE} \tag{2.16}$$

where the logarithmic mean temperature difference is given by Eq. (2.17), further assuming that the inlet and outlet user's water temperature are $T_{w,in} = 15$ °C and $T_{w,out} = 40$ °C, respectively.

$$LMTD_{CHE} = \frac{(T_3 - T_{w,out}) - (T_4 - T_{w,in})}{ln\frac{(T_3 - T_{w,out})}{(T_4 - T_{w,in})}} \tag{2.17}$$

In the same way, we can write for the heat flux balance in the evaporator heat exchanger, the Eq. (2.18). For the LMTD calculation, it has been assumed that the flue gases from the natural gas combustion cool from $T_{fg,in} = 1200$ ℃ down to $T_{fg,out} = 70$ ℃ in the evaporator.

$$\dot{Q}_{in} = \dot{m}_f[h_2 - h_1] = \dot{m}_{fg}\left[h_{fg,in} - h_{fg,out}\right] = U_{EHE} \cdot A_{EHE} \cdot LMTD_{EHE} \quad (2.18)$$

where the heat received by the fluid in the evaporator can be estimated with the energy balance of the whole cycle (neglecting the mechanical power input $\dot{W}_{in}$ at the pump):

$$\dot{Q}_{in} \approx \dot{Q}_{out} + \dot{W}_{out} \quad (2.19)$$

In Eqs. (2.16) and (2.18), to estimate the global heat transfer coefficients (U_{CHE}, U_{EHE}), typical values were assumed for the convective heat transfer coefficients on the side of the gases, working fluid and water in the heat exchangers [84]. More specifically, considering that the flue gases convection controls the heat transfer in the evaporator, a typical value of $U_{EHE} = 50\ \mathrm{W/m^2K}$ was assumed. In the condenser, both fluids exhibit high coefficients of heat transfer since the organic fluid experiences phase change and the water flow is turbulent, so it was assumed that $U_{CHE} = 1000\ \mathrm{W/m^2K}$. The cost function of the evaporator has also a parameter FC which is an increasing function of the maximum pressure P_2. Amicabile et al. define $FC = 0.1$ for a maximum pressure in the range 10-20 bar [82].

The diameter of the connecting ducts is calculated by imposing that the fluid speed does not surpass the values recommended in refrigeration applications: $V_{liq} = 1\ \mathrm{m/s}$ and $V_{gas} = 10\ \mathrm{m/s}$. As the evaporator is not a plates heat exchanger, a slight overestimation on the working fluid mass charge was applied compared to other micro-CHP ORCs in the literature [75].

Summing all the costs of Hebe, a total value of 3.924€ is achieved, relatively higher than the target price (2.750€). However, three factors can justify the difference: (1) an overestimation of several specifications was accounted for, (2) the cost functions of each component are for a single unit construction and (3) the evaporator cost, which is the largest cost term, can be substantially reduced since it will be an in-house product. The major price reduction will be obtained for sure on Factor (2), due to the economy of scale. On one hand, the negotiation and acquisition of a large number of units will decrease each mass component cost. On the other hand, the mass production of the whole system will decrease the global cost per unit. On the assumption of a 50% cut of the prototype price, the resulting raw margin of profit is around 30%. Nevertheless, the price for Hebe has yet some margin to be adjusted and an increase in the payback period is expected with the consequent market loss.

Chapter 3

ORC Modelling

This chapter provides an overview of the literature on the modelling of the Organic Rankine Cycle (ORC). In the first subchapter, a brief introduction to the challenges and present state of the technology of the micro-ORC is performed. The description of the most common simplified models and off-design models are presented in the second and third subchapters, respectively. Finally, the fourth subchapter contains the state-of-the-art of the charge-sensitive models, the most recent stage in steady-state ORC modelling.

3.1 Organic Rankine Cycle

The beginning of the Rankine Cycle technology development can be traced back to Carnot itself. Over the years, significant developments were achieved, but the first commercial exploration appeared only in 1952, on a geothermal site in Congo. However, a massive growth of this technology took place in Milano in the 60s and 70s, carried out by two university professors who led to the creation of Turboden company, afterwards [85]. Although the major developments in small-scale ORC systems appeared in the last two decades, theoretical [86],[87] and experimental [88] works have been developed since the earlies 70s, with reported thermodynamic efficiencies around 10%. Generally, volumetric vane expanders were used in the experimental tests along with high Ozone Depleting Potential (ODP) refrigerants, such as R11 or R13, now out of the market by environmental regulations [86],[89]. The first commercial applications appeared in the late 70s and 80s with medium-scale power plants developed for geothermal and solar applications.

Figure 3.1a presents the worldwide installed plants' capacity and the share referable to each one of the major manufacturers. This figure also reveals that most of these systems belong to ORMAT which, jointly with two other major companies (Turboden and Exergy), have 80% of the total units and 87.5% of the installed capacity. Moreover, these three major companies belong to the large-scale ORC segment with a power range usually higher than 1 MW_e. Figure 3.1b shows the share of the ORC systems per field of primary energy and a major portion corresponding to the geothermal ORC systems can be observed.

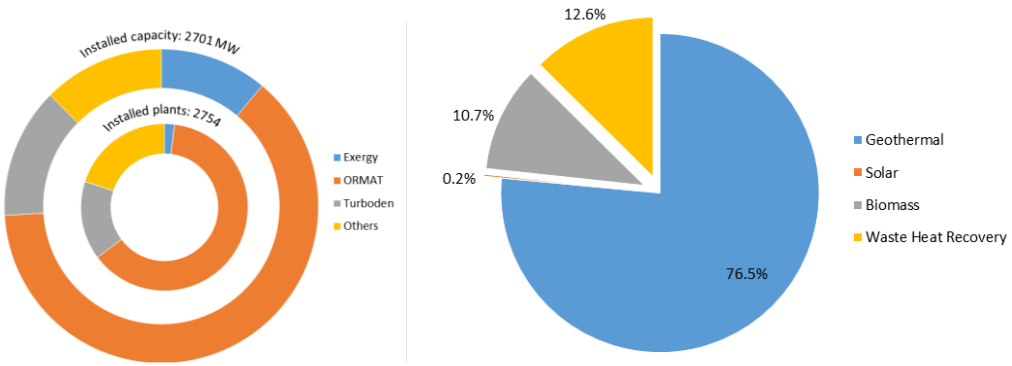

Figure 3.1 - Worldwide ORC systems by: a) installed capacity and plants; b) primary energy used (data from [70]).

The evolution of the ORC installed capacity and units were depicted by Tartiere in a world overview of the ORC market until 2017 and is illustrated in Figure 3.2a [70]. The ratio between installed capacity and number of units allows plotting the average size of the installed units up to 2017 (Figure 3.2b). A clear trend of increase can be seen in both, units and capacity, while the average unit capacity decreases. Furthermore, these data indicate that manufacturers are aware of the enormous potential of small and micro-scale applications and seeking to explore it.

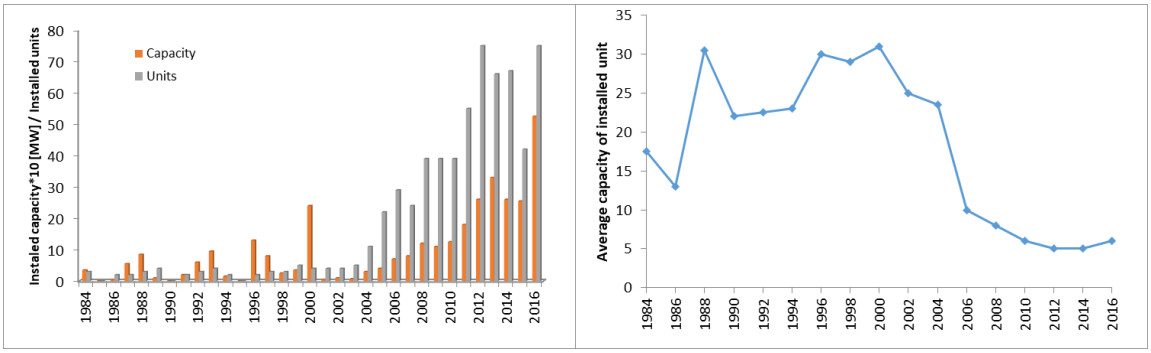

Figure 3.2 - ORC evolution in the world: a) Cumulative installed capacity and units, and b) average size of the installed units.

Several companies have developed and installed ORC systems worldwide from the large scale to small and micro-scale, most recently. For the sake of clarity, Table 3.1 summarises a non-exhaustive list of these companies, roughly ordered by decreasing power range of the systems.

Table 3.1 - Non-exhaustive list of ORC manufacturers with energy source, power range and turbine type of the respective products [90].

Company	Country	Primary Energy Source				Power Range [kW_e]	Turbine Type
		Geothermal	Biomass	WHR	Solar		
Ormat [67]	USA	x		x	x	200-70.000	Radial
Exergy [69]	Italy	x	x	x	x	100-240.000	Radial
GE clean energy[91]	USA			x		6900-16.000	Radial
Turboden [68]	Italy	x	x	x	x	200-15.000	Axial
GMK [92]	Germany	x	x	x		500-15.000	
Cryostar [93]	France	x		x	x	500-15.000	Radial
TAS [94]	USA	x		x		500-15.000	
Barber-Nichols [95]	USA	x		x		15-6.000	
Clear Power [96]	USA	x	x	x		1600-5.000	Radial
Enertime [97]	France	x	x	x	x	500-3.000	Axial
Maxxtec [98]	Germany		x			300-3.000	
Kaishan [99]	China	x	x	x	x	60-1.000	
Phoenix [100]	Australia	x	x	x	x	25-1.000	
Durr Cyplan [101]	Germany	x	x	x	x	50-1000	Axial
Opcon [102]	Sweden			x		<800	Axial
BEP-E-Rational [103]	Belgium	x	x	x		55-800	Single screw

Triogen [104]	Netherlands		x	x		95-170	Axial
Zuccato Energia [105]	Italy	x	x	x	x	30-500	Radial
ZE [106]	UK		x	x		95-130	Multi-stage Radial
Calnetix [107]	USA			x		125	Axial
Electratherm [108]	USA	x	x	x		35-110	Screw
Rank [8]	Spain	x	x	x	x	1-100	Screw
Enerbasque [109]	Spain	x	x	x	x	25-100	n.a.
Entropea Labs [110]	UK	x	x	x	x	25-100	Radial
Orcan [111]	Germany			x		20-100	Radial
Enogia [10]	France	x	x	x	x	10-100	Radial
Infinity Turbine [112]	USA	x	x	x	x	10-100	Radial
Exoes [113]	France			x		15	Piston
Kaymacor [9]	Italy	x	x	x	x	2-24	Scroll

Among all the technologies emerging for small and micro CHP applications, the Organic Rankine Cycle (ORC) is acknowledged as one of the most suitable technologies for valorising low-grade heat into electricity or mechanical power [114]. The organic Rankine cycle evolved from the Rankine cycle, where an organic fluid replaces the water used as a working fluid. Figure 3.3 shows the liquid and vapour saturation curves of water and typical organic fluids used in ORC applications in the thermodynamic *T-s* plane, and two main differences can be perceived. Firstly, the slope of the saturated vapour line is negative for water while it is slightly positive or vertical for organic fluids. In this way, for the latter fluids, the need for a substantially superheated vapour at the turbine inlet disappears as there is no risk of condensation at the end of the expansion. Secondly, the enthalpy difference is much smaller, which leads to a higher working fluid mass flow rate to obtain an equal thermal power delivery to the cold sink. Consequently, it leads to a higher pump consumption or even requires switching the pump type.

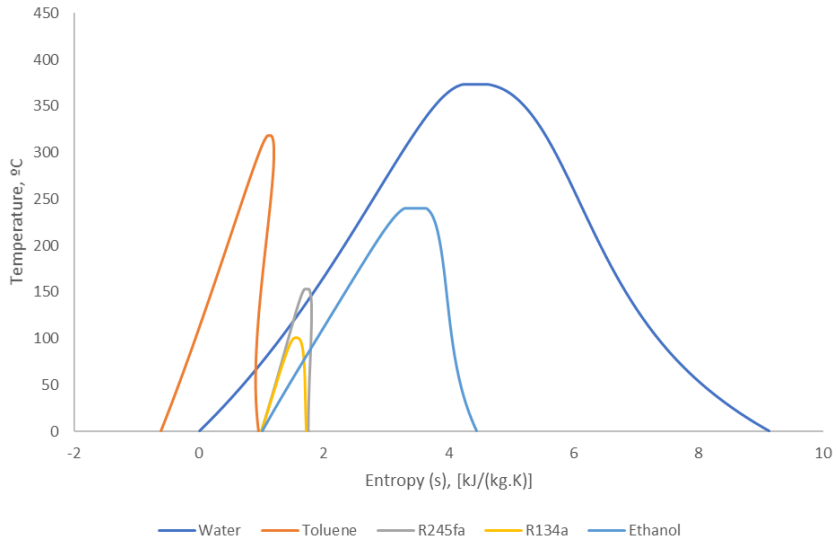

Figure 3.3 - Liquid and vapour saturation curves of water and typical organic fluids used in ORC, in the plane *T*−*s*.

Besides, organic fluids possess a lower boiling point enabling heat recovery at lower temperatures, i.e., to explore medium and low-grade heat sources. Also, due to the need of the superheating constraint in steam cycles, a maximum steam temperature usually higher than 450ºC is required which leads to higher thermal stresses and thus to higher costs. The high pressure of the steam cycle is about 60-70 bar and a very high-pressure ratio is standard, so turbines with multiples stages are commonly used while in ORC the high pressure does not exceed 30 bar and single stage turbines are usually employed. Additionally, the low pressure in steam cycle is generally lower than 100 mbar absolute which could lead to air infiltration in the cycle while organic fluids have a condensing pressure (at ambient temperature) higher or around atmospheric. Nevertheless, the steam cycle has some advantages, namely higher thermodynamic efficiency typically over 30% and, mainly, the low-cost, environmental-friendly, non-flammable and non-toxic working fluid (water) [115].

A simple Organic Rankine Cycle (ORC) consists of four main components: a pump, an evaporator, an expander (volumetric turbine) and a condenser, and also an organic working fluid. Its working principle may be briefly described as follows. The cycle starts with the pump feeding the organic fluid as a high-pressure liquid into the evaporator, where receives heat from a heat source and vaporizes (usually superheats). The pressurized vapour expands and cools while flowing through the expander producing work. The rotor shaft of the expander is coupled with the shaft of the electrical generator/converter ultimately responsible for the electricity output. The low-pressure but still relatively hot vapour at the exit of the expander enters into the condenser where cools down some more and condenses losing energy to a low temperature heat sink. The saturated/subcooled liquid fluid is then sucked by the pump, to be pressurized again, closing the cycle. A schematic representation of the basic configuration of the ORC, including the flows of the external hot and cold fluids, is shown in Figure 3.4a. Figure 3.4b indicates the thermodynamic loop transformation that the working fluid suffers in a *T-s* diagram.

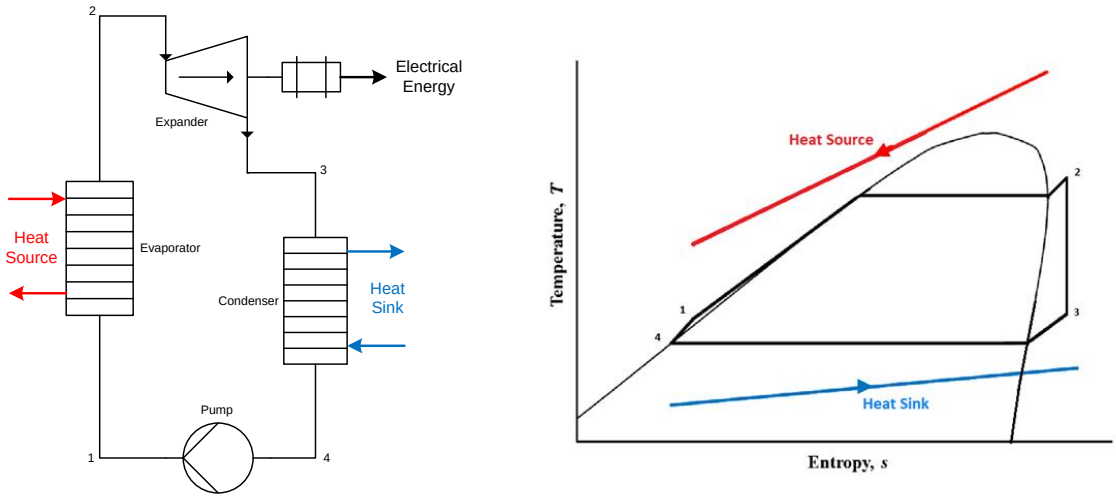

Figure 3.4 - Simple ORC system architecture a) Schematic b) *T-s* diagram

Numerous ORC architectures have been presented in the literature with variants relative to the basic one, to increase the performance of the system [116]. Several authors suggest a regenerator, as shown in Figure 3.5, to use the hot vapour after the expander to preheat the liquid before the evaporator (basic regenerative cycle) [117]. In a variant of the basic regenerative cycle, a part of the vapour flow is extracted from the mid of the turbine (so called, turbine bleeding) and mixes in a direct contact heat exchanger with the other part of the fluid flow, that was fully expanded, condensed and medium level pressurized, the resulting pre-heated saturated liquid flow suffering a second pressurization before entering the evaporator[118]. The cycle that uses a zeotropic mixture[1] of two fluids instead of a pure fluid is comparable to the simple ORC with non-isothermal phase change profiles in the evaporator and condenser, less prone to attain pinch point conditions [119]. The Organic Flash Cycle (OFC) uses a flash tank after the evaporator where the fluid is throttled, or flash evaporated, to a lower pressure liquid–vapour saturated mixture. The two phases are afterwards separated and the saturated vapour flows through the turbine while the saturated liquid goes directly to the condenser entrance after passing through a throttling valve [120]. Similar to the OFC, the Trilateral Cycle (TLC) directly feeds the expander with the flashed saturated mixture, which must be tolerant to it [121]. Finally, in the supercritical cycle, the working fluid is compressed up to a supercritical pressure and heated in the vapour zone of the *T*–*s* diagram of the fluid, effectively bypassing the two-phase liquid/vapour region [122]. However, in small-scale ORCs, a simpler plant schematic is usually preferred due to its lower specific cost [90].

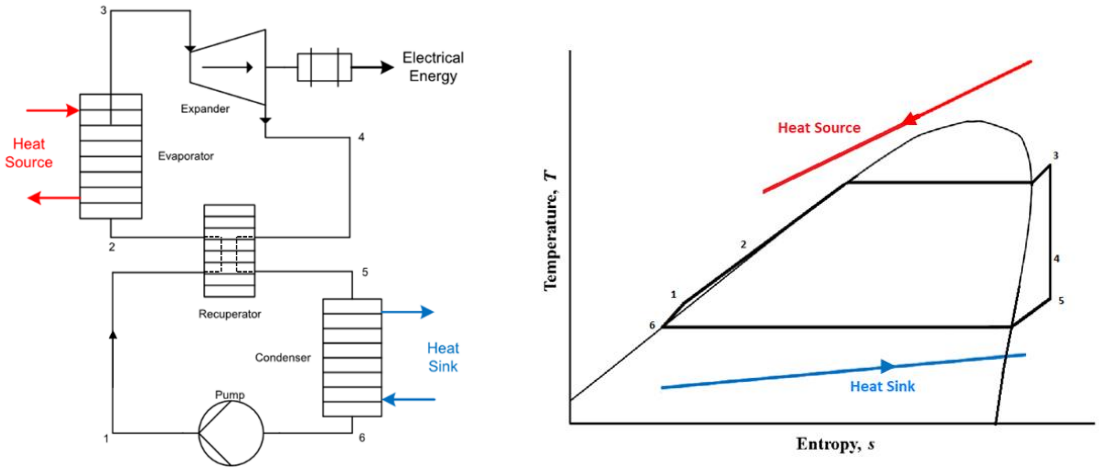

Figure 3.5 - Regenerative ORC system configuration: a) Schematic b) *T*-*s* diagram

[1] A zeotropic mixture, or non-azeotropic mixture, is a mixture of two pure fluids with different boiling points. In consequence, the mixture has a temperature phase transition glide, i.e., the phase change (condensation or boiling) occurs across a temperature range of about four to seven degrees Celsius, and not isothermally, as with pure fluids.

Over the past two decades, ORC systems have been widely proven to be an advantageous solution for power generation from multiple heat sources (including low-grade) in many different applications. Biomass and geothermal are the more conventional heat sources for electricity production. Recently, interest has increased in many innovative applications such as solar thermal power generation [123] and waste heat recovery from ICE on cars, trucks and ships [124]–[126], and from industrial processes [127]. In particular, cogeneration or CHP is also one of the most recognized applications of ORC to obtain electric and thermal energy simultaneously since it can be applied to most renewable heat sources as well as fossil fuels, increasing the overall energy conversion efficiency.

3.2 Overview and scope of the state-of-the-art

The Organic Rankine cycle theme has been increasingly studied by researchers and industry. Literature about ORC is vast due to different applications, processes and large variety of heat source and heat sink conditions. Further the operational conditions, an ORC system performance is also influenced by the working fluid, the components technology (specially the expander) and the cycle configuration. As a result of the continuous interest, the number of papers published about Organic Rankine Cycles depicted in Figure 3.6 has grown more than four times in the last decade.

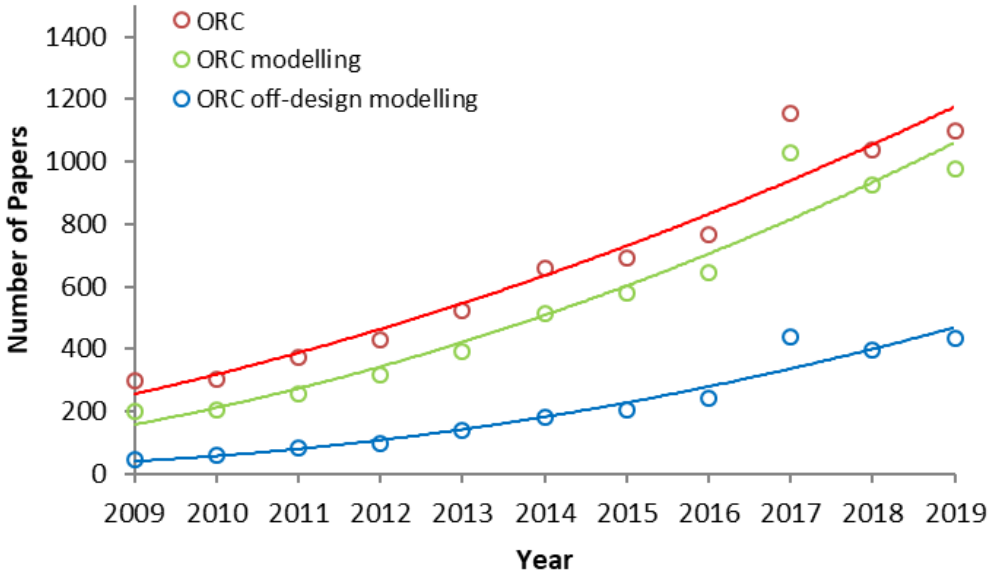

Figure 3.6 - Yearly number of publications on ORC from 2009 to 2019 (source: ScienceDirect) [128]

In particular, numerical simulations are an essential tool to analyse the performance and design of an ORC system because of the large variety of boundary conditions imposed by the heat source, heat sink, different applications and partial loads. Despite the apparent simplicity of the ORC systems, their design and modelling can be challenging, especially in off-design conditions, that can induce dangerous situations. Such situations can be prevented at the design stage with the help of models capable of simulating both nominal (typically at full load) and off-design (e.g., at partial load) steady-states of the ORC system. The simulation models can assist in working fluid screening [129] and components selection [130], in estimating the thermo-economic benefits of the system [131], in obtaining the key parameters of operation [132] and in developing control strategies [133]**.** System modelling also supports the design of experimental test-rigs [134]. In particular, the efficiency of micro-ORCs designed for low-grade heat recovery is especially sensitive to operating conditions and a careful choice of the components.

The ORC modelling often requires appropriate software tools to numerically solve the set of equations of the model, which is highly dependent on the type of model. A broad list of works can be found in the scientific literature on this regard. Bina et al. use EES optimization to perform a thermo-economic evaluation of various bottoming ORCs (i.e., ORCs using low grade heat sources) for a specific geothermal power plant and to obtain the optimum values of the operating parameters [135]. The Matlab software is used by most authors for ORC modelling. The off-design behaviour of the components and the whole ORC cycle was modelled in Matlab by Imran et al., Hu et al, Liu et al. and Chatzopoulou et al., among many others [136]–[139]. Sarah Van Erdeweghe implemented a two-step design and off-design optimization procedure for binary geothermal ORC using Python Programming Language for the thermodynamic and economic models [140]. A thermodynamic analysis and performance optimization of an ORC waste heat recovery system for marine diesel engines are performed with the help of a specific computer program written by Song et al. in FORTRAN [141]. Cao et al develop a procedure in Simulink software for off-design performance evaluation of a combined cycle with a topping gas turbine cycle and a bottoming ORC cycle [142]. Desideri et al. constructed a dynamic model of an ORC with nominal capacity 11 kW_e, based on Thermocycle Modelica library, that was validated against steady-state and transient experimental results obtained in a laboratory test-rig [143]. Rajabloo developed a thermodynamic model in Aspen Plus software environment, firstly, to design an ORC maximizing its efficiency in nominal conditions, and then, to carry out an off-design analysis of its performance [144].

In the ORC modelling software mentioned above, two main approaches can be distinguished: EES, Matlab, Phyton and Fortran are code-based high-level programming languages with a more or less wide scope of application. Simulink, Modelica, Amesim, Cycle-Tempo and Aspen are library-oriented software with user-friendly interfaces (e.g., graphical interfaces where the user can adequately connect the components and set the parameters). The main difference between the two approaches is the freedom to develop the set of equations, which is more restrained in the object-oriented libraries approach. The code-based approach further requires integration with available

and compatible fluid libraries to retrieve the thermodynamic and transport properties of the working fluids. Examples are REFPROP database, that represents the most extensive available library and also allows the introduction of user-defined mixtures, and CoolProp, an open-source library with the most used fluids.

Regarding the physical nature of the ORC models themselves, two main types can be recognized in the literature: steady-state and dynamic models, the former being the main target of this thesis. The most common steady-state models are the simplified models that are discussed in the next subchapter. The next grade steady-state models, following a scale of complexity, are the (incomplete) off-design models that are presented in subchapter 3.4. Finally, one more step ahead, at the front of the state-of-art, are the fully predictive charge-sensitive models addressed in subchapter 3.5.

3.3 Simplified thermodynamic models

As stated before, a simplified thermodynamic analysis is the most common approach for ORC systems modelling. Such models aim, under plausible simplifying hypotheses and given an appropriate set on inputs, to describe as detailed and realistically as possible the corresponding steady-state operation condition of the ORC system. The thermodynamic analysis is essentially an energy analysis based on the first law of thermodynamics. The basic equations described in Table 3.2 are applied to determine the thermodynamic steady-states of the working fluid at the main points of the cycle (these points are identified, e.g., in Figure 2.7). Afterwards, some parameters characterizing the overall performance of the system, such as, the power produced by the generator and the cycle efficiency, can be calculated. In some cases, a second law (of thermodynamics) analysis , so called exergy analysis, is also performed [145],[146]. Though theoretically appealing, because exergy quantifies the truly useful energy potentially available from a system in a given state, on the one hand, exergy analyses are often ambiguous, and, on the other hand, in practice, they add few or nothing to a rich energy analysis (namely, due to the natural constraints imposed to micro-CHP's operation). Anyway, the idea is to maximize the exergy efficiency of the system operation, identifying the components and design options that minimize the exergy losses.

Table 3.2 - Basic energy equations of ORC system's (see, e.g., Figure 2.7) simplified models

Component	Equations	
Pump & Motor	$\dot{W}_{in} = \frac{\dot{m}_f(h_{1i} - h_4)}{\eta_{i,pump}}$	(3.1)
	$P_{e,in} = \frac{\dot{W}_{in}}{\eta_{em,pump/motor}}$	(3.2)
Evaporator	$\dot{Q}_{EHE} = \dot{m}_f(h_2 - h_1)$	(3.3)
	$\dot{Q}_{EHE} = \eta_{EHE}\dot{Q}_{in}$	(3.4)
Expander & Generator	$\dot{W}_{out} = \dot{m}_f(h_2 - h_{3i})\eta_{i,exp}$ &	(3.5)
	$P_{e,out} = \eta_{em,exp/gen} \cdot \dot{W}_{out}$	(3.6)
Condenser	$\dot{Q}_{CHE} = \dot{m}_f(h_3 - h_4)$	(3.7)
	$\dot{Q}_{out} = \eta_{CHE}\dot{Q}_{CHE}$	(3.8)
Overall Cycle	$\eta_t = \frac{\dot{W}_{out} - \dot{W}_{in}}{\dot{Q}_{in}}$	(3.9)

In these models, the main components are described solely through nominal yields. The pump and the expander are commonly characterized by nominal isentropic efficiencies, assuming the compression and expansion are adiabatic (which they aren't). Regarding the evaporator and condenser losses to the ambient, they are characterized by nominal external heat exchanger efficiencies. Also, due to the incomplete character of these models, several *a priori* assumptions must be made, e.g., regarding the degrees of subcooling and/or superheating of the fluid at given points, and/or the evaporating and condensing temperatures or pressures. Machi and Astolfi report typical values of components' efficiencies that are gathered in Table 3.3, elaborated from the existent literature on the topic [147]. With respect to the components' behaviour, keeping the values of the efficiencies as constant is equivalent to assume that they behave in the same way across the whole range of operation, which is obviously not true.

Table 3.3 - Typical values assumed for the components' efficiencies

Efficiency	Value	Note
η_{pump}	0.50 – 0.70	
$\eta_{em,pump/motor}$	0.87 – 0.95	
η_{CHE}	0.98 – 0.99	brazed plates heat exchanger
η_{EHE}	0.90 – 0.98	other heat exchanger types
$\eta_{i,exp}$	0.70 – 0.85	flow turbines
	0.65 – 0.80	volumetric expanders
$\eta_{m,exp}$	0.93 – 0.97	
$\eta_{e,gen}$	0.94 – 0.98	

Regarding its applications, these models have been used to select suitable working fluids and components, particularly the expander, in a perspective of design optimization guided by thermodynamic or techno-economic indicators of the system. A summarized literature review of these topics will be presented next.

Working fluid selection

Simplified modelling appears extensively in ORC literature to perform a preliminary investigation of the effect of working fluids on the cycle performance. The working fluids physical properties, such as the critical temperature, the latent heat of vaporization, specific heat, standard boiling point, molecular weight and molecular composition, play a vital role in cycle performance [148]. In fact, from the sole knowledge of these properties it is already possible to devise an effective working fluid screening method given a set of desired working conditions. Moreover, the working fluid influences the system profitability, sizes the expander and other system components, affects the system stability and is relevant on safety and environmental grounds [115].

To commence with, a crucial feature that must be taken into consideration is the fluid environmental impact quantified by indicators, such as the Ozone Depletion Potential (ODP) and the Global Warming Potential (GWP). The cost, the safety (flammability and toxicity) and the compatibility with the materials (corrosion or proneness to induce the formation of condensates in the vapour expansion) of the various ORC components are other characteristics that affect the working fluid suitability.

In consequence, the appropriate choice of the ORC working fluid for different conditions and applications has always been studied but became a hot topic almost a decade ago, as reported in Table 3.4. Different ORC types, ranging from low temperature to high temperature heat sources (geothermal, solar, biomass and waste heat), mostly for power generation, and different cycle architectures were examined by several authors. To perform the working fluid screening, the most employed parameters in the simplified models are the hot $T_{H,in}$ and cold $T_{L,in}$ source inlet temperatures, the pinch point temperature difference in the heat exchangers ΔT_{pinch}, and the evaporation T_{evap} and condensation T_{cond} temperatures that implicitly define the corresponding pressures. Some of the authors use also as parameters the electric power output $P_{e,out}$ and the heat power output $\dot{Q}_{out}$ or the mass flow rates $\dot{m}_{H,L}$ of the hot or cold fluids which exchange heat with the working fluid. By default, the application of the ORC is power generation, when not mentioned as micro-CHP.

Table 3.4 - Non-exhaustive review of works on working fluid screening with simplified models

Author(s)	ORC Type	Parameters	Selection criteria	Working Fluid
Liu, 2004 [149]	- Low-grade WHR - Basic ORC	$T_{H,in} = 200$ °C $T_{L,in} = 30$ °C $\Delta T_{pinch} = 20$ °C	thermal efficiency η_{th} or recovery efficiency η_{rec}	(10 fluids) Toluene or R123
Tchanche, 2009 [150]	- Low temperature - Solar - Basic ORC	$T_{evap} = 75$ °C $T_{cond} = 35$ °C $P_{e,out} = 2$ kW	thermodynamic eff. η_t and environmental impact, safety	(10 fluids) R134a > R152a > R290 > R600
Mikielewikz, 2010 [151]	- Fuel combustion - Micro-CHP - Basic ORC	$T_{H,in} = 320$ °C $T_{evap} = 170$ °C $T_{cond} = 50$ °C $\dot{Q}_{out} = 20$ kW	thermodynamic eff. η_t	(20 fluids) ethanol, R123 and R141b
Liu, 2011 [152]	- Biomass - Micro-CHP - Basic ORC	$\dot{Q}_C = 20$ kW $P_{e,out} \approx 2$ kW $T_{L,in} = 10$ °C $T_{L,out} = 20,30,40$ °C	thermodynamic eff. η_t and electric efficiency η_e	(3 fluids) n-pentane
Qiu, 2012 [153]	- Medium-low temperature - Micro-CHP	(qualitative method)	environmental impact, safety, physical properties	(8 fluids) HFE7000
Wang, 2011 [154]	- ICE WHR - Regenerative ORC	$T_{H,in} = 327$ °C $T_{L,in} = 27$ °C $P_{e,out} = 10$ kW	environmental impact, safety thermodynamic eff. η_t exergy destruction $\dot{I}_t$	(8 fluids) R245fa
Shengjun, 2011 [155]	- Geothermal - Basic ORC	$T_{H,in} = 90$ °C $T_{L,in} = 20$ °C $\dot{m}_H = 1$ kg/s $\Delta T_{pinch} = 5$ °C	thermodynamic eff. η_t exergy efficiency η_{ex} recovery efficiency η_{rec} *LCOE* (see Table 3.6)	R123 R123 R218 R152
He, 2012 [156]	- Low-grade WHR - Basic ORC	$T_{H,in} = 85 - 145$ °C $T_{L,in} = 20$ °C $\dot{m}_H = 1$ kg/s $\Delta T_{pinch} = 5$ °C	exergy efficiency η_{ex}	(28 fluids) R236fa
Zhai, 2014 [157]	- Geothermal - Basic ORC	$T_{H,in} = 110 - 210$ °C $T_{L,in} = 10 - 30$ °C $\dot{m}_H = 1$ kg/s	output power $\dot{W}_{out}$	(11 fluids) R32
Long, 2014 [129]	- Low-grade WHR - Basic ORC	$T_{H,in} = 120$ °C $T_{cond} = 30$ °C $\Delta T_{pinch} = 5$ °C $\dot{m}_H = 30$ kg/s	internal exergy eff. $\eta_{ex,i}$ external exergy eff. $\eta_{ex,e}$	(10 fluids) R600a
Dong, 2014 [158]	- High-grade WHR - Regenerative ORC	$T_{H,in} = 280$ °C $T_{L,in} = 40$ °C $\Delta T_{pinch} = 35$ °C $\dot{Q}_{in} = 80$ kW	thermodynamic eff. η_t	Zeotropic 0.4/0.6 MM/MDM
Le, 2014 [159]	- WHR - Basic ORC	$T_{H,in} = 150$ °C $T_{L,in} = 20$ °C $\dot{m}_H = 50$ kg/s	exergy efficiency η_{ex} *LCOE* (see Table 3.6)	Zeotropic n-pentane/R245fa

Yu, 2015 [160]	- Low-grade WHR - Basic ORC	$T_{evap} = 70 - 170$ ℃ $T_{cond} = 40$ ℃	"predictor" heat recovered $\dot{Q}_{in}$ power output $\dot{W}_{out}$	(11 fluids) R245fa, R600
Vivian, 2015 [161]	- Low-to-medium grade WHR -Sub/Super critical ORC - Basic/ Reg. ORC	$T_{H,in} = 120 - 180$ ℃ $T_{cond} = 35$ ℃ $\Delta T_{pinch} = 10$ ℃ $\dot{m}_H = 10$ kg/s	thermodynamic eff. η_t heat recovery effectiveness ε_{hr} electrical efficiency η_e	(31 fluids) R227ea, R236fa
Zhai, 2016 [162]	- Medium-to-high grade heat source - Basic ORC	$T_{H,in} = 150 - 350$ ℃ $T_{L,in} = 10 - 60$ ℃ $\Delta T_{pinch} = 10$ ℃ $\Delta T_{sub}, \Delta T_{sup} = 5$ ℃ $\dot{m}_H = 1$ kg/s	thermodynamic eff. η_t exergy efficiency η_{ex}	(37 fluids) Depend on the temperatures $T_{H,in}, T_{L,in}, T_{crit}$
Lu, 2016 [163]	- Low temperature - Geothermal - Basic/ Reg. ORC	$T_{H,in} = 140$ ℃ $T_{L,in} = 20$ ℃ $\Delta T_{pinch} = 5$ ℃ $\dot{m}_H = 1$ kg/s $\dot{m}_L = 4 - 12$ kg/s	thermodynamic eff. η_t net power output $\dot{W}_{net}$	Zeotropic R601a/R600 R245fa/R600
Saloux, 2018 [164]	- Low temperature - Basic ORC	$T_{H,in} = 120{,}135$ ℃ $T_{L,in} = 10{,}15$ ℃ $\dot{W}_{net} = 1$ kW	environmental impact, safety thermodynamic eff. η_t	(4 fluids) R-600a
Chen, 2019 [165]	- Low temperature - Basic ORC	$T_{H,in} = 100 - 200$ ℃ $T_{evap} = 0.85 \cdot T_{crit}$ $T_{cond} = 40$ ℃	exergy efficiency η_{ex}	(18 fluids) 236ea, R245fa, R245ca,R365mfc

The thermodynamic efficiency η_t is predominantly used in the literature as the selection criteria. However, exergy efficiency η_{ex} is also commonly employed to optimize the matching between heat source and working fluid, in the spirit of exergy analyses. As shown in the last column of Table 3.4, the "optimum fluid" varies with the ORC application, desired operating conditions, and selection criteria adopted. While fluid selection studies in the scientific literature cover a broad range of working fluids, ultimately, only a few fluids are actually used in commercial ORC power plants, namely: HFC-134a, HFC-245fa, R1233zd, N-pentane, Solkatherm, OMTS and Toluene.

Thermodynamic Design Optimization

The design problematic of an ORC is not a new topic as it appears broadly in the literature. The need for more productive and efficient systems without ignoring the competitiveness through the minimization of the specific cost of power €/kW$_e$ has led to the investigation of enhanced solutions. The suitable choice of the most appropriate components and cycle configuration for specific applications or boundary conditions of operation are the major challenges in the ORC design stage. Additionally, the choice of the nominal condition represents also a hard task. Strategies such as parametric optimization and sensitivity analysis are sometimes used to solve this problem.

However, it is a hard and time-consuming process and, for that reason, an automatic optimization procedure is usually applied based on simplified models.

The optimization procedure of an ORC requires, firstly, the definition of an objective variable/function that can be the electric or the overall efficiency obtained from the thermodynamic model. The heat transfer areas of the condenser and evaporator, the built-in volume ratio and nominal flow rate of the expander, the nominal power of the pump and the volume of the circuit generally appear as optimization variables. Secondly, optimization is usually subjected to several constraints, such as the maximum temperature and pressure of the cycle or even the subcooling and superheating degrees at the outlet of the condenser and evaporator, respectively. Finally, simple nested cycle search algorithms and genetic algorithms are frequently used to solve the simpler optimization problems. However, more sophisticated optimization problems could require heavier and more complex algorithms.

Table 3.5 summarizes design optimization works present in the literature (the main state points of the cycle appear in Figure 2.7). Some authors use a so-called Turbine Size Parameter TSP, sometimes non-dimensional and others defined roughly as the diameter of the rotor, to size the turbine/expander.

Table 3.5 - Non-exhaustive review of ORC thermodynamic design optimization

Author(s)	ORC	Constraints & Algorithms	Parameters	Objective Function (max)
Facão, 2008 [166]	5 kW_e Solar CHP	Optimization in EES software $P_{evap} < 2500$ kPa	$P_{e,out} = 5$ kW $T_{cond} = 45$ °C $\Delta T_{sup} = 8$ °C	η_t(6.7%)
Peris, 2013 [167]	ICE-WHR	Safety and environmental indicators Iterative process maximization $\Delta T_{pinch} > 5$ °C $T_{H,in} > T_2 + 5$ °C $T_{H,out} > T_1 + 5$ °C	$T_{H,in} = 90$ °C $T_{cond} = 35$ °C $\Delta T_{sup} = 8$ °C $\Delta T_{sub} = 5$ °C	$\eta_e(6-7\%)$ TSP (4)
Wang, 2013 [168]	130 kW_t Solar Regenerative	Genetic Algorithm $T_2 < 70$ °C	$T_{cond} = 20$ °C $\Delta T_{sub} = 0$ °C $\Delta T_{sup} = 5$ °C $\Delta T_{pinch} = 8$ °C	η_t(7.8%) (day-averaged)
Sadeghi, 2016 [169]	10 MW_t Geothermal Power-plant	Genetic Algorithm $9°C > \Delta T_{pinch} > 4$ °C $15°C > \Delta T_{sup} > 5$ °C	$T_{H,in} = 100$ °C $\dot{m}_H = 50$ kg/s $T_{cond} = 25$ °C	$\dot{W}_{net}$ (877 kW_e) TSP (0.082 m)
Klonowicz, 2017 [170]	High-temperature biomass CHP	T_2 is the optimized variable $P_{evap} < 1500$ kPa $P_{cond} > 20$ kPa $T_{L,out} > 55$ °C	$\dot{Q}_{in} = 20$ kW $T_{evap} = 180$ °C $T_{cond} = 20$ °C $\Delta T_{pinch} = 10$ °C $\Delta T_{sub,sup} = 5$ °C	η_t (10.7%)

Thermo-economic Design Optimization

The last stage of ORC design optimization based on simplified models is the thermo-economic optimization, incorporating economic indicators in the objective and constraint conditions.

In that sense, the thermodynamic model is further extended with the cost functions of the components, materials and measure/control equipment, which depend on specific features of the components, such as, the heat transfer area of a heat exchanger, the working fluid flow rate or the consumed/generated power of the pump/expander. These cost models can be more or less sophisticated as they account for more components' features, direct costs (installation, piping, instrumentation and control) and indirect costs (engineering and transportation). The purchased equipment cost can be estimated with cost correlations for individual components and the obtained estimative has accuracy in the range of +40% to -25% [171]. In fact, the literature reveals a variety of approaches used to evaluate ORC costs [172]–[175].

Additionally, combinations of thermodynamic and economic criteria are used for the objective function and constraint conditions giving place to a variety of optimization problems. The ORC features optimized can be the working fluid, the components or even the ORC configuration. Regarding the latter aspect, for example, the introduction of an extra heat exchanger as regenerator turns the simple cycle in a regenerative ORC, which increases the overall cycle efficiency, but the increase of the system complexity and cost may not be cost-effective in the overall thermo-economic analysis. The most common indicators incorporated in the objective function are given in Table 3.6 and explained below.

Table 3.6 - Indicators applied in ORC thermo-economic optimizations

Indicator	**Formula**	
Specific Area *SA*	$SA[\mathrm{m^2/kW_e}] = \frac{A_{tot}}{\dot{W}_{net}}$	(3.10)
Specific Investment Cost *SIC*	$SIC[€/\mathrm{kW_e}] = \frac{C_{inv}}{\dot{W}_{net}}$	(3.11)
Simple Payback Period *PBP*	$PBP[\mathrm{years}] = \frac{C_{inv}}{R}$	(3.12)
Net Present Value *NPV*	$NPV[€] = \sum_{t=1}^{N} \frac{R_t}{(1+i)^t}$	(3.13)
Levelized Cost of Electricity	$NPV(LCOE[€/\mathrm{kW_e h}]) = 0$	(3.14)

In this table, the specific area *SA* (to minimize) given by Eq. (3.10), is the ratio between the total heat transfer area of the heat exchangers A_{tot} and the net power generated $\dot{W}_{net}$. The underlying assumption that the heat exchangers in the system are the most expensive parts of the ORC is valid in some cases, for instance when air cooled condensers are used [176]. However, a lot of studies refer that, usually, the expander accounts for the highest share in costs [147]. In addition, the

indicator *SA* does not have a direct economic interpretation and doesn't take into consideration the effects of economies of scale.

The specific investment cost *SIC* is probably the single most used techno-economic indicator in scientific literature and is equal to the amount of investment cost of the system per unit net power output. However, as the authors use several estimation methods, assumptions and cost functions, their results cannot be easily compared. Moreover, this criterion (minimization of the *SIC*) does not guarantee the highest revenue in the long run because the actual annual variation of the operating load is not considered.

The simple payback period *PBP* (to minimize), already used in the previous chapter, is obtained dividing the investment cost C_{inv} by the yearly cash flow R allowed by the operation of the system (in total energy savings) and indicates the number of years before the break-even point of the investment. Major drawbacks of this method are that it neither takes into account the variation of the value of the money with time nor the cash flow after the break-even point till the end of the lifetime of the system.

The net present value *NPV* (to maximize) is considered to be the most comprehensive and complete economic indicator for making investment decisions as it considers the time varying value of money and the cash flow during the total lifetime of the project [177]. *NPV* is calculated with Eq. (3.13), where R_t is the net cash flow generated by the system during year t after investment (at $t = 1$), and i is the average discount rate of money during the system lifetime $N[\text{years}]$. The discount rate i can be compared with the interest rate of an investment on the financial market. If $NPV > 0$, the investment has an added value while if $NPV < 0$, it results in a financial loss.

Finally, the levelized cost of electricity *LCOE* (to minimize) is an indicator specifically developed to compare the profitability of electrical power plants, that can be interpreted as the minimum price at which the plant should sell the electricity to avoid financial losses, or, in other terms, for the break-even of the economic project (plant investment and operation) to coincide with its lifetime [178]. Therefore, the *LCOE* is simply the price of electricity for which *NPV*=0, taking into consideration in the computation of the net cash flow R_t, all the costs to maintain the plant in operation (fuel, operational and maintenance costs). However, for the *LCOE* to be applied to a CHP system, it would be necessary, firstly, to put an economic value on the useful thermal energy generated together with the electricity. In this case, supposing that the electricity generated is self-consumed, the *LCOE* should be interpreted as the minimum price at which the client (CHP owner) should pay the electricity in order to have neither benefits nor losses at the end of the system life.

Finally, an illustrative review of thermo-economic works on the optimization of the design of micro-ORCs (unfortunately, purely electrical generators with one CHP exception) is given in Table 3.7 (see the main points of the ORC cycle in Figure 2.7).

Table 3.7 - Non-exhaustive review of ORC thermo-economic optimization works

Author(s)	ORC	Operational or Components Parameters	Algorithms & Constraints	Optimization Indicator(s) (max)
Schuster, 2009 [122]	35 kW_e WHR from biogas plants	$T_{H,in} = 490$ °C $r_v = 3$	-	*SIC* (3 755 €/kW_e)
Quoilin, 2011 [81]	2.5-5 kW_e WHR	$T_{H,in} = 180$ °C $T_{L,in} = 15$ °C $\Delta T_{sub,sup} = 5$ °C $r_v = 3.4$	Simplex algorithm T_{evap} is the optimized variable	*SIC* (2.136 €/kW_e)
Shengjun, 2011 [155]	5-10 kW_e Geothermal	$T_{H,in} = 90$ °C $T_{L,in} = 20$ °C $\Delta T_{pinch} = 5$ °C $\dot{m}_H = 1\ kg/s$	Matlab iterative algorithm of optimization T_{evap} and T_{cond} are the optimized variables $x_{exp,out} > 0.97$	*SA* (1.64 m^2/kW_e) *LCOE* (0,053 €/kW_eh)
Tempesti, 2013 [179]	50 kW_e Geothermal and Solar CHP	$T_{H,in} = T_2 + 10$ °C $T_{cond} = 45$ °C $P_{e,out} = 50\ kW$ $\Delta T_{pinch} = 5$ °C	EES iterative algorithm of optimization $T_2 < 147$ °C	*SIC* (~7.000 €/kW_e)
Algieri, 2014 [172]	~1 kW_e Biomass	$T_{cond} = 100$ °C $T_{evap} = 250$ °C $\Delta T_{sup} = 10$ °C $\Delta T_{pinch} = 10$ °C	Parametric optimization $260 < T_2 < 400$ °C	*PBP* (5 years) *SIC* (5.000 €/kW_e)
Amicabile, 2015 [82]	6-9 kW_e WHR of diesel engines	$T_{H,in} = 470$ °C $T_{L,in} = 25$ °C $\dot{m}_H = 0.188\ kg/s$ $\Delta T_{pinch} = 8$ °C	Safety and environmental indicators ΔT_{sup} and p_{evap} are the optimized variables	*PBP* (3.5-5 years)
Barse, 2016 [180]	250 kW_e Generic ORC	$T_{H,in} = 100$ °C $T_{cond} = 20$ °C $\Delta T_{sub} = 6$ °C $\Delta T_{pinch} = 6$ °C	Thermal eff. maximization with Aspen HYSYS $\dot{m}_f$ and p_{evap} are the optimized variables	*LCOE* (0,05 \$/kW_eh)
Galindo, 2016 [181]	~2.5 kW_e WHR	$\dot{Q}_C = 30kW$ $T_{H,in} = 678$ °C $\dot{m}_H = 0.048kg/s$ $\Delta T_{sup,sub} = 30$ °C $T_{L,in} = 50$ °C $\dot{m}_L = 0.275kg/s$	Genetic algorithm $T_{H,out}$, p_{evap} and p_{cond} are the optimized variables	*SA* (0.48 m^2/kW_e) *SIC* (2.515 €/kW_e)
Feng, 2018 [182]	Generic ORC	$T_{H,in} = 150$ °C $T_{cond} = 300$ °C $\Delta T_{sup} = 7$ °C $\Delta T_{sub} = 0$ °C $\Delta T_{pinch} = 5$ °C	Genetic Algorithm (NSGA-II) $T_2 + 5 < T_{H,in}$ $T_1 + 5 < T_{H,out}$ $T_3 + 5 < T_{L,out}$ $T_4 + 5 < T_{L,in}$	*LCOE* (0,11 \$/kW_eh)

Thesis Contribution

In Chapter 4, a novel simplified thermodynamic model and an also original optimization problem/algorithm are applied to design Hebe (or, indeed, any ORC micro-CHP), including the selection of the working fluid [183].

3.4 Off-design models

The ORC is receiving increasingly attention due to its features, such as, reliability and flexibility under various operating conditions [5]. Geothermal and biomass ORC applications are known to operate in a relatively stationary mode where the heat source and the heat sink conditions are practically constant or change very slowly with time. Solar, waste heat recovery and combined heat and power applications, on the other hand, have boundary conditions that often vary significantly in time, both from the supply energy and the load demand sides, which forces the ORC system to adapt its functioning point for performance or safety reasons. Consequently, an ORC system often operates more or less away from the point for which it was designed (nominal design point), in also referred as off-design or part-load conditions. This results ordinarily in a system efficiency degradation that must be taken into account. Off-design models can assist in the design of more efficient systems, in the optimal control of the system and in the assessment of the effective profitability of a given system in real conditions of operation.

Generally, an ORC system model uses physical fundamental and empirical or semi-empirical laws, the latter, typically, to describe the behaviour of some components. A common approach in the off-design modelling is to develop single component sub models and interconnect them to construct the global ORC system model. The model inputs are: components' characteristics and parameters (e.g., pump and expander displacements or heat exchangers geometry and heat transfer areas), operational or control variables, and boundary conditions (hot source and cold sink variables).

Among the fairly extensive off-design modelling work conducted on ORCs, different applications, power capacities and component types have been investigated and various models were developed. A non-exhaustive review of these works, mostly of micro-ORC, is displayed next, in Table 3.8. A common feature of all these models is their incomplete character in the sense that they need to impose *a priori* one or several non-evident and non-basic assumptions on the ORC functioning point of interest, the most common of which is the fluid subcooling ΔT_{sub} at the condenser outlet, typically, ranging from 0 to 10 ºC [184]. Another feature of these models is that they incorporate a steady-state control strategy which optimizes the off-design functioning of the system in some sense. Some features mentioned in Table 3.8 are explained in the following subsections. As usual,

$T_{H,in}$ and $T_{L,in}$ designate the temperatures of the heat source fluid (at the evaporator inlet) and of the heat sink fluid (at the inlet of the condenser), respectively.

Table 3.8 - Non-exhaustive review of ORC off-design models

Author(s)	ORC	Features	Assumptions
Quoilin, 2011 [185]	•2 kW_e WHR/Solar •Fluid: R123 •Scroll Expander •Diaphragm pump •Compact plates heat exchangers	• The pump imposes the fluid mass flow rate • The expander, running at constant speed, imposes its inlet pressure • Moving-boundary model for the heat exchangers • Maximization of the cycle efficiency with expander and pump rotational speeds	$\Delta T_{sub} = 5$ °C
Manente, 2013 [186]	•6 MW_e Geothermal •Fluids: isobutene, R134a •Shell-tube heat exchangers	• Hybrid dynamic/steady-state model • $T_{H,in} = \ 130 - 180$ °C; $T_{L,in} = \ 0 - 30$ °C • Control variables: pump speed, turbine nozzle vanes and air mass flow rate of the air-cooled condenser • Maximization of the electrical power output	$\Delta T_{sub} = 2$ °C
Wang, 2014 [187]	•250 kW_e Solar •Fluid: R245fa •Multi-stage turbine •Compact plates heat exchangers	• $T_{L,in} = 5 - 30$°C, $\dot{m}_{H,oil} = 11 - 20 kg/s$ • Sliding high pressure control. Turbine inlet valves fully opened to eliminate the throttling loss • Turbine backpressure kept constant with the cold sink (water) mass flow rate to maintain a constant temperature difference between the fluid and water in the condenser • Maximization of net power output and exergy efficiency	$\Delta T_{sub} = 0$ °C
Ibarra, 2014 [188]	•5 kW_e •Fluids: R245fa, SES36 •Scroll expander	• Partially off-design: expander, pump and regenerator heat exchanger • Part-load study that investigates the influence of $T_{in,exp}$, p_{cond}, p_{evap} and N_{exp} on the ORC performance • Control variables: required heat power input and expander speed • Maximization of the cycle efficiency for the demanded power output	$\Delta T_{sub} = 0$ °C
Hu, 2015 [189]	•67 kW_e Geothermal •Fluid: R245fa •Radial turbine •Compact plates heat exchangers	• Off-design performance analysis • Sliding high pressure and geothermal mass flow rate controlled to balance the nominal turbine speed and backpressure • The water mass flow rate of the cold sink is controlled to ensure saturated liquid at condenser outlet • Maximization of the cycle efficiency and net power.	$\Delta T_{sub} = 0$ °C N_{exp}=$N_{exp,nom}$

Song, 2016 [190]	•534 kW_e WHR •Fluid: R123 •Radial turbine	• Parametric analysis for design point and off-design analysis for different heat and cold sources • $T_{H,in} = 165 - 200$ °C; $T_{L,in} = 12,20,28$ °C • Maximization of net power output, thermodynamic and thermal efficiencies	$\Delta T_{sub} = 0$ °C
Chatzopolou, 2018	•11 kW_e ICE-WHR-CHP •Fluids: R1233zd/R245fa •Piston expander •Double pipe heat exchangers	• Maximization of the power output at full load for component sizing • Part-load simulation of the ICE (60-100%) with temperature and mass flow rate variation of the flue gases • Expander efficiency maximization at part load by adjusting the evaporating pressure	$\Delta T_{sub} = 0$ °C

The main components of an ORC system can be divided into two types: the heat exchangers (evaporator, condenser, regenerator) and the fluid mechanical devices (pump, expander), which sub modelling within the off-design models is reviewed below.

Condenser and Evaporator Heat Exchangers

The literature reveals two main approaches employed to model the heat exchangers (condenser and evaporator), from the side of the working fluid: the Finite Volume Models (FVM) and the Moving Boundary Models (MBM) [191]. The finite volume models discretize the heat exchanger into small contiguous cells or control volumes and solve the energy and mass balance equations in each cell consecutively, together with the fluid state equations. The moving boundary models solve the same equations in just three contiguous 1D integral cells with moving boundaries. In the left and right cells, the working fluid is in single phase (either liquid or vapour) and in the middle cell is in two-phase (saturated liquid and vapour phases), as depicted in Figure 3.7. High accuracy can be obtained in FVM but at a corresponding computation time expense. Indeed, the low computation cost of the MBM make them suited for control purposes due to the high number of simulations required.

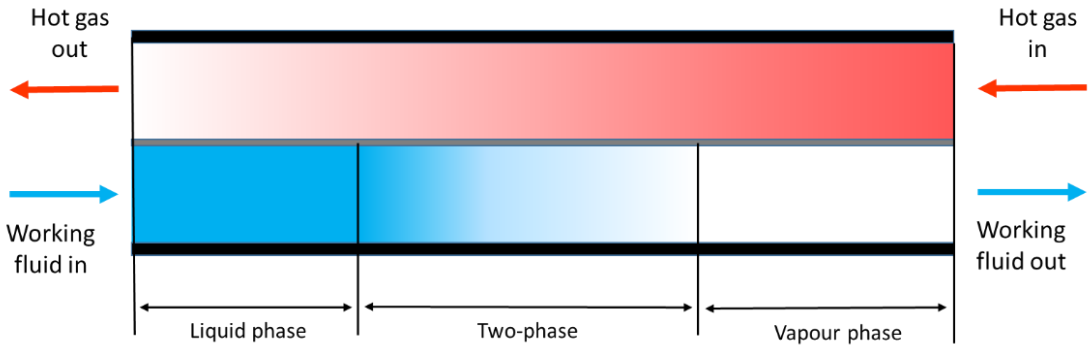

Figure 3.7 - Illustrative moving boundary model of an evaporator from the side of the working fluid

The proper length estimation of the three cells in the evaporator and condenser is particularly imperative for the outlet temperature calculation precision of MBM. Most turbines can be severally damaged if condensation occurs on their rotor blades. For this reason, a superheat degree superior to a prudent minimum must be achieved at the outlet of the evaporator. Besides, if the total condensation does not occur in the condenser, vapour bubbles enter into the pump leading to cavitation phenomena. Moreover, in different off-design part-load working conditions of the ORC, the three zones often shift, enlarge and contract over time causing possible harmful conditions.

The characterization of the three zones has been extensively studied along the time for various working fluids. The literature survey reveals several available empirical heat transfer correlations for single phase and two-phase zones that differ for boiling and condensing flows, and also for different heat exchanger types (e.g., compact plates, cross flow with finned tubes, shell-and-tube), as shown in Table 3.9. This table follows a review performed by Liu et al. and Ziviani et al.[192][193], but that should by no means be considered as exhaustive.

Table 3.9 - Basic heat transfer correlations for ORC systems' off-design modelling

Zone	Authors	Heat exchanger type/ Working Fluid	Correlations
Single-phase (vapour or liquid)	Wanniarachchi et al. [194]	Compact plates Water	$Nu = \left(j_{lam}^3 + j_{turb}^3\right)^{\frac{1}{3}} Pr^{\frac{1}{3}}$ $j_{lam} = 3.65(\pi/2-\theta)^{-0.455} Re^{-0.339c_2}$ $j_{turb} = \frac{12.6}{(\pi/2-\theta)^{1.142}} Re^{(0.646+0.00111(\pi/2-\theta))}$
	Thonon et al. [195]	Compact plates R410a/R134a	$Nu = C \cdot Re^m \cdot Pr^{1/3}$ $\begin{cases} \theta = 15°: C = 0.1000, m = 0.687 \\ \theta = 30°: C = 0.2267, m = 0.631 \\ \theta = 45°: C = 0.2998, m = 0.645 \\ \theta = 60°: C = 0.2946, m = 0.700 \end{cases}$ $50 < Re < 15000$
	Maslov and Kovalenko [196]	Compact plates	$Nu = 0.78 \cdot Re^{0.5} \cdot Pr^{1/3}$ $50 < Re < 20000;\ \beta \approx 30°$
	Gnielinski [197]	Fin-coil	$Nu = \frac{\frac{f}{8}(Re-1000)Pr}{1+12.7\left(\frac{f}{8}\right)^{0.5}\left(Pr^{\frac{2}{3}}-1\right)}\left[1+\left(\frac{d}{l}\right)^{\frac{2}{3}}\right]$ $f = (1.82\ logRe - 1.64)^{-2}$ $2000 < Re < 10^6$
Two-phase Condensation	Han et al. [198]	Compact plates R410a/R22	$Nu = Ge_1 Re^{Ge_2} Bo^{0.3} Pr^{1/3}$ $Ge_1 = 11.22\left(\frac{P_{co}}{D_h}\right)^{-2.83}\left(\frac{\pi}{2}-\beta\right)^{-4.5}$ $Ge_2 = 0.35\left(\frac{P_{co}}{D_h}\right)^{0.23}\left(\frac{\pi}{2}-\beta\right)^{1.48}$ $2500 < Re < 9000$
	Longo et al. [199]	Compact plates HFC134a/410a/236fa	$Nu = 0.943\Phi\frac{L}{k}\left[\frac{k_l^3 \rho_l^2 g \Delta h_{lat}}{\mu_l \Delta \mathrm{TL}}\right]^{0.25};\ Re \leq 1600$

		HC600a/290a/1270 HFO1234yf/1234ze	$Nu = 1.875\Phi Re^{0.445}Pr^{1/3}$; $Re > 1600$
	Yan et al. [200]	Compact plates R134a	$Nu = 4.118 \cdot Re^{0.4}Pr^{1/3}$; $\beta \approx 30°$
	Shah et al. [201]	Shell-tube R134a	$Nu = 0.023Re_l^{0.8}Pr_l^{0.4}\left[\frac{5}{9} + 2.2542\left(\frac{P_{cr}}{P}\right)^{0.38}\right]$ $2100 < Re < 42000$
Two-phase Boiling	Han et al [198]	Compact plates R410a	$Nu = Ge_1 Re^{Ge_2} Bo^{0.3} Pr^{0.4}$ $Ge_1 = 2.81\left(\frac{P_{co}}{D_h}\right)^{-0.041}\left(\frac{\pi}{2} - \beta\right)^{-2.83}$ $Ge_2 = 0.746\left(\frac{P_{co}}{D_h}\right)^{-0.082}\left(\frac{\pi}{2} - \beta\right)^{0.61}$ $2500 < Re < 9000$
	Amalfi et al. [202]	Compact plates R410a/R134a	$Nu = 982\left(\frac{\theta}{\theta_{max}}\right)^{1.101} We^{0.315} Bo^{0.32}\left(\frac{\rho_l}{\rho_v}\right)^{-0,224}$

Most of the ORC systems use compact plates heat exchangers, sketched in Figure 3.8, for the evaporator and condenser, since liquid fluids are commonly used to convey the heat of the hot source and cold sink. In fact, an intermediate thermal oil circuit interposed between the boiler and the ORC evaporator is commonly used as heat source and the domestic water plays the role of cooling medium. In the modelling scheme of the moving boundary method each zone is characterized by a global heat transfer coefficient U_i and a surface area A_i across which heat is transferred at rate $\dot{Q}_i$.

The shell-tube and fin-coil heat exchangers types are less common, being generally employed, respectively, for the evaporator in waste heat recovery applications from hot gases and for air-cooled condensers. In most cases, the working fluid flows inside the tubes.

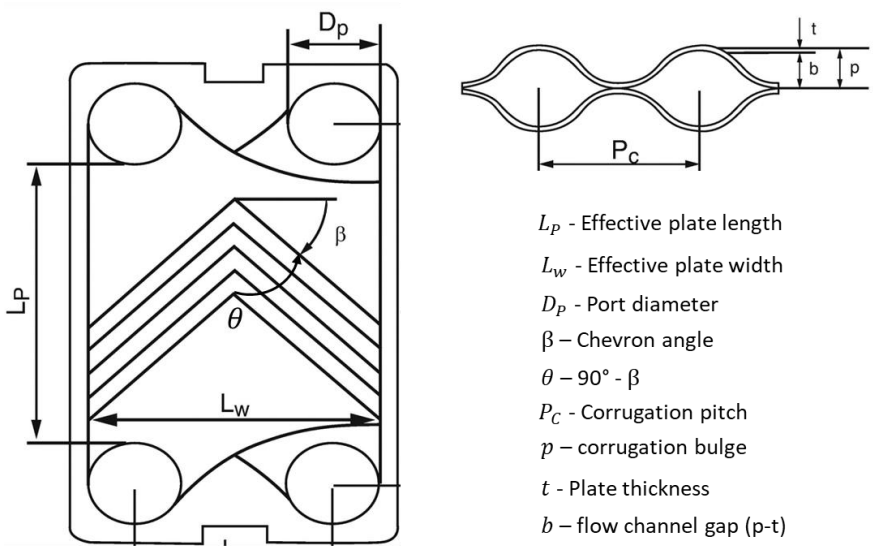

Figure 3.8 - Schematics of a compact plates-type heat exchanger [203].

Turbine/Expander

The efficiency of the expander heavily affects the overall system efficiency, especially in the small and micro-scale ranges, turning it the key component of the ORC system. In fact, among the fairly extensive modelling work conducted on ORCs, a significant portion is dedicated to the appropriate selection of the expander. However, for micro and small-scale ORCs, the choice of the "ideal" expander type and specifications is still an unresolved problem [204].

The turbines for ORC systems can be turbo-machines (simple open flow turbines) or volumetric turbines more commonly designated as expanders. Table 3.1 already identifies the different turbines used by the ORC manufacturers in the market-ready systems and some conclusions can be drawn from it. Firstly, axial and radial flow turbines are the most common for the large-scale systems. These turbomachines are rather efficient in the high-power range but they are not suitable for systems below 50 kW_e mainly due to the high cost, high rotational speed requiring special bearings, and the decrease of the efficiency with the downsizing [205]. Secondly, volumetric machines appear in the low range systems. Scroll, screw, piston and vane expanders, represented in Figure 3.9, are the most common types of expanders. In opposition to the turbines, their performance decreases with the increase of power while the cost increases as a consequence of the exponentially increase of the size in high power ranges [90]. Finally, a common feature among the reported manufacturers is the in-house development of their own turbines. The reasons are the specificity and the high cost of this component, usually the most expensive of the entire system. On the other hand, researchers, to diminish its cost, regularly restructure mass made volumetric compressors of the refrigeration industry to work in reverse mode as expanders.

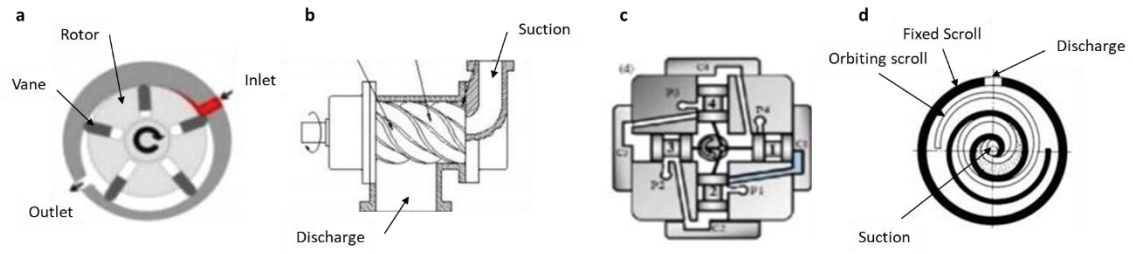

Figure 3.9 - The four main types of expanders; a) vane, b) single and double screw, c) piston and d) scroll (adapted from Alshammari et al. [206])

Scroll and single screw expanders are the most studied in the literature, whether in theoretical or practical works, as they possess a simpler construction. Qiu et al. carry out a market research on expanders with potential for domestic applications (1–10 kW_e) and highlighted the lack of commercially available expanders for ORC-based micro-CHP systems [204]. The analysis also showed that scroll expanders and vane-type expanders remain reasonable choices for micro-ORC systems. Park et al. review the experimental works regarding ORC's and report that scroll expanders are commonly used in small-scale ORCs with power output between 0.5 to 10 kW_e, screw expanders are suitable for mid-scale power output in the range 10-50 kW_e and turbo-machines above that range [75]. In general terms, expanders are used recurrently for small-scale

ORC systems because of the low flow rate, high-pressure ratio, low rotational speed, and tolerance to two-phase flows. Maximum isentropic efficiency of this turbine of about 70% is reported in several research works although experimental works experience difficulties in achieving this performance [75].

In alternative to fully empiric characteristic curves, the semi-empiric modelling approaches for expanders will be now highlighted [193]. The main inspiration is the semi-empirical modelling approach originally developed for volumetric compressors. Specifically for scroll expanders, Lemort et al. improve the model proposed by Winandy et al. [207] and Kane [208], by taking into account the internal (i.e., between the fluid and the stator and rotor surfaces) and external (i.e., to the ambient) heat transfers, under- and over-expansion of the fluid for pressure ratios above or below the built-in nominal value, and identifying the empirical parameters through a genetic optimization algorithm [209]. The thermodynamic state evolution of the working fluid through the expander is emulated by the following sequence of transformations which are sketched in Figure 3.10:

1. Adiabatic supply pressure drop emulated by an isentropic flow through a nozzle, (su→su,1);
2. Isobaric supply cooling to a fictitious isothermal envelope surface (su,1→su,2);
3. Isentropic expansion of the internal leakage flow from the supply to the discharge chambers, not performing work on the rotor (su,2→leak);
4. Isentropic expansion in closed system of the useful fluid flow (i.e., the one that transfers mechanical power to the rotor) from the supply to the discharge chambers, according with the built-in volume ratio of the expander (su,2→ad);
5. Adiabatic expansion/compression at constant volume of the useful fluid in the discharge chamber, when it opens, to equalize the pressures inside and outside (in the discharge duct), if the transformation of Step 4 leads to an under/over expansion of the fluid (ad→ex,2);
6. Adiabatic mixing of the useful and internal leakage flows in the opened discharge chamber (ex,2 & leak→ex,1); and, finally,
7. Isobaric exhaust heat transfer between the fluid and the fictitious isothermal envelope (ex,1→ex).

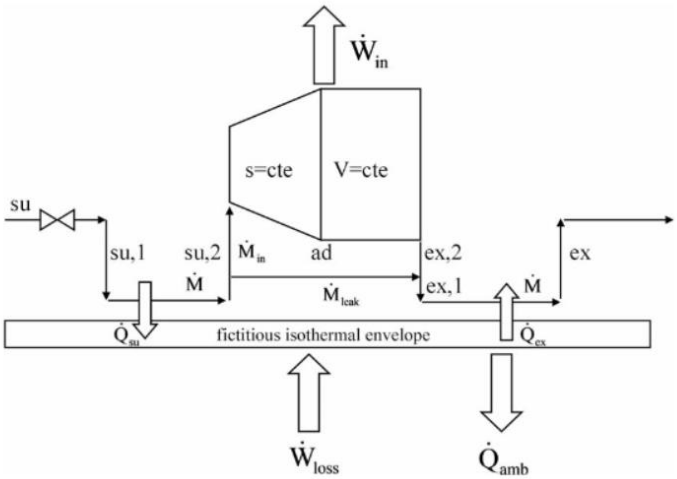

Figure 3.10 - Scheme of the expander model developed by Lemort et al. [209].

The set of transformations 1-7 of the fluid must finally be closed with the heat balance of the fictitious thermal envelope, taking into account the supply and exhaust heat exchanges with the fluid (transformations 2 and 7), the heat generated by the mechanical losses of the rotor and the heat loss to the ambient.

The scroll expander performance is globally characterized by the volumetric efficiency (Eq. 3.15), here written as a proper efficiency (i.e., lower than 1) and the isentropic efficiency (Eq.3.16):

$$\eta_v = \frac{V_{su} N \rho_{su}}{60 \cdot \dot{m}} \tag{3.15}$$

$$\eta_i = \frac{\dot{W}_{shaft}}{\dot{m}\left(h_{su} - h_{ex,i}\right)} \tag{3.16}$$

where: V_{su} is the volume of the supply chamber (when it closes), $N[\mathrm{rpm}]$ is the speed of rotation of the rotor, ρ_{su} and h_{su} are the supply fluid density and specific enthalpy, $\dot{m}$ is the mass flow rate through the expander, $\dot{W}_{shaft}$ is the power the fluid delivers to the shaft before mechanical losses, and $h_{ex,i}$ is the specific enthalpy of the fluid after an ideal isentropic expansion from the supply to the exit pressures.

Quoilin et al. validated this semi-empirical model with experimental data for a specific scroll expander, after fitting its empirical coefficients [209]. In fact, this approach has been widely used by the scientific community for semi-empirical modelling of scroll expanders [78], [210], [211]. The model has also been demonstrated to be applicable to different types of volumetric expanders, such as, screw and piston expander types [212], [213].

The literature also presents detailed models for turbines. Though turbines are rarely used in micro and small-scale ORCs, against the mainstream, Weiss and Zinn investigated the choice of volumetric expanders over small turbines and opine that the advantages of turbines outweigh their disadvantages [214]. Alshammari et al. discussed applications of turbomachines for waste heat

recovery and they favoured the performance of radial machines instead of axial for the mentioned scale [206]. Kang [215], Rahbar et al. [216] and Fiaschi et al. [217] proposed models for the design and performance evaluation of radial turboexpanders for ORC applications. The axial flow turbines, although they appear less in the literature, were studied by Lio et al. [218] and Talluri and Lombardi [219] to find optimum turbine geometry for a given range of operating conditions.

3.5 Charge-sensitive models – Case studies

The off-design models discussed in the previous subchapter describe with great detail the behaviour of an ORC system in a variety of functioning conditions, but they are not fully predictive. Analysing the reported works, it is possible to verify that, in all cases, a physically non-truly input variable (e.g., the fluid subcooling at the outlet of the condenser) is imposed *a priori*. The consequence is a mislead of the real ORC behaviour and performance prediction. In particular, assuming a constant preset subcooling makes the simulations blind to important phenomena susceptible to occur in off-design conditions, like the cavitation of the pump if the system is under-charged or the inability to reach a proper degree of superheating at the entrance of the expander if the system is overcharged [220]. In fact, all thermodynamic properties of the fluid throughout an ORC are determined by the boundary conditions: the hot source conditions, the cold sink conditions, the operation controls (e.g., expander and pump rotational speeds), the physical and geometric properties of the components and the working fluid mass existent in the circuit. The model should not only apply the mechanical and thermal energy balances but also the working fluid mass conservation equation in order to make the simulations free of assumptions [221]. Concretely, the total mass of the working fluid in the whole circuit (components and ducts), at any time instant, must remain constant and equal to what was initially charged (thence the qualifying "charge sensitive" given to these models) in the ORC system:

$$M_0 = \sum_{i}^{n_{components}} M_i + \sum_{j}^{nn_{ducts}} M_j \tag{3.17}$$

Models that account for the working fluid mass charge in the system are well-known for refrigeration systems [222][223], but in ORC units are very rare despite the working fluid charge plays a very important role in the system's off-design performance and has a non-negligible cost, especially for large-scale systems.

The determination of the mass of single-phase working fluid present in ducts and some components (pump, expander) is easily obtained by calculating the (average) fluid density from the pressure

and temperature and multiplying it by the volume of each element. However, the mass estimation inside the heat exchangers (evaporator, condenser) relies on the proper knowledge of the space occupied by each phase zone as well as on the estimation of the working fluid density throughout the zone. In the case of single-phase zones, the latter calculation is straightforward, but in the case of two-phase zones, the density depends not only on the pressure and temperature but also on the quality and flow regime through the void fraction (see below). This is one of the main research topics regarding charge-sensitive modelling. In particular, two papers investigate in-depth the selection of appropriate heat transfer correlations for heat exchangers, from the point of view of the working fluid mass calculation. A 3 kW_e system composed of a fin-tube evaporator and a shell-and-tube condenser is investigated by Pan et al. [224]. Dickes et al. also tested several correlations for mass estimation in plate and fan coil heat exchangers and compared them with the steady-state experimental values of a 2 kW_e unit [184].

The aforementioned void fraction variable α is commonly used to compute the density of two-phase flowing mixtures, further to the fluid temperature, pressure and quality [192]. It characterizes the flow pattern of the liquid and vapour phases, being defined as the ratio between the vapour and total flows cross-sectional areas. It is related with the two-phase fluid quality *x* through:

$$\alpha = \frac{A_{vap}}{A_t} = \frac{1}{1 + \frac{1-x}{x} \cdot \left(\frac{\rho_{vap}}{\rho_{liq}}\right) \cdot S} \tag{3.18}$$

where *S* is the slip (velocity) ratio between the vapour and liquid phases. A common approach to obtain the mass of fluid in the two-phase region is to assume a uniform heat flux of condensation/evaporation and thereby a linear evolution of the fluid quality along the length. However, this is not accurate because the actual variation of the quality along the heat exchanger is not linear. Such as the heat transfer correlations, the void fraction has been studied in the past years and several authors propose correlations for it. It is the case of Lockhart-Martinelli [225], Zivi [226], Premoli et al. [227] or Hughmark [228].

Following, the three works found in the literature on charge-sensitive modelling applied to ORC systems are presented.

Ziviani et al.

The first published paper on ORC modelling accounting for the fluid charge was proposed by Ziviani et al. in 2016 [229]. The developed model could either use a specified subcooling (common off-design approach) or the initial charge of working fluid (novel approach). The plates heat exchangers of the ORC (evaporator, condenser and regenerator) are modelled with a general steady-state, counter-flow, moving boundary approach. The Shah's correlation is used for the heat transfer coefficient for evaporating flow, while the Longo's correlation is used for condensing flow. No information regarding the single-phase correlation is provided in the paper. The working fluid mass estimation in each zone was carried out through Zivi's correlation [226]. The pump sub model is

based on the characteristic curves of volumetric efficiency and isentropic efficiency. The semi-empirical model applied to describe the expander is the one developed by Lemort et al., already mentioned in the previous subchapter. A simplified method to simulate the liquid receiver (component placed after the condenser to avoid that saturated vapour enters into the pump) and the oil separator (after the expander) is presented and the pressure drop in the ducts is also considered. Two regenerative ORC systems were used to validate the individual components sub models and the overall cycle model. The first one has a 5 kW_e scroll expander, diaphragm pump, R134a as working fluid and an oil flooding loop, while the second one has a 11 kW_e single-screw expander, centrifugal pump and R245fa as working fluid. The authors conclude that when the fluid charge is specified as input, the overall cycle efficiency is estimated with a mean relative error of 11% versus 16% for the subcooling-based model. Additionally, the charge-sensitive model predicts the subcooling of the fluid at the outlet of the condenser with an absolute error of less than 1.5 °C.

Liu et al.

The most relevant paper presented by Liu et al. in 2017 describes a working fluid charge-sensitive model for a small-scale ORC using the refrigerant R123 as working fluid, with the aim of estimating theoretically the optimum value of the working fluid charge for the system under rated conditions [230]. A fin-tube heat exchanger has been used as evaporator while the condenser is a shell and tube type heat exchanger. The system comprehends also a volumetric pump and a volumetric expander of the scroll type. The heat source is a hot air flow at a controlled temperature between 373-473 K and with an average mass flow rate of 0.427 kg/s, while the heat sink is water at 293 K. The sub models for the evaporator and condenser are steady-state MBM with detailed heat transfer correlations to determine the boundaries between the liquid, two-phase and vapour zones, together with the Logarithmic Mean Temperature Difference (LMTD) method. Finally, in the calculation of the working fluid charge, the amount of fluid in the expander, pump and connecting ducts is neglected. The complete model is implemented in Matlab using the pack of subroutines Refprop to compute the fluid properties. The authors firstly determined the optimum theoretical value of working fluid charge at rated conditions (33.6 kg), using the Lockhard-Martinelli method [225]. Afterwards, they ran the model at part-load (off-design) conditions, varying the expander output power in the range 1500−3000 W, and the working fluid charge in 1 kg steps. The authors conclude that the working fluid charge plays a very important role in the system's off-design performance. For instance, for lower working fluid charge mass, the system required higher degree of superheat of the vapour at the expander inlet and higher evaporator heat transfer capacity to ensure the same expander output power.

Therefore, Liu et al. decided to focus their research on a more correct prediction of the variation of the fluid properties along the two-phase zone of the heat exchangers, testing different void fraction models and heat transfer correlations. They also investigated the impact of the working fluid charge on the lengths of the different phase zones in the heat exchangers [224]. Not surprisingly, the

authors conclude that the working fluid mass was mostly concentrated in the liquid and two-phase zone of both heat exchangers, but more interestingly, they observed that the impact of various heat transfer correlations on the fluid mass calculations was insignificant in the evaporator but significant in the condenser, where the Shah correlation was found to be the best. Also, the corresponding impact of various void fraction models was found to be negligible in the evaporator but relatively larger in the condenser, where the Premoli correlation gave the best results.
A new paper was recently released by the authors on the working fluid charge subject [231]. They experimentally investigate the effect of three different working fluid charges in a 3 kW_e ORC prototype under off-design conditions. The results indicated that the stable and efficient operation of the system depends, not only on the characteristic curve of torque of the expander, but also on the working fluid charge. Overcharging leads to an increase of the average pressure across the expander, while undercharging has only a slight influence on this regard. However, the authors advise for special care to extreme part-load conditions in undercharging, regarding pump cavitation problems due to insufficient subcooling of the fluid at the outlet of the condenser.

Dickes et al.

Dickes et al. (2018) developed a charge-sensitive model for ORC power systems [184]. The Sun2power test-rig was used for model validation with 40 steady-state points gathered in the experimental campaign. It is a 2kW_e regenerative ORC system that uses R245fa as working fluid and is composed of a controlled-speed scroll expander, a diaphragm pump, a liquid receiver, two brazed plates heat exchangers for the evaporator and regenerator, and an air-cooled fin coil for the condenser. The authors pay particular attention to the heat exchangers modelling, both in properly identifying the convective heat transfer coefficients and in the investigation of the void fraction distribution in the two-phase zones. Among all the tested correlations, the single-phase correlation of Martin, the condensing correlation of Longo et al. [199], the boiling correlation of Amalfi et al. [202] for the convective heat transfer coefficients, and the void fraction model proposed by Hughmark [228] were considered the best to describe the heat exchangers behaviour. The authors conclude that a proper estimation of the mass enclosed in the heat exchangers is more important than the improvement of the heat transfer coefficients prediction.

Thesis Contribution

In Chapter 5, a general and rich modular modelling architecture was built, that enables the easy construction of fully predictive models of the charge-sensitive type, to simulate the quasi-steady behaviour of micro-CHP ORC [232]. This modelling work is believed to foster the state-of-the-art in some aspects, especially if it is taken into consideration the delay between its development and publication (and the pressure for cost-benefit effective options) induced by the engineering project of Hebe in the frame of Project HEBE (2012-2015), and the subsequent projects in which the author got involved.

Chapter 4

ORC design and construction

This chapter contains the paper "Design strategy for component and working fluid selection in a domestic micro-CHP ORC boiler" published in Applied Thermal Engineering. This work proposes an original design strategy for an innovative residential micro-CHP ORC (Hebe) that satisfies the hot waters and central heating domestic needs while generating some electricity. Firstly, the pre-specifications/assumptions of the basic design are stated followed by the presentation of a simplified thermodynamic steady-state model of the micro-CHP and an optimization problem in order to the control and design variables. Afterwards, taking advantage of the former tools, the selection of the working fluid, the main components of the system, and the instrumentation of its test bench is presented. Finally, preliminary experimental tests are carried out to assess the global ORC system performance, determine the influence of the basic control variables on the system behaviour and validate whole the design procedure.

Applied Thermal Engineering 169 (2020) 114945

Contents lists available at ScienceDirect

Applied Thermal Engineering

journal homepage: www.elsevier.com/locate/apthermeng

Design strategy for component and working fluid selection in a domestic micro-CHP ORC boiler

Márcio Santos*, Jorge André, Eduardo Costa, Ricardo Mendes, José Ribeiro

ADAI-LAETA, Department of Mechanical Engineering, University of Coimbra, Pólo II, 3030 Coimbra, Portugal

HIGHLIGHTS

- A design strategy for a novel micro-CHP combi-boiler home application is offered.
- The design strategy is demonstrated to be simple, truly useful and effective.
- A steady-state ORC model and a new optimization algorithm were developed.
- Test-rig selection based on realistic criteria and experimentally validated.
- At 30% load the ORC thermodynamic efficiency is still 6%, 1% below the prediction.

ARTICLE INFO

Keywords:
Micro-CHP
ORC
Design strategy
Optimization
Experimental validation

ABSTRACT

This paper presents an early design strategy for a micro Combined Heat and Power (micro-CHP with heat transfer rate less than 30 kW_t and electrical power up to 2 kW_e) based on organic Rankine cycle (ORC). The strategy consists of 3 steps: i) establish a set of pre-specifications; ii) conceive a thermodynamic steady-state model; and iii) formulate the optimization problem and develop a numerical algorithm to solve it. Through the described strategy, the selected working fluid for the domestic hot waters emulation test-rig was R245fa. The main components selected included a pre-specified scroll expander, a flexible rotary vane pump, an in-house direct evaporator coupled to the gas burner and a brazed plate heat exchanger as condenser. For last, a test-bench was built and the acquired measurement and control devices specified. The preliminary experimental results allowed to obtain a preliminary validation of the design procedure and revealed that the ORC components are not working far from the assumed nominal efficiencies. Also, the basic control variables are directly related to the model control variables and a reasonable agreement is obtained between the experimental and predicted overall thermodynamic efficiency.

1. Introduction

Nowadays, the energy dependence of our society leads to an increase of the power demands and consequently a decrease of the fossil fuel reservoirs. Moreover, the air pollutants emissions, climate change and global warming call for sustainable energy resources and more efficient methods of utilizing current technologies [1]. In this context, the organic Rankine cycle (ORC) is acknowledged as one of the most efficient and flexible solution for power production from thermal resources [2]. The general ORC technology has been extensively studied over the past two decades [3] and commonly uses heat sources such as geothermal [4], solar [5], biomass [6] or waste heat (WHR) [7] for power production. Nevertheless, a particular use of ORC is known as Combined Heat and Power (CHP) which allows the use of the cold sink for heating purposes and, simultaneously, the production of electric energy improving the overall system efficiency [8].

Although CHP systems are not a new topic, focusing on the micro range of power size (below 10 kW_e), the ORC-CHP technology is not mature and there are only few examples in the market [9]. The literature on ORC-based micro-CHP systems essentially concentrates in theoretical thermodynamic models in order to select an appropriate working fluid [10–13], thermo-economic assessment of the case study [14–17] and experimental performance evaluation [18–22]. However only a few of these performed analyses and optimizations take into account the design parameters and physical constraints, which makes them truly useful [23].

One step further but somewhat aside, some scientific studies have been published on the optimization of the design and working fluid

* Corresponding author.
E-mail address: marcio.santos@dem.uc.pt (M. Santos).

https://doi.org/10.1016/j.applthermaleng.2020.114945
Received 31 December 2018; Received in revised form 16 December 2019; Accepted 12 January 2020
Available online 20 January 2020
1359-4311/ © 2020 Elsevier Ltd. All rights reserved.

Nomenclature

Variables

A	Area [m^2]
c	Cost [€]
c_p	Specific heat [J/(kg.K)]
D	Diameter [m]
g	Gravity acceleration [m/s^2]
h	Specific enthalpy [kJ/kg]
m	Mass [kg]
M	Molar mass [kg/kmol]
$\dot{m}$	Mass flow rate [kg/s]
N	Rotational Speed [rpm]
p	Pressure [kPa, abs.]
P	Power [W]
$\dot{Q}$	Heat transfer rate [W]
r_p	Pressure ratio in the expander [–]
r_v	Volumetric ratio of the expander [–]
s	Specific entropy [J/(kg.K)]
S	Savings [€/h]
T	Temperature [°C]
v	Specific volume [m^3/kg]
V	Velocity [m/s]
$\dot{V}$	Volume flow rate [m^3/s]
$\dot{W}$	Mechanical power [W]
x	Working fluid quality [–]

Greek symbols

α	Expander displacement [m^3]
Δ	Difference [–]
η	Efficiency [–]
ρ	Density [kg/m^3]
μ	Dynamic viscosity [Pa·s]
ε	Effectiveness [–]
Ω	Flow pump specific velocity [–]

Acronyms

B	Boiler
BPHE	Brazed Plate Heat Exchanger
CH	Central Heating
CHE	Condenser Heat Exchanger
CHP	Combined Heat and Power
DHW	Domestic Hot Waters
EHE	Evaporator Heat Exchanger
FS	Full Scale
G	Generator
GWP	Global Warming Potential
HPR	Heat-to-Power Ratio
ICE	Internal Combustion Engine
LMTD	Logarithmic Mean
LMTD	Temperature Difference
M	Motor
MV	Measured Value
NPSH	Net Positive Suction Head
ODP	Ozone Depletion Potential
ORC	Organic Rankine Cycle
P	Pump
T	Turbine
Tr	Transmission (mechanic, magnetic)
WHR	Waste Heat Recovery

Subscripts

a	available
b	boiler
c	combustion
cr	critical
e	electrical
em	electro-mechanic
f	working fluid
g	gas
i	isentropic
in	inlet
m	mechanic
mag	magnetic
max	maximum
n	nominal
out	outlet
pinch	pinch-point
r	required
rf	radial flow
sat	saturated/saturation
t	thermodynamic
th	thermo-hydrodynamic
vap	vapor
w	water

selection of ORC systems majorly for power production and from medium-to-large scale [24,25]. The design of an ORC system is challenging due to the very large number of working fluid chemistries as well as structural and operating ORC parameters that need to be considered [26]. Amicabile et al. [27] perform a design optimization of the ORC for a 90 kW_t waste heat recovery from heavy-duty diesel engines (ICE). Wang et al. [28] carried out a dynamic simulation of a 130 kW_t solar driven regenerative ORC based on flat plate solar collectors using different organic working fluids just for electrical generation, as the heat is wasted to a low temperature sink. Tempesti et al. [29], propose an ORC CHP system designed to satisfy the central heating needs of a 30–40 flats residential building and produce 50 kW_e, powered jointly by geothermal water and by solar collectors. Lecompte et al. [30] optimize the design of a CHP system that satisfies the central heating needs of a large building and deliver the wasted heat to an ORC that produces electricity (< 300 kW_e) using ambient air as cold sink. Sadeghi et al. [31] optimize the nominal conditions of operation of an ORC with simple energy and exergy models for a 10 MW_t power plant using geothermal water at 90–120 °C as heat source, for three different configurations and various zeotropic working fluids. In these studies, generally, a simple thermodynamic model is used [28,31], the working fluid is universally optimized and the heat exchanger areas are commonly optimized [27,29,30]. The thermodynamic efficiency [28,31] and total investment cost [27,30] are usually the objective variables in the optimization.

The difference between this paper and the ones found in the literature are:

- the design of a micro-CHP, a much smaller scale and different application that mainly focuses on the customer demands (cold sink) instead of the heat source. At this scale and/or application there are only some theoretical works on working fluid selection or cycle configurations and thermo-economic assessment.
- The fact that the majority of these results cannot be directly applicable to a real ORC unit installation, because no limitations and constraints are imposed, which could lead to the need for

components with unrealistic characteristics and an erroneous prediction of the actual behavior of the system.

What pre-specifications can be done? What kind of model should be used? What constraints and objective should be adopted in the optimization, taking into consideration the specific application? The aim of this paper is to answer these questions and overpass in a rational manner its circular character. On the one hand, the selection is guided by any optimization of the system, respecting the basic design specifications. On the other hand, to perform the optimization, some modelling of the system must be done, but the information on its components and fluid is still lacking.

To the best of our knowledge, this paper is the first to describe a complete design strategy for a micro-CHP experimental test rig and present a preliminary validation of the design procedure.

The purpose of this work is to propose a design strategy for an innovative residential micro-CHP that satisfies the hot waters and central heating domestic needs from the very initial problem formulation to the construction and assessment of the experimental test-rig. Firstly, the pre-specifications/ assumptions of the basic design of the micro-CHP are stated followed by a thermodynamic steady-state model of the micro-CHP and an optimization problem in order to the control variables (Section 2). Afterwards, the selection of the working fluid, the main components of the system, and of the instrumentation of its test bench is presented (Section 3). Preliminary experimental tests are carried out to assess the global ORC system performance, determine the influence of the basic control variables on the system behavior and validate the design procedure (Section 4). Finally, conclusions are presented (Section 5).

2. Modeling methodology

2.1. System: Basic design, demands and pre-specifications

The micro-CHP in design uses an organic Rankine cycle to convert heat ($\dot{Q}_{in}$) delivered by a hot source simultaneously into heat delivered to a cold sink ($\dot{Q}_{out}$) and mechanical power ($\dot{W}_{out}$) ultimately converted into electrical power ($P_{e,out}$). A working fluid with a suitable organic composition flows through the closed circuit (Fig. 1a) following a thermodynamic loop (Fig. 1b).

The basic water heating demand conditions of the client are the ones of a domestic boiler without backup thermal cylinder, which are expressed in terms of inlet ($T_{w,in}$) and outlet ($T_{w,out}$) water temperature and either mass flow rate ($\dot{m}_w$ for the Domestic Hot Waters) or heating rate ($\dot{Q}_w$ for Central Heating):

- **DHW** - $T_{w,in}$ = 10–20 °C; $T_{w,out}$ = 40–50 °C; $\dot{m}_w$ = 0–0.15 kg/s;
- **CH** - $T_{w,in}$ = 30–50 °C; $T_{w,out}$ = 60–90 °C; $\dot{Q}_w$ = 6–12 kW_t

These conditions are represented graphically in the 3D space of client variables $T_{w,in}$[°C]-$T_{w,out}$[°C]– $\dot{Q}_w$ [kWt] in Fig. 2. Notice that:

$$\dot{Q}_w = \dot{m}_w c_{p_w} \bullet (T_{w,out} - T_{w,in}) \quad (1)$$

Given the low mass fluid rate $\dot{m}_f$ and high pressure ratios $r_p = p_2/p_3$ of operation expected for the turbine, together with the large variation of the client needs, a volumetric type turbine (also called expander) was initially chosen instead of a flow type turbine. In fact, the expander can be cheaper and easier to operate because it rotates at much lower speed, tolerates condensation and has a much wider window of tolerably efficient off-design operation conditions, in despite of a lower nominal efficiency [32–34]. Specifically, taking into consideration the few market options for micro expanders (P_e~1 kWe), a scroll expander with volumetric ratio $r_v = 3.5$ and maximum allowable temperature and pressure of 175 °C and 15 bar, respectively, was chosen.

Irrespective of the future selections of the working fluid and ORC components, the nominal efficiencies are assumed plausible [35]:

- Pump isentropic efficiency - $\eta_{i,P}$ = 0.98
- Pump/motor electro-mechanic efficiency - $\eta_{em,P/M}$ = 0.60
- Turbine isentropic efficiency - $\eta_{i,T}$ = 0.70
- Turbine/Generator electro-mechanic efficiency - $\eta_{em,T/G}$ = 0.90

Finally, the following variables are selected for optimization of the design of the micro-CHP: (i) the mass flow rate $\dot{m}_f$; (ii) the degree of vapor superheat ΔT_2; (iii) the mean pressure level p_0 in the cycle (*virtual* variable); and, in some instances that are explained in Section 2.2, (iv) the circuit high pressure p_1.

The mathematical statute of independent inputs of a simple model of the micro-CHP (Section 2.2) attributed to the former four variables is now physically justified from the high point of view of a complete physical model of the micro-CHP [36]. The first two variables ($\dot{m}_f$, ΔT_2) can be *really* and easily controlled independently of the micro-CHP working fluid and components, namely, $\dot{m}_f$, with a rotational speed controller of the pump P, and ΔT_2, by controlling the gas flow rate $\dot{V}_g$ feeding the gas burner of the boiler B. The third variable p_0 is determined by the initial fluid charge or mass m_{f0} in the circuit, which is also possible but harder to control in operation of the micro-CHP. In the absence of such a control, for a fully designed micro-CHP, once m_{f0} is arbitrated, p_0 becomes an output of the model. Finally, the fourth variable p_1 is truly impossible to control in the present design of the micro-CHP, in the sense that, once the working fluid and components are selected, the variable becomes an output of the model.

Just in passing, notice that, for a given micro-CHP (working fluid and components, namely, expander) and after the choice of variables

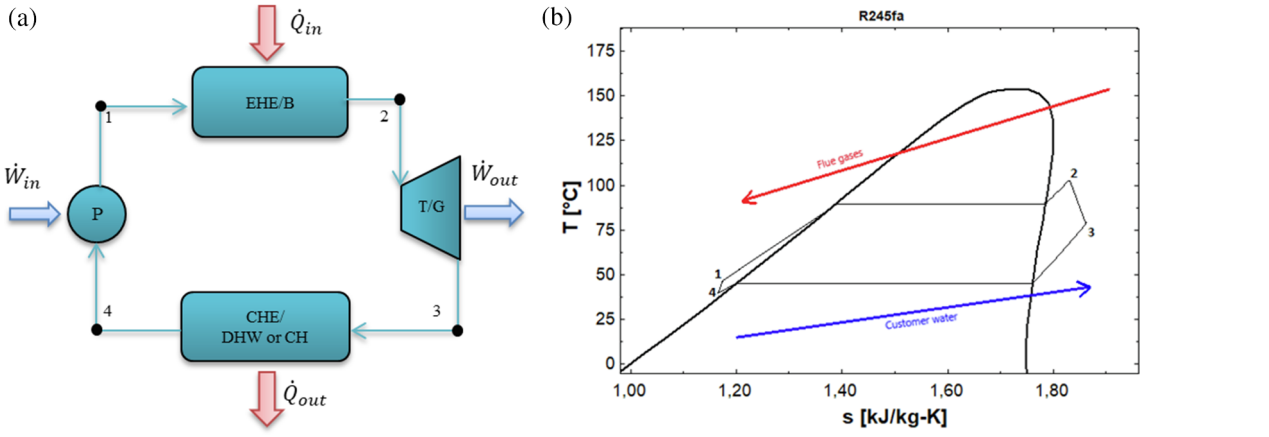

Fig. 1. (a) Schematic of an Organic Rankine Cycle. (b) Thermodynamic transformations suffered by the working fluid represented in diagram $T - s$.

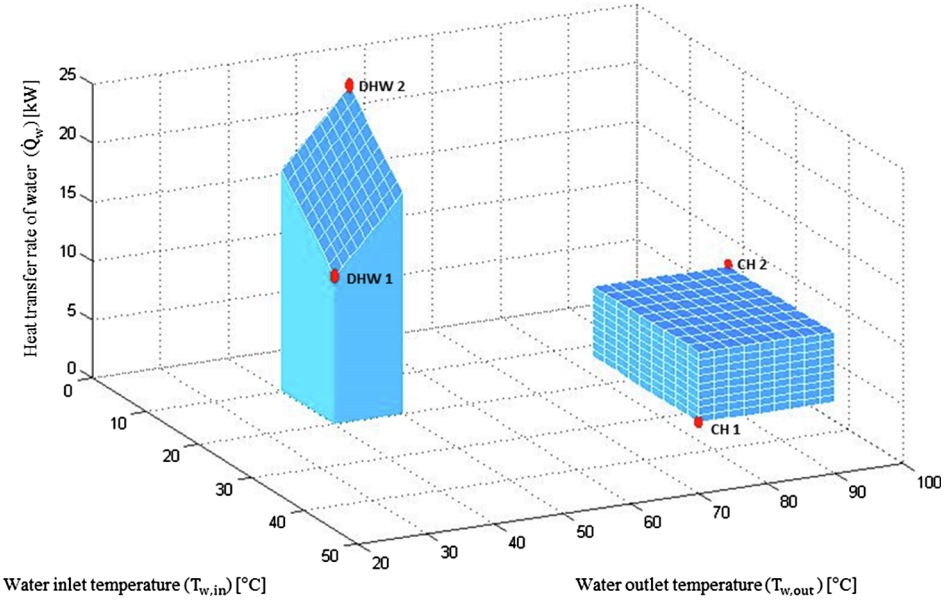

Fig. 2. Regions of demand operation conditions (for Domestic Hot Waters and Central Heating) of the micro-CHP represented in the 3D space of client variables.

($\dot{m}_f$, ΔT_2, p_0) as inputs, the speed of rotation N_T of the expander T, in despite of the fact that it can be easily controlled, becomes an output variable, i.e., its controller becomes fully constrained to assure a steady functioning of the micro-CHP.

2.2. Thermodynamic modelling

Now, a simplified steady model of the micro-CHP that given the following inputs, describes as detailed and realistically as possible the resulting steady-state operation conditions of the micro-CHP and thus guides the selection of the fluid and main components:

- the nominal efficiencies of the components;
- a working fluid;
- particular customer demand conditions ($T_{w,in}$, $T_{w,out}$, $\dot{m}_w/\dot{Q}_w$); and
- specific values for the free *virtual* control variables ($\dot{m}_f$, ΔT_2, p_0 [,p_1]);

Such a model coded in FORTRAN with the subroutine *Refprop* of NIST [37] for fluids properties calculation is presented below, under the following plausible simplifying hypotheses:

H1 The components operate in nominal conditions. In principle, this is possible through a judicious selection of the components and the given customer conditions should be envisaged as nominal.
H2 Neglect of the flow pressure losses in the condenser and evaporator. In consequence: $p_2 = p_1$ (cycle high pressure) and $p_4 = p_3$ (cycle low pressure).
H3 Neglect of the fluid heat losses at the evaporator and condenser. The components and ducts are thermally insulated.

Starting at point 4, the pump inlet, the relevant equations for the pump include the definition of the isentropic efficiency (Eq. (2)), the mechanical power delivered to the fluid (Eq. (3)), the electric power consumed by the motor (Eq. (4)), the pressure rise and flow rate at the inlet (Eqs. (5) and (6)) the mean cross section velocity at the inlet, which is the maximum velocity of a liquid in the cycle (Eq. (7)) and the Net Positive Suction Head available at the pump inlet (Eq. (8)). In fact, the kinetic term of the $NPSH_a$ formula is so low in this type of components that it can be neglected.

$$\eta_{i,P} = \frac{h_{1i} - h_4}{h_1 - h_4} \quad in \quad which \quad h_{1i} = h_f(p_1, s_{1i} = s_4) \tag{2}$$

$$\dot{W}_{in} = \dot{m}_f (h_1 - h_4) \tag{3}$$

$$P_{e,in} = \frac{\dot{W}_{in}}{\eta_{em,P/M}} \tag{4}$$

$$\Delta p_P = p_1 - p_4 \tag{5}$$

$$\dot{V}_4 = \frac{\dot{m}_f}{\rho_4} \tag{6}$$

$$V_4 = \frac{4\dot{V}_4}{\pi D_4^2} \tag{7}$$

$$NPSH_{a,P} = \frac{p_4 - p_{f,sat}(T_4)}{\rho_4 g} + \frac{V_4^2}{2g} \approx \frac{p_4 - p_{f,sat}(T_4)}{\rho_4 g} \tag{8}$$

The equations for the boiler/evaporator express the objective function of the controller of the superheat temperature at the outlet (Eq. (9)) and the heat flux (Eq. (10)).

$$T_2 - T_{f,sat}(p_2) = \Delta T_2 \tag{9}$$

$$\dot{Q}_{in} = \dot{m}_f (h_2 - h_1) \tag{10}$$

The equations for the expander/generator concern the design volumetric ratio (Eq. (11)) the definition of the isentropic efficiency (Eq. (12)) the pressure ratio (Eq. (13)), the mechanical power extracted from the fluid (Eq. (14)) and the generated electric power (Eq. (15)).

$$\frac{v_3}{v_2} = r_v \tag{11}$$

$$\eta_{i,T} = \frac{h_2 - h_3}{h_2 - h_{3i}} \quad \text{in which} \quad h_{3i} = h_f(v_3, s_{3i} = s_2) \tag{12}$$

$$r_p = \frac{p_2}{p_3} \tag{13}$$

$$\dot{W}_{out} = \dot{m}_f (h_2 - h_3) \tag{14}$$

$$P_{e,out} = \eta_{em,T/G} \bullet \dot{W}_{out} \tag{15}$$

In general off-design conditions of operation of the expander, Eq. (11) is not valid and the isentropic specific enthalpy in Eq. (12) should be considered a function of the pair of properties (p_3, s_{3i}) instead of (v_3, s_{3i}). In nominal conditions (cf. H1) both options lead to the same

result and Eqs. (11) and (12) simplify the calculations. In fact, in off-design conditions, the high pressure of the circuit can and should be considered a further independent input of the model in the sense explained in Section 2.1. This partial violation of H1 is legitimate for scroll expanders because they have a characteristic efficiency curve $\eta_{th,T}(r_p, N_T)$ with a wide plateau in r_p below the nominal pressure ratio r_{p_n}, across which $\eta_{th,T}(r_p, N_T) \approx \eta_{th,T_n} \equiv \eta_{th,T}$ [38].

The equations of the condenser CHE express the total heat flux extracted from the fluid (Eq. (16)), cumulatively in vapor sensible heat (Eq. (17)), latent heat of condensation (Eq. (18)) and liquid sensible heat (Eq. (19)) forms, the heating rate of the client's water (Eq. (20), based on H3), a safe indicator of the closeness to pinch point operation conditions (Eq. (21)) and the temperature difference between the working fluid at the condenser outlet and the inlet customer water (Eq. (22)).

$$\dot{Q}_{out} = \dot{m}_f (h_3 - h_4) \tag{16}$$

$$\dot{Q}_{out_1} = \dot{m}_f (h_3 - h_{f,sat}(p_3, x_3 = 1)) \tag{17}$$

$$\dot{Q}_{out_2} = \dot{m}_f (h_{f,sat}(p_3, x_3 = 1) - h_{f,sat}(p_4, x_4 = 0)) \tag{18}$$

$$\dot{Q}_{out_3} = \dot{m}_f (h_{f,sat}(p_4, x_4 = 0) - h_4) \tag{19}$$

$$\dot{Q}_w = \dot{Q}_{out} \tag{20}$$

$$\Delta T_{pinch} = T_{f,sat}(p_3) - \left(T_{w,out} - \frac{\dot{Q}_{out_1}}{\dot{m}_w c_{p_w}}\right) \tag{21}$$

$$\Delta T_{4,w} = T_4 - T_{w,in} \tag{22}$$

Notice that: $\Delta T_{pinch} > 0$ is a sufficient condition to avoid pinch point but a temperature difference close to 0 leads to an excessive heat transfer area and consequently to an expensive heat exchanger; $\Delta T_{4,w} \to 0^+ \Rightarrow A_{CHE} \to \infty$.

Finally, two useful global indicators of the micro-CHP performance, which in fact are closely interrelated, are the ORC thermodynamic efficiency (Eq. (23)) and the Heat-to-Power Ratio (Eq. (24)). A last global equation relates the mean pressure level (the third free control variable).

$$\eta_t = \frac{\dot{W}_{out} - \dot{W}_{in}}{\dot{Q}_{in}} \tag{23}$$

$$HPR = \frac{\dot{Q}_w}{P_{e,out}} \tag{24}$$

$$p_0 = \frac{1}{2} \bullet (p_4 + p_1) \tag{25}$$

A simple but effective numerical iterative algorithm was implemented to compute the outputs of the former model when H1 is strictly satisfied ($\dot{m}_f$, ΔT_2 and p_0 as free *virtual* control variables). The particular instance of the model in which H1 is partially violated for the expander T (p_1 as extra control variable) is even simpler to compute, namely requiring no iteration.

As a first illustration of the use of the former model and algorithm, for a micro-CHP working with R245fa and the following client conditions: $T_{w,in} = 20$ °C, $T_{w,out} = 40$ °C and $\dot{m}_w = 0.1$ kg/s, typical of domestic hot water needs, Fig. 3 shows the surfaces of global thermodynamic efficiency η_t [%] of the micro-CHP in the 2D-range of the *virtual* control variables $\dot{m}_f$ (kg/s) $\in [0.03, 0.05]$ and p_0 (kPa, abs.) $\in [200, 1000]$, for two degrees of superheat: $\Delta T_2 = 5, 20$ °C. Non-admissible functioning points were excluded from the graphic. A decrease of the operation range is noted as well as a slightly increase of the thermodynamic performance with an increase of the superheat temperature.

2.3. Optimization

After the design pre-specifications and the construction of the model simulating the micro-CHP behavior in nominal conditions, a rational procedure to select the working fluid and the main components still requires a third and last tool: the formulation of the optimization problem leading to the best design and a numerical algorithm to solve it.

The following optimization problem was chosen for that purpose:

$$max \eta_t(\dot{m}_f, \Delta T_2, p_0) \tag{26}$$

subject to the constraints or conditions of admissibility:

$$\Delta T_{pinch}(p_3, T_{w,out}) > \Delta T_{pinch_0} = 5 \ ^\circ C \tag{27}$$

$$T_4 - T_{w,in} > \Delta T_{4,w_0} = 5 \ ^\circ C \tag{28}$$

$$NPSH_{a,P} \approx \frac{p_4 - p_{f,sat}(T_4)}{\rho_4 g} > NPSH_{r,P_0} = 3m.f.h. \tag{29}$$

$$p_1 < p_{max} = 1500 \ kPa \tag{30}$$

$$T_2 < T_{max} = 150 \ ^\circ C \tag{31}$$

$$\Delta T_2 > \Delta T_{20} = 5 \ ^\circ C \tag{32}$$

Commencing by the objective function. The independent variables are the free control variables of the micro-CHP in order to assure its optimal control, obviously desirable. The client saving allowed by the micro-CHP relatively to the simple boiler B, when a water heating rate $\dot{Q}_w$ is being requested, is, roughly:

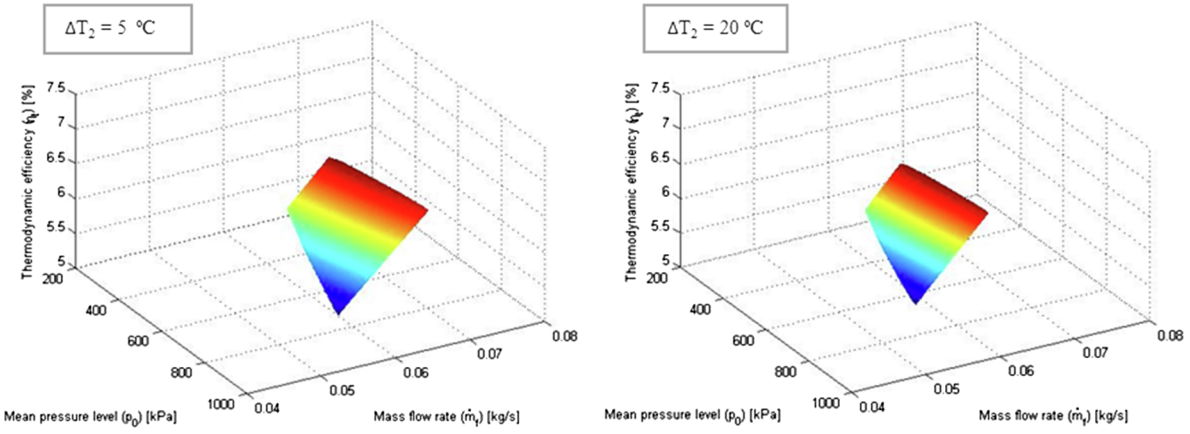

Fig. 3. Surfaces of global thermodynamic efficiency η_t of a micro-CHP working with fluid R245fa, for client conditions ($T_{w,in} = 20$ °C, $T_{w,out} = 40$ °C, $\dot{m}_w = 0.1$ kg/s), in an admissible range of the space of free *virtual* control variables ($\dot{m}_f$, p_0, ΔT_2).

$$S \approx P_{e,out} \bullet c_e - \left(\dot{Q}_B - \frac{\dot{Q}_w}{\eta_B} \right) \bullet c_B \tag{33}$$

Assuming that $P_{e,in} \ll P_{e,out}$ because $\dot{W}_{in} \ll \dot{W}_{out}$ (Table 2), and η_B is the same when the hot gases of combustion in the boiler transfer heat directly to the water (simple boiler) or to the working fluid in the evaporator of the ORC. The second term in the right-member expresses the extra consumption of primary fuel of the micro-CHP. Under the same assumptions, using the global energy balance of the working fluid in the ORC:

$$\dot{Q}_{in} + \dot{W}_{in} = \dot{Q}_{out} + \dot{W}_{out} \tag{34}$$

The Eq. (33) is thus equivalent to:

$$S \approx \left(\eta_{em,T/G} \bullet c_e - \frac{c_B}{\eta_B} \right) \bullet \dot{Q}_w \bullet \frac{\eta_t}{1 - \eta_t} \tag{35}$$

which shows that a maximum of $\eta_t \in [0, 1]$ corresponds effectively to a maximum of S and ultimately to an optimum of the micro-CHP business opportunity.

Turning now to the admissibility conditions (27–32).

- Condition (27) imposes a minimum distance (in the 3D-space of the free control variables) to the surface of pinch point operation conditions of the condenser CHE Together, conditions (27, 28) avoid that the heat transfer area, and so the cost of the condenser become too large, which is obviously desirable.
- Condition (29) prevents the cavitation of the pump P, assuring also that the working fluid is fully condensed at the outlet of the condenser.
- Conditions (30, 31) reflect the limitations of the main components, namely the previously selected expander T.
- Condition (32) avoids the formation of condensates inside the expander T.

To solve the former optimization problem for particular working fluid and client conditions (nominal conditions), a powerful numerical algorithm was developed and implemented in FORTRAN code along the following main steps:

1. *Step 1*. The ignition point P_0 in the space of control variables can be anywhere, including in the non-admissible region.
2. *Step 2*. At point P_k where the optimization path changes direction, the new direction is either: i) the direction of steepest ascent of the objective function η_t, if P_k is in the interior of the admissible region; or ii) the former direction orthogonally projected onto the hyperplane π_{P_k} tangent to the surface boundary of the admissible region at P_k, if P_k is on it (Gram-Schmidt method is here used to generate an orthonormal basis of plane π_{P_k}); or iii) the direction along which the boundary surface of the admissible region is nearest from P_k, if P_k is in the non-admissible region (the Lagrange multipliers method is used to find this direction).
3. *Step 3*. A clever algorithm is used for the 1D-advance along the direction found in Step 2, including a possible intermediate change of direction (e.g., to remain on a curved boundary surface), until Step 2 is applied at point P_{k+1}.

Fig. 4 shows the admissible region and the optimal point generated by the former algorithm in the 3D-space of the free *virtual* control variables ($\dot{m}_f$, ΔT_2, p_0), for a micro-CHP working with R245fa and nominal client conditions: $T_{w,in} = 20$ °C, $T_{w,out} = 40$ °C and $\dot{m}_w = 0.15$ kg/s (possible extremal scenery DHW 1 of Fig. 2). Each constraint is a face of the polyhedron that delimits the admissible region for a specific client condition.

The optimal operation point has coordinates ($\dot{m}_f = 0.0535$ kg/s, $\Delta T_2 = 35.0$ °C, $p_0 = 792$ kPa), and objective and constrained variables: $\eta_t = 7.13\%$, $\Delta T_{pinch} = 11.7$ °C, $\Delta T_{4,w} = 28.1$ °C, $NPSH_{a,P} = 3.00$m. f. h., $p_1 = 1221$ kPa, abs., $T_2 = 133.4$ °C.

3. Design results and discussion

3.1. Selection of working fluid

The design options and tools presented in Section 2 can now be applied to select the best working fluid for the intended application of

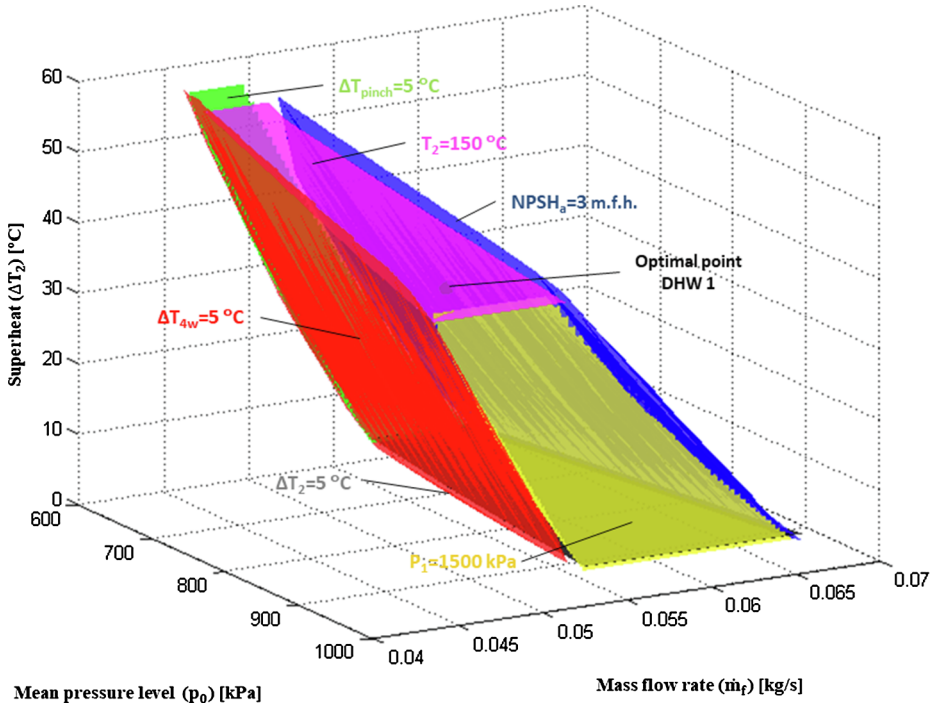

Fig. 4. Admissible region and optimal point in the 3D-space of free *virtual* control variables, for a micro-CHP working with R245fa and nominal client conditions.($T_{w,in} = 20$ °C, $T_{w,out} = 40$ °C, $\dot{m}_w = 0.15$ kg/s)

the micro-CHP.

The working fluid list can be qualitatively reduced *a priori* from the NIST database [37] considering the environmental impact (ODP and GWP), the cost, the safety (flammability and toxicity) and the compatibility with (corrosion or proneness to form condensates in a vapor expansion) or the influence on the performance (viscosity and thermal conductivity) of the ORC components. Summing up the preliminary stage of selection of the working fluid, the fluids R152a, R227ea, R236ea, R245fa, R-365MFC (SES36), R1234YF, R1234ZE, RE347mcc (HFE7000) and Novec 649 were approved for the next selection stage.

In the second stage of working fluid selection, nominal scenarios of client conditions at opposite vertices of both the upper boundary plane of the polygon of Domestic Hot Waters (DHW) demand conditions and of the polygon of Central Heating (CH) demand conditions (Fig. 2) were considered:

- **DHW 1** - $T_{w,in}$ = 20 °C; $T_{w,out}$ = 40 °C; $\dot{m}_w$ = 0.15 kg/s;
- **DHW 2** - $T_{w,in}$ = 10 °C; $T_{w,out}$ = 50 °C; $\dot{m}_w$ = 0.15 kg/s;
- **CH 1** - $T_{w,in}$ = 50 °C; $T_{w,out}$ = 60 °C; $\dot{Q}_w$ = 6 kW_t
- **CH 2** - $T_{w,in}$ = 30 °C; $T_{w,out}$ = 90 °C; $\dot{Q}_w$ = 12 kW_t

For each scenario and candidate working fluid, the optimization problem of Section 2.3 was either solved or shown to have no solution. For working fluids R152a, R1234yf and R1234ze there is no admissible solution in all scenarios, the constraint of Eq. (30) on the maximum pressure being systematically violated. For working fluids R227ea and R236ea there is no admissible solution for scenarios CH#, due to the violation of constraint of Eq. (31) on the maximum temperature.

Only the working fluids R245fa, R365mfc, RE347mcc and Novec649 allow an optimal solution in all scenarios. The global thermodynamic efficiency η_t (objective variable subject to constrained maximization) of the micro-CHP for the six working fluids in scenarios DHW#, and for four of them also in scenarios CH#, are compared in Fig. 5. If only the scenarios DHW# mattered, R245fa would be the best choice, but if the four scenarios are equally important for the business opportunity then R365mfc becomes the best choice.

For completeness, the coordinates (independent and constrained variables) of the micro-CHP optimal functioning points are given in Table 1. Figures marked in red denote optimal points partially violating the hypothesis H1 of the underlying incomplete model (Section 2.2), in the sense that the expander T is working in non-nominal conditions, the highest possible pressure ratio r_p laying below the expander nominal value.

3.2. Selection of components and instrumentation

Although the optimal fluid obtained for both services (DHW and CH) is the R365mfc, we chose to use the R245fa in the test-rig since for the initial tests only domestic hot water services are emulated. Central heating services require the inlet water temperature control which leads to a more sophisticated and complex experimental setup that, for now, the test-rig is not able to fulfill.

Once chosen the working fluid (R245fa), the selection of the main components and instrumentation can be addressed with the help of the design specifications and tools of Section 2. For the selection of the components, the critical nominal customer scenarios of section 3.1 continue to be useful. The corresponding optimal values of the output operational variables of the micro-CHP relevant to select the various components are grouped in Table 2.

3.2.1. Pump

In respect to the pump P, the first selection option concerns its main type, either flow or volumetric. The slowest rotating flow pumps are of the radial subtype (rfP). Typically, fine design radial pumps have non-dimensional specific velocity $\Omega > 0.15$ [39]. Table 2 shows that, irrespective of the critical nominal customer demand condition that is chosen, a flow pump would rotate at a prohibitively large velocity, turning it preferable to select a volumetric type pump.

The four nominal coordinates $(\dot{V}_4, \Delta p_P) \equiv (\dot{V}, \Delta p)$ of Table 2 are compatible with many subtypes of existing volumetric pumps (e.g., piston, diaphragm, internal or external gear, lobed, sliding or flexible rotary vane, peristaltic [40]). In a preselection, three of them stood out: rotary vane pumps, external gear pumps and diaphragm pumps. A final selection essentially taking into consideration the amplitude of pressure

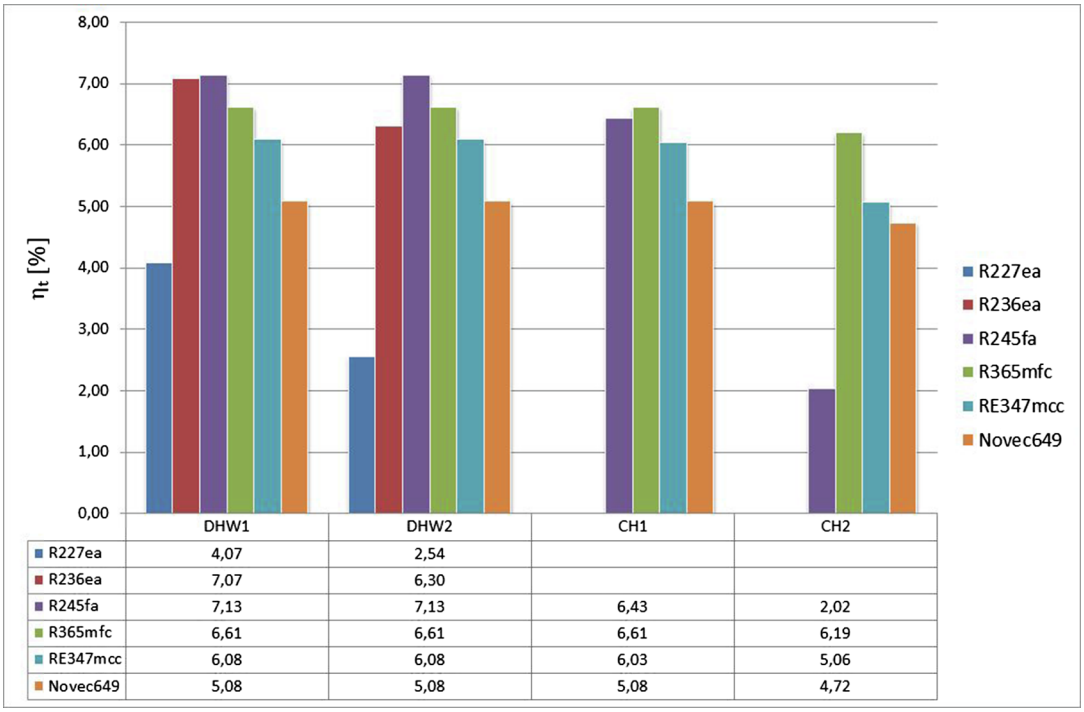

	DHW1	DHW2	CH1	CH2
R227ea	4,07	2,54		
R236ea	7,07	6,30		
R245fa	7,13	7,13	6,43	2,02
R365mfc	6,61	6,61	6,61	6,19
RE347mcc	6,08	6,08	6,03	5,06
Novec649	5,08	5,08	5,08	4,72

Fig. 5. Maximum thermodynamic efficiency of the micro-CHP (under optimal control) for the various working fluids in the four customer nominal demand scenarios considered.

Table 1
Coordinates of the optimal functioning points of the micro-CHP for each working fluid in all nominal scenarios considered (from top to bottom: DHW 1, DHW 2, CH 1, CH 2).

Variable	Working fluid					
	R227ea	R236ea	R245fa	R365mfc	RE347mcc	Novec649
$\dot{m}_f$ [kg/s]	0.0889	0.0664	0.0535	0.0584	0.0771	0.1001
	0.1919	0.1329	0.1066	0.1168	0.1545	0.2004
			0.0277	0.0279	0.0382	0.0479
			0.0616	0.0757	0.0850	0.1083
ΔT_2 [°C]	30.02	25.76	34.99	5.03	5.01	5.05
	30.18	28.82	37.26	5.03	5.00	5.05
			30.94	5.03	5.03	5.01
			39.14	6.37	9.03	5.04
p_0 [kPa, abs.]	1152	840	792	490	419	358
	1270	1013	872	489	427	358
			1016	490	562	358
			1315	1010	1053	741
ΔT_{pinch} [°C]	5.00	5.00	11.69	25.11	14.41	25.72
	5.00	5.05	5.04	15.10	5.05	15.72
			5.04	5.11	5.05	5.72
			5.03	5.00	5.00	5.01
$\Delta T_{4,w}$ [°C]	23.17	24.66	28.13	39.76	27.56	36.52
	43.56	42.30	41.79	49.76	38.33	46.52
			14.79	9.76	9.97	6.52
			63.74	62.44	62.53	60.78
$NPSH_{a,P}$ [m. f. h.]	3.00	3.00	3.00	3.00	3.00	3.00
	3.00	3.00	3.00	3.00	3.00	3.00
			3.00	3.00	3.00	3.00
			3.00	3.00	3.00	3.00
p_1 [kPa,abs.]	1500	1287	1221	749	638	542
	1500	1500	1344	749	650	542
			1500	749	849	542
			1500	1500	1500	1087
T_2 [°C]	100.4	116.6	133.4	115.5	102.1	113.1
	100.5	126.6	140.0	115.5	102.9	113.0
			138.8	115.5	114.7	113.0
			147.0	150.0	146.4	145.3

Table 2
Operational variables of the micro-CHP relevant for the components selection.

Component	Variable	Extreme customer scenarios	
		DHW 1	DHW 2
P	$minN_{rfP}$ [rpm]	29,319	22,440
	$\dot{V}_4$ [m^3/s]	4.24E-5	8.69E-5
	Δp_P [kPa]	859.1	943.4
	$P_{e,in}$ [kW$_e$]	0.075	0.167
	$NPSH_{a,P}$ [m. f. h.]	3.00	3.00
P, T	p_1 [kPa]	1221	1344
EHE	T_1 [°C]	48.6	52.3
	T_2 [°C]	133.4	140.0
	$\dot{Q}_{in}$ [kW$_t$]	13.50	27.01
EHE, T, CHE	$\dot{m}_f$ [kg/s]	0.0535	0.107
T/G	$r_p = p_2/p_3$ [−]	3.371	3.355
	$P_{e,out}$ [kW$_e$]	0.907	1.822
CHE	T_3 [°C]	51.7	55.0
	T_4 [°C]	48.1	51.8
	$\dot{Q}_{out}$ [kW$_t$]	12.56	25.12
Ducts	minD_2 [mm]	11.0	14.8
	minD_4 [mm]	4.2	6.1

pulsation, the lifetime, the noise and the time degradation of performance led to the ultimate choice of flexible rotary vane pumps.

Obviously, the selected pump must be compatible with the working fluid R245fa, have a characteristic curve of Net Positive Suction Head Required $NPSH_r(\Delta p, N)$ satisfactory, given the values of $NPSH_{a,P}$ of Table 2, and allow exit pressures up to $maxp_1 = 1500$ kPa(abs.).

The main characteristics of the selected rotary-vane pump are given in Table 3.

3.2.2. Condenser

The customer scenario DHW 2 dictates the selection condition of the condenser heat exchanger CHE, which is over determined but consistent (see Table 2): $\dot{m}_w = 0.15$kg/s, $T_{w,in} = 10$°C, $T_{w,out} = 50$°C

- Cold fluid (client water, in this case, domestic hot water, in the liquid phase) conditions:
- Hot fluid (R245fa, condensing) conditions: $\dot{m}_f = 0.107$kg/s, $T_{f,in} = 55.0$ °C, $T_{f,out} = 51.8$ °C
- Heat flux transfer: $\dot{Q} = 25.12$ kW

With this information, a suitable customized compact plates heat exchanger can be requested to any manufacturer, and roughly verified, e.g., with the LMTD method presented in [36]. The selected plate heat exchanger provided by GEA has the technical features presented in Table 3.

3.2.3. Expander

The scroll expander mentioned in Section 2.1, with the characteristics revealed in Table 3, was previously selected to play the role of the turbine T, and the subsequent design strategy followed is consistent with it, as can be verified in Table 2. For the moment, the expander is not coupled to an electric generator but to a servomotor and a set of resistive dissipaters that act as a brake with a speed (or torque) controller with speed and power ranges up to 3500 rpm and 2 kW.

3.2.4. Evaporator

The overwhelming majority of the ORC based systems use an indirect way to vaporize the organic fluid, usually an intermediate circuit with water or oil. The direct evaporation of the organic fluid is an attempt to avoid that intermediate circuit reducing the thermal inertia,

Table 3
Characteristics of the selected main components.

Component	Characteristic	Value
Pump	Model	Fluid-o-Tech TMFROT201A
	Pump Type	Rotary vane
	Max. operative temperature [°C]	70
	Displacement [l/h·rpm]	0.1297
	Speed range [rpm]	300 to 3500
	Max static pressure [bar]	20
Condenser	Model	GEA GBS240H
	Exchanger type	Brazed plate heat exchanger
	Number of plates	34
	Temperature range [°C]	70
	Maximum pressure [bar]	30
	Dimensions [mm]	465 × 90 × 85
	Surface area [m^2]	1.41
Expander	Model	Air Squared E15H022A-SH
	Expander type	Scroll
	Nominal Output [kW_e]	1
	Volume ratio [–]	3.5
	Displacement [cm^3/rev]	14.5
	Maximum speed [rpm]	3600
	Maximum inlet pressure [bara]	15
	Maximum inlet temperature [°C]	175
Premix gas burner	Model	Riello (RX 35 S/PV)
	Output [kW]	6–35
Evaporator Heat Exchanger	Type	Double helical coil
	Number of coils	22
	Tube diameter [mm]	17.2
	Coil Length [m]	19.06
	Surface area [m^2]	0.9

the system complexity and the energy losses. While the pump, the turbine and the condenser are considered off-the-shelf products, for the ORC-evaporator there isn't a ready-to-use component within this power range and for that reason, the EHE will be an in-house solution specially developed for it. What matters here is its critical thermal design condition, which corresponds to the customer scenario DHW 2 and can be formulated in this way:

- Cold fluid (R245fa) conditions: $\dot{m}_f = 0.107$kg/s, $T_{f,in} = 52.3^{\circ}$C, $T_{f,out} = 140.0^{\circ}$C
- Hot fluid (flue gases) conditions: $T_{h,in} = T_c$
- Heat flux transfer: $\dot{Q} = 27.01$kW

The in-house developed evaporator is a double concentric helical-coil divided in three parts: the external coil, the internal coil and a central combustion. The hot combustion gases flow around the tubes of the heat-exchanger, within which is the organic working fluid, in what can be described as a mixed counter flow/cross-flow arrangement [41]. The main features are revealed in Table 3

3.2.5. Connecting ducts

The minimum diameter of the ducts that link the main components was estimated in such a way that the maximum flow velocities in the liquid state (through the duct linking the condenser CHE and the pump P) and vapor state (through the duct linking the evaporator EHE and the expander T) don't overpass, respectively, $V_{40} = 4$ m/s and $V_{20} = 20$ m/s [42], i.e.:

$$D_i > minD_i = \sqrt{\frac{4\dot{V}_i}{\pi V_{i0}}} \; (i = 2, 4) \tag{36}$$

As can be seen in Table 2, even the larger duct can have a reasonable diameter $D_2 < 25.4$ mm = 1".

Table 4
Selected instrumentation for input/output variables measurement.

Measurement	Type	Range	Accuracy
T_1, T_2, T_3, T_4	Thermocouple K	−40 to 1100 °C	± 1.5 °C MV
p_1	Pressure transducer	0–25 bar	± 0.25% FS
p_2	High temperature pressure transducer	0–20.7 bar	± 0.25% FS
p_3, p_4	Pressure transducer	0–10 bar	± 0.25% FS
$\dot{V}_f$	Turbine flow meter	2.3–11.4 L/min	± 1% L/min
$T_{w,in}$, $T_{w,out}$	RTD (Pt100)	−50 to 200 °C	± 0.3 °C MV
$\dot{V}_w$	Inline dataflow transmitter	1–25 L/min	± 2% L/min
$T_{g,in}$, $T_{fg,out}$	Thermocouple K	−40 to 1100 °C	± 1.5 °C MV
p_g	Security Valve 20 mbar	0–6 m^3/h	(n.a.)
$\dot{V}_g$	Diaphragm gas meter	0.025–4 m^3/h	± 1.5% MV

Copper lines and threaded connections have been used to link the main components for a more versatile and flexible test rig. The main components and the copper lines were involved with glass wool and polyurethane foam, respectively, to reduce the thermal losses in the circuit.

3.2.6. Instrumentation and layout of the test rig

Finally, the data of Table 2 specify the approximate ranges of the main operational variables that can guide the selection of the corresponding measure and control instrumentation. The measure devices used in the test-rig are provided in Table 4 along with their range and accuracy. For easy viewing, a detailed schematic of the ORC test-and a picture of the installation is given in Fig. 6.

4. Experimental results and discussion

4.1. Test procedure

After the working fluid, component and measurement instrumentation selection, the test-rig was build and charged with the R245fa working fluid. The initial experimental tests, only controlling basic variables and not optimally, aim simply to obtain a preliminary validation of the design procedure, assess the global ORC system performance and also to experimentally determine the influence of the basic control variables on the system behavior. During the experimental tests, a total of 9 steady-state points were obtained that can be divided into 3 groups depending on the control variable that is being altered:

1. $\boldsymbol{N_P}$ **= 550, 600, 650 rpm**; N_T = 2500 rpm; $\dot{Q}_c$ = 6.6 kW; $\dot{m}_w$ = 0.1 kg/s
2. N_P = 650 rpm; N_T = 2500 rpm; $\boldsymbol{\dot{Q}_c}$ **= 6.5, 7.2, 8.0 kW**; $\dot{m}_w$ = 0.1 kg/s
3. N_P = 650 rpm; N_T = 2500 rpm; $\dot{Q}_c$ = 6.6 kW; $\boldsymbol{\dot{m}_w}$ **= 0.1; 0.08, 0.06 kg/s**

The turbine rotational speed N_T is imposed by the servomotor. The first two groups (N_P, $\dot{Q}_c$), $\dot{Q}_c$ being the thermal power generated by the combustion, can be easily controlled on the micro-CHP with a rotational speed controller of the pump P and by controlling the gas flow rate $\dot{V}_g$ burned in the combustion chamber, respectively. None of the basic control variables (N_T, N_P, $\dot{Q}_c$) are direct inputs of the model in Section 2.2, but (N_P, $\dot{Q}_c$) control indirectly the inputs ($\dot{m}_f$, ΔT_2). Finally, the water mass flow rate $\dot{m}_w$ is a client operating condition that can range from 0 to 0.15 kg/s, and appears in the third group.

A PC-based hardware and software solution composed of National Instruments (NI) plates, LabJacks, a Datalogger and LabVIEW was adopted to perform real-time acquisition, processing, control and data logging with user interface. This solution allows acquiring all the variables from the instrumentation with great versatility and ease of programming. The data were obtained in time intervals of 0.5 s

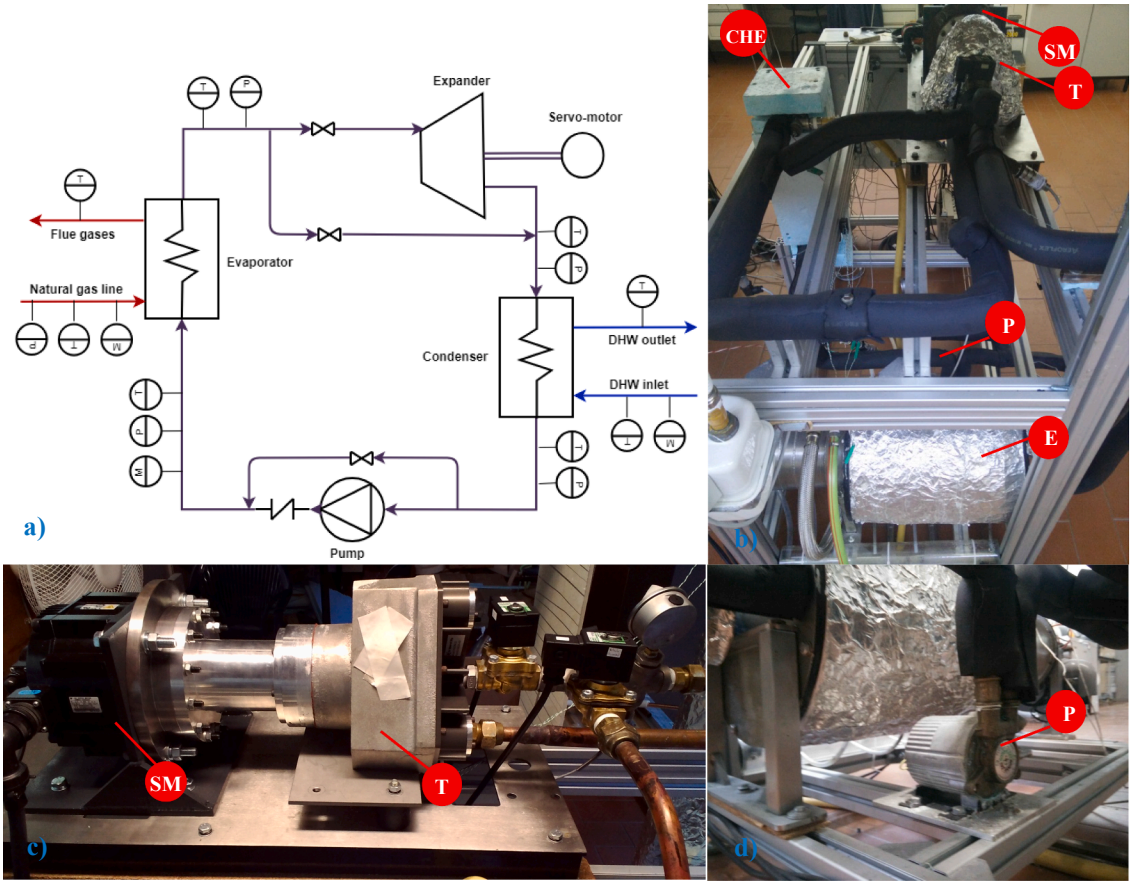

Fig. 6. (a) Test-rig full schematic and photographs of the (b) micro-CHP experimental test rig, (c) expander and servo-motor coupling, (d) rotary-vane pump (Legend: E –Evaporator, P-Pump, T – micro-turbine, SM – Servo-motor, CHE – Condenser heat exchanger).

presented to the user in real time and recorded in a file for future analysis. The experimental campaign lasted approximately 6.5 h from cold start until the ORC was safely switched off. The ORC starts up in simple boiler mode, with the working fluid flowing through a bypass to the turbine without electric generation. Afterwards, the turbine bypass is closed, forcing the flow through the turbine and steps to the micro co-generator mode of operation. The turbine bypass is opened again during the ORC shutdown procedure and keeping the pump running to allow the system to cool mainly because of the high thermal inertia of the evaporator.

4.2. Discussion

Just illustratively, Table 5 reports the average, minimum, maximum and standard deviation values measured for some variables in the test-rig for test #3 ($\dot{Q}_c$ = 6.6 kW, N_P = 650 rpm, N_T = 2500 rpm, $\dot{m}_w$ = 0.1 kg/s). The variables were read in a time window of 200 s at a frequency of 2 Hz. The fluctuation of the measures is of the same order than the accuracy of the instruments (Table 4), which means that the ORC steady functioning is rather stable. Notice that all variables are in the lower part of the predicted ranges (Tables 1 and 2) and, in agreement with the design hypotheses, $p_1 \approx p_2$ and $p_3 \approx p_4$.

As several variables are calculated based on the measured temperatures, pressures and volume flow rates, an average uncertainty analysis was carried out based on the sensor accuracy provided in Table 4. The uncertainty U_y of the variable y, collected in Table 6, is obtained by Eq. (37) and depends on the uncertainty U_{x_i} of each measured variable x_i:

$$U_y = \sqrt{\sum_{i=1}^{N} \left(\frac{\partial y}{\partial x_i}\right)^2 {U_{x_i}}^2} \tag{37}$$

The non-basic properties of the working fluid that depend on the pressure and temperature through state equations were computed with Refprop of NIST [37]. The uncertainties are mainly induced by the considerable error of type K thermocouples (± 1.5 °C), and could be reduced by replacing them for type T thermocouples (± 0.5 °C) that still have a suitable temperature range [−40 °C, 300 °C] for this application.

Fig. 7 (tests #1–9) shows that the external efficiency of the CHE

Table 5
Some variables measured in test #3.

Variable	Average	Min.	Max.	σ	Error
T_1 [°C]	17.4	17.2	17.6	0.08	± 1.5
T_2 [°C]	90.0	89.8	90.2	0.10	± 1.5
T_3 [°C]	66.5	66.2	66.8	0.16	± 1.5
T_4 [°C]	17.0	17.0	17.0	0.02	± 1.5
ΔT_{pinch} [°C]	5.6	–	–	–	± 0.51
$\Delta T_{4,w}$ [°C]	1.9	–	–	–	± 1.53
p_1 [kPa, abs]	524.5	505.4	547.4	6.45	± 6.33
p_2 [kPa, abs]	530.5	521.4	543.3	3.38	± 5.24
p_3 [kPa, abs]	166.2	165.1	167.4	0.34	± 2.53
p_4 [kPa, abs]	163.2	162.6	164.4	0.23	± 2.53
$NPSH_{a,P}$ [m. f. h.]	4.76	–	–	–	± 0.51
$\dot{m}_f$ [kg/s]	0.0197	0.0194	0.0199	0.0009	± 0.00021
$T_{w,in}$ [°C]	15.1	15.1	15.1	0.001	± 0.3
$T_{w,out}$ [°C]	26.4	26.3	26.5	0.048	± 0.3
$\dot{m}_w$ [kg/s]	0.100	0.098	0.104	0.001	± 0.002

Table 6
Average relative uncertainties.

Parameter	Uncertainty	Parameter	Uncertainty
$\dot{m}_f$	1.04%	$\Delta T_{4,w}$	75.09%
$\dot{m}_w$	2.00%	ΔT_{pinch}	15.32%
$\dot{Q}_{in}$	1.42%	ΔT_2	5.27%
$\dot{Q}_{out}$	1.43%	η_i	14.26%
$\dot{Q}_w$	3.71%	$\eta_m \eta_{mag}$	14.54%
$\dot{W}_{out}$	13.33%	η_t	22.07%
r_p	1.71%	η_{CHE}	3.98%
$NPSH_a$	11.14%		

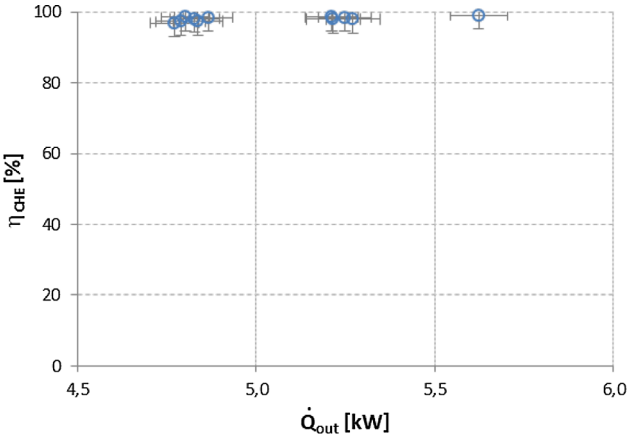

Fig. 7. External efficiency of the condenser heat exchanger (CHE).

(i.e., the ratio of the heat fluxes supplied to the water and extracted from the thermal fluid) is very high, $\eta_{CHE} \approx 1$, as assumed in the design hypotheses, i.e., $\dot{Q}_{out} \approx \dot{Q}_w$.

In tests #1–3, the mass flow rate $\dot{m}_f$ of R245fa, an input variable of the design model, is directly proportional to the rotational speed N_P of the pump, a basic control variable of the ORC, as can be seen in Fig. 8. Notice, however, that $\dot{m}_f$ is also affected by other ORC basic controls and client variables.

In Fig. 9 (tests #1–9) the characteristic curves of isentropic efficiency $\eta_{i,T}$, mechanical power $P_T = \dot{W}_{out} \cdot \eta_m \eta_{mag}$ at the shaft and mechanic and magnetic efficiency $\eta_m \eta_{mag}$ of the expander T are shown as a function of the normalized pressure ratio $r_{p,T} = r_{p,T}/r_{p,T_n}$. The measured turbine pressure ratio is $r_{p,T} = p_2/p_3$ and the nominal pressure ratio r_{p,T_n} is computed with the design model taking as inputs the experimental variables ($\dot{m}_f$, ΔT_2, p_0; $T_{w,in}$, $T_{w,out}$, $\dot{m}_w$). In particular, it can be seen that the extended design hypothesis $\eta_{th,T} \approx \eta_{th,T_n} = 0.7$ is not far from

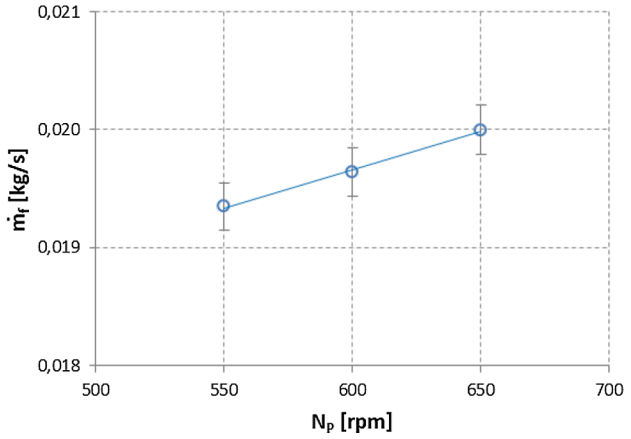

Fig. 8. Fluid mass flow rate *versus* pump rotational speed.

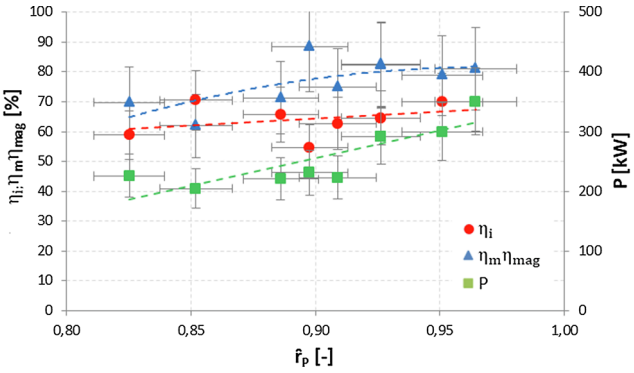

Fig. 9. Characteristic curves of the expander T.

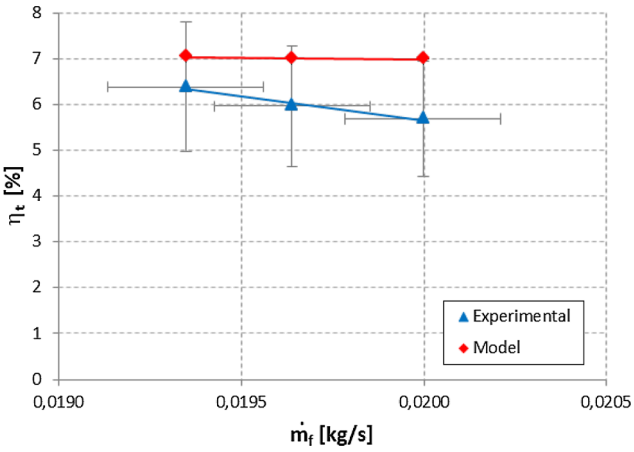

Fig. 10. Overall thermodynamic efficiency η_t of the ORC: experimental *versus* theoretical values.

reality.

For tests #1–3, Fig. 10 compares the experimental and predicted overall thermodynamic efficiency η_t of the ORC. The predicted values are computed with the design model taking as inputs the test measures of ($\dot{m}_f$, ΔT_2, p_0; $T_{w,in}$, $T_{w,out}$, $\dot{m}_w$). The agreement is reasonable, showing also that the ORC components are not working far from their nominal yields. The fact that η_t decreases with $\dot{m}_f$, more clear experimentally, seems to be due to the decrease of the degree of vapor superheat of R245fa at the outlet of the evaporator.

Finally, Fig. 11 (tests #4–6) shows the influence of the fluid thermal power input $\dot{Q}_{in}$ at the evaporator EHE, on both the degree of vapor superheat ΔT_2 at the exit of the EHE, and the client water outlet

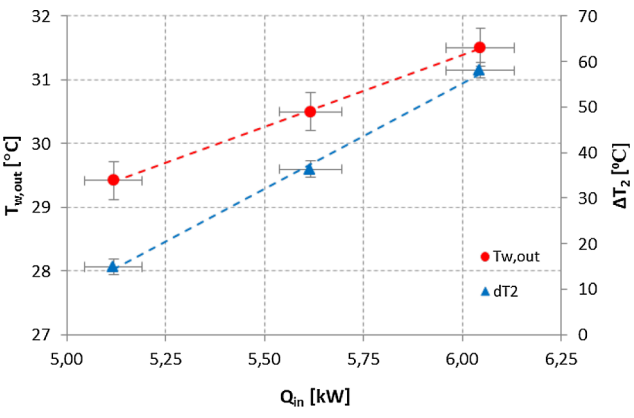

Fig. 11. Influence of the thermal input at the EHE on various ORC and client variables.

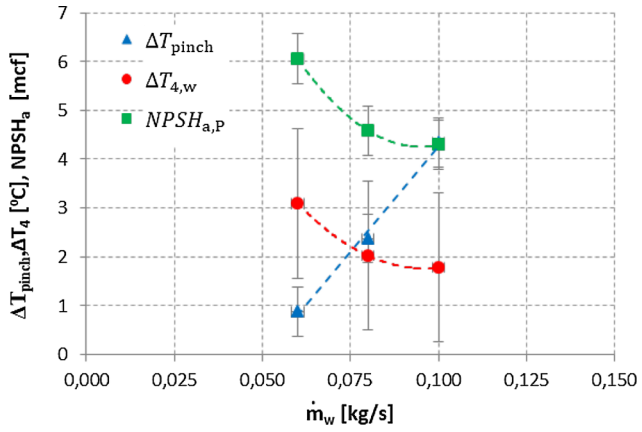

Fig. 12. Influence of the water mass flow rate of the customer on various ORC and client variables.

temperature $T_{w,out}$. Fig. 12 (tests #7–9) prove the influence of the customer water mass flow rate $\dot{m}_w$ on three ORC variables (ΔT_{pinch}, $\Delta T_{4,w}$, $NPSH_{a,P}$). Altough the user plain controls of the basic variables (N_T, N_P, $\dot{Q}_c$) are kept steady, the key control variables, such as ($\dot{m}_f$, ΔT_2), have slightly fluctuations in these tests, so these results are harder to interpret. However, it is interesting to observe that: i) there is no danger of cavitation of the pump ($NPSH_{a,P} > 3$m. c. f.); ii) the condenser is working with high internal thermal efficiency ε_{CHE}, which increases with $\dot{m}_w$ ($\Delta T_{4,w} \rightarrow 0^+$); and iii) for decreasing $\dot{m}_w$, the pinch point condition is approached ($\Delta T_{pinch} \rightarrow 0^+$), requiring a changing of the values of the basic control variables.

5. Conclusion

A strategy of early design of a basic ORC micro-CHP ultimately intended to replace domestic natural gas based combi-boilers is presented. The specific designed unit supplying just domestic hot waters is only the first step along this path, but ultimately also central heating water can be provided. Out of this study, the main outcomes can be summarized as follows:

- The strategy is applied, in the first place, to select the working fluid leading to the selection of the R365mfc (or of the R245fa if only the domestic hot waters matter).
- In the second place, a volumetric flexible rotary vane pump, an in-house solution of direct evaporator, a BPHE as condenser and a scroll expander were selected and dimensioned. Then, the experimental setup and the acquired measurement and control instruments are specified.
- The experimental results showed that the ORC components are not working far from the assumed nominal efficiencies and a reasonable agreement is obtained between the experimental and predicted overall thermodynamic efficiency. A direct influence of the basic controls is observed, both of the rotational speed of the pump on the mass flow rate (directly proportional) and of the thermal power input on the degree of vapor superheat at the outlet of the evaporator.
- On this basis, we conclude that the followed design procedure is suitable for component selection for an experimental facility.

Declaration of Competing Interest

The authors declare that they have no known competing financial interests or personal relationships that could have appeared to influence the work reported in this paper.

Acknowledgements

This research is partially sponsored by FEDER Funds through the program COMPETE – Programa Operacional Factores de Competitividade under the contract QREN-POFC-COMPETE-23101. This financial support is gratefully acknowledged.

Appendix A. Supplementary material

Supplementary data to this article can be found online at https://doi.org/10.1016/j.applthermaleng.2020.114945.

References

[1] P. Gao, L. Jiang, L.W. Wang, R.Z. Wang, F.P. Song, Simulation and experiments on an ORC system with different scroll expanders based on energy and exergy analysis, Appl. Therm. Eng. 75 (2015) 880–888, https://doi.org/10.1016/j.applthermaleng.2014.10.044.
[2] K. Rahbar, S. Mahmoud, R.K. Al-Dadah, N. Moazami, S.A. Mirhadizadeh, Review of organic Rankine cycle for small-scale applications, Energy Convers. Manag. 134 (2017) 135–155, https://doi.org/10.1016/j.enconman.2016.12.023.
[3] P. Song, M. Wei, L. Shi, S.N. Danish, C. Ma, A review of scroll expanders for organic rankine cycle systems, Appl. Therm. Eng. 75 (2015) 54–64, https://doi.org/10.1016/j.applthermaleng.2014.05.094.
[4] M. Kharseh, M. Al-khawaja, F. Hassani, Optimal utilization of geothermal heat from abandoned oil wells for power generation, Appl. Therm. Eng. 153 (2019) 536–542, https://doi.org/10.1016/j.applthermaleng.2019.03.047.
[5] J. Li, J. Zeb, G. Pei, J. Ji, P. Li, H. Fu, Effect of working fluids on the performance of a novel direct vapor generation solar organic Rankine cycle system, Appl. Therm. Eng. 98 (2016) 786–797, https://doi.org/10.1016/j.applthermaleng.2015.12.146.
[6] D. Prando, M. Renzi, A. Gasparella, M. Baratieri, Monitoring of the energy performance of a district heating CHP plant based on biomass boiler and ORC generator, Appl. Therm. Eng. 79 (2015) 98–107, https://doi.org/10.1016/j.applthermaleng.2014.12.063.
[7] S. Quoilin, S. Declaye, B.F. Tchanche, V. Lemort, Thermo-economic optimization of waste heat recovery Organic Rankine Cycles, Appl. Therm. Eng. 31 (2011) 2885–2893, https://doi.org/10.1016/j.applthermaleng.2011.05.014.
[8] A. Franco, F. Bellina, Methods for optimized design and management of CHP systems for district heating networks (DHN), Energy Convers. Manag. 172 (2018) 21–31, https://doi.org/10.1016/j.enconman.2018.07.009.
[9] J.S. Pereira, J.B. Ribeiro, R. Mendes, G.C. Vaz, J.C. André, ORC based micro-cogeneration systems for residential application – A state of the art review and current challenges, Renew. Sustain. Energy Rev. 92 (2018) 728–743, https://doi.org/10.1016/j.rser.2018.04.039.
[10] G. Qiu, Selection of working fluids for micro-CHP systems with ORC, Renew. Energy 48 (2012) 565–570, https://doi.org/10.1016/j.renene.2012.06.006.
[11] D. Mikielewicz, J. Mikielewicz, A thermodynamic criterion for selection of working fluid for subcritical and supercritical domestic micro CHP, Appl. Therm. Eng. 30 (2010) 2357–2362, https://doi.org/10.1016/j.applthermaleng.2010.05.035.
[12] B.F. Tchanche, G. Papadakis, G. Lambrinos, A. Frangoudakis, Fluid selection for a low-temperature solar organic Rankine cycle, Appl. Therm. Eng. 29 (2009) 2468–2476, https://doi.org/10.1016/j.applthermaleng.2008.12.025.
[13] O.A. Oyewunmi, C.J.W. Kirmse, A.M. Pantaleo, C.N. Markides, Performance of working-fluid mixtures in ORC-CHP systems for different heat-demand segments and heat-recovery temperature levels, Energy Convers. Manag. 148 (2017) 1508–1524, https://doi.org/10.1016/j.enconman.2017.05.078.
[14] P. Garg, M.S. Orosz, P. Kumar, Thermo-economic evaluation of ORCs for various working fluids, Appl. Therm. Eng. 109 (2016) 841–853, https://doi.org/10.1016/j.applthermaleng.2016.06.083.
[15] Y. Jang, J. Lee, Optimizations of the organic Rankine cycle-based domestic CHP using biomass fuel, Energy Convers. Manag. 160 (2018) 31–47, https://doi.org/10.1016/j.enconman.2018.01.025.
[16] F.A. Boyaghchi, P. Heidarnejad, Thermoeconomic assessment and multi objective optimization of a solar micro CCHP based on Organic Rankine Cycle for domestic application, Energy Convers. Manag. 97 (2015) 224–234, https://doi.org/10.1016/j.enconman.2015.03.036.
[17] M.T. White, O.A. Oyewunmi, M.A. Chatzopoulou, A.M. Pantaleo, B.A.J. Haslam, C.N. Markides, Integrated computer-aided working-fluid design and thermo-economic ORC system optimisation, Energy Procedia 129 (2017) 152–159, https://doi.org/10.1016/j.egypro.2017.09.095.
[18] M. Farrokhi, S.H. Noie, A.A. Akbarzadeh, Preliminary experimental investigation of a natural gas-fired ORC-based micro-CHP system for residential buildings, Appl. Therm. Eng. 69 (2014) 221–229, https://doi.org/10.1016/j.applthermaleng.2013.11.060.
[19] J.C. Chang, T.C. Hung, Y.L. He, W. Zhang, Experimental study on low-temperature organic Rankine cycle utilizing scroll type expander, Appl. Energy 155 (2015) 150–159, https://doi.org/10.1016/j.apenergy.2015.05.118.
[20] B. Peris, J. Navarro-Esbrí, F. Molés, J.P. Martí, A. Mota-Babiloni, Experimental characterization of an Organic Rankine Cycle (ORC) for micro-scale CHP applications, Appl. Therm. Eng. 79 (2015) 1–8, https://doi.org/10.1016/j.applthermaleng.2015.01.020.

[21] H.C. Jung, L. Taylor, S. Krumdieck, An experimental and modelling study of a 1kW organic Rankine cycle unit with mixture working fluid, Energy 81 (2015) 601–614, https://doi.org/10.1016/j.energy.2015.01.003.
[22] Y. Feng, T. Hung, Y. He, Q. Wang, S. Chen, S. Wu, C. Lin, Experimental investigation of lubricant oil on a 3 kW organic Rankine cycle (ORC) using R123, Energy Convers. Manag. 182 (2019) 340–350, https://doi.org/10.1016/j.enconman.2018.12.021.
[23] D. Ziviani, S. Gusev, S. Lecompte, E.A. Groll, J.E. Braun, W.T. Horton, M. Van Den Broek, M. De Paepe, Optimizing the performance of small-scale organic Rankine cycle that utilizes a single-screw expander, 189 (2017) 416–432.
[24] A. Gimelli, A. Luongo, M. Muccillo, Efficiency and cost optimization of a regenerative Organic Rankine Cycle power plant through the multi-objective approach, Appl. Therm. Eng. 114 (2017) 601–610, https://doi.org/10.1016/j.applthermaleng.2016.12.009.
[25] X. Liu, M. Wei, L. Yang, X. Wang, Thermo-economic analysis and optimization selection of ORC system configurations for low temperature binary-cycle geothermal plant, Appl. Therm. Eng. 125 (2017) 153–164, https://doi.org/10.1016/j.applthermaleng.2017.07.016.
[26] P. Linke, A.I. Papadopoulos, P. Seferlis, Systematic Methods for Working Fluid Selection and the Design, Integration and Control of Organic Rankine Cycles—A Review, (2015) 4755–4801. doi:10.3390/en8064755.
[27] S. Amicabile, J. Lee, D. Kum, A comprehensive design methodology of organic Rankine cycles for the waste heat recovery of automotive heavy-duty diesel engines, 87 (2015) 574–585.
[28] M. Wang, J. Wang, Y. Zhao, P. Zhao, Y. Dai, Thermodynamic analysis and optimization of a solar-driven regenerative organic Rankine cycle (ORC) based on fl at-plate solar collectors, 50 (2013) 816–825.
[29] D. Tempesti, G. Manfrida, D. Fiaschi, Thermodynamic analysis of two micro CHP systems operating with geothermal and solar energy, 97 (2012) 609–617. doi:10.1016/j.apenergy.2012.02.012.
[30] S. Lecompte, H. Huisseune, M. van den Broek, S. De Schampheleire, M. De Paepe, Part load based thermo-economic optimization of the Organic Rankine Cycle (ORC) applied to a combined heat and power (CHP) system, Appl. Energy 111 (2013) 871–881, https://doi.org/10.1016/j.apenergy.2013.06.043.
[31] M. Sadeghi, A. Nemati, A. Ghavimi, M. Yari, Thermodynamic analysis and multi-objective optimization of various ORC (organic Rankine cycle) configurations using zeotropic mixtures, Energy 109 (2016) 791–802, https://doi.org/10.1016/j.energy.2016.05.022.
[32] J. Bao, L. Zhao, A review of working fluid and expander selections for organic Rankine cycle, Renew. Sustain. Energy Rev. 24 (2013) 325–342, https://doi.org/10.1016/j.rser.2013.03.040.
[33] A.M. Pantaleo, M. Simpson, G. Rotolo, E. Distaso, O.A. Oyewunmi, P. Sapin, P. De Palma, C.N. Markides, Thermoeconomic optimisation of small-scale organic Rankine cycle systems based on screw vs. piston expander maps in waste heat recovery, Energy Convers. Manag. 200 (2019) 112053, https://doi.org/10.1016/j.enconman.2019.112053.
[34] E. Macchi, M. Astolfi (Eds.), Organic Rankine Cycle (ORC) Power Systems - Technologies and Applications, elsevier E, Woodhead Publishing Series in Energy, 2016.
[35] R. Bracco, D. Micheli, R. Petrella, M. Reini, R. Taccani, G. Toniato, Organic Rankine Cycle (ORC) Power Systems, 2017. doi:10.1016/B978-0-08-100510-1.00002-8.
[36] M. Santos, J. André, S. Francisco, R. Mendes, J. Ribeiro, Off-design modelling of an organic Rankine cycle micro-CHP: Modular framework, calibration and validation, Appl. Therm. Eng. 137 (2018), https://doi.org/10.1016/j.applthermaleng.2018.04.009.
[37] NIST - National Institute of Standards and Technology, Reference Fluid Thermodynamic and Transport Properties Database (REFPROP), 2018.
[38] M. Imran, M. Usman, B.S. Park, D.H. Lee, Volumetric expanders for low grade heat and waste heat recovery applications, Renew. Sustain. Energy Rev. 57 (2016) 1090–1109, https://doi.org/10.1016/j.rser.2015.12.139.
[39] R.H. Sabersky, A.J. Acosta, H.E. G., Fluid Flow: A First Course in Fluid Mechanics, Pearson, 1989.
[40] H. Institute, Pump fundamentals, 2009.
[41] J.S. Pereira, J.B. Ribeiro, R. Mendes, J.C. André, Analysis of a hybrid (topping/bottoming) ORC based CHP configuration integrating a new evaporator design concept for residential applications, 113984, Appl. Therm. Eng. 160 (2019), https://doi.org/10.1016/j.applthermaleng.2019.113984.
[42] A.J. Macintyre, Bombas e Instalações de Bombeamento, 04–1997th ed., Rio de Janeiro, 1997.

Chapter 5

Off-design and charge sensitive model

This chapter contains the paper "Off-design modelling of an organic Rankine cycle micro-CHP: Modular framework, calibration and validation" published in Applied Thermal Engineering. This work provides a modelling tool for predicting the ORC micro-CHP (Hebe) performance in any off-design condition given solely the system boundary conditions and the control strategy adopted. It begins with the presentation of the basic layout of the system to be modelled. The core of the paper contains the physical and mathematical framework of the model. The modular sub models of each component of the system are successively presented followed by the closure relationships of the model, expressing global conservation equations. The test facility is then presented, followed by the model calibration and preliminary validation against around 50 test points. Lastly, the main conclusions are presented.

Applied Thermal Engineering 137 (2018) 848–867

Contents lists available at ScienceDirect

Applied Thermal Engineering

journal homepage: www.elsevier.com/locate/apthermeng

Research Paper

Off-design modelling of an organic Rankine cycle micro-CHP: Modular framework, calibration and validation

Márcio Santos*, Jorge André, Sara Francisco, Ricardo Mendes, José Ribeiro

Department of Mechanical Engineering, University of Coimbra, Portugal

HIGHLIGHTS

- An off-design and charge-sensitive model for an ORC system is presented.
- Detailed submodels of the ORC main components are established.
- Steady modelling architecture of a micro-CHP: modular, realistic, fast computing.
- The experimental micro-CHP setup is fully described and characterized.
- Full calibration and preliminary validation of the micro-CHP model.

ARTICLE INFO

Keywords:
micro-CHP
Organic Rankine Cycle
Model
Off-design

ABSTRACT

A modular framework to model the steady off-design behavior of micro-CHP natural gas boilers based on Rankine technology is presented. The system charge integration into the model eliminates the use of any assumptions (i.e. subcooling, superheating, condensing pressure, etc.) which makes the presented model completely predictive. It is illustrated in the modelling a micro-CHP that satisfies the hot waters and central heating domestic needs (35 kW_t) and produces electricity ($\leq$1.5 kW_e). A library of sub models of components with empirical (rotary vane pump and vapor scroll expander), semi-empirical (compact plates condenser) and spatially detailed physical (gas burner and evaporator) models is used to construct a model, using R245fa as thermal fluid.

The model is calibrated and validated in tests in which 0.1 kg/s of water was heated from 20 °C to 30–36 °C, and 80–500 W mechanical power was delivered at the expander shaft, sweeping restrict ranges of three control variables: burner thermal power of combustion (10–14.5 kW_t), pump (500–740 rpm) and expander (2500–2750 rpm) rotation speeds. The model predicts most output variables with acceptable errors, e.g., less than ± 10% for the expander outlet pressure (190–220 kPa, abs) or the temperatures at the outlet of the evaporator (80–150 °C) or the expander (60–120 °C).

1. Introduction

Increased world-wide demand for energy (especially electricity), rising energy costs, and heightened environmental concerns are factors that continually press for the improvement and development of new technologies to promote energy savings and GHG (Green House Gases) emissions reduction. In this respect, not denying that this is controversial, the diffusion of CHP equipment throughout the EU domestic sector has been considered the most significant and easy to implement (e.g., cost-effective) individual measure to achieving the EU's CO_2 emissions reduction target to 2020, with a potential estimated in 150–800 Mton-CO_2 eq./year avoided emissions [1]. This justifies why some countries are supporting the corresponding technology development, e.g., through feed-in tariffs.

However, almost all CHP systems available in the market belong to the medium-high power range (0.01–3 MW) while domestic size systems are not so diffused yet [2]. Several technologies are emerging on the market for small and micro CHP applications, such as: Organic Rankine Cycle (ORC), Internal Combustion Engine (ICE) [3], Stirling Engine (SE), Fuel Cells (PEMFC) [4], Photovoltaic (CPVT) and Gas Turbine (GT) [5]. Although various micro-CHP gas boilers have come into market, even leaving aside the technological immaturity of these products relative to competitive condensing boilers, their prices are so high and their electric efficiencies so low that the pay-back periods of

* Corresponding author at: University of Coimbra, Rua Dr. Luís Reis Santos, 3030-788 Coimbra, Portugal.
E-mail address: marcio.santos@dem.uc.pt (M. Santos).

https://doi.org/10.1016/j.applthermaleng.2018.04.009
Received 11 December 2017; Received in revised form 10 March 2018; Accepted 2 April 2018
Available online 05 April 2018
1359-4311/ © 2018 Elsevier Ltd. All rights reserved.

Nomenclature

Symbols

A	area (m^2)
C	heat capacity rate (W/K)
c_p	specific heat (J/kg·K)
D	diameter (m)
F	F Factor
f	friction factor
g	constant gravity acceleration (m/s^2)
G	mass velocity ($kg/s·m^2$)
h	specific enthalpy (kJ/kg)
K	thermal conductivity (W/m·K)
L_p	length of plates of the CHE (m)
M	molar mass (kg/kmol)
$\dot{m}$	mass flow rate (kg/s)
N	rotational speed (rpm)
N_p	number of plates of the CHE
Nu	Nusselt Number
p	pressure (kPa, abs.)
P	power (W)
p_{co}	wavelets step distance of CHE plates (m)
Pr	Prandtl Number
$\dot{Q}$	heat flux (W)
q_{c0}	natural gas low heat value (MJ/kg)
$\dot{Q}_{pc}$	thermal power losses in the burner (W)
$\dot{Q}_{p_f}$	fluid thermal losses in the expander (W)
$\dot{Q}_{P_{mec+mag}}$	mech.-magnetic losses in the expander (W)
R	perfect gas constant (J/kg·K)
Re	Reynolds number
R_f''	fouling factor (m^2·K/W)
r_p	pressure ratio in the expander
s	specific entropy (kJ/kg·K)
T	temperature (K or °C)
ΔT_{lm}	logarithmic mean temperature difference
U	overall heat transfer coefficient (W/m^2·K)
v	specific volume (m^3/kg)
$\dot{V}$	flow rate (m^3/s)
ΔV_{adm}	expander admission chamber volume (m^3)
W_p	width of plates of the CHE (m)
$\dot{W}$	work

Acronyms

B	Burner
CHE	Condenser Heat Exchanger
CHP	Combined Heat and Power
CV	Control Volume
EU	European Union
GHG	Green House Gases
G/C	Generator/Conversor
LMTD	Logarithmic Mean Temperature Difference
NI	National Instruments
NPSH	Net Positive Suction Head
NTU	Number of (heat) Transfer Units
ORC	Organic Rankine Cycle
P	Pump
SM	Servomotor
T	Turbine

Greek letters

α	pump displacement (m^3)
β	chevron angle of the plates of the CHE
δ	excess air ratio of combustion
ε	heat exchanger efficiency
η	efficiency (various types)
ρ	density (kg/m^3)
μ	dynamic viscosity (Pa·s)

Subscripts

a	ambient
ad	adiabatic
b	burner
c	combustion
e	electric
f	thermal fluid
g	natural gas
gq	burnt gases
h	hydraulic
in	inlet
lm	logarithmic mean
mag	magnetic
mec	mechanic
out	outlet
pc	power losses
sat	saturated/saturation
st	stoichiometric
t	tube
th	thermo-hydrodynamic
v	volumetric
w	water

the implied extra investments largely exceed the maximum possible life-time of gas boilers [6]. In this respect, ORCs present good prospects of enabling the design of a profitable boiler/micro-CHP, as long as it is based on a sound enough comprehension of the physical processes involved in its operation.

Along this line of thought, this machine intends to be a micro-CHP natural gas boiler based on Rankine technology, that satisfies the hot waters and central heating domestic needs (~35 kW_t) and produces electricity (≤1.5 kW_e) that can be consumed at home or sold back to the public grid. Although consumes slightly more gas than a comparable state-of-the-art condensing gas boiler, as gas is usually much cheaper than electricity, for many dwellings, the annual saving in the energy bill (gas plus electricity) is supposed to pay-back the extra investment in less than 5–10 years, comparing with a lifetime of 12–15 years. For instance, it was estimated that, in a three bed semi-detached house very typical in the UK, a micro-CHP gas boiler can allow a 17–25% saving in the energy bill (of 739€/year for the state-of-the-art boiler) and is paid-back in 5–8 years [6].

Thinking now in this micro-CHP development, most models presented in the literature for ORC design, in order to achieve the maximum efficiency for given hot and cold sources, are simplified models based on integral conservation equations in steady-state conditions and characterizing the components solely through nominal yields, such as, the thermo-hydrodynamic isentropic efficiency (pump and turbine) and the heat transfer efficiency (evaporator and condenser). An abundant number of studies can be found in literature on the selections of the working fluid with these simplified models. Qiu et al. compares 8 of the most applied working fluids for the medium-to-low temperature ORC [7]. Tchanche et al. obtained the theoretical performance of a few fluids for a low-temperature solar ORC systems [8]. Mikielewicz et al. tested 20 fluids in subcritical and supercritical organic Rankine cycles for low-temperature domestic micro systems [9]. Kosmadakis et al. perform an

efficiency comparison between several organic fluids in a two-stage ORC [10]. Another use of such modelling approach was proposed and studied by several authors for the selection of the components and the evaluation of the cycle thermodynamic and economic performance for different costumer demand patterns and geographical zones. Mago et al. studied the use of CHP–ORC systems for small commercial buildings in various EUA cities [11], Peris et al. focused on waste heat recovery of jacket cooling water from Internal Combustion Engine and simulates six configurations using ten non flammable working fluid [12], Declaye et al. perform a experimental characterization of an open-drive scroll expander integrated into an Organic Rankine cycle using R245fa as working fluid [13] and Farrokhi et al. designed and constructed a natural gas-fired micro-scale CHP system with a vane expander and isopentane as the ORC working fluid [14]. However, they can only get a first approximation of the ORC steady-state behavior because the components do not behave in the same way in design and off-design conditions, and, in fact, the various components will never work simultaneously in design conditions except, possibly, in a very small region of the space of steady-state domestic customer demands.

Nevertheless, the literature presents also a few detailed simulation models of ORCs taking into account the off-design characteristics of the components. This is the case of Quoillin et al. [15], who model the evaporator and the condenser of a small scale ORC with the ε-NTU method for counter flow heat exchangers, subdividing both components into three distinct zones, respectively, of liquid, two-phase and vapor fluid. The scroll expander, converted *ad hoc* from a commercial air compressor, is modelled empirically through characteristic curves that had been previously obtained by the authors specifically for R245fa, the working fluid used in the present ORC [13]. Ibarra et al. [16] conducted a theoretical thermodynamic analysis and part-load simulation of a 5 kW_e ORC system using a scroll expander. The model only accounts for the expander, the pump and the recuperator off-design behaviors without modelling the evaporator, heat source or condenser. The authors investigate the influence of the evaporating pressure, the condensing temperature, the expander inlet temperature and the expander speed on the system performance. For larger scale ORCs, other models include even non-stationary conditions besides the off-design characteristics of the components. He et al. [17] presented a thermodynamic analysis of a 50 kW_e ORC power plant that uses a hot-water boiler or a solar collecting system as a low grade heat source. By fitting the experimental data with model results, the authors developed and validated the model to predict the net power output, thermal efficiency and exergetic efficiency. Wei et al. [18] developed a model of this kind for a small/medium scale ORC (100 kW_e) that recovers the exhaust gas heat from industrial processes. Only the heat exchangers are modelled in non-steady conditions. Pump and expander are modelled with steady lumped parameters because the authors state that these components evolve into stationary conditions much faster than the heat exchangers. Wang et al. [19] create a semi-empirical off-design model of an ORC driven by solar energy. The author's model interconnects each component submodel in order to examine the effects of the key thermodynamic parameters on the system performance and conducted also a parametric optimization using a genetic algorithm. In this work an experimental validation was not provided. Li et al. [20] investigate the potential of low temperature geothermal sources using a theoretical 1.5 MW_e Kalina cycle. The system performance was assessed by the variation effect of the geothermal source temperature, mass flow rate and heat sink temperature. The sliding pressure control was adopted to maintain the turbine inlet temperature at the design value.

As mentioned above, most of the literature papers focus on the working fluid selection, optimum cycle design and sensitive analysis using simplified models that not take into account the off-design behavior of the ORC components. The study of ORC systems in off-design conditions is a relative new issue and appears in some papers in the scientific literature despite most of them are for the medium-large scale. Also, most of these models employ a constant subcooling, overheating, pressure or another thermodynamic property that makes them not fully deterministic. A way to overcome this and achieve a better performance prediction is to use a charge-sensitive model. Although these types of models are well-known for refrigerant systems, in ORC systems are very rare and despite the little attention that has been paid to this parameter, the working fluid charge will play a very important role in the description of system's off-design performance besides it has a non-negligible cost, especially for the large-scale systems.

The present manuscript is the central part of a set of three papers on the modelling work of support of the design of the first prototypes of the micro-CHP, and of the corresponding test rig. This work began with the construction of a simplified model (described in the first paper of the set, still not published) to guide the selection of components and instrumentation for the first prototype and test facility, as a quick and effective response to the design requirements at an early stage. The present paper describes a second stage of the work, making use of a general and rich modular modelling architecture that enables the easy construction of more powerful and fully predictive models to simulate the quasi-steady behavior of the micro-CHP and, in fact, of any ORC. The aim of the present work is to provide a modelling tool for predicting the ORC performance in any off-design condition taking into account the system charge, which we believe to foster the state-of-the-art in some aspects. The predicted results and the experimental results are compared for a preliminary validation of the proposed model. Such models are very useful to optimize ORCs configuration, working fluid, components, operating conditions and, above all, control strategy.

The rest of the paper is organized as follows. In Section 2 the basic layout of the system to be modelled is presented. Section 3 is the core of the paper. The physical and mathematical framework of the model is explained in the introduction. The modular sub models of each component of the system are successively presented in Sections 3.1–3.4. Section 3.5 gathers the closure relationships of the model, expressing global conservation equations. The test facility is presented in Section 4. The strategy of calibration and preliminary validation of the model is illustrated in Section 5. The main conclusions are presented in Section 6.

2. System layout

This particular micro-CHP starts up in simple boiler mode, i.e., with the working fluid flowing through a bypass to the turbine, with no electric generation. Afterwards, the turbine bypass is closed, forcing the flow through the turbine and steps to the micro co-generator mode of operation which is the focus of this work.

Fig. 1 shows the basic scheme operating in this mode. The working fluid, in this case an organic fluid, flows in the liquid and vapor phases through the internal closed circuit $1 \rightarrow 2 \rightarrow 3 \rightarrow 4 \rightarrow 1$, following the well-known Rankine cycle [21].

i. Firstly ($1 \rightarrow 2$), the liquid fluid is heated and vaporizes in the gas burner and evaporator B.
ii. Then ($2 \rightarrow 3$), the vapor fluid expands and cools while flowing through the micro-turbine T. The rotor shaft of the micro-turbine is coupled with the shaft of the electrical generator/converter G/C ultimately responsible for the electricity output.
iii. Afterwards ($3 \rightarrow 4$), the vapor fluid cools down some more and condenses back to the liquid phase in the condenser heat exchanger CHE. The fluid condensation heats the water flowing through the open circuit of domestic hot water, i.e., (water company network) $\rightarrow 5 \rightarrow 6 \rightarrow$ (water drainage network), and the closed circuit of space heating, i.e., $7 \rightarrow 8 \rightarrow 7$.
iv. Finally ($4 \rightarrow 1$), the pump P1 forces the flow of the fluid around the internal circuit and pressurizes the liquid fluid back to its initial thermodynamic state.

In this work, the experimental tests were all performed using the

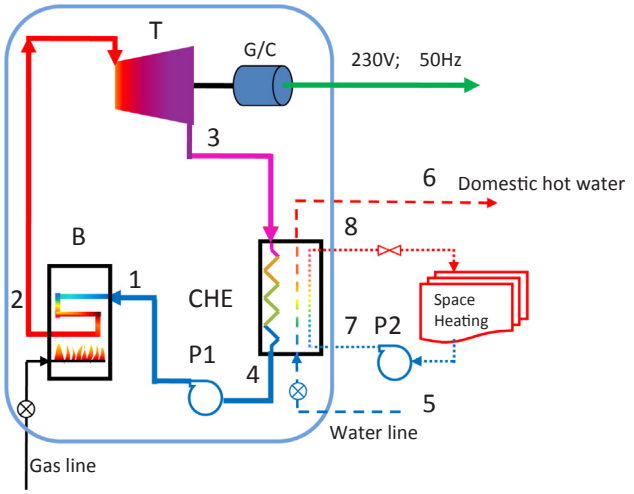

Fig. 1. Micro-CHP prototype basic scheme in the co-generator mode of operation (Legend: [B] gas Burner and evaporator, [T] micro vapor Turbine, [G/C] electrical Generator and Converser, [CHE] Condenser Heat Exchanger, [P1,2] circulating and pressurizing Pumps).

domestic hot water system where the heated water from the public grid after passes the condenser is discarded.

Previous work (to be reported in the first paper of the series) led to the selection of the turbine, in this case, a slow rotating semi-hermetic 1 kW scroll expander with maximum operating temperature and pressure of 175 °C and 13.8 bar, respectively. In the same vein, to avoid a radial centrifugal pump rotating at an exceedingly large speed, a pump P1 of the volumetric type, namely, a rotary-vane pump integrated in a pump-motor unit, was adopted. For the condenser, a compact plates heat exchanger with capacity to transfer up to 27 kW heat power was chosen. One of the basic design requirements was the direct vaporization of the fluid in the gas burner and heat exchanger B, but as such a component is not available in the market due to its small size, an in-house solution was specifically developed for it. Finally, the working fluid that was found to assure the best compromise (of performance, safety and commercial availability in the short-term, taking into consideration the needs of both circuits of domestic hot waters) is R245fa.

3. Model

The leitmotif of this work is to aid the design and control of a boiler/micro-CHP by affording an adaptive model capable of making realistic predictions of its quasi-steady behavior. This model has a modular architecture implemented in FORTRAN code, with a small general core and an open library of sub models for the components. The library includes the module *Refprop* of NIST [22], to compute thermodynamic and transport properties of a wide number of industrial fluids. The purpose of this architecture, which main concepts are presented below, is to ease the adaptation of the model to any micro-CHP, given its configuration and components.

Each sub model of the library corresponds to a functional component of the micro-CHP (e.g., pump, gas burner and evaporator, condenser, vapor turbine), that may include a controller (e.g., a speed controller of the shaft of the turbine), made concrete in a specific unit of a particular manufacturer. It can be a purely empirical model (e.g., manufacturer's characteristic curves of a turbine), a medium level semi-empirical model (e.g., a three zone Logarithmic Mean Temperature Difference model of a condenser heat exchanger) or a more or less complex semi-empirical model (e.g., a spatially detailed control volume model of an evaporator). In the latter case, to spare computation time, the sub model's main relationships among input/output variables can be emulated with pseudo-characteristic curves consisting, for instance, in a neural network.

In a model of a micro-CHP with m components (the overall micro-CHP itself can be envisaged as a "component") and n main output variables $(x_1,...,x_n)$, the sub model of component k is mathematically expressed by a set of m_k equations ($\sum_{k=1}^{m} m_k = n$):

$$f_i(x_1,...,x_n) = 0, i = i_k,...,i_k + (m_k - 1) \text{ with } i_1 = 1 \text{ and } i_k = i_{k-1} + m_{k-1} (k = 2,...,m) \quad (1)$$

Variables x_j can be thermodynamic (e.g., pressure, temperature, vapor quality of two-phase mixture, density or specific enthalpy) or hydrodynamic (mean cross section flow speed or mass flow rate) properties of the working fluid at notable points of the micro-CHP circuit (e.g., entrance or exit of components), or operating variables of components (e.g., rotation speed of the turbine shaft or heat flux transferred to the working fluid in the evaporator), characterizing the steady-state of the micro-CHP compatible with the user demand conditions and the controls imposed. Functions f_i depend effectively only on a more or less restrict subset of variables x_j, namely those concerning component k, and may have linear and non-linear parts, the latter of which, in some cases, isn't formalized analytically (i.e., it is only defined algorithmically). At the core of the code implementing the architecture is a powerful numerical solver of the non-linear system of equations (1), formally cast into the pseudo-linear matrix form:

$$A \cdot X = B(X) \quad (2)$$

In Eq. (2): $X(n \times 1)$ is the column-array of variables x_j; $A(n \times n)$ is a non-singular matrix of constant coefficients coping with the linear part of functions f_i, which, if non-existent, are numerically enforced (e.g., by adding a particular variable x_j to both members of the corresponding equation); and $B(n \times 1)$ stores the non-linear parts of functions f_i as pseudo-constant free terms. The system is solved with the following mixed direct-iterative scheme:

$$X^{(l+1)} = A^{-1} \cdot B(X^{(l)}), \quad \text{for } l = 0,1,2,... \quad (3)$$

It starts from an initial guess $X^{(0)}$, and ends after a stopping criterion is satisfied, e.g., when the norm of the residues column-array $R^{(l)} = B(X^{(l)}) - A \cdot X^{(l)}$ is lower than a given small positive threshold. Further numerical details, such as, the numerical dumping sub schemes, are not given here for lack of space.

In the following subsections, specific sub models for the components of the micro-CHP are presented. When no confusion arises, for simplicity, the notation used for the variables omits the reference to the respective component (usually denoted by a super index).

3.1. Condenser sub model

The condenser is a customized compact plates heat exchanger (cf. Section 2). The inputs of the condenser sub model can be split into:

(i) fixed design parameters (e.g.: length L_p, width W_p and number N_p of plates; Chevron angle β and step distance p_{co} of the plates' corrugation wavelets; and the configuration of the hot and cold fluids flow through the channels between the plates shown, in this case, in Fig. 2) determining notably the total heat transfer area A between the hot and cold fluids.
(ii) Fixed operation inputs, such as, the cold fluid (liquid water) and the hot fluid (condensing thermal fluid), and the fouling factors $(R''_{f_w}, R''_{f_f})[\text{m}^2 \cdot \text{K/W}]$ of the surfaces bathed by each fluid,
(iii) Variable operation external inputs (customer demand conditions), namely, the inlet ($T_{w,in}$) and outlet ($T_{w,out}$) temperatures and the mass flow rate $\dot{m}_w$ of water.
(iv) Variable operation internal inputs, i.e., the inlet temperature $T_{f,in}$ and pressure $p_{f,in}$ of the hot vapor fluid.

The main outputs of the sub model are:

(I) The mass flow rate $\dot{m}_f$ and the outlet temperature $T_{f,out}$ and pressure

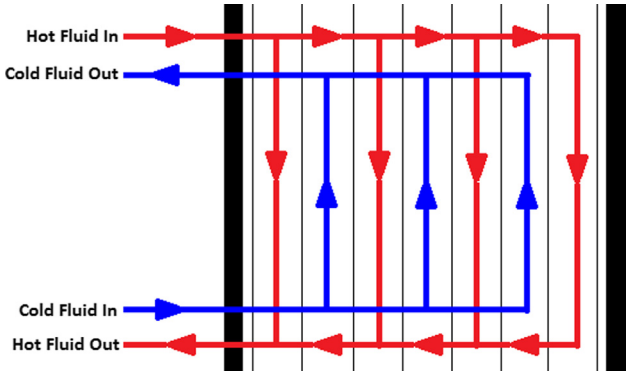

Fig. 2. Configuration of the hot (thermal fluid following the red lines) and cold (water following the blue lines) fluids flow through the channels between the plates of the heat exchanger. (For interpretation of the references to color in this figure legend, the reader is referred to the web version of this article.)

$p_{f,out}$ of the condensed thermal fluid;

(II) The heat flux $\dot{Q}$ transferred (and the corresponding overall heat transfer coefficient U [W/m^2·°C]) from the thermal fluid to the water (heat losses to the ambient are neglected) and the heat exchanger efficiency ε.

Within the micro-CHP overall model, the condenser sub model supplies the following three main functions (see Eq. (1)):

$$\dot{m}_f, T_{f,out}, p_{f,out} = \dot{m}_f, T_{f,out}, p_{f,out}(T_{f,in}, p_{f,in}) \tag{4}$$

The former equations are then coupled with the appropriate thermodynamic state equations of the thermal fluid in the liquid phase, to obtain the density $\rho_{f,out}$, specific enthalpy $h_{f,out}$ and specific entropy $s_{f,out}$ of the fluid at the exit of the condenser:

$$\rho_{f,out}, h_{f,out}, s_{f,out} = \rho_f, h_f, s_f(T_{f,out}, p_{f,out}) \tag{5}$$

As the pressure loss $|p_{f,out} - p_{f,in}|$ is more than one order of magnitude lower than either $p_{f,in}$ or $p_{f,out}$, and the same is true on the side of water, the condenser model is subdivided into a purely thermal sub model (taking $p_{k,out} \approx p_{k,in} \equiv p_k$ in the calculation of any thermodynamic and transport property of the thermal fluid [$k \equiv f$] and the water [$k \equiv w$]) and a hydraulic sub model (assuming that $T_{f,out} \approx T_{f,in}$), which are mutually decoupled.

The thermal part of the sub model is based on the general Logarithmic Mean Temperature Difference (LMTD) method of thermal analysis of heat exchangers [23]. To cope with the large variations of the global heat transfer coefficient U and of the rate of heat capacity C_f [W/K] of the thermal fluid induced by its phase change, the LMTD method is applied stepwise in three zones of the condenser, following the stream of the thermal fluid, in which this is, respectively, in: (1) vapor phase (superheated vapor), (2) vapor and liquid phases (condensing vapor), and (3) liquid phase (saturated or subcooled liquid). Properties of the fluids in each zone are denoted by a sub-index indicating if they refer to the entrance (*in*) or exit (*out*) of the zone in the sense of the fluids flow, and by a sub-sub-index with the zone number, such as, x_{f,in_1} or y_{w,out_2}. Notice that, following the streams of the fluids (in counter-flow): $x_{f,in_1} = x_{f,in}$, $x_{f,in_i} = x_{f,out_{i-1}} (i = 2,3)$ and $x_{f,out_3} = x_{f,out}$; but $y_{w,in_3} = y_{w,in}$, $y_{w,in_i} = y_{w,out_{i+1}} (i = 2,1)$ and $y_{w,out_1} = y_{w,out}$. Besides, as the phase changing fluid (f) does not invert the flow sense in the heat exchanger (see Fig. 2), the fundamental equation of the LMTD method is applied independently in each zone, i.e.:

$$\dot{Q}_i = A_i \cdot U_i \cdot (F_i \cdot \Delta_{lm_i}) \text{ with:} \tag{6}$$

$$\Delta T_{lm_i} = \frac{\Delta T_{1_i} - \Delta T_{2_i}}{ln(\Delta T_{1_i} / \Delta T_{2_i})} \tag{7}$$

where

$$\Delta T_{1_i} = T_{f,in_i} - T_{w,out_i} \tag{8}$$

$$\Delta T_{2_i} = T_{f,out_i} - T_{w,in_i} \tag{9}$$

This understood, the model is solved numerically in two parts.

The first part comprehends the direct sequential calculation of: (i) the specific enthalpies h_{w,in_3} and h_{w,out_1}, from the water thermodynamic state equations; (ii) the total rate of heat transfer $\dot{Q}$ from the thermal fluid to the water (neglecting losses to the ambient), computed with Eq. (10); (iii) the temperatures $T_{f,in_2} = T_{f,out_2} = T_{f,sat}(p_f)$ of isothermal condensation of the (simple) thermal fluid in zone 2; and (iv) the specific enthalpies $h_{f,in_2} = h_{f,out_2}$ and h_{f,in_1} (at the inlet) from the fluid thermodynamic state equations.

$$\dot{Q} = \dot{m}_w \cdot (h_{w,out_1} - h_{w,in_3}) \tag{10}$$

The second part is an iterative scheme starting with a first guess for $T_{f,out} = T_{f,out_3}$. After the calculation of $h_{f,out_3}(T_{f,out_3}, p_f)$, the mass flow rate $\dot{m}_f$ and the heat transfer rates $\dot{Q}_i$ in each zone can be computed successively in this way:

$$\dot{m}_f = \frac{\dot{Q}}{h_{f,in_1} - h_{f,out_3}} \tag{11}$$

$$\dot{Q}_i = \dot{m}_f \cdot (h_{f,in_i} - h_{f,out_i}) \quad \text{for } i = 1,2,3 \tag{12}$$

The next step is the determination of the intermediate specific enthalpies and temperatures of the water:

$$h_{w,out_3} = h_{w,in} + \frac{\dot{Q}_3}{\dot{m}_w} \tag{13}$$

$$h_{w,in_1} = h_{w,out} - \frac{\dot{Q}_1}{\dot{m}_w} \tag{14}$$

$$T_{w,out_i}(h_{w,out_i}, p_w) \quad \text{for } i = 1,3 \tag{15}$$

The global heat transfer coefficient U_i in zone i is then estimated (neglecting the conductive thermal resistance of the plates) through:

$$U_i = \frac{1}{\frac{1}{h_{f_i}} + R''_{f_f} + R''_{f_w} + \frac{1}{h_{w_i}}} \quad \text{for } i = 1,2,3 \tag{16}$$

To compute the convection coefficients at the hot (h_{f_i}) and cold (h_{w_i}) surfaces of the plates in the various zones, the empirical correlations of Muley and Manglik [24], Thonon [25], Maslov and Kovalenko [26], Kumar [27] and Wanniarachchi [28], for homogeneous fluids, and of Yan et al. [29] and Han et al. [30], for condensing fluids, were surveyed *a priori*. Ultimately, the following correlations were adopted: (i) Thonon [25] for h_{f_1}; (ii) Han et al. [30] for h_{f_2}; and (iii) Maslov and Kovalenko [26] for h_{f_3} and $h_{w_i} (i = 1,2,3)$. In the lack of information of the manufacturer, the parameters (β, p_{co}) of the plates were determined with reverse engineering by jointly fitting the manufacturer's selection calculations data for the total heat transfer area A, the overall mean coefficient $\overline{U}$ and the logarithmic mean temperature difference $\overline{\Delta T_m}$. Common procedures/parameters of the three correlations adopted are: (i) fluid properties computed at the mean fluid temperature in the zone; (ii) hydraulic diameter D_h of the flow through the channels between the plates; (iii) basic mass flow rate per unit cross section area G; (iv) Prandtl number of the fluid, $Pr = c_p \cdot \mu / K$; (v) basic Reynolds number of the flow, $Re = G \cdot D_h / \mu$; (vi) Nusselt number of convection, $Nu = D_h \cdot h / K$; and (vii) formal correlation for Nu:

$$Nu = C_1 \cdot Re'^{C_2} \cdot Pr^{1/3} \tag{17}$$

Specific parts of the correlations for this particular condenser ($\beta \approx 30°$ and $50 \leq Re \leq 15000$) are:

Thonon [25]:

$$C_1 = 0.2946, C_2 = 0.7, Re' = Re \tag{18}$$

Maslov and Kovalenko [26]:

$$C_1 = 0.78,\ C_2 = 0.5,\ Re' = Re \tag{19}$$

Han et al. [30]:

$$\begin{cases} C_1 = 11.22\cdot\left(\frac{p_{co}}{D_h}\right)^{-2.83}\cdot\left(\frac{\pi}{2}-\beta\right)^{-4.5}, \\ C_2 = 0.35\cdot\left(\frac{p_{co}}{D_h}\right)^{0.23}\cdot\left(\frac{\pi}{2}-\beta\right)^{1.48}, \\ Re' = \frac{G'\cdot D_h}{\mu_{sat\,l}}, \\ G' = G\cdot\left(1 + 0.5\cdot\left(\sqrt{\frac{\rho_{sat\,l}}{\rho_{sat\,v}}}-1\right)\right) \end{cases} \tag{20}$$

The calculation of the rates of heat capacity of both fluids through each zone follows:

$$C_{k_i} = \dot{m}_k\cdot\frac{h_{k,out_i}-h_{k,in_i}}{T_{k,out_i}-T_{k,in_i}} \quad \text{for } k = f,w \text{ and } i = 1,2,3 \tag{21}$$

Taking into account that $F_2 = 1$ (because $C_{f_2} \to \infty$ due to the thermal fluid isothermal condensation), Eqs. (6) and (7) can be immediately used to estimate the heat transfer area A_2. Afterwards, using the best available guess for area A_1 (the first guess can be, e.g., $A_1 = 0.7\cdot(A-A_2)$, recalling that the total area A can be computed at once from the model inputs), Kandlikar and Shah's [31] correlations for factor F, for a variety of plates heat exchangers, are applied to zone $i = 1$. Specifically, the condenser corresponds to the arrange #112 of these authors, Fluids 1 and 2 standing, respectively, for the water and the thermal fluid (see Fig. 2). Their extensive numerical tables for this arrange were found to be finely fitted with the following simple interpolation scheme, based on 12 coefficients $c_{jkl}(j,k = 1,2;l = 0,1,2)$:

$$F\left(NTU = \frac{U\cdot A}{C_{min}}, R = \frac{C_{min}}{C_{max}}, N_p\right) = 1 + a_1\cdot NTU + a_2\cdot NTU^2 \tag{22}$$

where

$$a_j = (b_{j1} + b_{j2}\cdot R)\cdot R \quad \text{for } j = 1,2 \tag{23}$$

$$b_{jk} = c_{jk0} + c_{jk1}\cdot N_p + c_{jk2}\cdot N_p^2 \quad \text{for } j,k = 1,2 \tag{24}$$

In Eq. (22): NTU is the non-dimensional Number of (heat) Transfer Units and $C_{min}, C_{max} = min,max\{C_1,C_2\}$, with C_m standing for the rate of heat capacity of Fluid $m = 1,2$.

Eqs. (6) and (7) are now used to get the heat transfer area A_1, from which A_3 can be estimated as:

$$A_3 = A - A_1 - A_2 \tag{25}$$

This allows a second use of Kandlikar and Shah's correlations to calculate factor F_3. The iteration closes at zone $i = 3$ of the condenser with the following two steps:

$$\Delta T_2 = \Delta T_1\cdot e^{-\frac{\Delta T_1-\Delta T_2}{\Delta T_{lm}}} \tag{26}$$

$$T_{f,out} = T_{f,out_3} = \Delta T_2 + T_{w,in_3} \tag{27}$$

In Eq. (26): the logarithmic mean temperature difference $\Delta T_{lm} \equiv \Delta T_{lm_3}$ is computed from $(\dot{Q}_3,F_3,U_3,A_3)$ with Eq. (6); and ΔT_1 and ΔT_2 in the right member side are best available guesses based on Eqs. (8) and (9), the latter of which is now updated. Eq. (26) itself derives from Eq. (7) in a way that assures the convergence of the iterative scheme. Finally, in Eq. (27), Eq. (9) is used again, this time with the updated guess of ΔT_2, to produce a new guess for the main output variable $T_{f,out}$.

The occurrence of a pinch point operation condition is further monitored by verifying if, at any iteration, one or both the following inequalities become true:

$$T_{w,out_3} > T_{f,in_3} \tag{28}$$

and

$$T_{w,in_1} > T_{f,out_1} \tag{29}$$

Obviously, in this case, the imposed input operation conditions are physically impossible. A sufficient condition to avoid this occurrence is:

$$T_{w,out} \leqslant T_{f,sat}(p_{f,in}) \tag{30}$$

However, if desired, the model can also be used to determine the maximum value of $T_{w,out}$ compatible with all the other given inputs, for a strict pinch point operation condition to occur. The numerical scheme used for this purpose is very simple but effective: to progressively lower $T_{w,out}$, starting from the initially given value, till inequality (28) (the most exigent of the two conditions) becomes a strict equality.

Finally, for completeness, the overall average global heat transfer coefficient $\overline{U}$ and thermal efficiency $\bar{\varepsilon}$ of the condenser are computed in this way (see, e.g., Kedziersky [32]):

$$\overline{U} = \sum_{i=1}^{3}\frac{A_i}{A}\cdot U_i \tag{31}$$

and

$$\bar{\varepsilon} = 1\Big/\sum_{i=1}^{3}\frac{\dot{Q}_i}{\dot{Q}}\cdot\frac{1}{\varepsilon_i} \tag{32}$$

The hydraulic part of the sub model gives directly the pressure drop Δp_f for the thermal fluid as:

$$(p_{f,out}-p_{f,in}) = \Delta p_f = \Delta p_{in} + \sum_{i=1}^{3}\Delta p_i + \Delta p_{out} + \Delta p_g \tag{33}$$

The terms Δp_{in} and Δp_{out} represent the pressure drop, respectively, at the entrance distributor and at the exit collector, being given by (Kumar [27]):

$$\Delta p_k = -0.7\cdot\frac{1}{2}\frac{G_k^2}{\rho_{f,k}} \quad \text{with } k = in,out \tag{34}$$

In Eq. (33): G_k is the mass flow rate per unit area of cross section of manifold k (e.g., for a circular duct with diameter D_k, it would be: $G_k = 4\dot{m}_f/\pi D_k^2$).

The intermediate terms Δp_i are the pressure drops in the various condenser zones. Following Kumar [27], for the homogeneous phase zones, the pressure drop is due to friction at the walls of the channels and can be quantified by a friction factor f:

$$\Delta p_i = -4f_i\cdot\frac{L_i}{D_h}\cdot\frac{1}{2}\frac{G^2}{\rho_{f,i}} \quad \text{for } i = 1,3 \tag{35}$$

with

$$f_i = 915\cdot Re_i^{-0.25} \quad \text{for } i = 1,3 \tag{36}$$

In Eqs. (35) and (36): G and Re are already introduced above (before Eq. (12)); L_i is the zone length along the flow; and all fluid properties are calculated at the mean temperature in the zone.

The computation of Δp_2 in the condensation zone is made according with Han et al. [30], in the following way:

$$\Delta p_2 = \Delta p_{2f} + \Delta p_{2m} \tag{37}$$

with:

$$\Delta p_{2f} = -4f_2\cdot\frac{L_2}{D_h}\cdot\frac{1}{2}\frac{G'^2}{\rho_{f,satl}} \tag{38}$$

$$\Delta p_{2m} = G^{prime2}\cdot(v_{f,satv}-v_{f,satl})\cdot\Delta x_{f_2} \tag{39}$$

$$f_2 = C_3\cdot Re_i^{C_4} \tag{40}$$

$$C_3 = 3521.1\cdot\left(\frac{p_{co}}{D_h}\right)^{4.17}\cdot\left(\frac{\pi}{2}-\beta\right)^{-7.75} \quad (41)$$

$$C_4 = -1.024\cdot\left(\frac{p_{co}}{D_h}\right)^{0.0925}\cdot\left(\frac{\pi}{2}-\beta\right)^{-1.3} \quad (42)$$

In Eqs. (37)–(39): Δp_{2f} is the pressure loss due to friction, with friction factor f_2 given by Eqs. (40)–(42) (note the similarity among Eqs. (41), (42) and (20)); Δp_{2m} is the pressure gain due to linear momentum conservation in the condensation process; G' is the modified G defined by Eq. (20); $v_f = 1/\rho_f$ designates the fluid specific volume; and the factor $\Delta x_{f_2} = (x_{f,in_2} - x_{f,out_2})$ in Eq. (39) is the drop of vapor quality of the thermal fluid in zone 2, which, in our case, is equal to one (total condensation).

Finally, the gravity term Δp_g represents a pressure gain in this case (see Fig. 2), given by:

$$\Delta p_g = -g\cdot\overline{\rho_f}\cdot(z_{f,out} - z_{f,in}) \approx g\cdot\overline{\rho_f}\cdot L_p \quad (43)$$

3.2. Pump sub model

The present sub model models a specific component composed of a rotary vane pump, a hermetic magnetic coupling and an electrical motor with a rotational speed controller. The sub model inputs can be subdivided into:

(i) Constant characteristics of the component, such as: the pump displacement α [m³] and suction duct diameter D_s, and the component characteristic curves supplied by the manufacturer (given below).
(ii) Constant operating conditions: working fluid (in the liquid phase).
(iii) Variable operating conditions: of the component (the rotational speed N) and of the fluid (mass flow rate $\dot{m}_f$, pressure and temperature at the entrance of the pump, $(p_{f,in}, T_{f,in})$).

The outputs are:

(I) main set of iterated variables: fluid properties at the outlet $(p_{f,out}, T_{f,out})$.
(II) Auxiliary set of iterated variables: fluid properties at the inlet $(\rho_{f,in}, s_{f,in}, h_{f,in})$ and outlet $(h_{f,out})$, flow rate $\dot{V}_{f,in}$ (referred to the entrance conditions, though $\dot{V}_{f,out} \approx \dot{V}_{f,in}$) and fluid pressure rise Δp_f.
(III) Set of variables computed directly in the end: inlet fluid variables (speed $V_{f,in}$ and available net positive suction head $NPSH_{af}$) and component variables of operation (pump net positive suction head required $NPSH_{rf}$ to avoid cavitation, hydraulic power $\dot{W}_{f,in} \equiv P_h$ supplied to the fluid and volumetric efficiency η_v; electrical power consumption P_e of the motor; and overall efficiency η of the component).

The ordered body of equations for the iterated variables is:

$$\rho_{f,in}, s_{f,in}, h_{f,in} = \rho_f, s_f, h_f(p_{f,in}, T_{f,in}) \quad (44)$$

$$\dot{V}_{f,in} = \frac{\dot{m}_f}{\rho_{f,in}} \quad (45)$$

$$\Delta p_f:\ \dot{V}_{f,in} = \alpha\cdot N\cdot\eta_{vw}\left(\Delta p_f\cdot\frac{\rho_{w0}}{\rho_{f,in}}, N\right) \quad (46)$$

$$p_{f,out} = p_{f,in} + \Delta p_f \quad (47)$$

$$h_{f,out} = h_{f,in} + \frac{h_{f,out_i} - h_{f,in}}{\eta_{th}} \quad (48)$$

with

$$h_{f,out_i} = h_f(p_{f,out}, s_{f,in}) \quad (49)$$

$$T_{f,out} = T_f(p_{f,out}, h_{f,out}) \quad (50)$$

Only Eqs. (47) and (50) are explicitly incorporated in the main system (1) of the micro-CHP model, thus forming the core of the group. The others are auxiliary equations. Eqs. (44), (49) and (50) use thermodynamic state functions of the fluid. Eq. (46), implicit in the output variable Δp_f, involves the manufacturer's characteristic curve of volumetric efficiency $\eta_{vw}(\Delta p, N)$ of the pump for water in reference conditions (to which correspond, namely, the density ρ_{w0}). The extrapolation of this curve for the micro-CHP working fluid is based on the usual similarity hypotheses in turbomachinery (both fluids viscosity are of the same order of magnitude, namely, $\mu_f < \sim \mu_{w0}$). From the literature (e.g., Cherkasski [33]) and the analysis of the manufacturer's characteristic data of the pump, the following empirical form can be assumed for this curve:

$$\eta_{vw}(\Delta p, N) = 1 - c(N)\cdot\Delta p \quad (51)$$

with

$$c(N) = a\cdot N^b (b < 0) \quad (52)$$

In Eqs. (48) and (49): h_{f,out_i} is the specific enthalpy of the fluid at the outlet for an ideal isentropic compression in the pump, and η_{th} is the thermo-hydrodynamic isentropic efficiency of the pump, roughly given by its characteristic curve of hydraulic efficiency η_h, which, for this type of pumps, is very high and practically constant, namely, $\eta_h \sim 0.98-1$ [33,34], allowing η_{th} to be treated as a simple input parameter of the sub model.

At the end of the iteration, the group (III) of output variables of the sub model can be calculated with the following equations:

$$V_{f,in} = \frac{4\dot{V}_{f,in}}{\pi D_s^2} \quad (53)$$

$$NPSH_{af} = \left(\frac{p_{f,in}}{\rho_{f,in}\cdot g} + \frac{V_{f,in}^2}{2g}\right) - \frac{p_{f,sat}(T_{f,in})}{\rho_{f,in}\cdot g} \quad (54)$$

$$NPSH_{rf} = NPSH_{rw}\left(\Delta p_f\cdot\frac{\rho_{w0}}{\rho_{f,in}}, N\right) \quad (55)$$

$$\dot{W}_{in} = \dot{V}_{f,in}\cdot\Delta p_f \quad (56)$$

$$P_e = \frac{\rho_{f,in}}{\rho_{w0}}\cdot P_{ew}\left(\Delta p_f\cdot\frac{\rho_{w0}}{\rho_{f,in}}, N\right) \quad (57)$$

$$\eta_v = \eta_{vw}\left(\Delta p_f\cdot\frac{\rho_{w0}}{\rho_{f,in}}, N\right) \quad (58)$$

$$\eta = \frac{\dot{W}_{in}}{P_e} \quad (59)$$

In Eq. (54), $p_{f,sat}(T_{f,in})$ is a thermodynamic state function of the fluid. In Eqs. (55), (57) and (58) appear, respectively, the characteristic curves of net positive suction head required to avoid cavitation of the pump $NPSH_{rw}(\Delta p, N)$, electric power consumed by the motor $P_{ew}(\Delta p, N)$ and volumetric efficiency $\eta_{vw}(\Delta p, N)$ of the pump, supplied by the manufacturer for water in reference conditions. The same similarity hypotheses mentioned above were used to extrapolate these curves for the micro-CHP working fluid. Notice that the characteristic curve $P_{ew}(\Delta p, N)$ and the overall efficiency η (Eq. (59)) characterize the behavior not only of the pump but of the whole component (pump, magnetic transmission and electrical motor). Just illustratively, for this particular component, $\eta \sim 0.4–0.5$ for $(1250 \leqslant N\,[\text{rpm}] \leqslant 2750)$ and $(3 \leqslant \Delta p\,[\text{bar}] \leqslant 12)$, and the function $P_{ew}(\Delta p, N)$ can be empirically fitted in the following way:

$$P_{ew}(\Delta p,N) = a_0 + a_1\cdot\Delta p + a_2\cdot\Delta p^2 \quad (60)$$

with

$$a_i = b_{0i} + b_{1i}\cdot N + b_{2i}\cdot N^2 (i = 0,1,2) \quad (61)$$

Finally, a cavitation condition of operation of the pump occurs presumably when: $NPSH_{af} \leq NPSH_{rf}$.

3.3. Burner and evaporator sub model

This sub model models the component shown in Fig. 3 (except for the exit duct of the flue gases, at the right, the whole set has cylindrical symmetry), comprehending a gas burner and a heat exchanger between the flue gases and the thermal fluid, capable of performing the direct evaporation of the latter. To reduce the burner head surface temperature, to ensure a proper and safe operation of the gas-burner and to reduce the combustion gases temperature and the risk of the working fluid thermal degradation an water cooled external chamber was designed (at the left in Fig. 3) and placed outside the heat exchanger [35]. A finely controlled (gas flow rate) and tuned (air-to-fuel ratio) premixed combustion of natural gas and air generates high temperature flue gases that flow mostly axially, to and fro, along the evaporator, as indicated by the arrows in Fig. 3. The thermal fluid flows in the spiral tubes, entering (liquid) at the top of the rightmost outer spire and exiting (superheated vapor) at the bottom of the rightmost inner spire. The heat exchange between the hot gases and the thermal fluid occurs mostly in crossflow but as the coaxial cylindrical plates confining the flow of the gases are thermally insulated at both surfaces, the gases follow a perfect energy cascade assuring an essentially counter-current heat exchange between the gases and the fluid. The component is assumedly peculiar and far from optimal but this is irrelevant here.

The sub model of the component contributes to the main system of equations (1) of the overall model with just two equations:

$$T_{f,out},p_{f,out} = T_{f,out},p_{f,out}(T_{f,in},p_{f,in},\dot{m}_f,\dot{Q}_c) \quad (62)$$

These equations, in which $\dot{Q}_c$ designates the thermal power liberated by the combustion of the gas, come from the models of the burner (combustion model) and the evaporator (heat exchanger model). For lack of space, the two models are only summarized below.

The inputs of the combustion model are: the molar composition of the natural gas (sub index g), $\nu'_{g,i}$ [kmol of component C_i/kmol of g] for $i = 1,...,m$ (from which the low heat value q_{c0} [MJ/kg] and the molar mass M_g [kg/kmol] can be estimated); the excess air ratio $\delta_{air} = \frac{\dot{m}_{air} - \dot{m}_{air,st}}{\dot{m}_{air,st}} = \frac{\nu'_{air} - \nu'_{air,st}}{\nu'_{air,st}}$, $st\equiv$ (stoichiometric conditions); the gas feeding pressure p_g and the ambient temperature $T_g = T_a$ at which both the gas and the air are admitted in the combustion chamber; the chamber's pressure p_b (the combustion is assumed isobaric); the thermal power $\dot{Q}_c$; and the thermal power losses $\dot{Q}_{pc} = \alpha_{pc}\cdot\dot{Q}_c$ from the hot gases to the refrigerating water and the ambient, which can be substituted for a set of more accessible inputs by incorporating a sub model for the losses.

The main outputs of the model are: the mass flow rate $\dot{m}_g$ of gas consumption; and the composition x_j= (mass fraction of product j) with $j = CO_2,H_2O,N_2,O_2$, the mass flow rate $\dot{m}_{gq}$ and the temperature $T_{gq,b}$ of the burnt gases (sub index gq).

The equations of a simple but useful combustion model express, in the first place, the molar conservation of atoms of each specie k = C,H,O,N, from which the mass composition x_j (and also the specific moles number ν'_{gq} [kmol of gq/kmol of g] and the molar mass M_{gq}) of the flue gases can be computed, assuming a complete combustion. The mass flow rates of fuel and combustion gases can then be estimated as:

$$\dot{m}_g = \frac{\dot{Q}_c}{q_{c0}} \quad (63)$$

$$\dot{m}_{gq} = \dot{m}_g\cdot\nu'_{gq}\cdot\frac{M_{gq}}{M_g} \quad (64)$$

Finally, the energy conservation equation of combustion, coupled with the state equations for the specific enthalpies h_j [kJ/kg] of the products j, can be used to compute the temperature $T_{gq,b}$:

$$(h_{gq}(T_{gq,b},p_b) - h_{gq}(T_a,p_b))\cdot\dot{m}_{gq} = (1-\alpha_{pc})\cdot\dot{Q}_c \quad (65)$$

where

$$h_{gq} = \sum_j x_j\cdot h_j \quad (66)$$

The inputs of the heat exchanger model are:

(i) The geometrical and physical parameters of the evaporator, such as: the internal and external diameters of the cylindrical plates and of the spiral tube, the material of the tube, the number n_t and spacing of the inner and outer spires.
(ii) The inlet properties of the burnt gases computed with the combustion model, namely, $(x_j,\dot{m}_{gq},T_{gq,in} = T_{gq,b},p_{gq,in} = p_b)$.
(iii) The mass flow rate $\dot{m}_f$ and the properties of the thermal fluid at the inlet $(T_{f,in},p_{f,in})$.

The outputs can be subdivided into four groups:

(I) The main global outputs: the outlet properties of the flue gases $(T,p,x_j)_{gq,out}$ and, above all, of the thermal fluid $(T,p)_{f,out}$ (see Eq. (61)).
(II) the main detailed outputs: the evolution of the properties $(T,p,x_j)_{gq}$ of the hot gases with the axial coordinate z_{gq} along the first and second passages (in crossflow with the tube), and the evolution of the properties $(T,p,x)_f$ of the thermal fluid (x_f is the vapor quality)

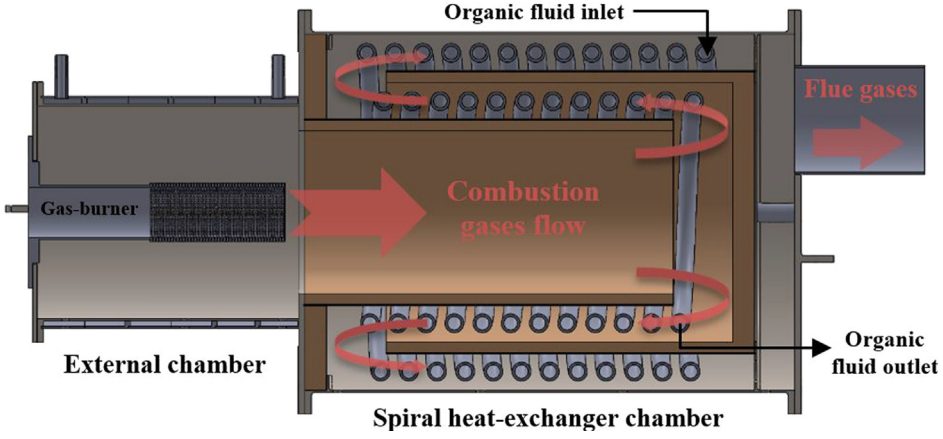

Fig. 3. 3D CAD view of an axial cut of the gas burner and evaporator of the first prototype of the micro-CHP.

with the curvilinear coordinate s_f (not to be confused with the specific entropy) along the axis of the spiral tube, crossing three main regions: $s_f \leqslant s_{f,eb}^-$ (liquid, $x_f = 0$), $s_{f,eb}^- < s_f < s_{f,eb}^+$ (two-phase, $0 < x_f < 1$) and $s_f \geqslant s_{f,eb}^+$ (vapor, $x_f = 1$).

(III) The secondary detailed outputs, such as: the evolutions of the local heat transfer coefficient U [W/m^2·K](s_f) and of the temperatures at the internal $T_t^-(s_f)$ and external $T_t^+(s_f)$ surfaces of the tube.

(IV) The secondary global outputs, such as: the overall efficiency ε of the heat exchanger.

The model main hypotheses and equations can only be described in very synthetic terms.

The hydraulic part of the model, dealing with the pressure variation of both fluids along the flow, is neglected due to its scarce relevance, i.e., it is simply assumed that: $p_{f,out} \approx p_{f,in}$ and $p_{gq,out} \approx p_{gq,in}$.

The thermal part of the model is presented successively for the hot gases and the thermal fluid.

The flow of the gases between each pair of cylindrical plates, from the beginning of the first passage to the end of the second passage, in cross flow with the spiral tubes of the thermal fluid, goes through adjacent control volumes CV_i, each one with a toroidal form with the same cylindrical symmetry as the whole drawing (Fig. 3) and enclosing one spire. The mass composition x_j of the gases is supposed to be frozen, except for the possible condensation of part of the water vapor near the exit of the evaporator, which occurs in high efficiency operation conditions of condensing boilers (typically, for $T_{gq} < 50$ °C). In this case, it is admitted that the condensates are drained out of the vapor flow. The energy conservation equation of the gases flowing through CV_i is:

$$(h_{gq,out_i} - h_{gq,in_i}) \cdot \dot{m}_{gq} = \sum_{j=j_{in_i}}^{j_{out_i}} -\dot{Q}_{ij} \tag{67}$$

with:

$$h_{gq,k_i} = h_{gq}(T_{gq,k_i}, p_{gq,k_i}) \quad \text{for } k = in,out \tag{68}$$

In Eq. (67), $\dot{Q}_{ij}$ (see Eq. (71)) is the heat flux from the hot gases in CV_i to the thermal fluid in CV_j (explained below). Eq. (68) involves a thermodynamic state function of the hot gases mixture.

On the side of the thermal fluid, control volume $CV_j (j_{in_i} \leqslant j \leqslant j_{out_i})$ is a section of the spire i of the tube (surrounded by the hot gases in CV_i) with variable length Δs_{f_j} along the tube axis. The energy conservation equation for the fluid flowing through CV_j is:

$$\left[(h_{f,out_j} - h_{f,in_j}) + \frac{1}{2}(V_{f,out_j}^2 - V_{f,in_j}^2) \right] \cdot \dot{m}_f = \dot{Q}_{ij} \tag{69}$$

with:

$$h_{f,k_j} = h_f(T_{f,k_j}, p_{f,k_j}, x_{f,k_j}) \quad \text{for } k = in,out \tag{70}$$

$$\dot{Q}_{ij} = U_{ij} \cdot (\Delta s_{f_j} \cdot \pi D_i^+) \cdot (\overline{T}_{gq_i} - \overline{T}_{f_j}) \tag{71}$$

In Eq. (69), the kinetic energy term is, most of the times, negligible. Eq. (70) involves a thermodynamic state function of the thermal fluid in the region of the tube (liquid, two-phase or vapor) where CV_j is located, which is indicated by the vapor quality x_{f,k_j}. In Eq. (71), the bars over the temperature symbols denote appropriate spatial averages in the respective control volumes, and U_{ij} is the local overall heat transfer coefficient (here referred to the outer surface of the tube section of CV_j) between the hot gases in CV_i and the thermal fluid in CV_j. In the computation of coefficient U_{ij}, the internal convection coefficient $h_{int_{ij}}$, in the regions where the thermal fluid is in homogeneous phase, is calculated with the fine empirical correlation of Gnielinski [23] for the Nusselt number:

$$Nu = \frac{(f/8) \cdot (Re - 1000) \cdot Pr}{1 + 12.7 \cdot (f/8)^{1/2} \cdot (Pr^{2/3} - 1)} \tag{72}$$

The Darcy friction factor f in Eq. (72) can be approximated by the correlation of Haaland [36] for the Moody diagram (in turbulent regime with $Re > 3000$). In the two-phase region, where the fluid is evaporating ($0 < x_{f,k_j} < 1$), the much more complex empirical procedure recommended by Coulson and Richardson [37] is used. The external convection coefficient $h_{ext_{ij}}$, on the side of the hot gases, is computed with a combination of empirical correlations taken from Grimson [38] and Incropera and DeWitt [23], for a cross flow with a cylindrical tube placed at a certain position along a row of tubes confined by upper and lower plates (but neglecting the curvature of both the tubes axis and the plates).

The group of equations for the thermal fluid in the CV_j is closed with the following mass conservation and state equations:

$$\rho_{f,out_j} \cdot V_{f,out_j} = \rho_{f,in_j} \cdot V_{f,in_j} \tag{73}$$

$$(\rho, T, x)_{f,out_j} = \rho_f, T_f, x_f(p_{f,out_j}, h_{f,out_j}) \tag{74}$$

The numerical scheme of calculation of the evaporator model involves various levels of nested iterative cycles. The outer (1st) cycle initiates with a guess for the exit properties of the flue gases (mainly, $T_{gq,out}$), and goes upstream the gas flow, from the outlet to the inlet of each $CV_i (i = n_t, n_t-1, \ldots, 2, 1)$, stopping when the corresponding guesses for the entrance properties, namely, for $T_{gq,in}$, approach sufficiently the input values. The 2nd cycle iterates the properties $(T, p, x; h, \rho, V)_{f,out_j}$ of the thermal fluid, going downstream the flow, from the inlet to the outlet of $CV_j (j = j_{in_i}, \ldots, j_{out_i})$ for each CV_i. In the homogeneous regions, the numerical integration is performed in order to the curvilinear coordinate s_f along the tube axis, with a constant step Δs_{f_j}, different for the liquid and vapor phase regions. In the liquid phase region, the overpassing of the border with the two-phase region (when $s_{f_j} > s_{f,eb}^-$) is detected through the condition $x_{f_j} > 0$. In the two-phase region, the numerical integration is performed in order to the vapor quality x_f, with a constant step Δx_{f_j}, so the length Δs_{f_j} of the CV_j becomes variable. This requires a special iterative procedure (3rd level cycle) at the end section of a spire. The crossing of the border with the vapor region (when $s_{f_j} > s_{f,eb}^+$) is also detected. The inner (4th level) iteration cycle serves to calculate the heat fluxes $\dot{Q}_{ij}$.

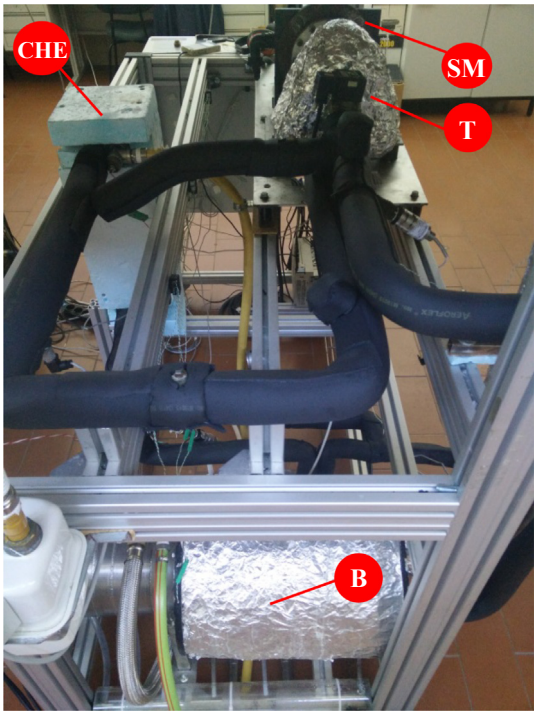

Fig. 4. Photograph of the micro-CHP experimental test rig (Legend: B – Gas burner and evaporator, T – micro-turbine, SM – Servo-motor, CHE – Condenser heat exchanger).

Table 1
Main components of the micro-CHP test rig.

Component	Type	Manufacturer	Characteristics
Turbine (T)	Scroll Expander	Air Squared (E15H022A-SH)	Nominal Output: 1 kWe Volume ratio: 3.5 Displacement: 14.5 cm^3/Rev. Max. speed: 3600 RPM Max. inlet pressure: 13.8 bara Max. Inlet temperature: 175 °C Net weight: 9 kg
Condenser (CHE)	Plate Heat Exchanger	GEA (GBS240H – 34)	Total Number of Plates: 34 Connection Diameter mm: 27 wt Empty: 6.8 kg Surface: 1,41 m^2
Pump (P1)	Rotary vane	Fluid-o-Tech (TMFROT201A)	Max. operative temperature: 70 °C Displacement: 0.1297 dm^3/h.rpm Speed range: 300 to 3500 rpm Max static pressure: 20 bar Unit weight: 2.7 kg
Burner (B)	Premix burner	Riello (RX 35 S/PV)	Output: 6–35 kW Fuel: Natural gas - LPG Operation: Modulating Modulation: Fan variable speed drive Combustion head: Cylindrical

The former detailed sub model of the component (specially the model of the evaporator), though much lighter than a standard CFD model, is still computationally too heavy to render its direct incorporation in the overall model convenient. In alternative, a large campaign of calculations was conducted throughout the relevant region of the space of the main inputs ($T_{f,in}$: 7.5–65 °C, $p_{f,in}$: 1–15 bara, $\dot{m}_f$: 0.02–0.17 kg/s, $\dot{Q}_c$: 5–35 kW_t) in order to emulate with a fast computing neural network the functions of Eq. (62), which can be considered the characteristic curves of the component. Some more details of the emulation methodology adopted are given in Section 5, in the context of the calibration and preliminary validation of the component sub model.

3.4. Scroll expander sub model

Scroll micro-expanders, contrary to scroll micro-compressors, are still little used in industry. Even in the literature [39] their behavior and characterization are still not settled. Specifically, the scroll expander (non-lubricated and with a hermetic magnetic coupling) is a "one-of-a-kind" component, incompletely characterized by the manufacturer and with some flaws of design. In fact, the sub model presented below is the result of a deep research on this expander that can't be presented here (e.g., Woodland et al. [40,41] and André et al., Costa et al. [42–45]. For the moment, the component doesn't include an electrical generator, the exposed shaft being directly coupled to a servomotor that acts as a brake with a speed N[rpm] (or torque) controller. So, the power output of the component is the mechanical power P delivered at the shaft and not an electrical power.

This understood, the component sub model inputs are:

(i) Constant characteristics of the expander: geometric parameters (volume ΔV_{adm} of the admission chamber and diameter D_{in} of the entrance duct) and volumetric efficiency or filling factor curve $\eta_v^*(N)$ for a reference gas or vapor fluid f^* (functions with super index) and, possibly, curve of thermo-hydrodynamic isentropic efficiency in adiabatic conditions $\eta_{th,ad}^*(N,r_p)$, $r_p = (p_{f,in}/p_{f,out})$ being the (absolute) pressure ratio of operation.
(ii) Constant characteristics of the whole component: instead of $\eta_{th,ad}^*(N,r_p)$, curve of mechanic and magnetic power losses $\dot{Q}_{p_{mec+mag}}(N)$ (independent of the fluid), curve of thermal power losses $\dot{Q}_{p_f}(T_{f,in})$ and curve of mechanic and magnetic efficiency $\eta_m\eta_{mag}^*(N,r_p)$.
(iii) Variable conditions of operation of the expander with the working fluid: inlet temperature and pressure $(T_{f,in},p_{f,in})$, outlet pressure $p_{f,out}$ or pressure ratio r_p, and mass flow rate $\dot{m}_f$.

Without entering into details, a well-designed component (which, unfortunately, is not the case) would have negligible thermal power losses (i.e., $\dot{Q}_{p_f} \approx 0$ corresponding to adiabatic operation conditions), as this is obviously desirable and simplifies the component modelling. In our case, the curve $\dot{Q}_{p_f}(T_{f,in})$ of the component, which makes it dispensable to measure the loss $\dot{Q}_{p_f}$ in the operating condition of interest, was obtained afterwards through the calibration process described in Section 5.

The outputs of the model can be subdivided into:

(I) the outlet temperature $T_{f,out}$ of the fluid (main output);
(II) the operational properties of the component: rotational speed N (main output) and mechanic power P delivered at the shaft (secondary output);
(III) The performance properties of the component (all secondary outputs): volumetric efficiency η_v, thermo-hydrodynamic isentropic efficiency η_{th} and mechanic-magnetic efficiency $\eta_m\eta_{mag}$.

The sub model commences by using the thermodynamic state equations of the working fluid (sub index f) and of the reference fluid (sub index f^*) to complete the characterization of the state of both fluids at the inlet of the expander, for the same $(T_{f,in} = T_{f^*,in}, p_{f,in} = p_{f^*,in})$ conditions:

$$v_{k,in},h_{k,in},s_{k,in} = v_k,h_k,s_k(T_{k,in},p_{k,in}) \quad \text{for } k = f,f^* \tag{75}$$

For the working fluid, the cross section mean speed $V_{f,in}$, the stagnation specific enthalpy $h_{f_0,in}$ and temperature $T_{f_0,in}$, and the isentropic stagnation pressure $p_{f_0,in}$ are determined additionally through:

$$V_{f,in} = \frac{4\dot{m}_f \cdot v_{f,in}}{\pi D_{in}^2} \tag{76}$$

$$h_{f_0,in} = h_{f,in} + \frac{V_{f,in}^2}{2} \tag{77}$$

$$T_{f_0,in},p_{f_0,in} = T_f,p_f(h_{f_0,in},s_{f,in}) \tag{78}$$

Applying the usual similarity hypotheses for compressible flows

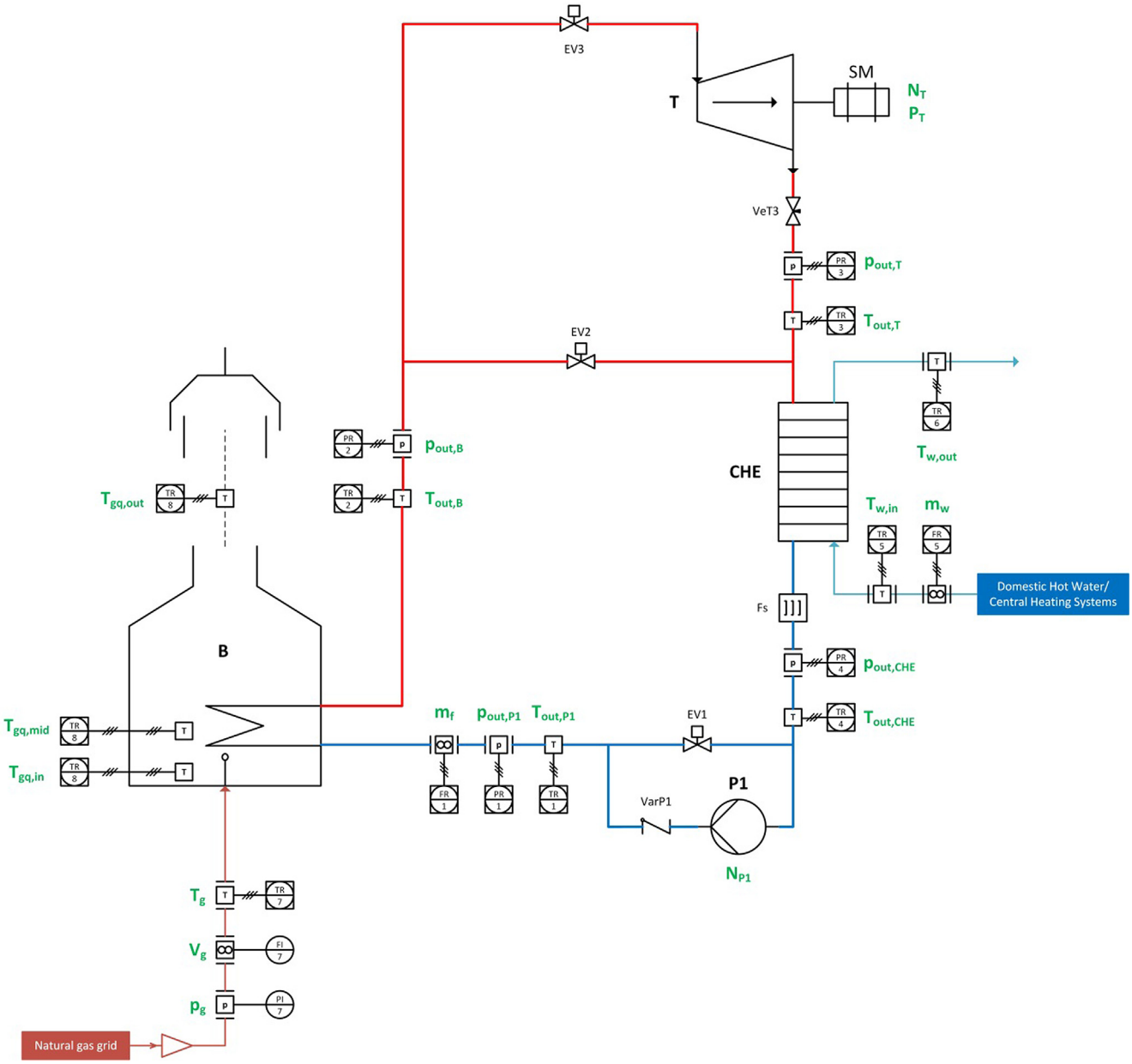

Fig. 5. Complete test rig sketch with all the components and measuring instruments. *Legend*: T – temperature sensor, p – pressure sensor, ∞ – flow sensor, ⋈ – electro-valve.

through turbomachines [46] (in this case, the inherent approximation is supposed to be admissible because the superheated vapors of organic thermal fluids $f \equiv$ R245fa and $f^* \equiv$ R134a have properties not too disparate), the inlet properties and mass flow rate $\dot{m}_{f^*}$ of the reference fluid flowing through the expander in physically similar conditions to the given inlet conditions of the working fluid are then computed with the following iterative procedure: a guess is made/available for $\dot{m}_{f^*}$; equations similar to (76)–(78) are used to produce new guesses successively for $V_{f^*,in}$, $h_{f_0^*,in}$, $T_{f_0^*,in}$ and $p_{f_0^*,in}$; and, closing the cycle, the old guess for $\dot{m}_{f^*}$ is substituted for the new one:

$$\dot{m}_{f^*} = \frac{p_{f_0^*,in}}{p_{f_0,in}} \cdot \sqrt{\frac{R_f \cdot T_{f_0,in}}{R_{f^*} \cdot T_{f_0^*,in}}} \cdot \dot{m}_f \tag{79}$$

In Eq. (79), R_f and R_{f^*} are the perfect gas constants, respectively, of the working and reference fluids. The speed N^* at which the expander must rotate to admit the mass flow rate $\dot{m}_{f^*}$ of the reference fluid, can now be computed from the curve of volumetric efficiency $\eta_v^*(N)$, by solving the following equation:

$$N^* \cdot \eta_v^*(N^*) = \frac{60 \cdot \dot{m}_{f^*} \cdot v_{f^*,in}}{\Delta V_{adm}} \tag{80}$$

Under the similarity hypotheses mentioned above, the speed N (first main output) at which the expander rotates when crossed by the working fluid in the given inlet conditions, to operate in physically similar conditions to the ones computed above for the reference fluid, is given by:

$$N = \sqrt{\frac{R_f \cdot T_{f_0,in}}{R_{f^*} \cdot T_{f_0^*,in}}} \cdot N^* \tag{81}$$

Depending on the inputs that are supplied, the mechanical power P_m delivered at the shaft before (in the perspective of the energy cascade through the component) mechanic and magnetic losses can be computed with the following equations:

Table 2
Instrumentation used to measure input/output variables.

Variables	Type	Model/Manufacturer	Accuracy
$T_{gq,in}$ $T_{gq,mid}$ $T_{gq,out}$	Thermocouple K	Type 'K' to IEC 584 mineral insulated 310 St. Steel 1.5 mm diameter; −40 to +1100 °C	± 0.4%
$T_{out,CHE}$ $T_{out,P1}$ $T_{out,B}$ $T_{out,T}$	Thermocouple K	Type 'K' to IEC 584 1.5 mm diameter; −40 to +1100 °C	± 0.4%
$T_{w,in}$ $T_{w,out}$ T_g	Pt100	Pt100 element to IEC 751 Class B	± 0.3%
$\dot{m}_w$	Dataflow Compact Transmitter	Grilamid TR55; 18% PTFE; 1–25 LPM	± 2%
$\dot{m}_f$	Magnetic Pickup	Omega, Turbine Flow Meter FTB-1411, 2.3–11.4 LPM	± 0.25%
$p_{out,CHE}$ $p_{out,T}$	Pressure transmitter	GEM 3100B 0010G, 0–10 bar, −40 to 120 °C	± 0.25%
$p_{out,P1}$	Pressure transmitter	GEM 3100B 0025G, 0–25 bar, −40 to 120 °C	± 0.25%
$p_{out,B}$	Pressure Transducer	OMEGA PXM35D0–300GV −70 to +149 °C 0–20.7 bar	± 0.25%
N_{P1}	DRIVER TMFE2	Fluid-o-tech, Driver TMFE2 for TMFR-TSFR PUMP; input: φ 230 V, 0–5 V; output: 3φ, 180 V, 30–120 Hz	(n.a.)
p_g	Security Valve	RECGAS RG-90 VIS MIN; 6 m^3(n)/h; 20 mbar	(n.a.)
$\dot{V}_g$	Diaphragm Gas Meter	Gallus G2.5, 0.025–4 m^3/h,	± 1.5%
N_T P_T	Servo Motor & Drive	Yaskawa Three-phase 400 V, SGDV-2R8A01 Model	(n.a.)

$$P_m = \begin{cases} \eta^*_{th,ad}(N^*,r^*_p)\cdot\dot{m}_f\cdot(h_{f,in}-h_{f,out_i})-\dot{Q}_{pf}(T_{f,in}) \\ \dot{Q}_{p_{mec+mag}}(N)/(1-\eta_m\eta^*_{mag}(N^*,r^*_p)) \end{cases} \quad (82)$$

with

$$h_{f,out_i} = h_f(p_{f,out},s_{f,in}) \quad (83)$$

$$r^*_p = r_p = \frac{p_{f,in}}{p_{f,out}} \quad (84)$$

The specific enthalpy $h_{f,out}$ and temperature $T_{f,out}$ (second main output) of the working fluid at the outlet of the expander derive, respectively, from the energy conservation equation for the fluid flow through the expander and from a thermodynamic state function of the fluid:

$$h_{f,out} = h_{f,in}-\frac{P_m+\dot{Q}_{pf}(T_{f,in})}{\dot{m}_f} \quad (85)$$

$$T_{f,out} = T_f(p_{f,out},h_{f,out}) \quad (86)$$

Finally, the various efficiencies ($\eta_v,\eta_{th},\eta_m\eta_{mag}$) of the component and the effective mechanical power P it delivers at the shaft (all secondary outputs), in the given condition of operation with the working fluid, derive either from similarity theory or from the definition of the efficiencies it selves:

$$\eta_v = \eta^*_v(N^*) \quad (87)$$

$$\eta_{th} = \frac{P_m}{\dot{m}_f\cdot(h_{f,in}-h_{f,out_i})}, \quad (88)$$

$$\eta_m\eta_{mag} = \eta_m\eta^*_{mag}(N^*,r^*_p) \quad (89)$$

$$P = \eta_m\eta_{mag}\cdot P_m \quad (90)$$

Summing up, the equations of the expander sub model in the main system (1) of the overall model can be cast into the form:

$$N,T_{f,out} = N,T_{f,out}(T_{f,in},p_{f,in},p_{f,out},\dot{m}_f) \quad (91)$$

3.5. Closure of the overall model

The present section uses a slightly alleviated notation from the one used in Sections 3.1–3.4. In particular, the reference to the fluid is substituted for a reference to the component: P1≡ (Pump), B≡ (Burner and evaporator), T≡ (Turbine or expander, in this case, not coupled to a generator) and CHE ≡ (Condenser Heat Exchanger). For example, the temperature $T_{f,out}$ in Eq. (4) of Section 3.1 (condenser sub model), is now denoted by $T_{out,CHE}$.

A first group of closure relationships of the overall model of the micro-CHP express the conservation of mechanical and thermal energy in the flow of the thermal fluid through the ducts linking the various components. In this case, taking into consideration, in what respects the mechanical energy, the large variations of pressure in the expander (T) and the pump (P1), and, in what respects the thermal energy, that the ducts are thermally insulated, these relationships are simply:

$$p_{in,k+1} \approx p_{out,k} \quad \text{for } k = (1,2,3,4) \equiv (\text{P1,B,T,CHE}) \quad (92)$$

$$T_{in,k+1} \approx T_{out,k} \quad \text{for } k = (1,2,3,4) \equiv (\text{P1,B,T,CHE}) \quad (93)$$

In these equations, the component sub index k varies in a cyclic permutation through the sequence (1,2,3,4), i.e., 5 ≡ 1.A second closure relationship expresses the mass conservation of the thermal fluid in the whole circuit, i.e., that, at any time instant, the mass m_0 of fluid initially injected into the circuit remains constant:

$$\sum_{k=1}^{4}(m_{k,k+1}+m_k) = m_0 \quad (94)$$

The same convention adopted for the component k sub index in Eqs. (92) and (93) applies to Eq. (94). The term $m_{k,k+1}$ represents the mass of fluid instantaneously occupying the duct linking the pair of components $(k,k+1)$, which, taking into account Eqs. (92) and (93), is simply given by:

$$m_{k,k+1} = \rho_{out,k}(T_{out,k},p_{out,k})\cdot V_{k,k+1} \quad (95)$$

where $V_{k,k+1}$ is the volume of the duct. The term m_k in Eq. (94) is the mass of fluid inside the component k (instantaneously) and, so, can be considered an extra output of the component sub model. Namely:

$$m_{P1} = m_{P1}(T_{in,P1},p_{in,P1},\dot{m}_f,N_{P1}) = \overline{\rho_{P1}}\cdot V_{P1} \quad (96)$$

$$m_B = m_B(T_{in,B},p_{in,B},\dot{m}_f,\dot{Q}_c) = \int_0^{s_{f,out}}\rho_f\cdot\frac{\pi D_i^{-2}}{4}\cdot ds_f \quad (97)$$

$$m_T = m_T(T_{in,T},p_{in,T},p_{out,T},\dot{m}_f) \approx 3.5\cdot\frac{60\cdot\dot{m}_f}{N_T[\text{rpm}]} \quad (98)$$

$$m_{CHE} = m_{CHE}(T_{in,CHE},p_{in,CHE}) \quad (99)$$

In Eq. (96), $\overline{\rho_{P1}}$ is the average fluid density inside P1, which can be approximated by: $\overline{\rho_{P1}} \approx (\rho_{in,P1}+\rho_{out,P1})/2 \approx \rho_{in,P1}$ and the density is a thermodynamic state function of the pair of basic properties (T,p). In Eq. (97): the sub index f of the thermal fluid is retained for clarity; and the integration is in order to the curvilinear coordinate s_f along the axis of the spiral tube of the evaporator. The coefficient 3.5 in Eq. (98) is, approximately, the number of turns of the scroll expander axis during which a fluid particle remains inside the internal chambers (see Spínola [47] for more details). Eq. (99), of the condenser sub model, is based on a linear hypothesis regarding the variation of the fluid temperature T_f (in the homogeneous phase regions) or the vapor quality x_f (in the two-phase region of condensation) throughout the condenser (Section 3.1).

Summing up, the main system (1) of 18 equations of the micro-CHP overall model operating in steady cogeneration mode is composed of:

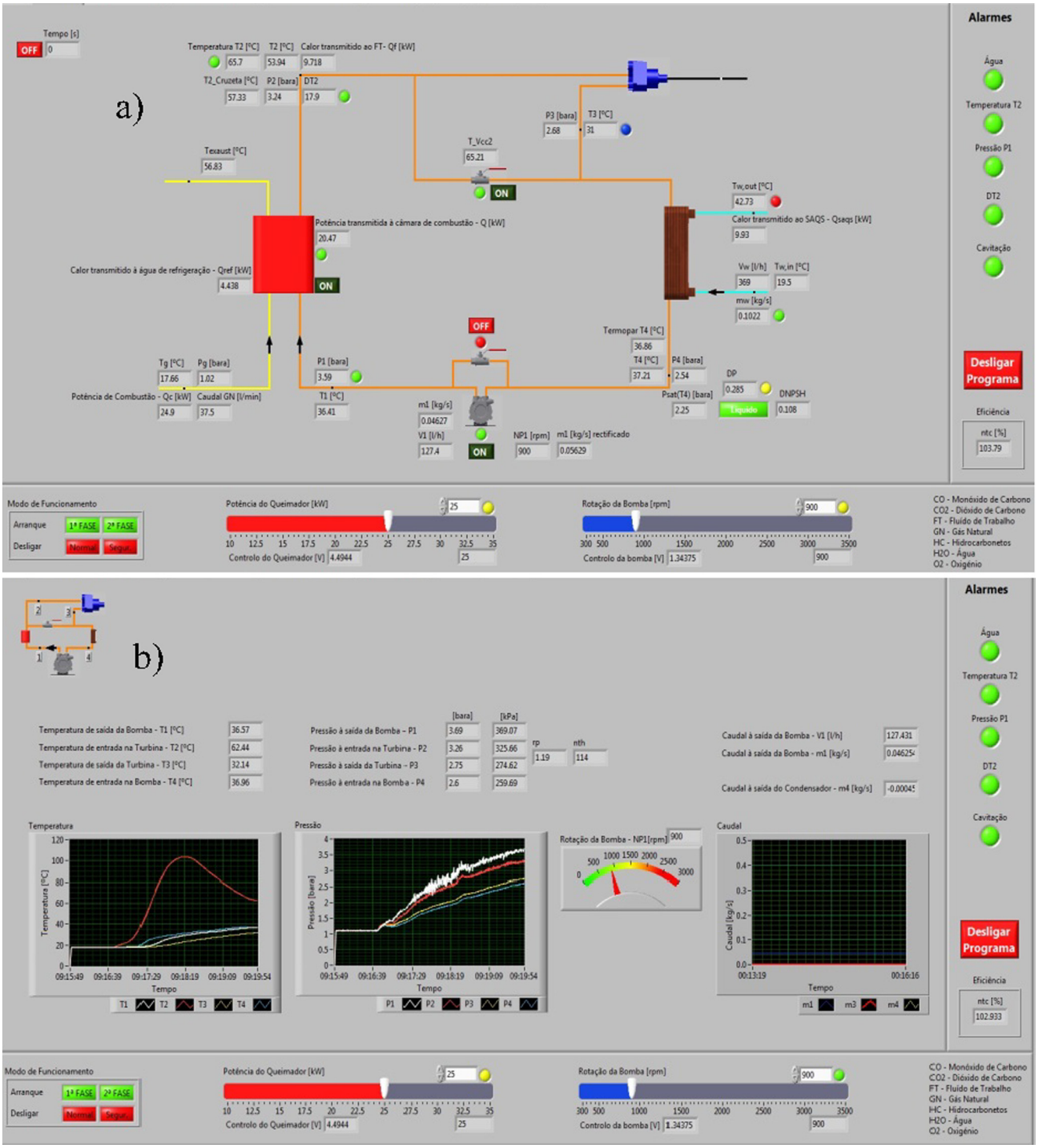

Fig. 6. LabVIEW user interface of micro CHP experimental rig: two illustrative panels (a) General control panel, (b) Measured data variation over time (temperature, pressure, mass flow).

(i) The Eq. (4) of the sub model of the condenser CHE.
(ii) The Eq. (47) (coupled with Eqs. (44)–(46)) and (50) (coupled with Eqs. (44), (48) and (49)) of the sub model of the pump P1.
(iii) The Eq. (62) of the sub model of the burner and evaporator B.
(iv) The Eq. (91) of the sub model of the expander T.
(v) The Eqs. (92) and (93) of mechanical and thermal energy conservation of the flow in the linkage ducts; and
(vi) The Eq. (94) (coupled with Eqs. (95)–(99)) of global mass conservation.

The natural (so to say) inputs of the model are the various sets of input parameters and fixed variables of the sub models of each component (Sections 3.1–3.4), together with the water client variables and the control variables of thermal power of combustion $\dot{Q}_c$ of the burner B (controlled via the natural gas flow rate $\dot{V}_g$) and rotational speed N_{P1} of the pump P1.

The 18 natural main output variables of the model are: the pairs of basic thermodynamic properties $(T_{in,k},p_{in,k})$ and $(T_{out,k},p_{out,k})$ of the thermal fluid at the inlet and outlet of each component k = P1,B,T,CHE; the mass flow rate $\dot{m}_f$ of the fluid through the circuit; and the control

Table 3
Output variables received by the measuring devices for a specific customer condition.

Cycle point	Temperature [°C]	Pressure [kPa]	Mass flow [kg/s]
1 (P1-B)	21.84	604.58	0.074
2 (B-T)	107.18	630.53	
3 (T-CHE)	81.87	199.04	
4 (CHE-P1)	20.70	183.77	
5 $Water_{in}$	20.85	–	0.10
6 $Water_{out}$	34.48	–	
Natural gas	23.13	102.00	0.26

variable of the speed of rotation N_T of the expander T. Secondary outputs of the model characterize more fully the flow of the thermal fluid and the operation, performance and control of the components.

4. Experimental setup

The micro-CHP has been designed and constructed in the laboratory at University of Coimbra without any concerns regarding space or volume in order to obtain ease of access to all components and sensors installed in the experimental test rig (Fig. 4).

The rotating vane pump (not visible in Fig. 4) that circulates and pressurizes the fluid through the pipeline has been positioned in the bottom in order to minimize cavitation risk. The direct evaporator (Burner + heat exchanger) (B) specially designed for this purpose has been placed also in the bottom in order to assure that, at startup, the fluid inside is completely in liquid phase thus avoiding hot spots and vapor bubbles inside. The scroll expander (T) is magnetically coupled to a servomotor (SM) instead of an electric generator and the generated electrical power is dissipated in a series of resistances. This expander has been placed at the top of the installation to ensure that the fluid inside is permanently in the vapor phase. Finally, the compact heat exchanger (CHE) is a plate type and is located at medium height. In this component both liquid and vapor phases can be found either when the system is shut down or in operation mode. Table 1 lists the type, parameters and manufacturers of the components available in the market and acquired for the micro-CHP test-rig.

Copper lines have been used to link the main components. Threaded connections have also been preferentially used for a more versatile and flexible test rig but in the future for pre-commercial equipment, the copper pipes should be welded for sealing purposes and reliability. The main components and the copper lines were involved with glass wool and polyurethane foam, respectively, to reduce the thermal losses in the circuit.

A schematic sketch of the facility is shown in Fig. 5 and includes the layout, all the micro-CHP components and the measuring devices. The measured variable appears in Fig. 5 in a green color next to each measuring instrument so as to read more conveniently. A temperature sensor and a pressure transducer were installed at the inlet and outlet of each main component. The mass flow rate of the R245fa, the pump rotation speed and the expander power generation and rotation speed were also measured.

The main characteristics of the control and measuring devices used in the test bench are given in Table 2. The natural gas feeding pressure p_g is kept constant at 20 mbar. Unfortunately, during the course of preliminary tests, the turbine flow meter (placed before the pump P1) planned to measure the mass flow rate $\dot{m}_f$ of the thermal fluid stopped working correctly.

Due to its great versatility and ease of programming, a PC-based hardware and software solution composed of National Instruments (NI) plates, LabJacks (LBJ), a Datalogger (DLO) and LabVIEW (acronym for Laboratory Virtual Instrument Engineering Workbench) was adopted to perform real-time acquisition, processing, control and data logging with user interface (Fig. 6) [48].

The recorded data by the LabVIEW developed program using the instrumentation referred in Table 2, point by point is presented in Table 3. This is an example of a specific case also used in the calibration where the micro-CHP operates in steady-state with the following imposed controls:

- thermal power of combustion of the burner B - $\dot{Q}_c$ = 13.82 kW
- rotational speed of the pump P1 - N_{P1} = 550 rpm
- speed of rotation of the expander T - N_T = 2750 rpm

In addition to the above data, the temperature of the flue gases within the heat exchanger is also measured by thermocouples. The inlet temperature, at the transition between inner and outer spirals and at the outlet, for this specific case, is 816.80 °C, 211.02 °C and 112.65 °C, respectively.

5. Results

Essentially for illustrative purposes, the model of the micro-CHP with the simplified scheme of Fig. 1 (in steady cogeneration mode of

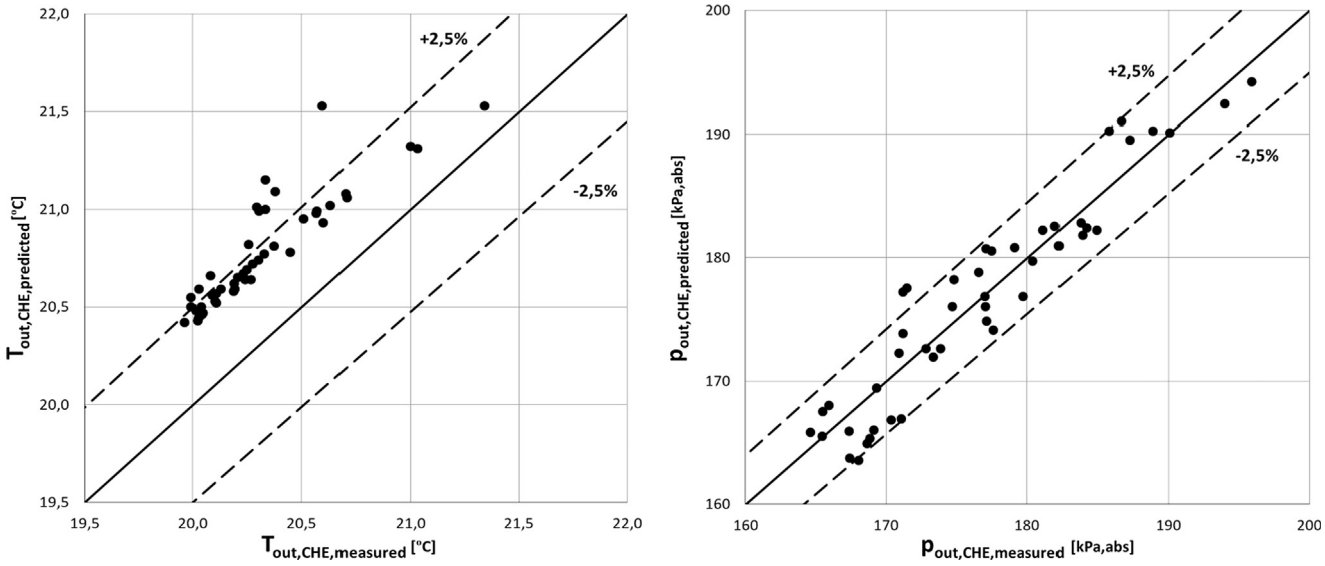

Fig. 7. Predicted *versus* measured values in the condenser, for the thermal fluid: (a) outlet temperature $T_{out,CHE}$; and (b) outlet pressure $p_{out,CHE}$.

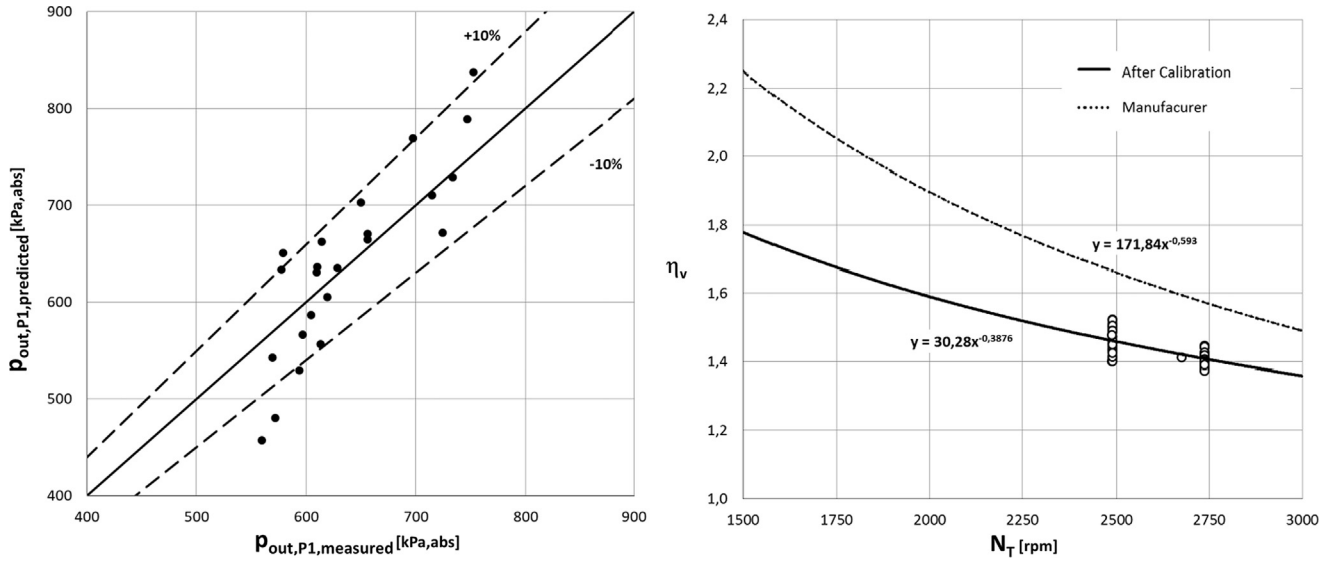

Fig. 8. (a) Predicted *versus* measured values of outlet pressure $p_{out,P1}$ of the pump P1. (b) Curves of volumetric efficiency $\eta_v(N_T)$ of the scroll expander T for R245fa, either supplied indirectly by the manufacturer (originally for R134a) or obtained directly through calibration.

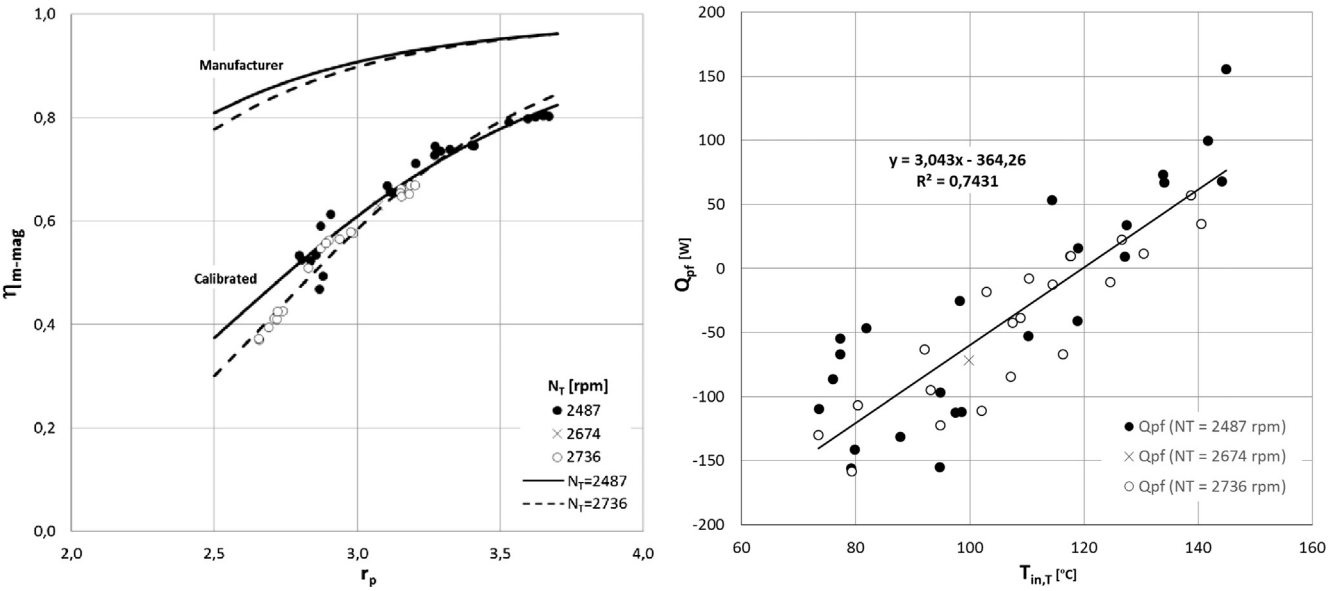

Fig. 9. Characteristic curves of the scroll expander T for R245fa: (a) Curves of mechanic and magnetic efficiency $\eta_m\eta_{mag}(N_T,r_{p,T})$ of the manufacturer (originally for R134a) and calibrated; and (b) curve of heat power losses $\dot{Q}_{pf}$ obtained by calibration.

operation), equipped with the components which sub models are presented in Sections 3.1–3.5 and coupled only to the open circuit of the water public network, was subjected to a careful calibration and a preliminary validation based on around 50 test points in the facility shown in Figs. 4 and 5. In these tests, the mass flow rate and inlet temperature of the water were $\dot{m}_w \approx 0.1$ kg/s and $T_{w,in} \approx 20$ °C (input variables not finely controlled but rather stable), and the control variables were varied in the ranges: speed of rotation of the pump P1, N_{P1}: 330–740 rpm (normal full range: 500–3500 rpm); thermal power of combustion of the gas burner B, $\dot{Q}_C$: 10–14.5 kW_t (full range: 5–35 kW_t); and speed of rotation of the expander T, $N_T \approx$ 2500,2750 rpm (full range: 1500–3000 rpm). The outlet temperature of the water ranged within $T_{w,out}$: 30–36 °C.

Below, the notation of Section 3.5 for the variables of the thermal fluid is retained. To quantify the error of prediction of the output variable y, the relative error $\varepsilon = (y_{predicted} - y_{measured})/y_{measured}$ [%] is used. Regarding the dependence of ε on the units scale of some variables y, which is immaterial in this context, the following conventions are adopted: T [°C] and p [kPa,abs.]. In the independent calibration and test of each sub model, when not mentioned otherwise, all its variable inputs and outputs are measured or indirectly estimated in an independent way.

5.1. Calibration and test of the sub model of the condenser CHE (Section 3.1)

The condenser CHE sub model contains a thermal part based on a three zone Logarithmic Mean Temperature Difference method, namely, capable of predicting abnormal pinch point operating conditions, and a simple hydraulic model for the head losses. The plates geometrical parameters not given by the manufacturer were obtained by reverse engineering from the available data.

The fouling factors (R''_{f_w}, R''_{f_f}) were neglected due to the small time of use of the component. In all test points, it was verified that the Reynolds

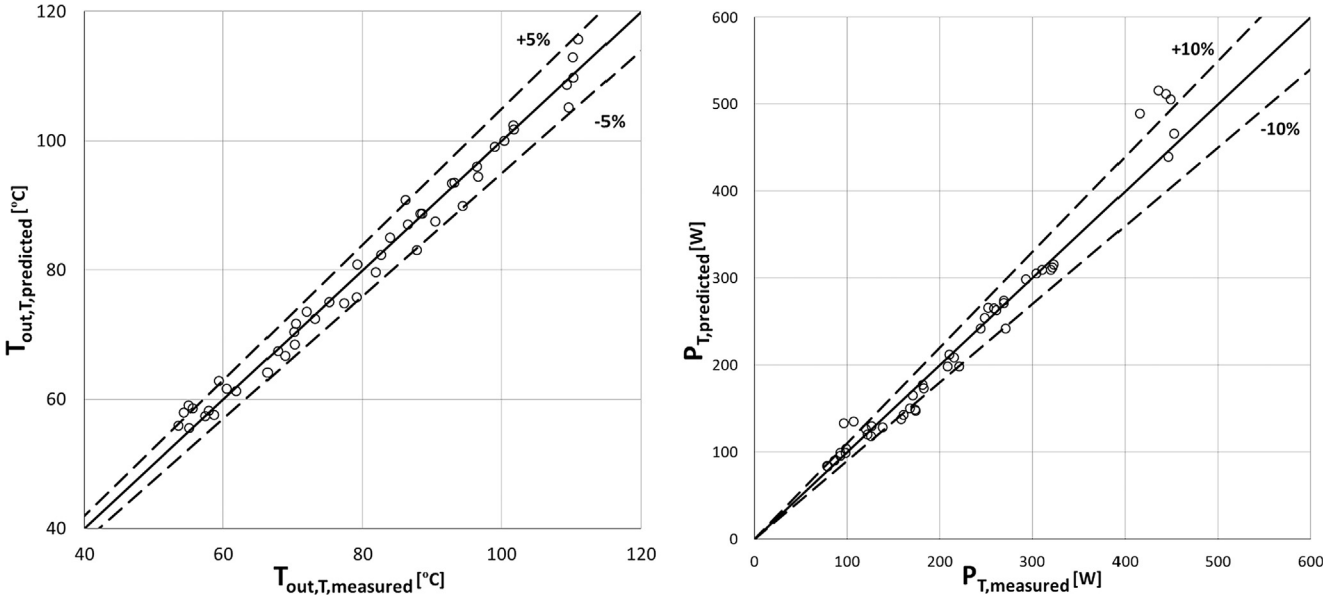

Fig. 10. Predicted *versus* measured values for the scroll expander T: (a) thermal fluid outlet temperature $T_{out,T}$; and (b) mechanical power P_T delivered at the shaft.

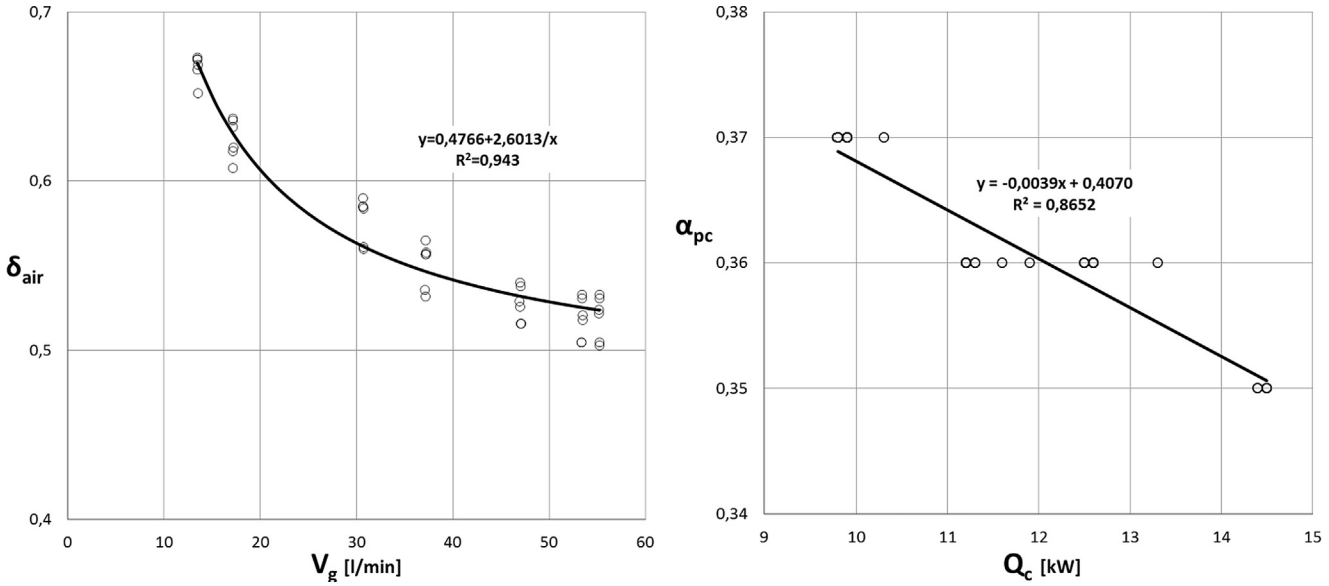

Fig. 11. Characteristic curves of the gas burner B obtained through specific calibrations: (a) Curve of the excess air ratio δ_{air} as a function of the gas flow rate $\dot{V}_g$; and (b) curve of the heat power losses coefficient α_{pc} as a function of the thermal power $\dot{Q}_c \equiv Q_c$ of combustion.

and Prandtl numbers stayed always within the ranges of application of the empirical correlations adopted for the convection coefficients, and that the pinch point temperature difference was never null. Without calibration, the predictions of the thermal part of the sub model for the output variable $T_{out,CHE}$ are compared with the measured values in Fig. 7a. The prediction error range and mean are, respectively: $\varepsilon = (+0.9\%)–(+4.5\%)$ and $\bar{\varepsilon} = +2.3\%$. In fact, the absolute error $|\varepsilon|$ can be even smaller because the measures of $T_{out,CHE}$ are probably a little below the true value, as it was observed that $T_{out,CHE} < T_{w,in}$ (obviously, a physical impossibility) in a few test points, and the measure of $T_{w,in}$ is considered more reliable than the one of $T_{out,CHE}$. Without any calibration, the sub model predicts the outlet temperature of the condensed fluid with less than ± 5% error. This encouraged the use of the sub-model, throughout the rest of the calibration and validation process, to indirectly estimate the mass flow rate of R245fa (another output variable of the sub model), in substitution of the lately flawed flow rate meter deployed for that purpose.

After a calibration offset of −9.75 kPa which remains unexplained (perhaps an extra head loss at a flawed valve), the predictions of the hydraulic part of the sub model for the output variable $p_{out,CHE}$ are compared with the measured values in Fig. 7b. The prediction error range and mean are, respectively: $\varepsilon = (-2.7\%)–(+3.6\%)$ and $\bar{\varepsilon} \approx 0\%$.

5.2. Calibration and test of the sub model of the pump P1 (Section 3.2)

The pump P1 sub model is based on a good physical understanding of the functioning of this type of volumetric pumps, including similarity theory, to fit and extrapolate the characteristic data on the volumetric efficiency, net positive suction head required (to avoid cavitation) and electric power consumed, supplied by the manufacturer for water in reference conditions, to the variable operating conditions of R245fa. In the course of the calibration and validation of the sub model, it was unfortunate to verify that the pump is rotating near the lower limit of normal operation (500 rpm) and, in some cases that ultimately had to

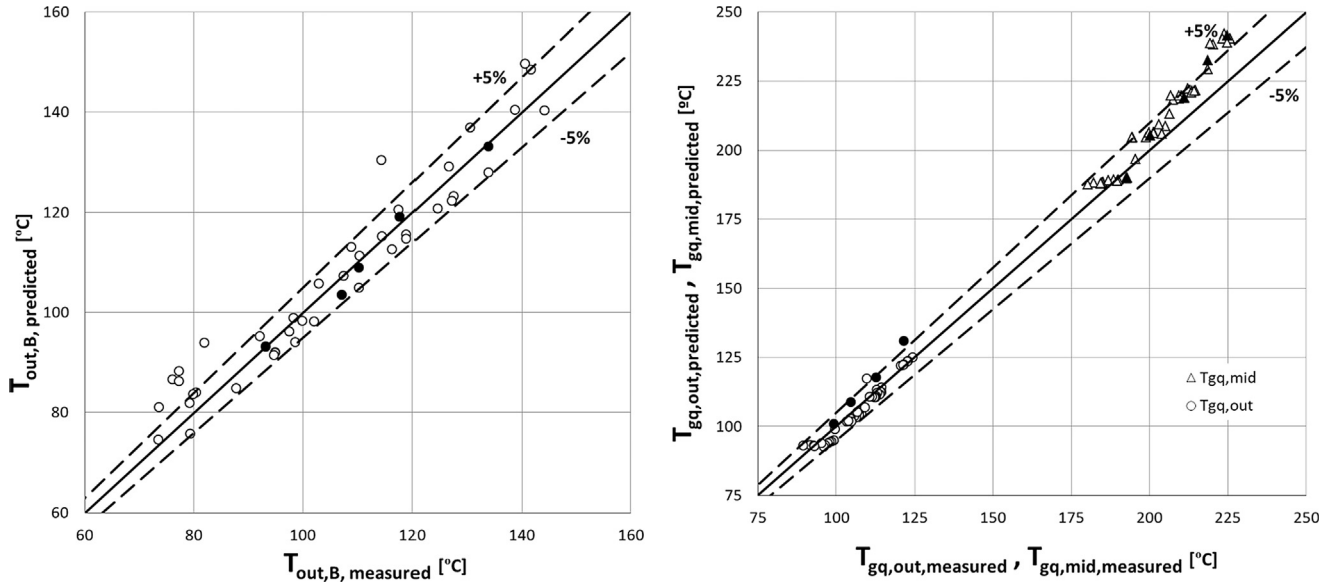

Fig. 12. Predicted *versus* measured values in the evaporator B for: (a) the outlet thermal fluid temperature $T_{out,B}$; and (b) the middle $T_{gq,outn1} \equiv T_{gq,mid}$ (between the first and second gas passages) and outlet $T_{gq,out}$ flue gas temperatures. The closed symbols indicate the test points used for the calibration of the sub model.

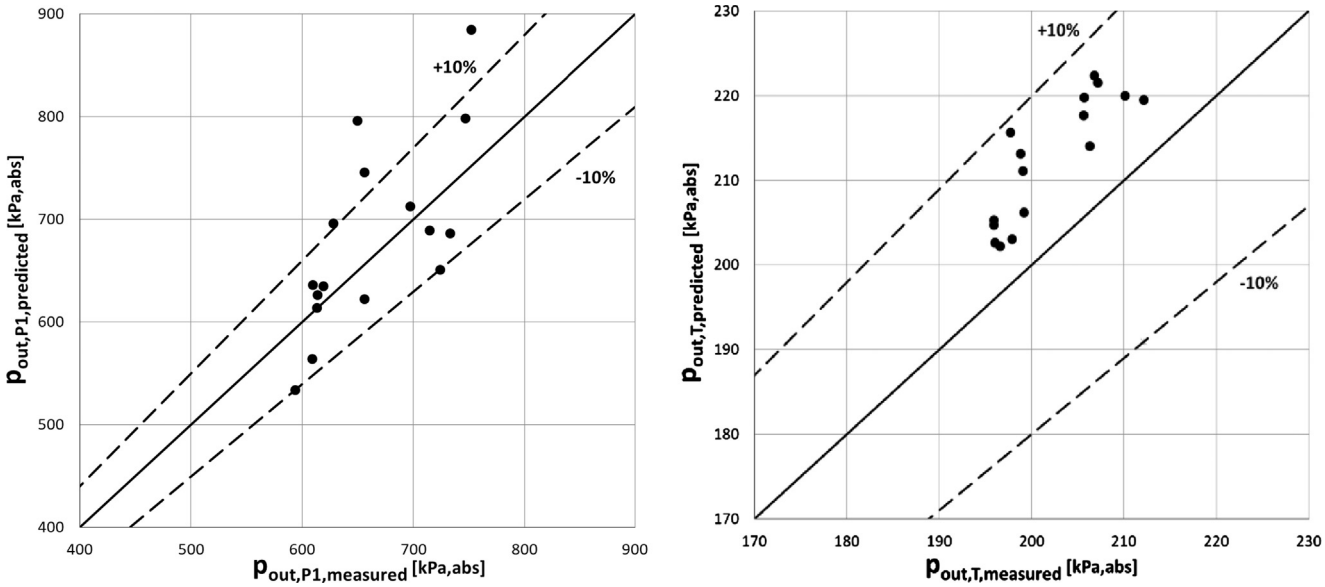

Fig. 13. Predicted *versus* measured values for the thermal fluid outlet pressures: (a) in the pump P1, $p_{out,P1}$; and (b) in the scroll expander T, $p_{out,T}$.

be discarded, even below.

Only the test points with $N_P > 500$ rpm were used because for various characteristic curves (namely, of volumetric efficiency $\eta_{vw}(\Delta p_{w,P1}, N_P)$, cf. Eqs. (51) and (52)), the empirical fittings to the manufacturer's data are not reliable below this threshold. This restriction is maintained heretofore. In what respects the output variable $p_{out,P1}$ of the sub model, a slight trend of underprediction was corrected with a calibration factor of 1.068 (see the comparison with the measured values in Fig. 8a). The resultant range and mean value of the relative error of prediction are, respectively: $\varepsilon = (-18.3\%)–(+12.4\%)$ and $\bar{\varepsilon} \approx 0\%$. A possible explanation for this correction is some change occurred in the manufacturer's linear calibration function $N_P(V)$, of the speed N_P controller of the pump as a function of the control voltage V. Unfortunately, this wasn't possible to verify due to the hermetic character of the component, that inhibits the direct measurement of N_P. Finally, the error of prediction of the output variable $T_{out,P1}$, taking as input a thermo-hydrodynamic isentropic efficiency $\eta_{th} \approx 1$, is negligible (specifically, $|\varepsilon| < 0.2\%$).

5.3. Calibration and test of the sub model of the scroll expander T (Section 3.4)

The sub modelling of the expander T posed a particular challenge for three reasons: (i) the state-of-the-art of this type of expanders is still deficient; (ii) the manufacturer's data is insufficient and partly inappropriate (for a different unit and fluid); and, above all, (iii) the unit suffered various deteriorations and, due to a deficient design, exhibited significant rates of heat exchange with the ambient and with the servomotor that was used as brake, which, at some test points, acted as a heat sink, and at others, as a heat source. In consequence, the calibration of the sub model afforded an unexpected but consistent full characterization of the peculiar behavior of the component coupled to the servomotor of the test rig.

In this case, as the manufacturer's data is either insufficient or inappropriate (e.g., it refers to a lubricated unit tested with the thermal fluid R134a), a deep calibration leading to revised or new characteristic curves revealed necessary. These curves are specific of the unit installed

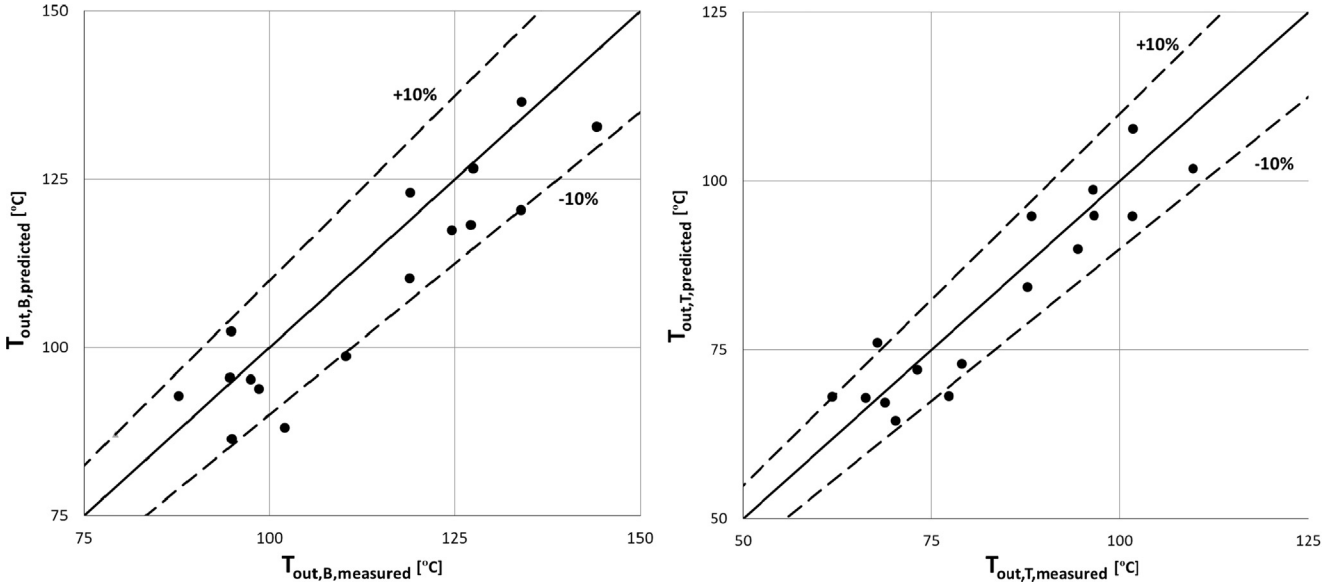

Fig. 14. Predicted *versus* measured values for the thermal fluid outlet temperatures: (a) in the evaporator B, $T_{out,B}$; and (b) in the scroll expander T, $T_{out,T}$.

in the facilities, operating with R245fa. The volumetric efficiency curves $\eta_v(N_T)$ obtained either directly through calibration or indirectly from the manufacturer's data applying similarity theory (see Section 3.4) are compared in Fig. 8b. Notice that, on this particular aspect, the performance or our unit is clearly superior to the reference of the manufacturer. A similar comparison for the curve of mechanic and magnetic efficiency $\eta_m\eta_{mag}(N_T,r_{p,T})$ of the component is shown in Fig. 9a. The measurement of the efficiency $\eta_m\eta_{mag}$ is based on Eq. (90), with $P \equiv P_T$ and the mechanical power P_m delivered at the shaft before mechanic and magnetic losses given by:

$$P_m = P_T + \dot{Q}_{p_{mec+mag}}(N_T) \tag{100}$$

The curve $\dot{Q}_{p_{mec+mag}}(N_T)$ of mechanic and magnetic power losses of the component was obtained in a special vacuum test [43], in which the component shaft was directly coupled to the shaft of an electric motor with variable speed. In Fig. 9a it is apparent the very significant degradation of the performance of our unit relative to the reference of the manufacturer, which can be attributed to the absence of lubrication and to defects of the mechanic bearings and magnetic coupling (the latter were, in fact, visually confirmed). The curve of thermal power losses $\dot{Q}_{p_f}(T_{in,T})$ of the component was also obtained with the help of Eqs. (85) and (100) and is shown in Fig. 9b. The in-depth explanation of this curve can't be made here [45], except to say that the high thermal losses (right part of the curve, with $\dot{Q}_{p_f} > 0$) flow through the large exposed surface of the mechanical coupling and the abnormal thermal gains (left part of the curve, with $\dot{Q}_{p_f} < 0$) are due to the heat conduction bridge between the component and the servomotor, the latter acting as a thermal source.

A preliminary validation of the calibrated sub model of component T is shown in Fig. 10, by comparing the predicted and measured values for the outlet temperature of the thermal fluid $T_{out,T}$ (Fig. 10a) and the mechanical power at the shaft P_T (Fig. 10b). The ranges and mean values of the relative errors of prediction of the three main output variables are, respectively: $\varepsilon = (-7\%)–(+5\%)$ and $\bar{\varepsilon} \approx -0.2\%$ for $T_{out,T}$; $\varepsilon = (-7\%)–(+7\%)$ and $\bar{\varepsilon} \approx 0\%$ for N_T; and $\varepsilon = (-15\%)–(+38\%)$ and $\bar{\varepsilon} \approx +1.3\%$ for P_T.

5.4. Calibration and test of the burner and evaporator B sub model (Section 3.3)

The burner and evaporator component B was specifically designed for this micro-CHP prototype (Fig. 3) and, in line with the design needs, was heavily sub modelled. The gas combustion model of the burner is simple but sound. The thermal modelling of the evaporator is based directly on the conservation equations for the flows of the burnt gases (external) and the thermal fluid (inside a spiral tube), through a sequence of infinitesimal control volumes, from the respective inlets to the outlets. The calibration of this model uses only five test points to fit two normalized coefficients controlling the calculation of the convection coefficients from the side of the combustion gases (one of these coefficients masks the absence of radiation terms in the conservation equations for the combustion gases, which are deemed relevant in the first spires of the first passage of the gases), and a third coefficient to correct the average reading of two thermocouples for radiation losses difficult to estimate independently.

Commencing by the combustion model, the detailed molar composition of the natural gas $\nu'_{g,i}$[kmol of C_i/kmol of g]$(i = 1,2,...,11)$, as well as other gas properties (e.g., molar mass M_g and low heat value q_{c0}), are supplied by the gas provider. The flow rate of combustion air is controlled via the speed of the air fan of the burner (continuous control by a voltage signal feeding the speed controller of the fan) but the corresponding control of the gas flow rate $\dot{V}_g$ (measured variable) is made internally by the burner, after a previous manual tuning of two trimmers. The resultant curve of excess air ratio $\delta_{air}(\dot{V}_g)$ of combustion, obtained in preliminary tests of calibration of the burner with the help of a gas analyzer, is shown in Fig. 11a (the empirical fitting function has a physical rationale behind which is related with the burner control of $\dot{V}_g$). A second calibration function $\alpha_{pc}(\dot{Q}_c)$ (Fig. 11b) was obtained for the thermal power losses $(\dot{Q}_{pc} = \alpha_{pc}\cdot\dot{Q}_c)$ of the external refrigerated combustion chamber (Fig. 3), by minimizing the prediction error of the output variable $T_{gq,b} = T_{gq,in}$ of the temperature of the combustion gases at the entrance of the (nearly adiabatic) cylindrical inner chamber of the evaporator. Just in passing, notice that, due to the large rate of heat extraction of the refrigeration system, the effective thermal power of combustion available in the evaporator ranged only from 6.2 to 9.4 kW_t in the tests. The preliminary validation of the calibrated combustion model against the whole set of tests, led to the following errors of prediction of various output variables: $|\varepsilon| < 0.5\%$ for M_g; $\bar{\varepsilon} \approx 0\%$ for q_{c0}; and $\varepsilon = (-1.7\%)–(+1.2\%)$ and $\bar{\varepsilon} \approx +0.1\%$ for $T_{gq,in}$.

The heat exchanger model (thermal part) was calibrated relatively to only three non-dimensional coefficients: a coefficient α_c of correction of the average reading of the two thermocouples measuring the inlet gas temperature $T_{gq,in}$, to take into account the radiation losses (so, it is expected that $\alpha_c > 1$); and a pair of normalized (to the range 0–1)

coefficients $(\alpha_{h_1},\alpha_{h_2})$ used to compute the external convection coefficients h_{extij} (on the gas side) at the surface of the spiral tube inside which flows the thermal fluid, respectively, in the first (in cross flow with the inner spiral) and second (in cross flow with the outer spiral) passages of the burnt gases. Among other things, the coefficients α_{h_k} mask the omitted radiation terms in the thermal energy conservation equation of the gas flow through the control volumes CV_i, which are deemed important in the first inner spirals, where the gas temperatures T_{gq,in_i} are still rather high. The calibration coefficients were fitted to minimize the relative errors of prediction of the outlet thermal fluid temperature $T_{out,B}$ and the gas temperatures at the exit of the first passage ($T_{gq,out_{n1}}$) and at the outlet ($T_{gq,out}$), in a subset of only five test points sweeping more or less evenly the range of $\dot{Q}_c = 10-14.5\text{kW}_t$. It resulted: $\alpha_c = 1.01$, which seems a bit low but can be explained by the adiabatic character of the inner surface of the entrance chamber of the evaporator; and $(\alpha_{h_1} = 0.9,\alpha_{h_2} = 0)$, which is plausible. A preliminary validation of the calibrated model, making use of all the test points, led to the following errors of prediction: $\varepsilon = (-5\%)-(+15\%)$ and $\bar{\varepsilon} \approx +1.5\%$ for $T_{out,B}$ (Fig. 12a); $\varepsilon = (-2\%)-(+9\%)$ and $\bar{\varepsilon} \approx +3.5\%$ for $T_{gq,out_{n1}}$ (upper part of Fig. 12b); and $\varepsilon = (-4\%)-(+7\%)$ and $\bar{\varepsilon} \approx -1\%$ for $T_{gq,out}$ (lower part of Fig. 12b).

As the complete sub model of the component B is computationally heavy, for incorporation in the overall model, the two characteristic functions relating the main output variables of the sub model (outlet temperature of the thermal fluid and mass of fluid inside the component at any instant) with the four main input variables (inlet fluid temperature and pressure, mass flow rate and thermal power of the combustion in the gas burner) were emulated with neural networks, practically without increasing the prediction errors. The error analysis of the characteristic curves $T_{out,B}$,m_B($T_{in,B} \in [7.5,65\ °C]$, $p_{in,B} \in [1,15\ \text{bara}]$, $\dot{m}_f \in [0.02,0.17\ \text{kg/s}]$, $\dot{Q}_c \in [5,35\ \text{kW}_t]$) (cf. Eqs. (62) and (97)) of emulation of the overall sub model of the component B (combustion model and thermal part of the heat exchanger model) with neural networks, alluded in the last paragraph of Section 3.3, led to the identification of two additional independent sources of error: (i) the freezing of the natural gas composition (physical error); and (ii) the fitting of the neural network (numerical error). Just for illustrative purposes, after an advanced (but not final) phase of calibration of the model, the errors of prediction of the output variable $T_{out,B}$ (for the whole set of test points) were: (I) $\varepsilon = (-5\%)-(+17\%)$ and $\bar{\varepsilon} \approx +1.5\%$, for the base model; (II) $\Delta\varepsilon = (-0.8\%)-(+2.2\%)$ and $\overline{\Delta\varepsilon} \approx +0.3\%$, for the additional error induced by Source (i) alone; (III) $\Delta\varepsilon = (-2.7\%)-(+1.5\%)$ and $\overline{\Delta\varepsilon} \approx -0.5\%$, for the additional error induced by Source (ii) alone; and (IV) $\varepsilon = (-7\%)-(+18\%)$ and $\bar{\varepsilon} \approx +1.3\%$, for the final emulated model.

5.5. Test of the overall model

The closure relationships of the micro-CHP overall model (Section 3.5) require no calibration. An interesting point on the mass conservation Eqs. (94)–(99) concerns the order of magnitude of its various terms (in percentage of the total fluid mass m_0) for a typical test point: the mass m_B of fluid in the evaporator B represents 60% of the total mass; the mass m_{CHE} of fluid in the condenser CHE represents 30%; the mass ($m_{CHE,P1} + m_{P1,B}$) of liquid fluid in the ducts represents 9%; and the mass of vapor fluid ($m_{B,T} + m_{T,CHE}$) in the ducts and m_T in the expander T, and the mass m_{P1} of liquid fluid in the pump P1 represent, jointly, only 1%. Unfortunately, due to unknown thermal fluid leaks caused by some accidents occurred in preliminary tests, the total mass m_0 during the calibration/validation tests can only be estimated *a priori* to be within the interval: $m_0 \in [2.60,4.26\ \text{kg}]$. However, a physically rigorous reverse engineering procedure that can't be presented here led to the unexpectedly fine plausible estimate of $m_0 = 3.26(7)$ kg.

At last, the prediction errors of the micro-CHP overall model for some of the most relevant output variables, throughout the whole set of test points, are: $\varepsilon = (-10\%)-(+22\%)$ and $\bar{\varepsilon} \approx +2\%$, for $p_{out,P1}(\approx p_{out,B})$ (Fig. 13a); $\varepsilon = (+3\%)-(+9\%)$ and $\bar{\varepsilon} \approx +5\%$, for $p_{out,T}(\approx p_{out,CHE})$ (Fig. 13b); $\varepsilon = (-14\%)-(+8\%)$ and $\bar{\varepsilon} \approx -4\%$, for $T_{out,B}$ (Fig. 14a); $\varepsilon = (-12\%)-(+12\%)$ and $\bar{\varepsilon} \approx +1\%$, for $T_{out,T}$ (Fig. 14b); and $\varepsilon = (-33\%)-(+21\%)$ and $\bar{\varepsilon} \approx -3\%$, for N_T.

6. Conclusions

A modular open architecture to model in a realistic though computationally fast way (typically, a few minutes in a normal PC) the steady behavior of a micro-CHP is proposed. After a general exposition, this modelling architecture is richly illustrated by applying it to a particular ORC in normal cogeneration mode of operation, including the model calibration and (preliminary) validation. This particular micro-CHP uses R245fa as thermal fluid and has four main components, which are sub modelled in a modular way: a compact plates condenser (CHE), a rotary vane pump hermetically coupled to an electrical motor with a speed controller (P1), a non-commercial natural gas burner and evaporator (B), and a scroll expander hermetically coupled to an electromagnetic brake with a speed controller (T). The three control variables are: the thermal power of combustion in the gas burner B, and the speeds of rotation of the pump P1 and the expander T. No additional input is required since this model is charge-sensitive what makes it fully predictive.

In the whole set of tests used to calibrate and validate the model, these variables ranged, respectively, within: 10–14.5 kW_t (5–35 kW_t full range), of which only 6.2–9.4 kW_t are effectively available in the evaporator; 330–740 rpm (500–3500 rpm normal full range; the points with speed below 500 rpm were ultimately discarded); and 2500–2750 rpm (1500–3000 rpm full range).

The main results obtained for each sub-model and the overall model are summarized as follows:

(1) For the CHE, without any calibration, the sub model predicts the outlet temperature of the condensed fluid with less than ± 5% error. The prediction of the pressure loss across the component revealed errors lower than ± 4% after correction by an offset of around +10 kPa, which, unfortunately, remains unexplained.
(2) In the pump P1, with a simple calibration factor of 1.068 (which can be due to a deficient calibration of the speed controller supplied by the manufacturer, difficult to verify), the outlet fluid pressure is predicted with no mean bias and errors below ± 18% in the range 550–800 kPa (abs.), and the outlet temperature (less relevant) is predicted with virtually no error.
(3) The turbine resultant error predictions are less than ± 7% for both the outlet fluid temperature (range: 50–110 °C) and rotation speed (range: 2500–2750 rpm), and typically less than ± 15% (attaining +40% at rare test points) for the mechanical power delivered at the shaft (range: 80–500 W).
(4) For the evaporator which comprises the burner and the heat exchanger, after a calibration for the thermal losses in the external refrigerated combustion chamber, the temperature of the combustion gases at the entrance of the evaporator is predicted with less than ± 2% error in the range 780–860 °C. The resulting predictions for the whole set of test points have errors: lower than ± 7% (with mean error lower than 3%) for the gas temperatures at the middle (range: 175–225 °C) and at the outlet (range: 85–125 °C) of the evaporator; and typically lower than ± 5% (at rare test points the error can attain +15%, but the mean error is lower than 2%) for the outlet thermal fluid temperature (range: 70–150 °C).
(5) The overall model exhibited the following maximum prediction errors (practically with unbiased mean) throughout the whole set of test points: ± 10% for the thermal fluid pressure at the outlet of the expander T (range: 190–220 kPa, abs.); ± 12% for the fluid temperatures at the outlet of the evaporator B (range: 80–150 °C) and the expander T (range: 60–120 °C); ± 20% for the fluid pressure at the outlet of the pump P1 (range: 600–800 kPa, abs.); and ± 30%

for the rotation speed of the expander T (range: 2500–2750 rpm).

Requiring as inputs only truly accessible data on the components, the water client demand variables and two of the control variables of operation (thermal power of combustion in the burner B and speed of rotation of the pump P1), the overall calibrated model of the micro-CHP affords a rich characterization of its off-design steady behavior, including the thermal fluid properties throughout the circuit, its mass flow rate and the third control variable (speed of rotation of the expander T).

Such a modelling tool is ideal to optimize/refine the micro-CHP design, selection of components and control, the demonstration of which is the main purpose of the next paper of the series along with a detailed description of the modular framework.

Acknowledgements

This research is partially sponsored by FEDER Funds through the program COMPETE – Programa Operacional Factores de Competitividade under the contract QREN-POFC-COMPETE-23101. This financial support is gratefully acknowledged.

References

[1] J. Harrison, Potential Benefits os micro-CHP, Energy Saving Trust, 2001.
[2] M. Bianchi, a. De Pascale, Bottoming cycles for electric energy generation: parametric investigation of available and innovative solutions for the exploitation of low and medium temperature heat sources, Appl. Energy 88 (2011) 1500–1509, http://dx.doi.org/10.1016/j.apenergy.2010.11.013.
[3] I. Vaja, A. Gambarotta, Internal Combustion Engine (ICE) bottoming with Organic Rankine Cycles (ORCs), Energy 35 (2010) 1084–1093, http://dx.doi.org/10.1016/j.energy.2009.06.001.
[4] A. Arsalis, M.P. Nielsen, S.K. Kær, Modeling and off-design performance of a 1kWe HT-PEMFC (high temperature-proton exchange membrane fuel cell)-based residential micro-CHP (combined-heat-and-power) system for Danish single-family households, Energy 36 (2011) 993–1002, http://dx.doi.org/10.1016/j.energy.2010.12.009.
[5] H.I. Onovwiona, V.I. Ugursal, Residential cogeneration systems: review of the current technology, Renew. Sustain. Energy Rev. 10 (2006) 389–431, http://dx.doi.org/10.1016/j.rser.2004.07.005.
[6] J. André, J.B. Ribeiro, E. Costa, J.P. Pinto, R. Mendes, Projecto Hebe – Business Plan (2011), Coimbra, 2012.
[7] G. Qiu, Selection of working fluids for micro-CHP systems with ORC, Renew. Energy 48 (2012) 565–570, http://dx.doi.org/10.1016/j.renene.2012.06.006.
[8] B.F. Tchanche, G. Papadakis, G. Lambrinos, A. Frangoudakis, Fluid selection for a low-temperature solar organic Rankine cycle, Appl. Therm. Eng. 29 (2009) 2468–2476, http://dx.doi.org/10.1016/j.applthermaleng.2008.12.025.
[9] D. Mikielewicz, J. Mikielewicz, A thermodynamic criterion for selection of working fluid for subcritical and supercritical domestic micro CHP, Appl. Therm. Eng. 30 (2010) 2357–2362, http://dx.doi.org/10.1016/j.applthermaleng.2010.05.035.
[10] G. Kosmadakis, D. Manolakos, S. Kyritsis, G. Papadakis, Comparative thermodynamic study of refrigerants to select the best for use in the high-temperature stage of a two-stage organic Rankine cycle for RO desalination, Desalination 243 (2009) 74–94, http://dx.doi.org/10.1016/j.desal.2008.04.016.
[11] P.J. Mago, A. Hueffed, L.M. Chamra, Analysis and optimization of the use of CHP–ORC systems for small commercial buildings, Energy Build. 42 (2010) 1491–1498, http://dx.doi.org/10.1016/j.enbuild.2010.03.019.
[12] B. Peris, J. Navarro-Esbrí, F. Molés, R. Collado, A. Mota-Babiloni, Performance evaluation of an Organic Rankine Cycle (ORC) for power applications from low grade heat sources, Appl. Therm. Eng. 75 (2015) 763–769, http://dx.doi.org/10.1016/j.applthermaleng.2014.10.034.
[13] S. Declaye, S. Quoilin, L. Guillaume, V. Lemort, Experimental study on an open-drive scroll expander integrated into an ORC (Organic Rankine Cycle) system with R245fa as working fluid, Energy 55 (2013) 173–183, http://dx.doi.org/10.1016/j.energy.2013.04.003.
[14] M. Farrokhi, S.H. Noie, a.a. Akbarzadeh, Preliminary experimental investigation of a natural gas-fired ORC-based micro-CHP system for residential buildings, Appl. Therm. Eng. 69 (2014) 221–229, http://dx.doi.org/10.1016/j.applthermaleng.2013.11.060.
[15] S. Quoilin, V. Lemort, J. Lebrun, Experimental study and modeling of an Organic Rankine Cycle using scroll expander, Appl. Energy 87 (2010) 1260–1268, http://dx.doi.org/10.1016/j.apenergy.2009.06.026.
[16] M. Ibarra, A. Rovira, D.-C. Alarcón-Padilla, J. Blanco, Performance of a 5kWe Organic Rankine Cycle at part-load operation, Appl. Energy 120 (2014) 147–158, http://dx.doi.org/10.1016/j.apenergy.2014.01.057.
[17] Z. He, Y. Zhang, S. Dong, H. Ma, X. Yu, Y. Zhang, X. Ma, N. Deng, Y. Sheng, Thermodynamic analysis of a low-temperature organic Rankine cycle power plant operating at off-design conditions, Appl. Therm. Eng. 113 (2017) 937–951, http://dx.doi.org/10.1016/j.applthermaleng.2016.11.006.
[18] D. Wei, X. Lu, Z. Lu, J. Gu, Dynamic modeling and simulation of an Organic Rankine Cycle (ORC) system for waste heat recovery, Appl. Therm. Eng. 28 (2008) 1216–1224, http://dx.doi.org/10.1016/j.applthermaleng.2007.07.019.
[19] J. Wang, Z. Yan, P. Zhao, Y. Dai, Off-design performance analysis of a solar-powered organic Rankine cycle, Energy Convers. Manage. 80 (2014) 150–157, http://dx.doi.org/10.1016/j.enconman.2014.01.032.
[20] H. Li, D. Hu, M. Wang, Y. Dai, Off-design performance analysis of Kalina cycle for low temperature geothermal source, Appl. Therm. Eng. 107 (2016) 728–737, http://dx.doi.org/10.1016/j.applthermaleng.2016.07.014.
[21] Y.A. Cengel, M.A. Boles, Thermodynamics: An Engineering Approach, fourth ed., McGraw-Hill, 2002.
[22] NIST - National Institute of Standards and Technology, Reference Fluid Thermodynamic and Transport Properties Database (REFPROP), 2016.
[23] F.P. Incropera, D.P. DeWitt, T.L. Bergman, A.S. Lavine, Fundamentals of Heat and Mass Transfer, John Wiley & Sons, 2007. http://doi.org/10.1016/j.applthermaleng.2011.03.022.
[24] A. Muley, R.M. Manglik, Experimental study of turbulent flow heat transfer and pressure drop in a plate heat exchanger with chevron plates, J. Heat Transfer. ASME 121 (1999) 110–117.
[25] B. Thonon, A review of hydrocarbon two-phase heat transfer in compact heat exchangers and enhanced geometries, Int. J. Refrig. 31 (2008) 633–642, http://dx.doi.org/10.1016/j.ijrefrig.2008.02.006.
[26] A. Maslov, L. Kovalenko, Hydraulic resistance and heat transfer in plate heat exchangers, Molochnaya Promyshlennost. 10 (1972) 20–22.
[27] H. Kumar, The plate heat exchanger: construction and design, in: Proc. First UK Natl. Conf. Heat Transf. Univ. Leeds, Inst. Chem. Symp., 1984, pp. 1275–1288.
[28] A.S. Wanniarachchi, U. Ratman, approximate correlations for chevron-type plate heat exchangers, in: Proc. 30th Natl. Heat Transf. Conf. ASME-vol, 1995, pp. 145–151.
[29] Y.Y. Yan, H.C. Lio, T.F. Lin, Condensation heat transfer and pressure drop of refrigerant R134a in a plate heat exchanger, Int. J. Heat Mass Transf. 42 (1999) 993–1006.
[30] D.H. Han, K.J. Lee, Y.H. Kim, The characteristics of condensation in brazed plate heat exchangers with different chevron angles, J. Korean Phys. Soc. 43 (2003) 66–73.
[31] S.G. Kandlikar, R.K. Shah, Multipass plate heat exchangers - Effectiveness-NTU Results and guidelines for selecting pass arrangements, 1989, pp. 300–313.
[32] M.A. Kedzierski, J.M. Goncalves, Horizontal convective condensation of alternative refrigerants within a micro-fin tube, Enhanc. Heat Transf. 6 (1999) 161–178.
[33] V.M. Cherkasski, Pumps, fans, compressors, Moscow Mir, 1980.
[34] A.J. Macyntire, Bombas e instalações de bombeamento, second ed., Rio de Janeiro, 1987.
[35] J.P. Pereira, R. Mendes, G.C. Vaz, J.C. André, J.B. Ribeiro, Development of a direct concept helical-coil evaporator for an ORC based micro-CHP system, Energy Proc. 129 (2017) 474–478, http://dx.doi.org/10.1016/j.egypro.2017.09.162.
[36] S.E. Haaland, Simple and explicit formulas for the friction factor in turbulent pipe flow, J. Fluid Eng. 105 (1983) 242–243.
[37] J.M. Coulson, J.F. Ricardson, Chemical Engineering, vol. VI: An Introduction to Chemical Engineering Design, 2005.
[38] J. Grimson, Advanced Fluid Dynamics and Heat Transfer, McGraw-Hill, London, 1972.
[39] L. Guangbin, Z. Yuanyang, L. Liansheng, S. Pengcheng, Simulation and experiment research on wide ranging working process of scroll expander driven by compressed air, Appl. Therm. Eng. 30 (2010) 2073–2079, http://dx.doi.org/10.1016/j.applthermaleng.2010.05.015.
[40] B. Woodland, J.E. Braun, A.E. Groll, W.T. Horton, Experimental testing of an organic Rankine Cycle with scroll-type expander, Publ. Ray W Herrick Lab. 52, 2012.
[41] B. Woodland, J.E. Braun, A.E. Groll, W.T. Horton, Improved detailed results of tests of E15H22N4.25 – 1 kW Scroll Expander with fuid R-134a, Purdue, 2012.
[42] J. André, E. Costa, J. Borges, J. Ribeiro, Air Squared scroll expander E15H22N4.25 [v 3.2], Internal Report R-T3.1-AS1 of Project Hebe., Coimbra, 2012.
[43] I. Costa, J. André, J. Borges, Air Squared scroll expander E15H22N4.25 [v 1.2], Internal Report R-T3.1-AS2 of Project Hebe., Coimbra, 2013.
[44] I. Costa, J. André, J. Borges, R. Mendes, M. Brett, Air Squared scroll expander E15H22N4.25 Experimental Setup [v 2.2], Internal Report R-T3.1-AS3 of Project Hebe., Coimbra, 2013.
[45] I. Costa, J. André, J. Borges, R. Mendes, M. Brett, Air Squared scroll expander E15H22N4.25: Tests with Low Pressure Compressed Air [v 2.5], Internal Report R-T3.1-AS4 of Project Hebe., Coimbra, 2014.
[46] R.S.R. Gorla, A.A. Khan, Turbomachinery: Design and Theory, 2003.
[47] J. Spínola, Estudo de micro-turbinas de vapor do tipo scroll, University of Coimbra, 2011.
[48] R.H.C. Elliott, V. Vijayakumar, W. Zink, National instrument LabVIEW: a programming environment for laboratory automation and measurement, SLAS Technol. Transl. Life Sci. Innov. 12 (2007) 17–24.

Chapter 6

Quasi-steady behaviour and control

This chapter contains the paper "Quasi-steady state behaviour and control of an Organic Rankine Cycle (ORC) micro-CHP", submitted for publication in Applied Thermal Engineering. This work develops a suitable control strategy for a micro-CHP ORC system (Hebe) under variable user demand conditions, using the stationary off-design and charge-sensitive model of the previous chapter. The experimental setup and main structure and set of I/O of the model are described first. Afterwards, a preliminary analysis of the model/algorithm behaviour is carried out and the control maps of the system, forming the basis of its steady-state control strategy, are generated. Finally, an empirical dynamic control strategy is tentatively proposed for the micro-CHP system, based on three independent PID controls, with the ultimate goal of guiding the system through start-ups and changings of steady-state functioning point, as fast and safely as possible.

Quasi-steady state behavior and control of an Organic Rankine Cycle-based micro combined heat-and-power system

Márcio Santos*, Jorge André, Eduardo Costa, Cátia Augusto, Ricardo Mendes and José Ribeiro

University of Coimbra, ADAI, Department of Mechanical Engineering
* Corresponding author: marcio.santos@dem.uc.pt, University of Coimbra, Rua Dr. Luís Reis Santos, 3030-788 Coimbra, Coimbra, Portugal

KEYWORDS
micro-CHP; Off-design Modeling; Quasi-steady simulation; Organic Rankine Cycle; Control Strategy

ABSTRACT

A steady-state off-design charge sensitive model is used to develop a control strategy for an Organic Rankine Cycle (ORC) micro Combined Heat-and-Power (micro-CHP) combi-boiler, satisfying real-time hot waters domestic needs (water temperature and heating power up to 40 ºC and 35 kWt, respectively) while producing up to 1 kWe of electricity. The hot source of the ORC is a natural gas burner that directly evaporates the fluid R245fa. The control variables are the heat power of combustion, the rotational speed of the volumetric pump, and the rotational speed of the scroll expander. In a first stage, after a thorough physical and numerical evaluation, the model is used to draw steady-state 2D control maps of the ORC that delimit the admissible region and the optimal point of operation compatible with the given inputs, in the 3D-space of the control variables. The best pairs of control and controlled variables are also identified. In a second stage, a tentative empirical dynamic control strategy is devised based on independent 1D-PID controls. The aim is, on the one hand, to lead the ORC as fast and safe as possible through start-ups and in response to changes in the user demands, and, on the other hand, to maintain a stable optimal operation under uncontrolled perturbations of some inputs. The results demonstrate that the developed control strategy kept the maximum temperature of the ORC at secure values while maintaining the steady operation of the system. Additionally, in start-ups, the hot water is supplied at a given temperature in less than 1.5 or 5 minutes whether the boiler is in simple-boiler mode or cogeneration mode, respectively. A variation in the user demand does not cause significant system instability. The new steady-state is attained in less than 2 minutes. Compared to a manual start, reductions of 5 minutes for steady operation and of 2 minutes for electricity production are achieved.

NOMENCLATURE:

Symbols:

$\dot{m}$	Mass flow rate (kg/s)
N	Rotational Speed (rpm)
p	Pressure (kPa, abs.)
P	Power (W)
$\dot{Q}$	Heat flux (W)
$\dot{Q}_{p_{mec+mag}}$	Mech.-magnetic losses in the expander (W)
r_p	Pressure ratio in the expander
T	Temperature (K or ºC)
U	Overall heat transfer coefficient (W/m^2·K)
$\dot{V}$	Flow rate (m^3/s)
$\dot{W}$	Mechanical Power (W)

Acronyms:

B	Burner
CHE	Condenser Heat Exchanger
CHP	Combined Heat and Power
EHE	Evaporator Heat Exchanger
EV	Electro-Valve
G/C	Generator/Conversor
I/O	Input/Output
NI	National Instruments™
NPSH	Net Positive Suction Head
ORC	Organic Rankine Cycle
P	Pump
PID	Proportional, Integral and Derivative
SM	Servomotor
SP	Setpoint
T	Turbine
WHR	Waste Heat Recovery

Greek Letters:

α	Thermal losses coefficient
δ	Excess air
ε	Error
η	Efficiency

Subscripts:

a	available
b	burner
c	combustion
e	electric
f	thermal fluid
fg	flue gases
g	natural gas
h	hydraulic
in	inlet
mag	magnetic
max	maximum
mec	mechanic
mid	middle
out	outlet
pinch	pinch-point
t	thermodynamic
tl	thermal losses
v	volumetric
w	water

1. Introduction

In the last decades, there is a growing interest in reducing energy consumption and associated greenhouse gas emissions in every sector of the economy. Wood et al. state that significant proportions of total energy-consumption accounts in the residential sector and developing low energy domestic equipment is a route to reduce it [1]. Dentice d'Accadia et al. refers that the combined heat-and-power (CHP) has been considered, worldwide, as the major alternative to traditional systems in terms of significant energy savings and environmental conservation [2]. Replacing the conventional combi-boilers by a fully operational micro-CHP ORC-based natural gas boiler that satisfies the hot waters and central heating domestic needs is the ultimate goal of the current work.

Research on ORC systems has been widely investigated in the literature. The bulk of investigations on ORC subject are related to thermodynamic analysis [3–5], working fluids selection [6–8], performance analysis and integration of specific components [9–12] and experimental study of ORC facilities [13–15]. The previous referred works have a particular feature in common, they only analyze the nominal design condition that maximizes certain variables, generally, the thermodynamic efficiency or the electric generation. However, in real applications, ORC systems operate frequently in different conditions from the nominal design point. The heat source quality or the load demand often changes, depending on the application, and the system must adapt itself in order to guarantee stable and safe operation. Also, a system able to operate efficiently at any off-design condition is required and critical for a broader approval of these systems. Therefore, an appropriate control strategy should be developed to guarantee safety, feasibility, and the best performance, maximizing the power generated at any predictable off-design condition.

The real behavior of ORC systems under off-design conditions has gained significant interest over recent years. A standard approach is the development of steady-state off-design models for the performance evaluation of ORC systems under real operating conditions, which are variable and non-nominal most of the time. This approach, on the one hand, must postulate *a priori* a quasi-steady control strategy of the ORC in off-design conditions. On the other hand, it neglects the transient behavior of the ORC following any variation of boundary conditions. Ibarra et al. [16] investigate the performance of a small regenerative ORC system at part load operation. The scroll expander rotational speed and working pressure were adjusted to meet the load requirement and maximize the efficiency for a conceptual given heat source and cold sink temperature. The authors conclude that the performance of the ORC is influenced strongly by the isentropic efficiency of the expander and its irreversibilities. Fu et al. [17] analyzed the influence of the heat source temperature out of the design conditions in the ORC system. The control of the operating high pressure of the cycle allows that R245fa reaches the saturation liquid and vapor states at the outlet of the preheater and evaporator, respectively. However, the ORC model uses fixed efficiencies for the main components, which are not accurate in off-design modeling. Dickes

et al. [18] compares different off-design modeling approaches for the simulation of ORC-based power systems and experimentally validated it in two facilities. The results show that semi-empirical models are the most reliable, while constant-efficiency and polynomial-based models are both demonstrating a lack of accuracy and/or robustness. Mondejar et al. [19] carried out a quasi-steady state simulation with an off-design model, based on optimized design conditions, to estimate the average net power production during a passenger ship standard round trip. The authors used the experimental data of the exhaust gas temperatures and engine loads as model inputs confront the estimated average net power production of the ORC with the electricity demand on board. Chatzopolou et al. [9] developed an optimization tool to predict the impact of recovering heat from the exhaust gases of an internal-combustion engine (ICE). The results showed that by accounting for the performance variability of the main components, the ORC engine's thermal efficiency could be maintained at off-design conditions. Moreover, the authors state that the design of real-time controllers capable of monitoring the temporal heat-source variations and instructing the ORC engine to adjust its operation accordingly is a key challenge.

The stationary off-design models can be additionally employed to assist the control of the ORC system. In fact, performing successive steady-state calculations allows the development of quasi-stationary optimal control strategies by controlling some variables to obtain the best ORC performance in response to changing boundary conditions, with no concern with the system evolution between two optimal equilibrium states. Cao and Dai [20] assessed the off-design performance of a combined gas turbine-ORC system under different operation approaches. Mainly concerned with control strategies for the turbine, the results showed that the sliding pressure operation afforded the best off-design performance. Hu et al. [21] presented a control strategy for different mass flow rates and temperatures of the geothermal hot source based on the off-design model analysis of a variable inlet guide vane ORC system. The authors assess different control approaches using the guide vane outlet angle and evaporating pressure as control variables to maximize the net power generated. Manente et al. [22] developed an off-design model for a geothermal binary cycle power plant. The main plant components were modeled through steady-state characteristic curves and the control variables are the dependent variables of these curves. In the first stage, the model runs in a partially transient mode to dimension two capacities added to the plant layout to stabilize its behavior. In a second stage, based on the steady-state solutions of the model, the authors conceive an optimal control strategy that maximizes the power generated for any ambient temperature and/or geo-fluid temperature. The results show that the cold source temperature substantially influences the power output.

Dynamic models are a more sophisticated approach to address the ORC control strategy. The central goal is to maintain or lead the system to equilibrium safely and in the shortest possible time in response to uncontrolled or desired variations of any boundary variables [23]. Dynamic models allow not only to determine the best sensitivity pairing between control and controlled variables, as the quasi-steady models, but also to find the optimal dynamic matching between them [24]. Such type of model further

enables an a priori estimation of the optimal PI/PID coefficients [23] and grant fast and safe transients (over/under-shoots) in response to quick variations, for instance, of the heat-source or cold-source of the system [25] [26]. One of the first papers on dynamic ORC control strategies is Quoilin et al. [27], applied to the recovering of energy from a variable flow rate and temperature waste heat source. The authors proposed a dynamic model of the ORC focused specifically on the time-varying performance of the heat exchangers. The simulation results show that a model predictive control strategy of PI controllers based on a previously established steady-state optimization of the cycle under various conditions produces the best results. Bamgbopa et al. [28] developed a strategy to maintain optimal stable operation of an ORC by adjusting evaporator flow rates according to the available solar heat source temperature and flow rate. Steady sub models for some components and transient for the heat exchangers were formulated to study its dynamic response when available thermal energy gradually or abruptly changes. Jolevski et al. [24] proposed a decentralized control structure by loop pairing using the non-square relative, and dynamic non-square relative gain array methods. A linear model is used to analyze the interaction effects among the control and disturbance inputs, taking into account the coupling of the dynamics between different inputs and outputs of the ORC. In fact, waste heat recovery (WHR) systems are known for unsteady heat sources, with variations of the temperature and mass flow rate, which causes disturbances in the system and consequently fast transients that need to be handled. Zhang et al [25] and Shi et al. [26] addressed the control strategy problem in WHR systems using dynamic models in power plants and automotive engines, respectively. In particular, the first authors apply a promising multi-variable predictive control strategy. The choice between quasi-steady state and dynamic simulation depends on the variability of the heat source, on the computational time that can be tolerated and on the desired level of detail of the description of the transient behavior of the system [29]. The literature survey shows that only a few studies have used stationary off-design models to develop optimal control strategies capable of maximizing the ORC performance for any given boundary conditions. The majority of the works employ dynamic models for control purposes, while stationary off-design models are mostly used for performance evaluation in real operating conditions. Moreover, the start-up problem is hardly discussed since it does not often occur in continuously operating ORC applications such as geothermal, biomass, or waste heat recovery, mostly concerned about heat source quality. At the same time, to the authors knowledge, the control of ORC micro-CHP under user demand (cold sink) variations in terms of water mass flow rate and end-user temperature was not addressed.

This work aims to develop a suitable control strategy for an ORC micro-CHP system under variable user demand conditions using a stationary off-design and charge-sensitive mode already partially validated [30]. In the first stage, the model is employed to thoroughly characterize the steady-state behavior of the micro-CHP, identify its stable operation regions and generate its complete control maps. In a second stage, a complementary empirical dynamic control strategy based on PIDs is established to

guide the system through a quick and safe operation path during start-ups and user demand variations, towards the compatible best performance steady-state maximizing the power generated.

2. ORC SYSTEM SETUP AND MODEL

2.1. The experimental setup

The ORC system considered in this work is a micro-CHP unit built in the University of Coimbra assembled with off-the-shelf components except for the evaporator, which is an in-house developed component. The ORC test setup is shown in Figure 2 and its schematic representation is given in Figure 1. This experimental setup has a nominal electrical power output of 1 kWe and uses R-245fa as working fluid. The high-quality ORC heat source is the stream of hot gases resulting from the natural gas combustion that will directly evaporate the working fluid while the cold source is the water that will meet the user's demands of domestic hot water. As depicted in Figure 2, the ORC system is composed of:

- A scroll expander magnetically coupled to a controlled speed servo-motor which generates the electrical power ultimately dissipated in a set of resistances;
- A hermetic rotary-vane pump magnetically coupled to an electrical motor with a speed controller that circulates and pressurizes the working fluid through the pipeline;
- A thermally-insulated brazed plate compact heat exchanger (condenser) entrusted with the heat transfer from the condensing working fluid for the user hot water; and
- A controlled (gas flow rate) and tuned (air-to-fuel ratio) premixed natural gas burner, which produces hot combustion gases connected to a double-helical heat exchanger (evaporator), ensuring a counter flow between the hot gases and the ORC working fluid [31].

The test rig is fully instrumented with temperature and pressure sensors at each point of the thermodynamic cycle. Moreover, a liquid flow meter and a power meter allow to characterize the behavior of each component and assess the global cycle performance. The complete description of the ORC test-rig is presented in Santos et al. [32]**.** The data acquisition, real-time processing, and control system are established through NI data loggers connected to a pc running an application developed in LabVIEW [33].

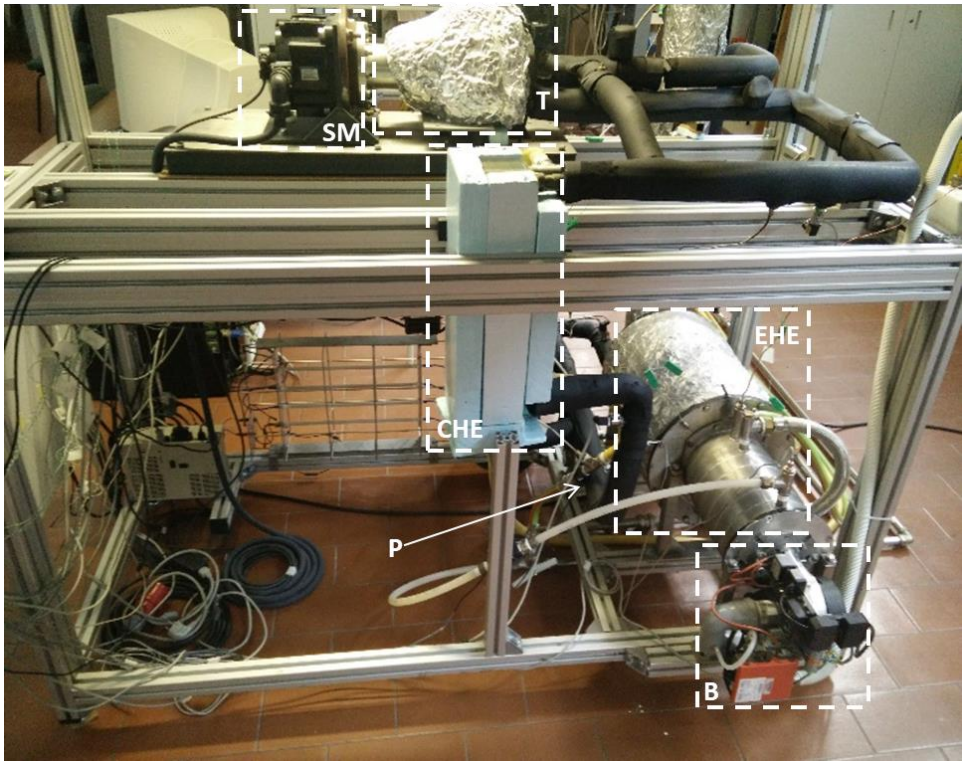

Figure 1 - Photograph of the micro-CHP experimental test rig (Legend: B-Burner, EHE –Evaporator Heat Exchanger, P-Pump, T – micro-turbine (scroll expander), SM – Servo-motor, CHE – Condenser Heat Exchanger)

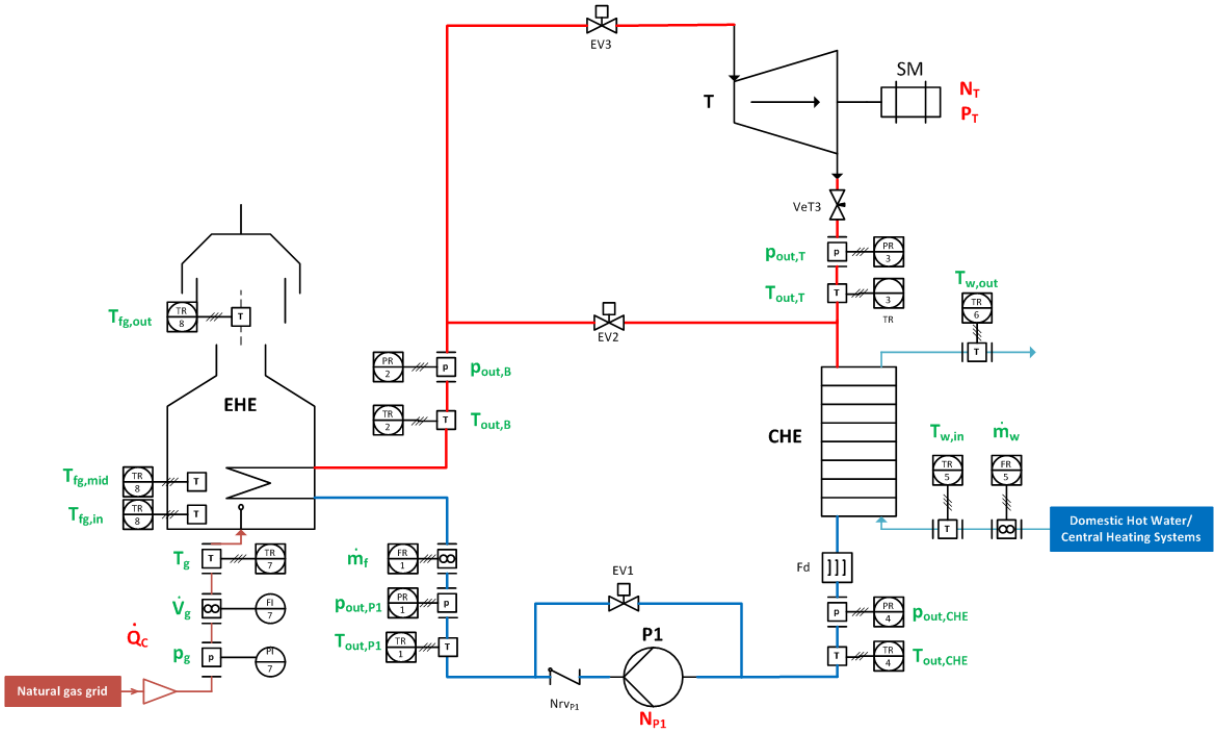

Figure 2- Complete test rig sketch with all the components and measuring instruments. *Legend*: T – temperature sensor, p – pressure sensor, ∞ – flow sensor

2.2 The charge-sensitive off-design model

Off-design models afford the complete thermodynamic state of the ORC based on known boundary conditions, such as, the heat source and the heat sink supply conditions, as well as the pump and the expander speeds. Pre-specifying the sub-cooling at the condenser outlet and the superheating at the expander inlet is a common approach in such type of modeling, but in real operating conditions, they are not precisely known *a priori*. However, if the conservation equation of the ORC's working fluid mass is incorporated in the model, these inputs shall not be required. In this way, a charge-sensitive and fully-predictive model can be attained. This type of model is advantageous for evaluating ORC performance in an extensive range of conditions, obtaining the optimal values of control inputs, and thus assisting in the ORC's control strategy, the ultimate goal of this paper.

In this work, the complete modular off-design and charge-sensitive model described in Santos et al. [30] is employed to assess the impact of the operating parameters and guide the control implementation. The model developed in FORTRAN code incorporates the Refprop fluid library for thermodynamic physical properties calculation [34]. Empirical submodels are applied for the pump and expander employing the manufacturers' characteristic curves. The condenser submodel is a three-zone moving boundary model with variable heat transfer coefficients. In contrast, the evaporator submodel is a finite volume model that discretizes the heat exchanger into multiple cells and solves the energy and mass balance equations consecutively in each cell. Afterwards, the sub-models of the main components are interconnected according to their physical interrelationships to create the overall system model, which main structure is sketched in Figure 3.

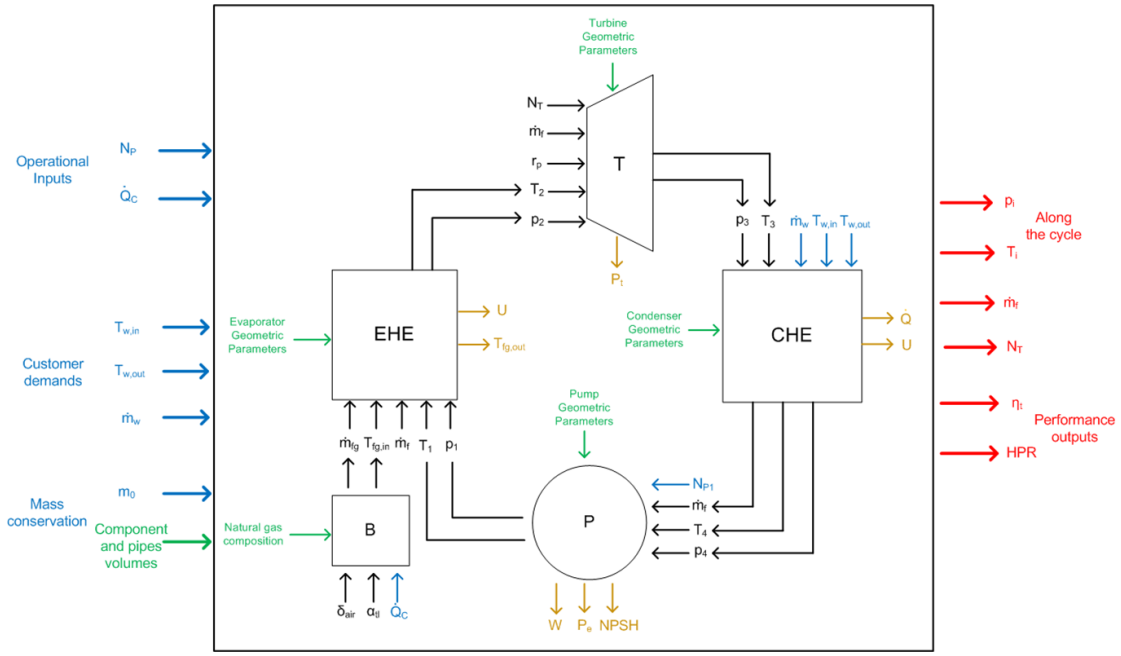

Figure 3 – The complete ORC model schematics. Legend: Main variable inputs (in blue) and outputs (in red), input parameters (in green), components' models specific outputs (in orange) and iteration variables (in black).

3. STUDY OF THE ORC STEADY-STATE CONTROL

The three control variables of the ORC are:

i) $\dot{Q}_c$, the heat power of combustion, controlled through the natural gas flow rate $\dot{V}_g$ control valve;

ii) N_{P1}, the rotational speed of the working fluid volumetric pump P1, directly controlled with a motor speed controller; and

iii) N_{T}, the rotational speed of the expander T, controlled with the servomotor.

For given natural gas, ambient and user $(T_{w,in}, \dot{m}_w)$ input conditions, the control variables' values $(\dot{Q}_c, N_{\mathrm{P1}}, N_{\mathrm{T}})$ determine the water temperature $T_{w,out}$ to the user and all steady-state ORC thermodynamic variables. The corresponding functioning point is admissible only if the following constraints (or conditions of admissibility) are satisfied:

$$p_1 < p_{max}\ (= 1500\ \text{kPa}) \tag{1}$$

$$T_2 < T_{max}\ (= 150\ ^\circ\text{C}) \tag{2}$$

$$\Delta T_2 > \Delta T_{2_0}\ (= 5\ ^\circ\text{C}) \tag{3}$$

$$\Delta T_{pinch}(p_3, T_{w,out}) > \Delta T_{pinch_0} (= 5\ ^\circ\text{C}) \tag{4}$$

$$N_{\mathrm{T}} < N_{\mathrm{T}_0}\ (= 3000\ \text{rpm}) \tag{5}$$

Conditions (1) and (2) are specified by the manufacturer as required to protect the expander while condition (3) assures a minimum superheat to avoid condensation inside the expander. Condition (4) is not strictly necessary; however, it prevents reaching too close to a pinch point operating condition of the condenser. It is formally equivalent to impose a variable lower bound to the temperature T_3 at the inlet of the condenser. In condition (5), the limit value of $N_{\mathrm{T}_0} = 3000$ is imposed by the servomotor presently coupled to the expander, but the expander itself withstands up to $N_{\mathrm{T}_0} = 3500$ rpm. Other conditions (e.g., full condensation of the thermal fluid at the outlet of the CHE) are practically assured, not requiring to be explicitly imposed. An admissible point is considered optimum if it maximizes the ORC thermodynamic efficiency η_t:

$$\eta_t = \frac{\dot{W}_{out} - \dot{W}_{in}}{\dot{Q}_{in}} \tag{6}$$

3.1 Model and algorithm behavior assessment

Before the model can guide the conception of the control strategy of the ORC, it is necessary to master the basic behavior both of the numerical algorithm that implements the model (ignition, stability, speed

of convergence and errors) and of the model physics itself (single, multiple or no solution; stable and instable solutions), which are indeed intermingled. For that purpose, it is preferable to work with the natural inputs of the model/algorithm, fully specifying the user conditions, including $T_{w,out}$, and leaving the control variable N_{T} as an output.

In this vein, several steady-state calculations with different pairs of the heat power of combustion and rotational speed of the pump ($\dot{Q}_c$, N_{P1}), forming a grid, were performed for typical natural gas, ambient and user hot waters specification $\left(T_{w,in} = 15\ °\mathrm{C}, T_{w,out} = 40\ °\mathrm{C}, \dot{m}_w = 0.1\ \mathrm{kg/s}\right)$ conditions, and a fluid charge of $m_{f_0} = 3.74$ kg. Figure 4 depicts some level lines of a set of operational variables of the ORC in the region $\left(\dot{Q}_c = 14.6 - 15.8\ \mathrm{kW_t}, N_{\mathrm{P1}} = 750 - 1050\ \mathrm{rpm}\right)$ of the control plane $\dot{Q}_c - N_{\mathrm{P1}}$. The model exhibits no solution to the right of the dashed line, which indicates that no steady-state can be achieved for the ORC in this zone.

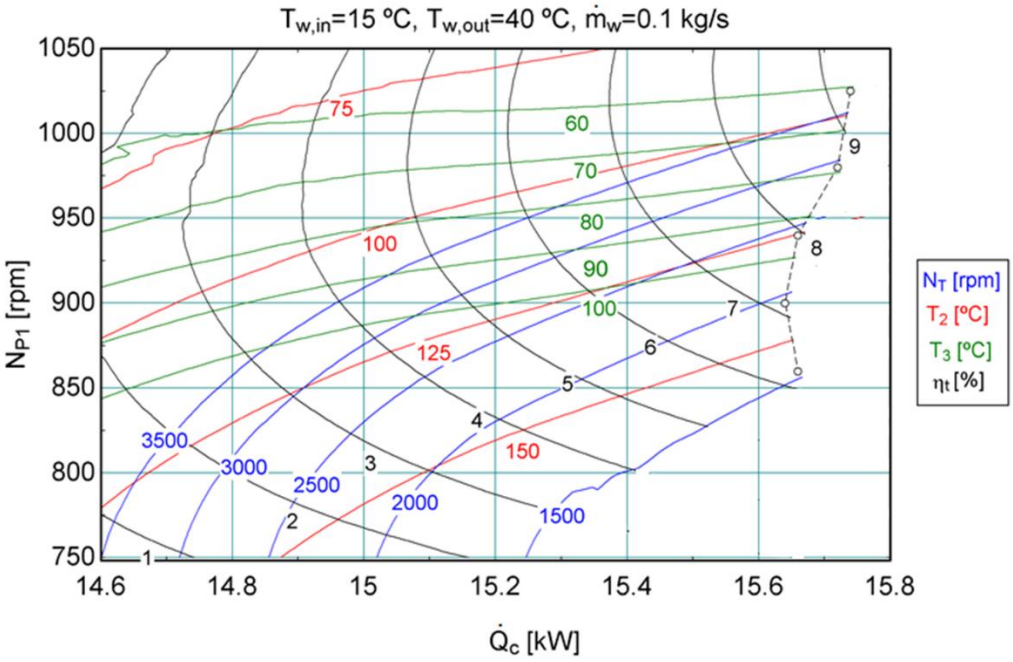

Figure 4 - Level lines of the variables $(N_{\mathrm{T}}, T_2, T_3, \eta_t)$ in the control plane $\dot{Q}_c - N_{\mathrm{P1}}$ of the ORC, for given costumer conditions (typical of hot water needs).

In general, three main regions of steady-state solutions (or no solution) of the model/algorithm were found in the control plane, represented qualitatively in Figure 5: I) single stable and admissible solution (but, for some user conditions and in some sub-regions, one or two more numerical solutions, unstable and either physically spurious or uninteresting); II) seemingly, single stable but either non-admissible or uninteresting solution; and III) region outside zones I and II, where there is no solution.

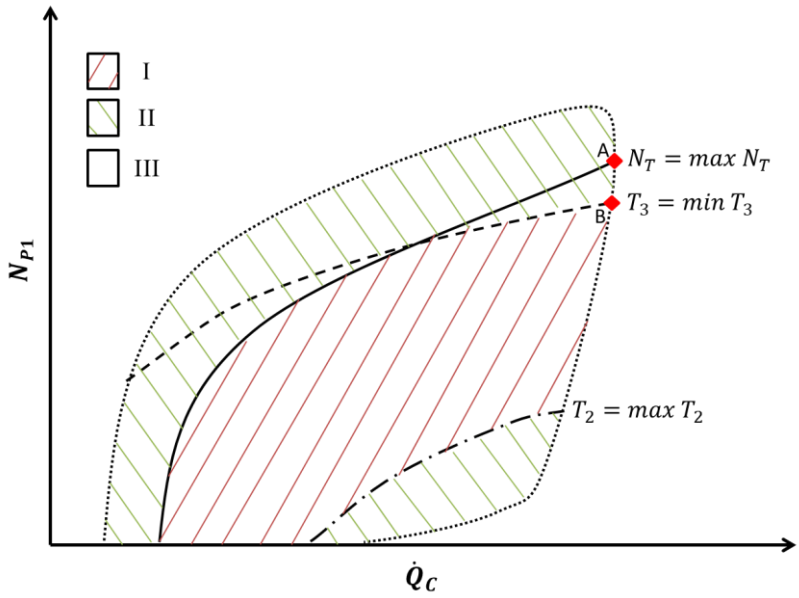

Figure 5 - Regions of steady state solutions of the model/algorithm of the ORC system for given user conditions.

In regions I and II, numerically unstable solutions are found by varying the seed of the iteration very finely and carefully for some user conditions and sub-regions. These solutions are either non-admissible or have bizarre values for some variables (e.g., abnormally low speed of rotation of the expander N_{T}) that seem physically meaningless. When the solution seems to be physically possible, it is quite probable that the above-mentioned numerical instability has a physical origin that would turn difficult the ORC control. Given the form of the level lines of the ORC thermodynamic efficiency η_t in the $\dot{Q}_c - N_{\mathrm{P1}}$ plane (see Figure 4), in Figure 4, Point B is the optimal functioning point, with maximum η_t. For other user conditions, Point A, with a value of η_t still higher than Point B, may lay in the admissible region, becoming the optimal point of operation thence. In particular, notice that the nominal point of the ORC (where the efficiency η_t reaches the absolute maximum) is not far away in the plane of Figure 4.

3.2 ORC steady-state control maps

The previous understanding of the model/algorithm of the ORC allows now the (computationally heavy) construction of the control maps of the ORC for any user condition. Keeping all the former input values (namely, the user inputs: $T_{w,in} = 15$ °C, $\dot{m}_w = 0.1$ kg/s), except for $T_{w,out}$ that now exchanges the role of I/O with N_{T}, four illustrative control maps are shown in Figure 6 a-d for $N_{\mathrm{T}} = 1500, 2000, 2500, 3000$ rpm, respectively. In each control plane $\dot{Q}_c - N_{\mathrm{P1}}$ for a given value of N_{T}, the following lines are represented:

i) upper and lower (the latter, except for $N_{\mathrm{T}} = 1500$ rpm) limiting lines of steady operation, which are discussed below;

ii) level line $T_2 = 150$ ℃ (upper admissible limit), below which the operation is inadmissible when this line falls inside the steady operation region (for $N_\mathrm{T} \leq 2500$ rpm);

iii) level line $\Delta T_2 = +5$ ℃ (lower admissible limit), above which the operation is inadmissible when this line falls inside the steady operation region (for $N_\mathrm{T} \geq 2500$ rpm);

iv) level lines $T_{w,out} = 30, 35, 40, 45, 50$ ℃; and

v) a set of level lines of η_t[%].

For the present four values of N_T, no more variables (e.g., p_1 or T_3) limit the operation of the ORC, so the corresponding level lines are not represented. It may be observed that for these particular input and control conditions, the ORC has practically no admissible region of operation for the lowest speed of rotation of the expander $N_\mathrm{T} = 1500$ rpm, because the level line $T_2 = 150$ ℃ is very close to the upper limiting line of the steady-state region. In the case of the two highest speeds of rotation, the admissible zone of the ORC is quite broad, causing additional variables to limit the ORC operation. It is the case of the superheat degree at the expander inlet (ΔT_2) and the expander outlet temperature (T_3).

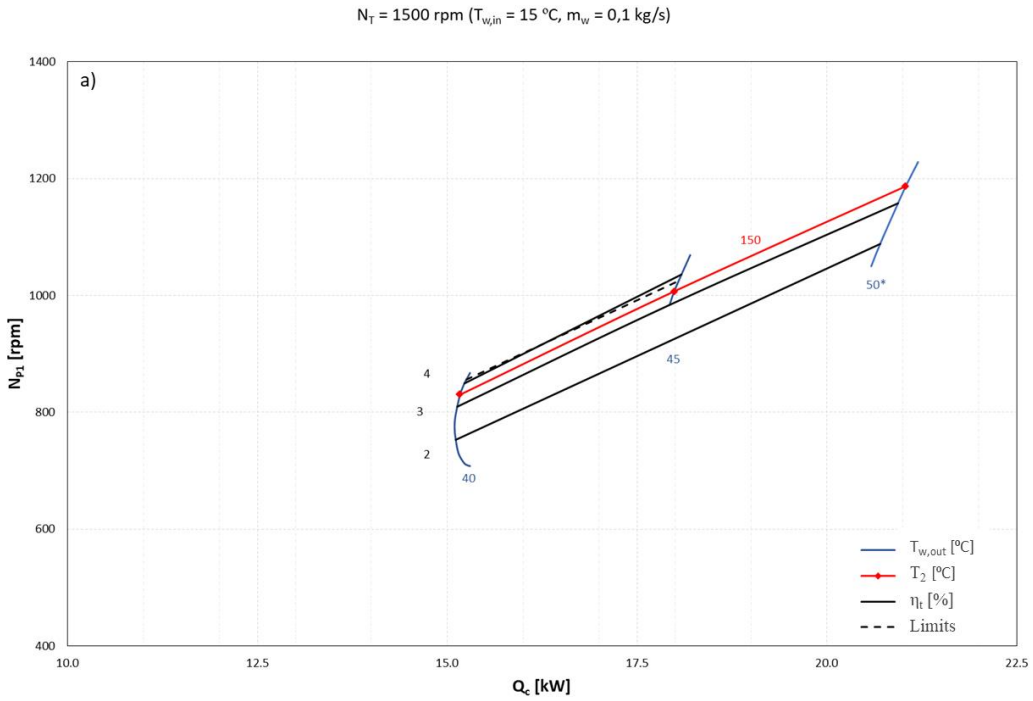

N_T = 2000 rpm ($T_{w,in}$ = 15 °C, m_w = 0,1 kg/s)

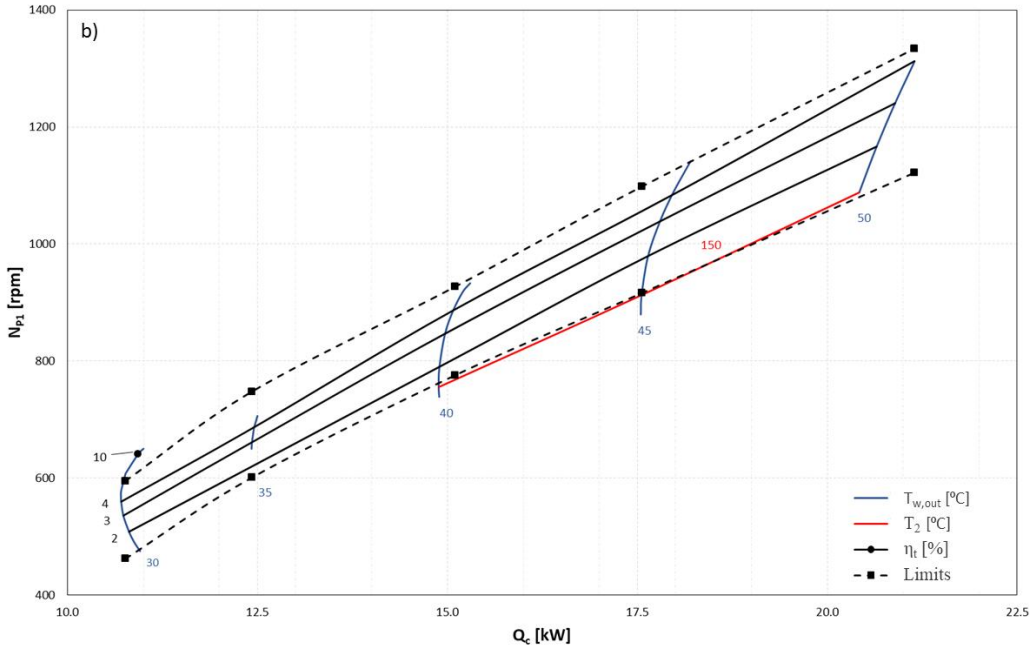

N_T = 2500 rpm ($T_{w,in}$ = 15 °C, m_w = 0,1 kg/s)

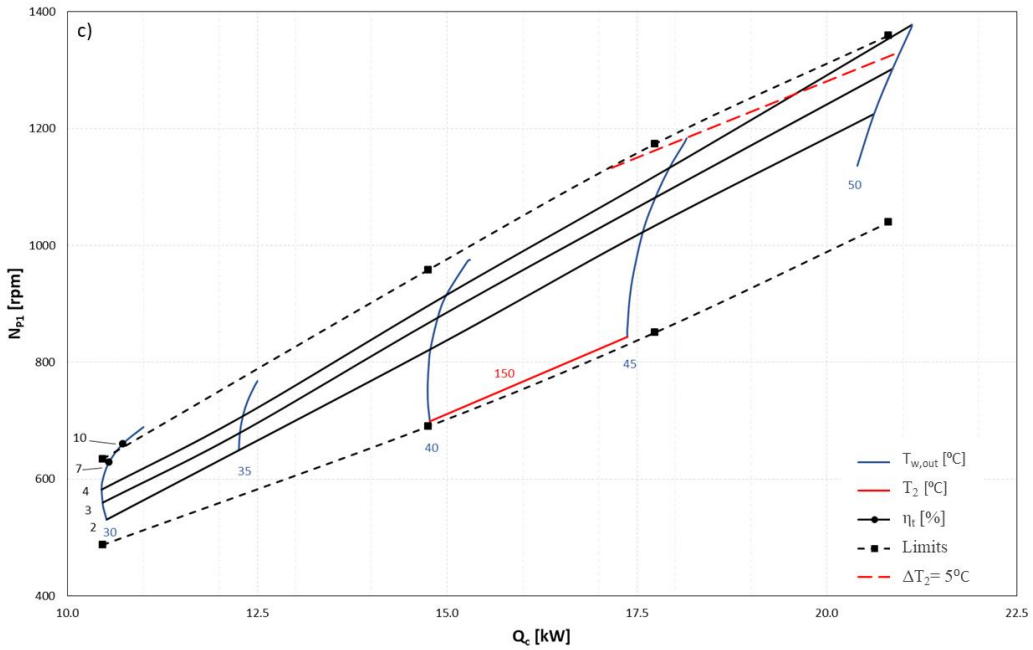

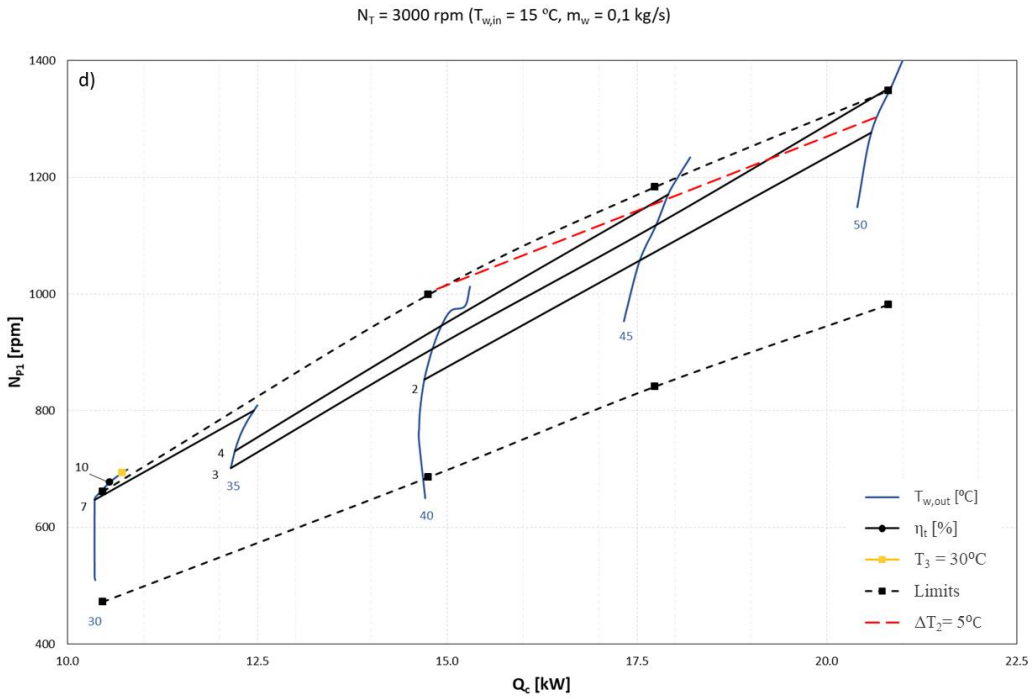

Figure 6 – Control maps of the ORC for $N_{\mathrm{T}}[\mathrm{rpm}] = 1500\,(a), 2000(b), 2500(c), 3000(d)$.

It is rather interesting to physically interpret the upper limiting line of the steady region of operation in the control plane for a given value of N_{T}. In fact, above this line, the two speed controllers, of the pump P1 and the expander T, collide. The first one is trying to enforce a mass flow rate $\dot{m}_f$ (which increases practically linearly with N_{P1}) of fluid through the expander that this cannot cope with while limited, by its speed controller, to rotate at the given N_{T}. The result is an unsteady behavior of the ORC, namely, characterized by sharp fluctuations of the pressure p_2 at the inlet of the expander. This prediction is confirmed in the tests shown in Figure 7. Obviously, this conflict is solved out by increasing the value of N_{T} above a threshold that depends on the input conditions and on the other control variables $(\dot{Q}_c, N_{\mathrm{P1}})$, as can also be seen in Figure 7. The physical interpretation of the lower border of the steady region of operation in a particular control plane is analogous. In fact, for low enough N_{T} (in this case, for $N_{\mathrm{T}} \leq 1500$ rpm), this line falls inside the bottom part of the inadmissible region and, so, it is not restrictive.

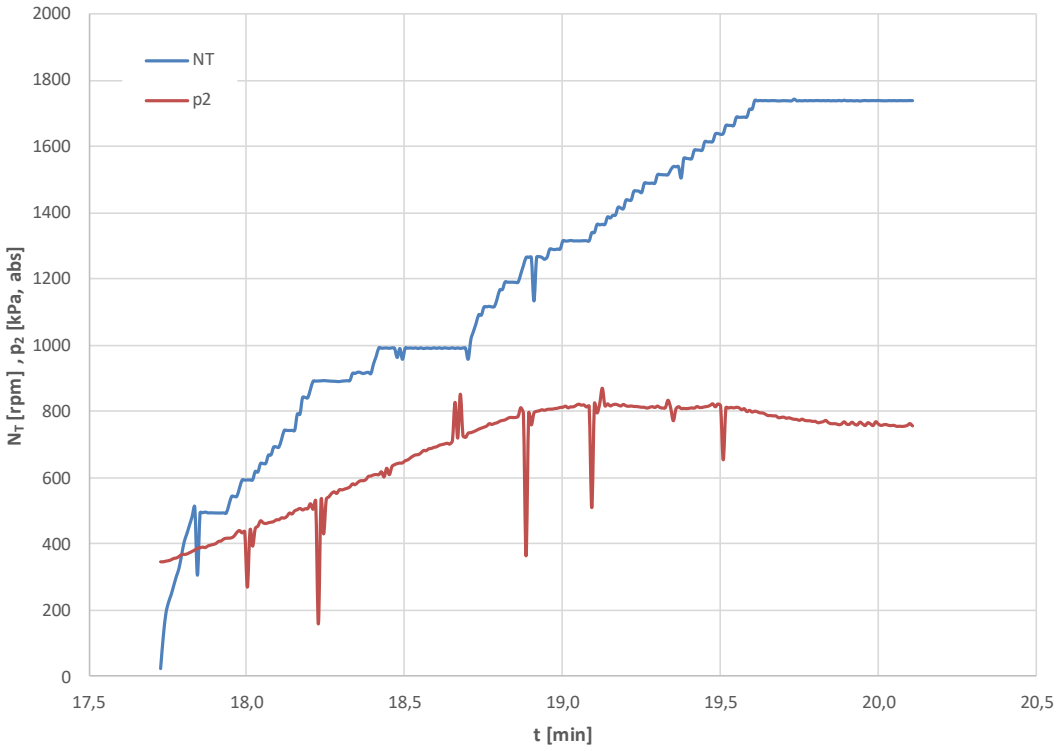

Figure 7 – Instability of the ORC shown up by the fluctuation bursts of the pressure at the inlet of the expander when this is rotating at a low speed.

The fact that the highest admissible value of the efficiency η_t of the ORC occurs on the upper border of the steady operation region (for a given N_{T}), at the intersection with the level-line of $T_{w,out}$ desired by the user (optimal point), poses a challenge to the control algorithm. Summing-up, from the point of view of the ORC control, the analysis of the former control maps shows that:

i) as the value of η_t at the optimal point increases with N_{T}, the latter should be maximized, perhaps by simply setting $N_{\mathrm{T}} = N_{\mathrm{T}_0}$;

ii) the control variable $\dot{Q}_c$ should be used to match the objective condition on $T_{w,out}$ because the slope $\left(\frac{\partial N_{\mathrm{P1}}}{\partial \dot{Q}_c}\right)_{T_{w,out}=cte}$ of the level lines of $T_{w,out}$ is rather high; and

iii) the control variable N_{P1} should be used to approach the optimal point of operation, e.g., by controlling the variable T_2, taking due attention to the challenge referred above.

4. TRANSIENT CONTROL STRATEGY

In summary, each one of the three controllers must pursuit an objective in order to allow the ORC to attain the optimal steady-state satisfying a given demand of hot waters. The rotational speed of the expander N_{T} should be kept constant, say at N_{T_0}, either at the maximum value allowed (Section 3.2) or

at a lower value still to be defined. The heat power of combustion $\dot{Q}_c$ should be adjusted (via the position of the valve of control of the natural gas flow rate $\dot{V}_g$) to assure the outlet water temperature $T_{w,out}$ demanded by the user. The pump speed $N_{\mathrm{P}1}$ should be used to control the vapor temperature T_2 at the outlet of the evaporator, either to approach the most possible the upper border of the steady-state region of operation of the ORC in the control map of $N_{\mathrm{T}} = N_{\mathrm{T}_0}$ (Section 3.2) or to assure that $T_2 < 150$ °C.

Now, the second step of the development of the ORC control strategy has two goals of a dynamic nature. The first goal is that the transient of approach of the optimal steady-state condition at start-up and when there is a deliberate change of the user demand is as fast and safe (e.g., regarding over or under-shoots of constrained ORC variables) as possible. The second goal is to keep the ORC at the desired steady-state regardless of the possible occurrence of small uncontrolled disturbances of some variables (e.g., gas properties, inlet temperature or mass flow rate of the user water).

For that purpose, as the experimental tests and the subsequent model calibration revealed conjuncture setup or design flaws of the particular set of components formed by the expander, magnetic coupling and servomotor reported in Santos et al. [30], the parameters $N_{\mathrm{T}_0} = 2000$ rpm and $T_{2_0} = 120$ °C of the steady-state control strategy were set *a priori* without concern with the full steady-state optimization of the ORC (i.e., the steady-state value of the efficiency η_t will stay somewhat below the maximum possible).

The dynamic control strategy adopted makes use of two independent PID controllers, respectively, for the two pairs of variables $(N_{\mathrm{P}1}[\mathrm{rpm}], T_2[°\mathrm{C}])$ [pump controller] and $\left(\dot{Q}_c[\mathrm{kW}], T_{w,out}[°\mathrm{C}]\right)$ [burner controller]. The servomotor coupled to the expander has an efficient autonomous controller to assure that $N_{\mathrm{T}} = N_{\mathrm{T}_0}$. In fact, PID's are widely used in industrial control environments. Synthetically, the PID controller compares the set-point value y_{SP} with the present value $y(t)$ of the controlled variable in the process in order to obtain the error $\varepsilon(t)$, from which computes an optimized response $u(t)$ of the control variable in order that $\varepsilon(t) \to 0$ (Figure 8).

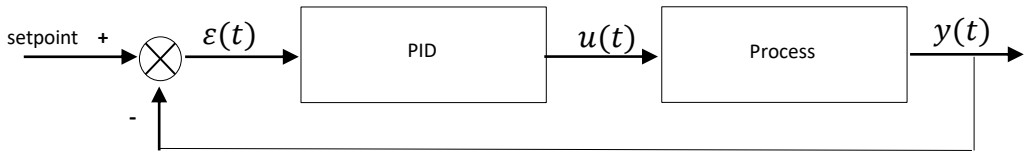

Figure 8 – Block diagram of a generic PID controller integrated in a typical feedback loop involving the process.

Specifically, the control signal $u(t)$ of a PID is described by the equation:

$$u(t) = k_P \left(\varepsilon(t) + \frac{1}{T_I}\int_0^t \varepsilon(\tau)\, d\tau + T_D \frac{d}{dt}\varepsilon(t)\right) \quad (7)$$

where: i) k_P is the proportional gain; ii) T_I is the time constant of the integral correction term, which considers for how long and by how far the process variable was separated from the set point during the time-interval $[0, t]$ with given origin; and iii) T_D is the time constant of the differential correction term, which is interpreted as the controller's anticipated action to the future error evolution.

At first, the simple open-loop Ziegler-Nichols [35] calibration method was applied independently to each PID, affording the coefficients of Table 1. Unfortunately, when both controllers are active, inadmissible instabilities appear, requiring a more sophisticated approach, in this case, empirical.

Table 1 - Pump and burner PID controllers' coefficients obtained with the Ziegler-Nichols calibration method.

	Pump controller	Burner controller
k_p	−19.23	16.55
T_I	0.566	0.423
T_D	0.141	0.105

The control algorithm for a full start-up, from when the system is off till it is steadily (in this case, more or less near to optimally) supplying heat and electricity to the user, encompasses six stages. In each stage, each of the three controllers is in a specific mode (off, preset, PID) and is characterized by specific parameters (set-point of the controlled variable, coefficients, allowed range of the control variable). Depending on the temperature value at a reference point inside the evaporator, three start-ups procedures were conceived: cold, semi-cold and hot. Figure 9 shows an example of a semi-cold start-up, very near to a cold start-up. In all stages, the speed controller N_{P1} of the pump is in PID mode but with evolving parameters.

In stages I to IV, the system works in boiler mode, with the vapor flowing almost integrally through the bypass to the expander. In stages I to III, the controller of the burner is in preset mode with a value of $\dot{Q}_{c_0}$ (in this case, $\dot{Q}_{c_0} = 20$ kW) neither too high to cause a dangerous over-shoot of the temperature T_2 nor too low that the increase rate of $T_{w,out}$ becomes too small. The transition between stages I and II occurs when $T_2 = T_{2_{01}} - 10$ ℃ ($T_{2_{01}}$ is the set-up of the controller when the system is in boiler mode, in this case, $T_{2_{01}} = 75$ ℃). The transition between stages II and III occurs at the bottom of the first under-shoot of T_2, following the first over-shoot. Throughout the first three stages, the configuration of the pump controller suffers various changes with the aim of accelerating the process while avoiding a dangerous over-shoot of T_2, to which the system is prone. The transition condition between stages III and IV is more cumbersome, trying to detect the attainment of the steady condition of T_2 around its set-point and that $T_{w,out}$ is also near or above its set-point (prescribed by the user). In stage IV, the PID controller of the pump is set to its steady-state configuration and the controller of the burner changes from Preset to PID mode to lead the system to its fully steady condition in boiler mode.

In stages V and VI, the system steps from simple boiler to CHP mode, supplying both heat and electricity. The transition between stages IV and V occurs as soon as the expander can be safely put into operation, i.e., the vapor superheat degree ΔT_2 at the inlet is high enough to avoid condensation inside (in this case, somewhat conservatively, it was imposed that $\Delta T_2 > 20$ ºC). Moreover, it must assure that there is no danger of cavitation of the pump P1 due to the strong decrease of pressure p_3 at the outlet of the expander (again on the safe side, assured jointly by $\Delta NPSH_a > 9$ m. f. h and $p_2 > 2.6$ kPa). The valve of the bypass to the expander is closed, forcing the whole flow through the expander, accelerating it. Above a certain threshold of the speed N_T of the expander, the controller of the servomotor drives the rotor to the preset control condition $N_T = N_{T_0}$, maintaining it afterwards. The set-up value of the pump controller rises from $T_{2_{01}}$ (in boiler mode) to the optimal value in CHP mode, established by the steady-state control strategy (in this case, $T_{2_{02}} = 120$ ºC). Additionally, its PID coefficients are also adapted, but the burner controller PID parameters remain unchanged. A collateral effect still not satisfactorily solved is the undershoot of the outlet temperature of the water to the user $T_{w,out}$ (see Figure 9). Finally, at the bottom of the undershoot following the first overshoot of T_2, the system enters in stage VI. The last adjustment of the range of the control variable of the burner controller is performed in order to speed-up the approach to the optimal steady-state of the system in CHP mode compatible with the user demand.

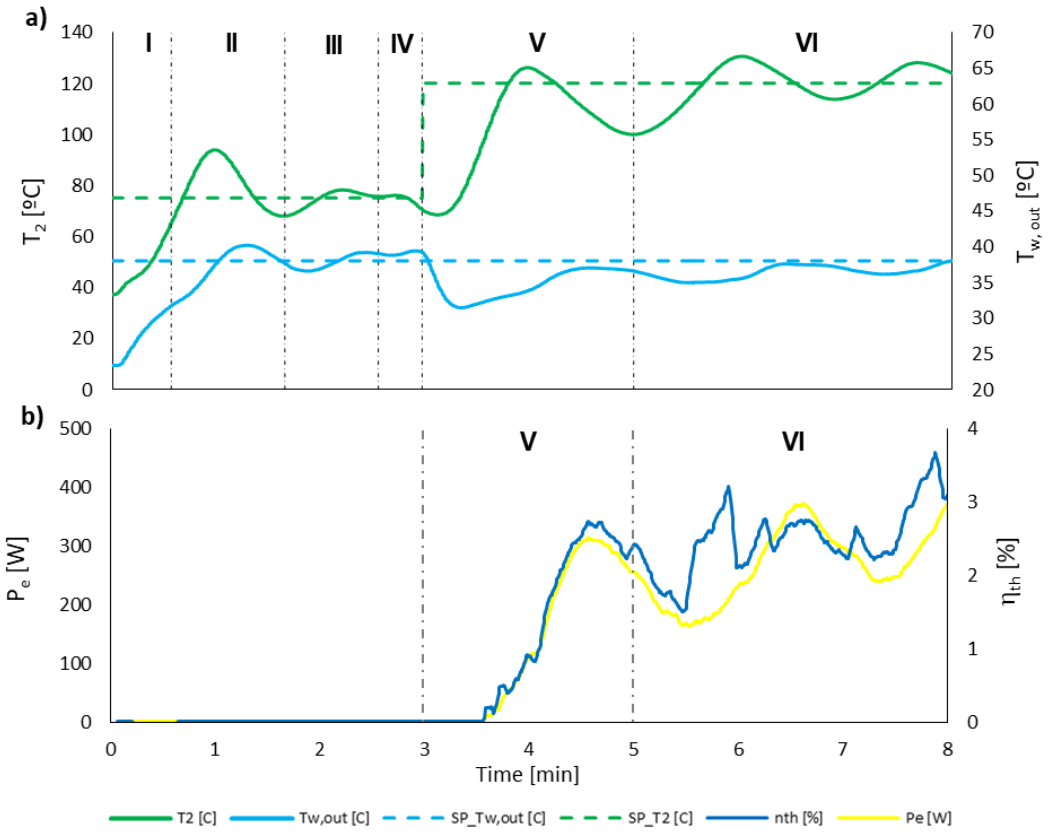

Figure 9– Practical illustration of the empirical control algorithm implemented in a semi-cold start-up.

The progress represented by the present transient control algorithm relative to manual regulation is illustrated in Figure 10. There is a clear improvement in the response time of the machine, as well as in the hot water temperature stabilization around the level desired by the user. The beginning of the production of electrical energy (CHP mode) is triggered at 3 minutes after start-up using automatic control, while in manual control only after 5min 30s it is possible to do it. The control developed for this machine allowed not only to automate the ORC but also to speed up the process to reach the user's target temperature for the hot water, and to produce electricity faster and more effectively.

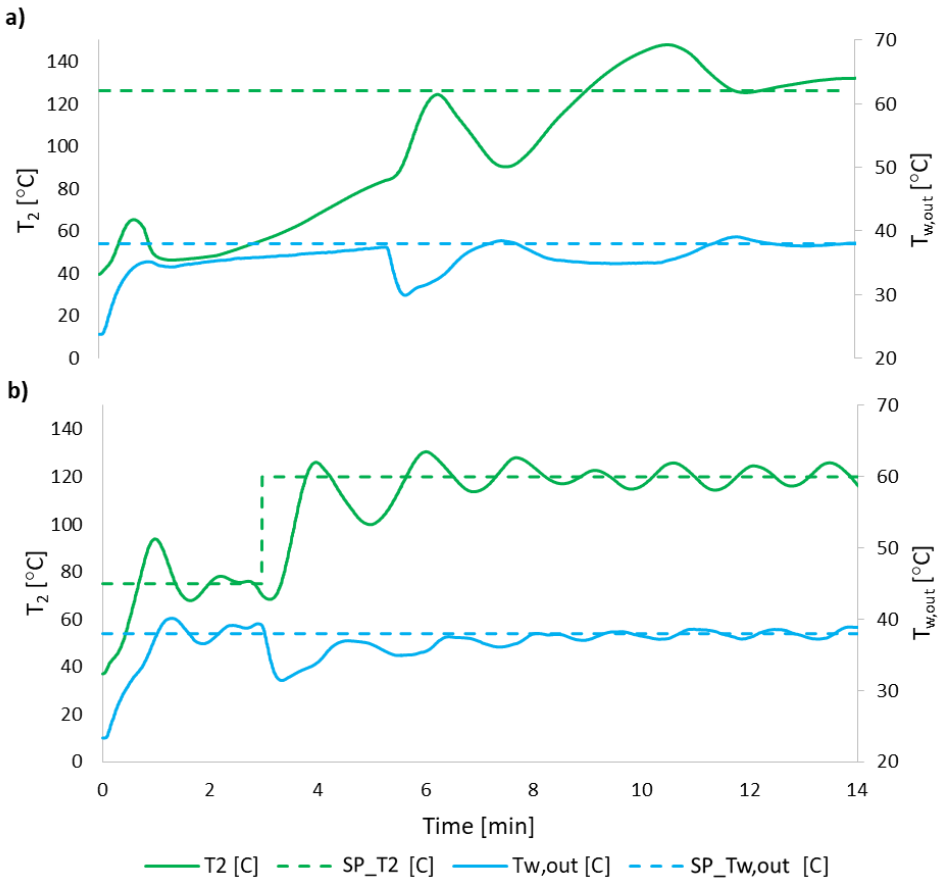

Figure 10– ORC start-up comparison between a) manual regulation of the control variables and b) automatic control by PID controllers

Another instance in which dynamic control is relevant occurs when the user suddenly changes a variable. Figure 11 demonstrates a small shift upwards in the hot water temperature $T_{w,out}$, from 38 to 40 ºC, followed by a symmetrical shift 10 minutes later. Figure 11a show the evolution of the controlled variables $(T_{w,out}, T_2)$. After the user intervention, it can be seen that both temperatures fluctuate more significantly than in steady-state, but with an amplitude that is attenuated over time. Figure 14b shows how the control variables act over time. Figure 11c indicates the corresponding variation of the electrical

power that is produced. The developed control manages to meet user requests without compromising the stability and security of the system. In this case, the conditions imposed by the user require a thermal power supply of 10-15 kW_t and allow the production of electrical energy in the range of 300-500 W. The system reaches an efficiency between 3 and 4% that can be enhanced using the pump speed control to maximize the efficiency, instead of just keeping $T_2 = 120ºC$.

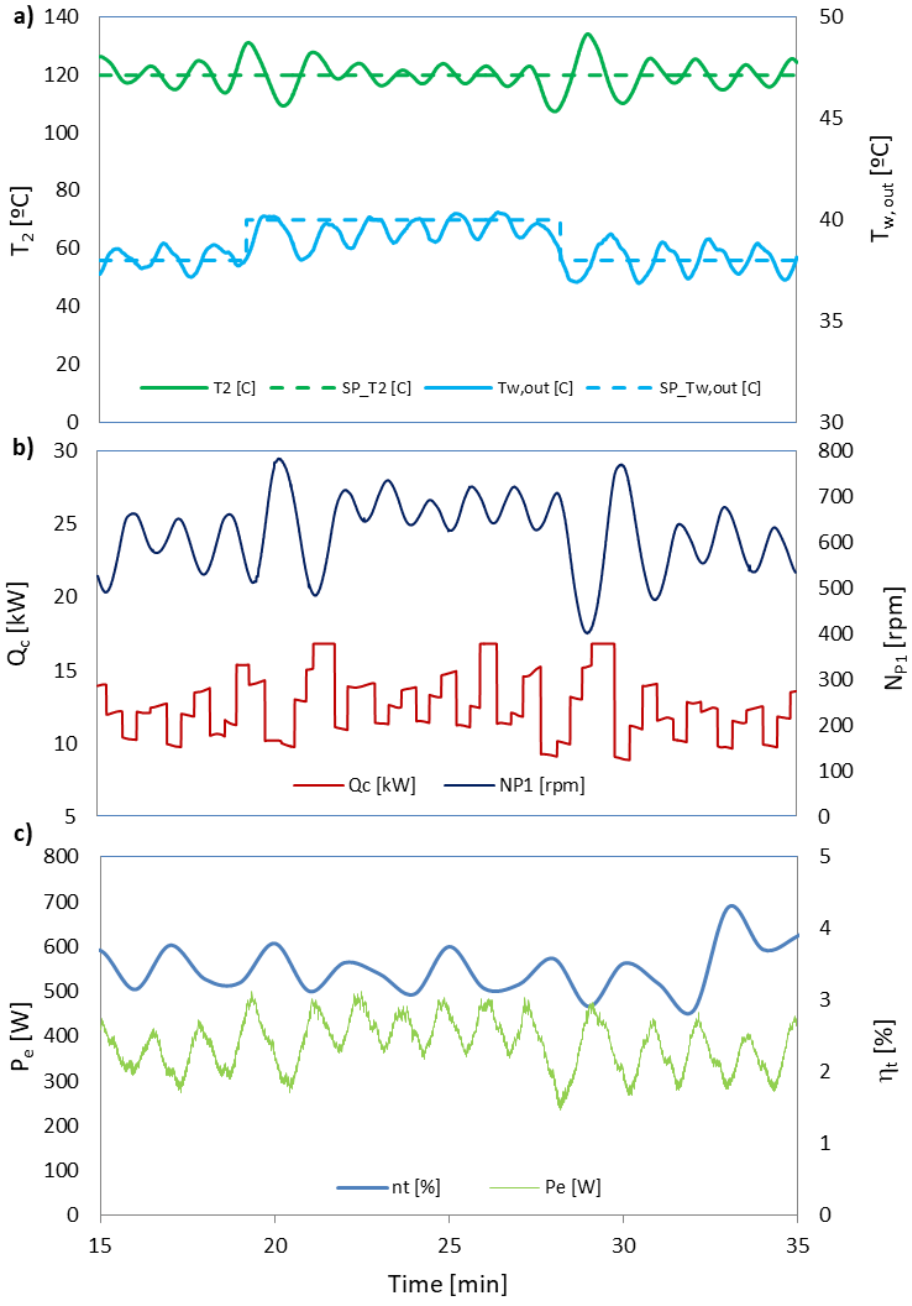

Figure 11 – ORC system response to a user temperature change: a) Controlled variables $(T_2, T_{w,out})$; b) Control variables$(\dot{Q}_c, N_{P1})$, c) Electrical power output P_e.

5. CONCLUSIONS

A steady-state off-design charge sensitive semi-empirical and fully predictive model is used to develop a control strategy for a micro-CHP ORC satisfying typical hot waters domestic needs ($T_{w,out} \leq 40$ ℃, $\dot{Q}_w \leq 35$ kW_t) while producing up to 1 kW_e of electricity. The hot source of the ORC is a natural gas burner that directly evaporates the organic fluid R245fa. Its control variables are the heat power of combustion $\dot{Q}_C$, the rotational speed N_{P1} of the volumetric pump and the rotational speed N_T of the scroll expander.

For given input conditions of the hot source (natural gas) and the cold source (user demands), the model allows the drawing of the steady-state control maps of the ORC in the form of level lines of important operational variables in a collection of planes $\dot{Q}_C - N_{P1}$ for a set of values of N_T. Important qualitative conclusions on the ORC steady control strategy are:

- In some of the control planes $\dot{Q}_C - N_{P1}$, the admissible region of operation is delimited by upper and/or lower lines above/below which the speed controllers of (N_{P1}, N_T) become mutually incompatible, causing an unsteady functioning of the ORC that can be observed, notably, through bursts of high fluctuations of the pressure p_2 at the expander inlet. Other limiting lines of the admissible region can be, at the bottom, the highest admissible level line of the temperature T_2, and, at the top, the lowest admissible level line of degree of vapor superheat ΔT_2, both variables referring to the expander inlet.
- The control variable $\dot{Q}_c$ should be used to match the objective user condition on $T_{w,out}$. The control variable N_{P1} is best suited to lead the ORC to the optimal point of the pertinent plane $N_{P1} - \dot{Q}_c$, with maximum thermodynamic efficiency η_t, through the direct control of variable T_2. The control variable N_T can be kept at a practically constant optimal value.

An empirical transient control strategy is also devised for the ORC making use of two PID's for the pairs of variables $(N_{P1} \rightarrow T_2)$ and $(\dot{Q}_c \rightarrow T_{w,out})$, and of a third autonomous controller of the servomotor for N_T. For cold, semi-cold and hot start-ups, this strategy may change the state (off/on) and the mode (preset/PID) of each controller, and, in the PID mode, some of its parameters, throughout six stages, leading the ORC as fast and safely as possible to its optimal steady functioning condition compatible with the user requirements, firstly in simple boiler mode (first to fourth stages) and lately in CHP mode (fifth and sixth stages). Typical achievements of the strategy in a semi-cold (very near to cold) start-up are:

- The maximum temperature T_2 of the ORC never attains dangerous values.
- In simple boiler mode, the temperature $T_{w,out}$ is stabilized within ± 1 ℃ in 1.5 min.
- The steady CHP operation is attained in $5 - 7$ min.

- In CHP mode of operation, the water temperature to the user $T_{w,out}$ may fluctuate ± 2 ℃ and the electrical power output P_e, ± 50 W.

A sub strategy of the former, dealing with sudden shifts of the user temperature requirements of $\Delta T_{w,out} = \pm 2$ ℃, demonstrates the following performance indicators, not quite satisfactory:

- The maximum temperature T_2 may fluctuate by $\pm(12 - 15)$ ℃, and the power output P_e by ± 100 W, but the water temperature to the user $T_{w,out}$ has no significant over or undershoots.
- The new steady-state is attained in less than 2 min.

For future work, the control strategy can be further improved by decreasing fluctuations, reducing the start-up duration and minimizing some undershoots in the simple to cogeneration boiler transition and in the user demand transitions.

ACKNOWLEDGEMENTS

This research is partially sponsored by FEDER Funds through the program COMPETE – Programa Operacional Factores de Competitividade under the contract QREN-POFC-COMPETE-23101 concerning Project HEBE. This financial support is gratefully acknowledged.

REFERENCES

[1] Wood G, Newborough M. Dynamic energy-consumption indicators for domestic appliances: Environment, behaviour and design. Energy Build 2003;35:821–41. https://doi.org/10.1016/S0378-7788(02)00241-4.

[2] Dentice d'Accadia M, Sasso M, Sibilio S, Vanoli L. Micro-combined heat and power in residential and light commercial applications. Appl Therm Eng 2003;23:1247–59. https://doi.org/10.1016/S1359-4311(03)00030-9.

[3] Fan W, Han Z, Li P, Jia Y. Analysis of the thermodynamic performance of the organic Rankine cycle (ORC) based on the characteristic parameters of the working fluid and criterion for working fluid selection. Energy Convers Manag 2020;211:112746. https://doi.org/10.1016/j.enconman.2020.112746.

[4] White MT, Oyewunmi OA, Chatzopoulou MA, Pantaleo AM, Haslam AJ, Markides CN. Computer-aided working- fl uid design , thermodynamic optimisation and thermoeconomic assessment of ORC systems for waste-heat recovery. Energy 2018;161:1181–98. https://doi.org/10.1016/j.energy.2018.07.098.

[5] Liu H, Shao Y, Li J. A biomass-fired micro-scale CHP system with organic Rankine cycle (ORC) - Thermodynamic modelling studies. Biomass and Bioenergy 2011;35:3985–94. https://doi.org/10.1016/j.biombioe.2011.06.025.

[6] Guo T, Wang HX, Zhang SJ. Selection of working fluids for a novel low-temperature geothermally-powered ORC based cogeneration system. Energy Convers Manag 2011;52:2384–91. https://doi.org/10.1016/j.enconman.2010.12.038.

[7] Oyewunmi OA, Kirmse CJW, Pantaleo AM, Markides CN. Performance of working-fluid mixtures in ORC-CHP systems for different heat-demand segments and heat-recovery temperature levels. Energy Convers Manag 2017;148:1508–24. https://doi.org/10.1016/j.enconman.2017.05.078.

[8] Qiu G. Selection of working fluids for micro-CHP systems with ORC. Renew Energy 2012;48:565–70. https://doi.org/10.1016/j.renene.2012.06.006.

[9] Chatzopoulou MA, Simpson M, Sapin P, Markides CN. O ff -design optimisation of organic Rankine cycle (ORC) engines with piston expanders for medium-scale combined heat and power applications. Appl Energy 2019;238:1211–36. https://doi.org/10.1016/j.apenergy.2018.12.086.

[10] Ziviani D, James NA, Accorsi FA, Braun JE, Groll EA. Experimental and numerical analyses of a 5 kWe oil-free open-drive scroll expander for small-scale organic Rankine cycle (ORC) applications. Appl Energy 2018;230:1140–56. https://doi.org/10.1016/j.apenergy.2018.09.025.

[11] Santos M, André J, Mendes R, Ribeiro JB. Design and modelling of a small scale biomass-fueled CHP system based on Rankine technology. Energy Procedia, vol. 129, 2017. https://doi.org/10.1016/j.egypro.2017.09.143.

[12] White MT, Oyewunmi OA, Haslam AJ, Markides CN. Industrial waste-heat recovery through integrated computer-aided working-fluid and ORC system optimisation using SAFT-Γ Mie. Energy Convers Manag 2017;150:851–69. https://doi.org/10.1016/j.enconman.2017.03.048.

[13] Cao Y, Gao Y, Zheng Y, Dai Y. Optimum design and thermodynamic analysis of a gas turbine and ORC combined cycle with recuperators. Energy Convers Manag 2016;116:32–41. https://doi.org/10.1016/j.enconman.2016.02.073.

[14] Han Z, Fan W, Zhao R. Improved thermodynamic design of organic radial-inflow turbine and ORC system thermal performance analysis. Energy Convers Manag 2017;150:259–68. https://doi.org/10.1016/j.enconman.2017.08.025.

[15] Farrokhi M, Noie SH, Akbarzadeh AA. Preliminary experimental investigation of a natural gas-fired ORC-based micro-CHP system for residential buildings. Appl Therm Eng 2014;69:221–9. https://doi.org/10.1016/j.applthermaleng.2013.11.060.

[16] Ibarra M, Rovira A, Alarcón-padilla D, Blanco J. Performance of a 5 kW e Organic Rankine Cycle at part-load operation. Appl Energy 2014;120:147–58. https://doi.org/10.1016/j.apenergy.2014.01.057.

[17] Fu B, Hsu S, Lee Y, Hsieh J, Chang C, Liu C. Effect of off-design heat source temperature on heat transfer characteristics and system performance of a 250-kW organic Rankine cycle system.

Appl Therm Eng 2014;70:7–12.

[18] Dickes R, Dumont O, Daccord R, Quoilin S, Lemort V. Modelling of organic Rankine cycle power systems in off-design conditions : An experimentally-validated comparative study. Energy 2017;123:710–27. https://doi.org/10.1016/j.energy.2017.01.130.

[19] Mondejar ME, Ahlgren F, Thern M, Genrup M. Quasi-steady state simulation of an organic Rankine cycle for waste heat recovery in a passenger vessel. Appl Energy 2017;185:1324–35. https://doi.org/10.1016/j.apenergy.2016.03.024.

[20] Cao Y, Dai Y. Comparative analysis on off-design performance of a gas turbine and ORC combined cycle under different operation approaches. Energy Convers Manag 2017;135:84–100. https://doi.org/10.1016/j.enconman.2016.12.072.

[21] Hu D, Zheng Y, Wu Y, Li S, Dai Y. Off-design performance comparison of an organic Rankine cycle under different control strategies. Appl Energy 2015;156:268–79. https://doi.org/10.1016/j.apenergy.2015.07.029.

[22] Manente G, Toffolo A, Lazzaretto A, Paci M. An Organic Rankine Cycle off-design model for the search of the optimal control strategy brine. Energy 2013;58:97–106. https://doi.org/10.1016/j.energy.2012.12.035.

[23] Rech S, Zandarin S, Lazzaretto A, Frangopoulos CA. Design and off-design models of single and two-stage ORC systems on board a LNG carrier for the search of the optimal performance and control strategy. Appl Energy 2017;204:221–41. https://doi.org/10.1016/j.apenergy.2017.06.103.

[24] Jolevski D, Bego O, Sarajcev P. Control structure design and dynamics modelling of the organic Rankine cycle system. Energy 2017;121:193–204.

[25] Zhang J, Zhou Y, Li Y, Hou G, Fang F. Generalized predictive control applied in waste heat recovery power plants. Appl Energy 2013;102:320–6.

[26] Shi R, He T, Peng J, Zhang Y, Zhuge W. System design and control for waste heat recovery of automotive engines based on Organic Rankine Cycle. Energy 2016;102:276–86.

[27] Quoilin S, Aumann R, Grill A, Schuster A, Lemort V, Spliethoff H. Dynamic modeling and optimal control strategy of waste heat recovery Organic Rankine Cycles. Appl Energy 2011;88:2183–90. https://doi.org/10.1016/j.apenergy.2011.01.015.

[28] Bamgbopa MO, Uzgoren E. Numerical analysis of an organic Rankine cycle under steady and variable heat input. Appl Energy 2013;107:219–28.

[29] Spliethoff H, Pili R, Romagnoli A, Jim M, Wieland C. Simulation of Organic Rankine Cycle e Quasi-steady state vs dynamic approach for optimal economic performance. Energy 2019;167. https://doi.org/10.1016/j.energy.2018.10.166.

[30] Santos M, André J, Francisco S, Mendes R, Ribeiro J. Off-design modelling of an organic Rankine cycle micro-CHP: Modular framework, calibration and validation. Appl Therm Eng

2018;137. https://doi.org/10.1016/j.applthermaleng.2018.04.009.

[31] Pereira JS, Ribeiro JB, Mendes R, André JC. Analysis of a hybrid (topping / bottoming) ORC based CHP configuration integrating a new evaporator design concept for residential applications. Appl Therm Eng 2019;160:113984. https://doi.org/10.1016/j.applthermaleng.2019.113984.

[32] Santos M, André J, Costa E, Mendes R, Ribeiro J. Design strategy for component and working fluid selection in a domestic. Appl Therm Eng 2020;169:114945. https://doi.org/10.1016/j.applthermaleng.2020.114945.

[33] Bitter R, Mohiuddin T, Nawrocki M. LabVIEW: Advanced programming techniques. 2018.

[34] NIST - National Institute of Standards and Technology, Reference Fluid Thermodynamic and Transport Properties Database (REFPROP) 2018.

[35] Ohri J. FUZZY Based PID Controller for Speed Control of D . C . Motor Using LabVIEW 2 DC Motor Mathematical Model 2015;10:154–9.

Chapter 7

Conclusions and perspectives

This last chapter summarises the main findings and results of this work. Perspective themes and improvements for future work are also revealed.

Conclusions and Perspectives

7.1 Conclusions

This thesis can be envisaged as a research co-product of a larger industrial R&D project (Project HEBE) aiming at designing an innovative micro-CHP (Combined Heat and Power) gas boiler based on Rankine technology, heretofore named Hebe. This project was developed in a context of co-promotion among companies and R&D institutions with a clear focus on the market, with the inherent pressures of time, resources and results. Consequently, the research co-products as the scientific papers and the academic theses were delayed about their development and subsequent publication. The beginning of this thesis took place in the academic year of 2014/15, roughly in the middle of Project HEBE, but it was only well after the end of the project that scientific papers were written out and published. Because the PhD work was developed in a company instead of a purely academic domain, more elaborated scientific products and without delays could have been achieved.

As stated in the general introduction, the goal of this PhD work is to assist in the thermodynamic project and the development of Hebe. In order to accomplish it, a set of modelling tools able to simulate the system's operational behaviour was required to develop. An engineering cost-benefit effective bottom-up approach was followed, from simple thermodynamic models, evolving to more sophisticated component sub models and complex global ORC model. Ultimately, a precise and fully predictive model is constructed to describe the system steady-state off-design behaviour requiring solely the operating and boundary conditions. Such tool constitutes the core of this thesis. A concise summary of the main outcomes, achievements and issues met through this work is reported below.

Chapters 2 and 3

Prior to the beginning of the present thesis, a micro-CHP (Combined Heat and Power) capable of replacing the current domestic combi-gas boilers was identified as a global business opportunity in countries with a sufficiently large domestic segment of medium-high thermal demand. In particular, for an ORC (Organic Rankine Cycle) based micro-CHP, such as Hebe, a low payback period and fine market acceptance can be expected if a good performance and above all, a very competitive price (2.750€-5.000€) can be achieved. Although this solution is not completely new, this

opportunity has not been properly explored by any product (of whatever technology) in the market so far.

An innovative and challenging engineering project of Hebe, which is the motivation of the thesis, framed in the Business Plan behind the R&D Project HEBE, is intrinsic to this business opportunity. Some basic design options for Hebe were initially conceived based on the technological state-of-the-art and market analysis, which were deepened in the present work, including, namely, a more careful cost analysis of Hebe.

Chapter 4 (Paper 1/3)

An original strategy of early design of a basic ORC micro-CHP was developed and specifically applied to Hebe, with the aim of selecting the main components and test-rig instrumentation. The work fosters the state-of-art as develops a design methodology from the scratch to a fully operational experimental test-rig mostly accounting on the user demands (cold source). The main outputs of the design of Hebe are (fully specified):

- The working fluid best choice: R365mfc if Hebe is supposed to serve both central heating and domestic hot waters (DHW), or R245fa if only the DHW matter;
- A volumetric flexible rotary vane pump;
- A volumetric scroll-type expander coupled to a servomotor and a set of resistive dissipaters that act as a brake with speed control;
- An in-house developed direct evaporator in which the R245fa receives heat directly from the combustion gases of a natural gas burner;
- A compact brazed plates heat exchanger as condenser; and
- The operational ranges of the measure and control test-rig instrumentation.

The following tools were developed to implement the design strategy:

- A simplified thermodynamic steady model of the micro-CHP, requiring as inputs the nominal efficiencies of the components, the user demand conditions and three control variables, and giving as output the steady-state operation point of the system, accurately enough if not too far away from the design point.
- An optimization problem for the design point, and a corresponding numerical algorithm to efficiently solve it.

The detailed design (in particular, of the built-in evaporator), the construction and assembly of Hebe and its test bench were carried out by the HEBE Project team, in which the author was integrated, but of which he does not claim significant authorship in the context of the thesis.

The experimental results, in which the ORC components are not working far from the assumed nominal efficiencies, showed a reasonable agreement between the experimental and predicted overall thermodynamic efficiency. Additionally, the expected influence of the basic controls is

observed, both of the rotational speed of the pump on the mass flow rate of R245fa and of the thermal power input on the degree of R245fa vapour superheat at the outlet of the evaporator. These results validate the developed design strategy.

Chapter 5 (Paper 2/3)

The development of the complete semi-empirical stationary model of Hebe, which, at the date, was at front of state-of-art, occurred in parallel with the acquisition of components, construction and assembly of the test-rig, but finished earlier. In this way, it was possible to reduce the risk, anticipate and save testing time by achieving an adequate understanding of Hebe's quasi-stationary operation. This model, more realistic and detailed than the simplified model used in Hebe's design, constitutes the most original core of the thesis. In fact, more than a single model, a very general modular modelling architecture was developed, which, by simple replacement or expansion of modules, allows the generation of several models, capable of guiding the evolutionary design of Hebe's prototypes, until reaching a commercial stage.

Each module is composed by a sub model of one of the components of Hebe. Purely empirical models encompassing the manufacturer's characteristic curves were proposed for the turbine/expander and for the pump. A medium level semi-empirical model using a one-dimensional moving-boundary method was applied to the condenser. A complex semi-empirical finite volume model was developed for the evaporator, including the boiler's combustion chamber. By combining the various components' sub models and introducing the working fluid mass conservation equation, a charge-sensitive model of Hebe was ultimately obtained. The model predicts the system performance from its boundary and control conditions only, making it completely predictive and thus fulfils the initial goal of this thesis.

Hebe's model was calibrated and validated in a limited but illustrative range of the control variables. A summary of the model's prediction errors, satisfactory in the context of an innovative engineering project, can be found in the conclusions section of Paper 2 (Chapter 5).

Notably, the calibrated model made it possible to identify an anomalous behaviour of the component set formed by the expander, magnetic coupling and servomotor. In fact, in the scope of HEBE Project, the model allowed to identify other design/construction deficiencies of Hebe's first laboratory prototype, pointing out possible paths of correction for each, that are not reported here.

Chapter 6 (Paper 3/3)

To develop an optimal steady-state control strategy for Hebe, a large set of simulations were conducted with the model developed in the previous chapter, ultimately leading to the construction of Hebe's control maps and operation limits for any given user demand, which were experimentally confirmed. In the state-of-the-art context, this strategy is original and is close to the front line.

A complementary dynamic control strategy based on PIDs was further established on purely empirical grounds, to guide the system through a quick and safe operation path during start-ups and transients following changes of the user's request, and to stabilize the stationary operation of Hebe. Within the HEBE Project team, without claiming special authorship in the context of this thesis, the author also contributed to its development.

7.2 Recommendations and perspective work

In accordance with the underlying motivation of the thesis, but largely transcending it, it can be said that the laboratory prototype of Hebe that was materialized and partially tested certainly served to prove the concept. However, it is still far from a commercial product. As an illustration, the following points are to be corrected or completed:

- Functionality: The Hebe's laboratory prototype was tested in a broad range of the domestic hot water service. Nevertheless, the central heating service, with higher inlet and outlet temperatures, was not tested since an additional refrigeration circuit must be implemented. Also, the direct injection of the generated electricity in the grid was not accomplished: it has simply been dissipated in a set of resistances.
- Components: The in-house developed evaporator exhibits low thermal efficiency and a new upgraded design was carried out and tested with promising results. The previously referred problems of the expander must be solved by acquiring/developing a new expander.

Regarding the main goal of this thesis, the development of a fully predictive steady-state model, the following remarks and hints may be worthy for future investigations:

- Estimate the working fluid mass in the evaporator and condenser more precisely, taking advantage of the advances in the sate-of-the-art that occurred meanwhile;
- Extend the 3D space region of Hebe's control variables, of the calibration/validation tests; and
- Strengthen and accelerate the solver algorithm to meet the intensive calculation needs of control refinement.

The stationary control strategy does not require substantial improvements. However, the dynamic control of Hebe can be optimized and further implemented with:

- Operation: Diminish the risk of the evaporator outlet temperature over-shoot. Smooth the pressure fluctuations in a short phase of start-up, and develop a safe shut-down procedure after a sudden cut of the user's hot water demand.

- Functionality: Reduce the time for the hot water to attain the demanded temperature, and the disturbance in the temperature of the water when the turbine is put into service. Improve the stability of the electricity supply. Achieve a fully automate system, from start-up to shut-down.

References

[1] IEA, "World Energy Outlook 2011," Paris, 2011. [Online]. Available: https://www.iea.org/reports/world-energy-outlook-2011.

[2] M. Bianchi, L. Branchini, A. De Pascale, and A. Peretto, "Application of environmental performance assessment of CHP systems with local and global approaches," *Appl. Energy*, vol. 130, pp. 774–782, 2014, doi: 10.1016/j.apenergy.2014.04.017.

[3] M. Dentice d'Accadia, M. Sasso, S. Sibilio, and L. Vanoli, "Micro-combined heat and power in residential and light commercial applications," *Appl. Therm. Eng.*, vol. 23, no. 10, pp. 1247–1259, 2003, doi: 10.1016/S1359-4311(03)00030-9.

[4] M. M. Maghanki, B. Ghobadian, G. Najafi, and R. J. Galogah, "Micro combined heat and power (MCHP) technologies and applications," *Renew. Sustain. Energy Rev.*, vol. 28, pp. 510–524, 2013, doi: 10.1016/j.rser.2013.07.053.

[5] F. Vélez, J. J. Segovia, M. C. Martín, G. Antolín, F. Chejne, and A. Quijano, "A technical, economical and market review of organic Rankine cycles for the conversion of low-grade heat for power generation," *Renew. Sustain. Energy Rev.*, vol. 16, no. 6, pp. 4175–4189, 2012, doi: 10.1016/j.rser.2012.03.022.

[6] K. Alanne and A. Saari, "Sustainable small-scale CHP technologies for buildings: The basis for multi-perspective decision-making," *Renew. Sustain. Energy Rev.*, vol. 8, no. 5, pp. 401–431, 2004, doi: 10.1016/j.rser.2003.12.005.

[7] "FlowEnergy micro CHP boiler." https://www.renewableenergyhub.co.uk/main/micro-combined-heat-and-power-micro-chp-information/the-flow-micro-chp-boiler/ (accessed Jul. 02, 2020).

[8] Rank, "Rank-ORC," 2020. https://www.rank-orc.com/es/ (accessed Jul. 02, 2020).

[9] "Kaymacor Srl." https://www.kaymacor.com/en⟩ (accessed Jul. 02, 2020).

[10] "Enogia - The Small Turbine Company." http://enogia.com/wp/ (accessed Jul. 02, 2020).

[11] B. Dudley, "Full Report - BP Statistical Review of World Energy 2018," *Stat. Rev. World Energy*, vol. 67, p. 40, 2018.

[12] EIA, "EIA Database," 2018. https://www.eia.gov/international/data/world (accessed May 30, 2020).

[13] S. Murugan and B. Horák, "A review of micro combined heat and power systems for residential applications," *Renew. Sustain. Energy Rev.*, vol. 64, pp. 144–162, 2016, doi: 10.1016/j.rser.2016.04.064.

[14] A. Rong, H. Hakonen, and R. Lahdelma, "A dynamic regrouping based sequential dynamic programming algorithm for unit commitment of combined heat and power systems," *Energy Convers. Manag.*, vol. 50, no. 4, pp. 1108–1115, 2009, doi: 10.1016/j.enconman.2008.12.003.

[15] B. F. Kolanowski, "History of Cogeneration," *Cogener. Compet. Power J.*, vol. 14, no. 1, pp. 74–79, 1999, doi: 10.1080/10668683.1999.10530325.

[16] "DIRECTIVE 2012/27/EU OF THE EUROPEAN PARLIAMENT AND OF THE COUNCIL of 25 October 2012," *Off. J. Eur. Union*, pp. 1–56, 2012.

[17] M. Bianchi, A. De Pascale, and P. R. Spina, "Guidelines for residential micro-CHP systems design," *Appl. Energy*, vol. 97, pp. 673–685, 2012, doi: 10.1016/j.apenergy.2011.11.023.

[18] T. Elmer, M. Worall, S. Wu, and S. B. Riffat, "Fuel cell technology for domestic built environment applications: State of-the-art review," *Renew. Sustain. Energy Rev.*, vol. 42, pp. 913–931, 2015, doi: 10.1016/j.rser.2014.10.080.

[19] CODE 2 - Cogeneration Observatory and Dissemination Europe, "Micro-CHP potential analysis - European level report," 2014. [Online]. Available: https://ec.europa.eu/energy/intelligent/projects/en/projects/code2.

[20] C. Roselli, M. Sasso, S. Sibilio, and P. Tzscheutschler, "Experimental analysis of microcogenerators based on different prime movers," *Energy Build.*, vol. 43, no. 4, pp. 796–804, 2011, doi: 10.1016/j.enbuild.2010.11.021.

[21] J. Harrison and E. On, *Small and Micro Combined Heat and Power (CHP) Systems*. Energy, Woodhead Publishing, 2011.
[22] S. Martinez, G. Michaux, P. Salagnac, and J. L. Bouvier, "Micro-combined heat and power systems (micro-CHP) based on renewable energy sources," *Energy Convers. Manag.*, vol. 154, no. June, pp. 262–285, 2017, doi: 10.1016/j.enconman.2017.10.035.
[23] M. J. Moore, *Micro Turbine Generators*. IMech, 2002.
[24] P. A. Pilavachi, "Mini- and micro-gas turbines for combined heat and power," *Appl. Therm. Eng.*, vol. 22, no. 18, pp. 2003–2014, 2002, doi: 10.1016/S1359-4311(02)00132-1.
[25] W. P. J. Visser, S. A. Shakariyants, and M. Oostveen, "Development of a 3 kW Microturbine for CHP Applications," *J. Eng. Gas Turbines Power*, vol. 133, no. 4, Nov. 2010, doi: 10.1115/1.4002156.
[26] R. Napoli, M. Gandiglio, A. Lanzini, and M. Santarelli, "Techno-economic analysis of PEMFC and SOFC micro-CHP fuel cell systems for the residential sector," *Energy Build.*, vol. 103, pp. 131–146, 2015, doi: 10.1016/j.enbuild.2015.06.052.
[27] A. Arsalis, "A comprehensive review of fuel cell-based micro-combined-heat-and-power systems," *Renew. Sustain. Energy Rev.*, vol. 105, no. January, pp. 391–414, 2019, doi: 10.1016/j.rser.2019.02.013.
[28] A. Adam, E. S. Fraga, and D. J. L. Brett, "Options for residential building services design using fuel cell based micro-CHP and the potential for heat integration," *Appl. Energy*, vol. 138, pp. 685–694, 2015, doi: 10.1016/j.apenergy.2014.11.005.
[29] T. C. Fubara, F. Cecelja, and A. Yang, "Modelling and selection of micro-CHP systems for domestic energy supply: The dimension of network-wide primary energy consumption," *Appl. Energy*, vol. 114, pp. 327–334, 2014, doi: 10.1016/j.apenergy.2013.09.069.
[30] G. Di Marcoberardino, L. Chiarabaglio, G. Manzolini, and S. Campanari, "A Techno-economic comparison of micro-cogeneration systems based on polymer electrolyte membrane fuel cell for residential applications," *Appl. Energy*, vol. 239, no. March 2018, pp. 692–705, 2019, doi: 10.1016/j.apenergy.2019.01.171.
[31] V. Liso, M. P. Nielsen, and S. K. Kær, "Influence of anodic gas recirculation on solid oxide fuel cells in a micro combined heat and power system," *Sustain. Energy Technol. Assessments*, vol. 8, pp. 99–108, 2014, doi: 10.1016/j.seta.2014.08.002.
[32] S. Pezzutto, S. Croce, S. Zambotti, L. Kranzl, A. Novelli, and P. Zambelli, "Assessment of the space heating and domestic hot water market in Europe—open data and results," *Energies*, vol. 12, no. 9, 2019, doi: 10.3390/en12091760.
[33] A. S. B. Ankit Gupta, "GLOBAL BOILER MARKET SIZE," 2018.
[34] F. Filippidou, N. Nieboer, and H. Visscher, "Energy efficiency measures implemented in the Dutch non-profit housing sector," *Energy Build.*, vol. 132, pp. 107–116, 2016, doi: 10.1016/j.enbuild.2016.05.095.
[35] T. Sakai and S. Takata, "DIRECTIVE 2009/125/EC - Ecodesign directive," *Off. J. Eur. Union*, vol. 61, no. 1, pp. 21–26, 2009, doi: 10.1016/j.cirp.2012.03.121.
[36] BSRIA, "Trends in the World Traditional & Renewable Heating Markets," UK, 2015.
[37] AMBITEMP, "Caldeiras Ambitemp," *2020*. https://www.ambitemp.pt/category/caldeira (accessed Jul. 02, 2020).
[38] G. M. Insights, "GMInsights micro CHP market," 2019. https://www.gminsights.com/industry-analysis/micro-combined-heat-and-power-market.
[39] E. Costa *et al.*, "HEBE Business Plan," Coimbra, 2011.
[40] B. J. Schweitzer and T. Formanski, "Toward New Technologies for the gas Market."
[41] Honda, "Household Gas Engine Cogeneration Unit," 2020. https://global.honda/innovation/technology/power/cogeneration-picturebook.html (accessed Jul. 02, 2020).
[42] I. Staffell, D. J. L. Brett, N. P. Brandon, and A. D. Hawkes, *Domestic Microgeneration: Renewable and Distributed Energy Technologies, policies and economics*. Housing Studies, 2015.
[43] Senertec, "Senertec smart Cogeneration," 2020. https://senertec.com/dachs/ (accessed Jul.

02, 2020).
[44] “RMB Energie,” 2020. https://www.rmbenergie.com/ (accessed Jul. 02, 2020).
[45] M. Engines, “Marathon Ecopower.” https://www.marathonengine.com/ (accessed Jul. 02, 2020).
[46] ECPower, “ECPower.” https://www.ecpower.eu/en/ (accessed Jul. 02, 2020).
[47] A. Seiki, “CHP, AISIN Seiki: GECC 46 A2 mini CHP,” 2020. http://www.bhkw-prinz.de/aisin-seiki-gecc-46-a2-np-r-mini-bhkw/2596 (accessed Jul. 02, 2020).
[48] Senertec, “Senertec Dachs 5.5,” 2020. https://senertec.com/dachs-the-original/ (accessed Jul. 02, 2020).
[49] RMBEnergie, “Yanmar neoTower products.” https://www.rmbenergie.com/en/products/ (accessed Jul. 02, 2020).
[50] Qnergy, “Qnergy.” https://www.qnergy.com/ (accessed Jul. 02, 2020).
[51] Inspirit-energy, “inspirit-energy.” https://www.inspirit-energy.com/ (accessed Jul. 02, 2020).
[52] J. R. Garcıa-Cascales, F. Vera-Garcıa, and J.M. Corberan-SalvadorJ. Gonzalvez-Macia, “Assessment of boiling and condensation heat transfer correlations in the modelling of plate heat exchangers,” vol. 30, pp. 1029–1041, 2007, doi: 10.1016/j.ijrefrig.2007.01.004.
[53] Microchap, “micro Combined Heat & Power,” 2013. http://www.microchap.info/micro_chp_products.htm (accessed Jul. 02, 2020).
[54] “BDR Thermea Group.” https://www.bdrthermeagroup.com/ (accessed Jul. 02, 2020).
[55] Viessman, “Viessman Vitovalor 300,” 2018. http://viessmann.com.ua/images/uploads/pdfs/Vitotwin_Micro_CHP_units.pdf (accessed Jul. 02, 2020).
[56] E. Group, “Elliot Energy System.” https://www.elliott-turbo.com/ (accessed Jul. 02, 2020).
[57] “Capstone Turbine.” https://www.capstoneturbine.com/ (accessed Jul. 02, 2020).
[58] “ABB Group.” https://new.abb.com/ (accessed Jul. 02, 2020).
[59] “enertwin.” https://www.enertwin.com/ (accessed Jul. 02, 2020).
[60] K. Valeriy and V. Pandian, *Handbook of Research on Energy-Saving Technologies for Environmentally*. ICI Global, 2019.
[61] Pace-Energy, “Pace Project,” 2020. http://www.pace-energy.eu/about-pace/ (accessed Jul. 02, 2020).
[62] “Energypost.” https://energypost.eu/fancy-having-your-own-power-plant-fuel-cell-micro-cogeneration-is-market-ready/ (accessed Jul. 02, 2020).
[63] “SolidPower.” https://www.solidpower.com/en/ (accessed Jul. 02, 2020).
[64] “Viessman.” https://www.viessmann.co.uk/products/combined-heat-and-power/fuel-cell/vitovalor (accessed Jul. 02, 2020).
[65] “Sunfire.” https://www.sunfire.de/en/products-and-technology/sunfire-home (accessed Jul. 02, 2020).
[66] PACE, “Summary report on specifications for newest model deployment in PACE (April 2020),” 2020. [Online]. Available: http://www.pace-energy.eu/wp-content/uploads/2020/04/PACE-D1.7-FV.pdf.
[67] “ORMAT.” https://www.ormat.com/en/home/a/main/ (accessed Jul. 02, 2020).
[68] “Turboden.” https://www.turboden.com/ (accessed Jul. 02, 2020).
[69] “Exergy - ORC.” http://exergy-orc.com/ (accessed Jul. 02, 2020).
[70] T. Tartière, “ORC market: a world overview,” 2017. http://orc-world-map.org/analysis.%0Ahtml (accessed Jul. 02, 2020).
[71] “Viking Development Group.” http://vikingenergy.co.za/#craftengine (accessed Jul. 02, 2020).
[72] A. Druckman and T. Jackson, “Household energy consumption in the UK: A highly geographically and socio-economically disaggregated model,” *Energy Policy*, vol. 36, no. 8, pp. 3177–3192, 2008, doi: 10.1016/j.enpol.2008.03.021.
[73] Pordata, “Pordata - Environment, Energy and Territory.” https://www.pordata.pt/en/Theme/Europe/Environment++Energy+and+Territory-34

(accessed Jul. 02, 2020).
[74] J. Cooke, “Condensing boiler technology, Presentation to the Puget Sound ASHRAE Chapter,” 2005.
[75] B. S. Park, M. Usman, M. Imran, and A. Pesyridis, “Review of Organic Rankine Cycle experimental data trends,” *Energy Convers. Manag.*, vol. 173, no. July, pp. 679–691, 2018, doi: 10.1016/j.enconman.2018.07.097.
[76] DGC, *Facts and figures about domestic gas boilers A compilation of results covering 25 years of testing at DGC’s laboratory*, no. February 2016. 2016.
[77] I. Tzanakis, “Sustainable design and durability of domestic micro combined heat and power scroll expander systems,” U. Bournemouth, UK, 2010.
[78] S. Clemente, D. Micheli, M. Reini, and R. Taccani, “Energy efficiency analysis of Organic Rankine Cycles with scroll expanders for cogenerative applications,” *Appl. Energy*, vol. 97, pp. 792–801, 2012, doi: 10.1016/j.apenergy.2012.01.029.
[79] O. Dumont, R. Dickes, and V. Lemort, “Experimental investigation of four volumetric expanders,” *Energy Procedia*, vol. 129, pp. 859–866, 2017, doi: 10.1016/j.egypro.2017.09.206.
[80] A. Bejan, G. Tsatsaronis, and M. Moran, *Thermal Design and Optimization*. 1996.
[81] S. Quoilin, S. Declaye, B. F. Tchanche, and V. Lemort, “Thermo-economic optimization of waste heat recovery Organic Rankine Cycles,” *Appl. Therm. Eng.*, vol. 31, no. 14–15, pp. 2885–2893, 2011, doi: 10.1016/j.applthermaleng.2011.05.014.
[82] S. Amicabile, J. I. Lee, and D. Kum, “A comprehensive design methodology of organic Rankine cycles for the waste heat recovery of automotive heavy-duty diesel engines,” *Appl. Therm. Eng.*, vol. 87, pp. 574–585, 2015, doi: 10.1016/j.applthermaleng.2015.04.034.
[83] G. Carraro, S. Rech, A. Lazzaretto, G. Toniato, and P. Danieli, “Dynamic simulation and experiments of a low-cost small ORC unit for market applications,” *Energy Convers. Manag.*, vol. 197, no. April, p. 111863, 2019, doi: 10.1016/j.enconman.2019.111863.
[84] Y. A. Çengel and A. J. Ghajar, *Heat and Mass Transfer - Fundamentals & Applications*, Fourth Edi. McGraw-Hill Education, 2014.
[85] J. S. Pereira, J. B. Ribeiro, R. Mendes, G. C. Vaz, and J. C. André, “ORC based micro-cogeneration systems for residential application - A state of the art review and current challenges,” *Renew. Sustain. Energy Rev.*, vol. 92, no. May, pp. 728–743, 2018, doi: 10.1016/j.rser.2018.04.039.
[86] T. A. Davidson, “Design and analysis of a 1 kw Rankine power cycle, employing a multi-vane expander, for use with a low temperature solar collector,” 1977.
[87] S. D. Probert, M. Hussein, P. W. O’Callaghan, and E. Bala, “Design optimisation of a solar-energy harnessing system for stimulating an irrigation pump.,” *Appl. Energy*, vol. 15, no. 4, 1983, doi: 16/0306- 2619(83)90059-4.
[88] J. Monahan, “Development of a 1-kW, Organic Rankine Cycle Power Plant for remote applications.,” 1976.
[89] O. Badr, P. W. O’Callaghan, and S. D. Probert, “Rankine-cycle systems for harnessing power from low-grade energy sources,” *Appl. Energy*, vol. 36, no. 4, 1990, doi: 16/0306-2619(90)90002-U.
[90] L. Tocci, T. Pal, I. Pesmazoglou, and B. Franchetti, “Small scale Organic Rankine Cycle (ORC): A techno-economic review,” *Energies*, vol. 10, no. 4, pp. 1–26, 2017, doi: 10.3390/en10040413.
[91] G. E. (Institution), “GE clean energy.” https://www.ge.com/power/applications/chp (accessed Jul. 02, 2020).
[92] GMK, “GMK - Clean energy efficiency.” http://www.gmk.info/home.html (accessed Jul. 02, 2020).
[93] Cryostar, “Cryostar - more than cryogenics,” [Online]. Available: https://cryostar.com/.
[94] TAS, “TAS Engineered Modular Solutions,” [Online]. Available: http://turbineairsystems.com/.
[95] BNI, “Barber-Nichols.” https://www.barber-nichols.com/industries/energy/ (accessed Jul.

02, 2020).
[96] Clearpower, “Clearpower systems - Heat to power generator systems.” https://clearpowersystems.com/ (accessed Jul. 02, 2020).
[97] Enertime, “Enertime - Clean energy harvesting.” https://www.enertime.com/en/home (accessed Jul. 02, 2020).
[98] Maxxtec, “Maxxtec - hot solutions for high demands.” https://www.maxxtec.co.id/ (accessed Jul. 02, 2020).
[99] Kaishan, “Kaishan USA.” https://kaishanusa.com/ (accessed Jul. 02, 2020).
[100] Phoenix, “Phoenix thermal energy conversion.” http://www.phoenixorc.com.au/ (accessed Jul. 02, 2020).
[101] “Durr Cyplan.” https://www.durr.com/en/products/decentral-power-generation/cyplan-orc (accessed Jul. 02, 2020).
[102] OPCON, “SMA Technologies.” https://smatechnologies.com/opcon-automation (accessed Jul. 02, 2020).
[103] BEP, “E-rational - value for heat.” https://www.e-rational.net/ (accessed Jul. 02, 2020).
[104] Triogen, “Triogen - power from heat.” http://www.triogen.nl/.
[105] Zuccato, “Zuccato Energia.” http://www.zuccatoenergia.it/it/ (accessed Jul. 02, 2020).
[106] ZEgroup, “ZE International Group - Zero emission generation solutions.” https://www.zeintlplc.com/?page_id=463# (accessed Jul. 02, 2020).
[107] “Calnetix Technologies.” https://www.calnetix.com/system-integration/heat-power-systems (accessed Jul. 02, 2020).
[108] BITZERgroup, “Electratherm.” https://electratherm.com/ (accessed Jul. 02, 2020).
[109] Enerbasque, “Enerbasque.” http://enerbasque.com/en/ (accessed Jul. 02, 2020).
[110] “Entropea Labs.” http://entropea.com/ (accessed Jul. 02, 2020).
[111] Orcan-Energy, “Orcan - the efficiency company.” https://www.orcan-energy.com/en/ (accessed Jul. 02, 2020).
[112] “INFINITY TURBINE LLC.” https://infinityturbine.com/.
[113] Exoes, “Exoes.” http://exoes.com/en/ (accessed Jul. 02, 2020).
[114] B. F. Tchanche, G. Lambrinos, A. Frangoudakis, and G. Papadakis, “Low-grade heat conversion into power using organic Rankine cycles - A review of various applications,” *Renew. Sustain. Energy Rev.*, vol. 15, no. 8, pp. 3963–3979, 2011, doi: 10.1016/j.rser.2011.07.024.
[115] S. Quoilin, M. Van Den Broek, S. Declaye, P. Dewallef, and V. Lemort, “Techno-economic survey of organic rankine cycle (ORC) systems,” *Renew. Sustain. Energy Rev.*, vol. 22, pp. 168–186, 2013, doi: 10.1016/j.rser.2013.01.028.
[116] S. Safarian and F. Aramoun, “Energy and exergy assessments of modified Organic Rankine Cycles (ORCs),” *Energy Reports*, vol. 1, pp. 1–7, 2015, doi: 10.1016/j.egyr.2014.10.003.
[117] H. Chen, D. Y. Goswami, and E. K. Stefanakos, “A review of thermodynamic cycles and working fluids for the conversion of low-grade heat,” *Renew. Sustain. Energy Rev.*, vol. 14, no. 9, pp. 3059–3067, 2010, doi: 10.1016/j.rser.2010.07.006.
[118] P. J. Mago, L. M. Chamra, K. Srinivasan, and C. Somayaji, “An examination of regenerative organic Rankine cycles using dry fluids,” *Appl. Therm. Eng.*, vol. 28, no. 8–9, pp. 998–1007, 2008, doi: 10.1016/j.applthermaleng.2007.06.025.
[119] M. Chys, M. van den Broek, B. Vanslambrouck, and M. De Paepe, “Potential of zeotropic mixtures as working fluids in organic Rankine cycles,” *Energy*, vol. 44, no. 1, pp. 623–632, 2012, doi: 10.1016/j.energy.2012.05.030.
[120] T. Ho, S. S. Mao, and R. Greif, “Increased power production through enhancements to the Organic Flash Cycle (OFC),” *Energy*, vol. 45, no. 1, pp. 686–695, 2012, doi: 10.1016/j.energy.2012.07.023.
[121] M. Yari, A. S. Mehr, V. Zare, S. M. S. Mahmoudi, and M. A. Rosen, “Exergoeconomic comparison of TLC (trilateral Rankine cycle), ORC (organic Rankine cycle) and Kalina cycle using a low grade heat source,” *Energy*, vol. 83, pp. 712–722, 2015, doi: 10.1016/j.energy.2015.02.080.

[122] A. Schuster, S. Karellas, and R. Aumann, “Efficiency optimization potential in supercritical Organic Rankine Cycles,” *Energy*, vol. 35, no. 2, pp. 1033–1039, 2010, doi: 10.1016/j.energy.2009.06.019.
[123] J. Freeman, I. Guarracino, S. A. Kalogirou, and C. N. Markides, “A small-scale solar organic Rankine cycle combined heat and power system with integrated thermal energy storage,” *Appl. Therm. Eng.*, vol. 127, pp. 1543–1554, 2017, doi: 10.1016/j.applthermaleng.2017.07.163.
[124] M. Usman, M. Imran, Y. Yang, and B. S. Park, “Impact of organic Rankine cycle system installation on light duty vehicle considering both positive and negative aspects,” *Energy Convers. Manag.*, vol. 112, pp. 382–394, 2016, doi: 10.1016/j.enconman.2016.01.044.
[125] L. Guillaume, A. Legros, A. Desideri, and V. Lemort, “Performance of a radial-inflow turbine integrated in an ORC system and designed for a WHR on truck application: An experimental comparison between R245fa and R1233zd,” *Appl. Energy*, vol. 186, pp. 408–422, 2017, doi: 10.1016/j.apenergy.2016.03.012.
[126] E. Baldasso, J. G. Andreasen, M. E. Mondejar, U. Larsen, and F. Haglind, “Technical and economic feasibility of organic Rankine cycle-based waste heat recovery systems on feeder ships: Impact of nitrogen oxides emission abatement technologies,” *Energy Convers. Manag.*, vol. 183, no. January, pp. 577–589, 2019, doi: 10.1016/j.enconman.2018.12.114.
[127] R. Pili, A. Romagnoli, H. Spliethoff, and C. Wieland, “Techno-Economic Analysis of Waste Heat Recovery with ORC from Fluctuating Industrial Sources,” *Energy Procedia*, vol. 129, pp. 503–510, 2017, doi: 10.1016/j.egypro.2017.09.170.
[128] Elsevier, “Sciencedirect,” 2020. https://www.sciencedirect.com/.
[129] R. Long, Y. J. Bao, X. M. Huang, and W. Liu, “Exergy analysis and working fluid selection of organic Rankine cycle for low grade waste heat recovery,” *Energy*, vol. 73, pp. 475–483, 2014, doi: 10.1016/j.energy.2014.06.040.
[130] J. Kicinski and G. Zywica, “Prototype of the domestic CHP ORC energy system,” *Bull. Polish Acad. Sci. Tech. Sci.*, vol. 64, no. 2, pp. 417–424, 2016, doi: 10.1515/bpasts-2016-0047.
[131] N. B. Desai and S. Bandyopadhyay, “Thermo-economic analysis and selection of working fluid for solar organic Rankine cycle,” *Appl. Therm. Eng.*, vol. 95, pp. 471–481, 2016, doi: 10.1016/j.applthermaleng.2015.11.018.
[132] M. Astolfi, S. Lasala, and E. Macchi, “Selection Maps for ORC and CO2 Systems for Low-Medium Temperature Heat Sources,” *Energy Procedia*, vol. 129, pp. 971–978, 2017, doi: 10.1016/j.egypro.2017.09.217.
[133] J. Zhang, Y. Zhou, R. Wang, J. Xu, and F. Fang, “Modeling and constrained multivariable predictive control for ORC (Organic Rankine Cycle) based waste heat energy conversion systems,” *Energy*, vol. 66, pp. 128–138, 2014, doi: 10.1016/j.energy.2014.01.068.
[134] G. Zywica, J. Kicinski, T. Z. Kaczmarczyk, E. Ihnatowicz, T. Turzynski, and S. Bykuc, “Prototype of the domestic CHP ORC system : construction and experimental research,” *Proc. 3rd Int. Semin. ORC Power Syst.*, no. 2011, p. Paper ID: 58, Page 1-9, 2015.
[135] S. Mohammadzadeh Bina, S. Jalilinasrabady, and H. Fujii, “Thermo-economic evaluation of various bottoming ORCs for geothermal power plant, determination of optimum cycle for Sabalan power plant exhaust,” *Geothermics*, vol. 70, no. April, pp. 181–191, 2017, doi: 10.1016/j.geothermics.2017.06.007.
[136] M. Imran, M. Usman, B. S. Park, and Y. Yang, “Comparative assessment of Organic Rankine Cycle integration for low temperature geothermal heat source applications,” *Energy*, vol. 102, pp. 473–490, 2016, doi: 10.1016/j.energy.2016.02.119.
[137] D. Hu, S. Li, Y. Zheng, J. Wang, and Y. Dai, “Preliminary design and off-design performance analysis of an Organic Rankine Cycle for geothermal sources,” *Energy Convers. Manag.*, vol. 96, pp. 175–187, 2015, doi: 10.1016/j.enconman.2015.02.078.
[138] C. Liu and T. Gao, “Off-design performance analysis of basic ORC, ORC using zeotropic mixtures and composition-adjustable ORC under optimal control strategy,” *Energy*, vol. 171, pp. 95–108, 2019, doi: 10.1016/j.energy.2018.12.195.

[139] M. A. Chatzopoulou, M. Simpson, P. Sapin, and C. N. Markides, "O ff -design optimisation of organic Rankine cycle (ORC) engines with piston expanders for medium-scale combined heat and power applications," *Appl. Energy*, vol. 238, no. July 2018, pp. 1211–1236, 2019, doi: 10.1016/j.apenergy.2018.12.086.
[140] S. Van Erdeweghe, J. Van Bael, B. Laenen, and W. D'haeseleer, "Design and off-design optimization procedure for low-temperature geothermal organic Rankine cycles," *Appl. Energy*, vol. 242, no. February, pp. 716–731, 2019, doi: 10.1016/j.apenergy.2019.03.142.
[141] J. Song, Y. Song, and C. wei Gu, "Thermodynamic analysis and performance optimization of an Organic Rankine Cycle (ORC) waste heat recovery system for marine diesel engines," *Energy*, vol. 82, pp. 976–985, 2015, doi: 10.1016/j.energy.2015.01.108.
[142] Y. Cao and Y. Dai, "Comparative analysis on off-design performance of a gas turbine and ORC combined cycle under different operation approaches," *Energy Convers. Manag.*, vol. 135, pp. 84–100, 2017, doi: 10.1016/j.enconman.2016.12.072.
[143] A. Desideri, A. Hernandez, S. Gusev, M. van den Broek, V. Lemort, and S. Quoilin, "Steady-state and dynamic validation of a small-scale waste heat recovery system using the ThermoCycle Modelica library," *Energy*, vol. 115, pp. 684–696, 2016, doi: 10.1016/j.energy.2016.09.004.
[144] T. Rajabloo, "Thermodynamic study of ORC at different working and peripheral conditions," *Energy Procedia*, vol. 129, pp. 90–96, 2017, doi: 10.1016/j.egypro.2017.09.165.
[145] H. Nami, A. Nemati, and F. Jabbari Fard, "Conventional and advanced exergy analyses of a geothermal driven dual fluid organic Rankine cycle (ORC)," *Appl. Therm. Eng.*, vol. 122, pp. 59–70, 2017, doi: 10.1016/j.applthermaleng.2017.05.011.
[146] H. W. Hevert and S. C. Hevert, "Second law analysis: An alternative indicator of system efficiency," *Energy*, vol. 5, no. 8, pp. 865–873, 1980, doi: https://doi.org/10.1016/0360-5442(80)90102-4.
[147] E. Macchi and M. Astolfi, *Organic Rankine Cycle (ORC) Power Systems*, 1st editio. Woodhead Publishing, 2016.
[148] J. Bao and L. Zhao, "A review of working fluid and expander selections for organic Rankine cycle," *Renew. Sustain. Energy Rev.*, vol. 24, pp. 325–342, 2013, doi: 10.1016/j.rser.2013.03.040.
[149] B. T. Liu, K. H. Chien, and C. C. Wang, "Effect of working fluids on organic Rankine cycle for waste heat recovery," *Energy*, vol. 29, no. 8, pp. 1207–1217, 2004, doi: 10.1016/j.energy.2004.01.004.
[150] B. F. Tchanche, G. Papadakis, G. Lambrinos, and A. Frangoudakis, "Fluid selection for a low-temperature solar organic Rankine cycle," *Appl. Therm. Eng.*, vol. 29, no. 11–12, pp. 2468–2476, 2009, doi: 10.1016/j.applthermaleng.2008.12.025.
[151] D. Mikielewicz and J. Mikielewicz, "A thermodynamic criterion for selection of working fluid for subcritical and supercritical domestic micro CHP," *Appl. Therm. Eng.*, vol. 30, no. 16, pp. 2357–2362, 2010, doi: 10.1016/j.applthermaleng.2010.05.035.
[152] H. Liu, Y. Shao, and J. Li, "A biomass-fired micro-scale CHP system with organic Rankine cycle (ORC) - Thermodynamic modelling studies," *Biomass and Bioenergy*, vol. 35, no. 9, pp. 3985–3994, 2011, doi: 10.1016/j.biombioe.2011.06.025.
[153] G. Qiu, "Selection of working fluids for micro-CHP systems with ORC," *Renew. Energy*, vol. 48, pp. 565–570, 2012, doi: 10.1016/j.renene.2012.06.006.
[154] E. H. Wang, H. G. Zhang, B. Y. Fan, M. G. Ouyang, Y. Zhao, and Q. H. Mu, "Study of working fluid selection of organic Rankine cycle (ORC) for engine waste heat recovery," *Energy*, vol. 36, no. 5, pp. 3406–3418, 2011, doi: 10.1016/j.energy.2011.03.041.
[155] Z. Shengjun, W. Huaixin, and G. Tao, "Performance comparison and parametric optimization of subcritical Organic Rankine Cycle (ORC) and transcritical power cycle system for low-temperature geothermal power generation," *Appl. Energy*, vol. 88, no. 8, pp. 2740–2754, 2011, doi: 10.1016/j.apenergy.2011.02.034.
[156] C. Liu, C. He, H. Gao, X. Xu, and J. Xu, "The optimal evaporation temperature of subcritical

ORC based on second law efficiency for waste heat recovery," *Entropy*, vol. 14, no. 3, pp. 491–504, 2012, doi: 10.3390/e14030491.
[157] H. Zhai, L. Shi, and Q. An, "Influence of working fluid properties on system performance and screen evaluation indicators for geothermal ORC (organic Rankine cycle) system," *Energy*, vol. 74, no. C, pp. 2–11, 2014, doi: 10.1016/j.energy.2013.12.030.
[158] B. Dong, G. Xu, Y. Cai, and H. Li, "Analysis of zeotropic mixtures used in high-temperature Organic Rankine cycle," *Energy Convers. Manag.*, vol. 84, pp. 253–260, 2014, doi: 10.1016/j.enconman.2014.04.026.
[159] V. L. Le, A. Kheiri, M. Feidt, and S. Pelloux-Prayer, "Thermodynamic and economic optimizations of a waste heat to power plant driven by a subcritical ORC (Organic Rankine Cycle) using pure or zeotropic working fluid," *Energy*, vol. 78, pp. 622–638, 2014, doi: 10.1016/j.energy.2014.10.051.
[160] H. Yu, X. Feng, and Y. Wang, "A new pinch based method for simultaneous selection of working fluid and operating conditions in an ORC (Organic Rankine Cycle) recovering waste heat," *Energy*, vol. 90. pp. 36–46, 2015, doi: 10.1016/j.energy.2015.02.059.
[161] J. Vivian, G. Manente, and A. Lazzaretto, "A general framework to select working fluid and configuration of ORCs for low-to-medium temperature heat sources," *Appl. Energy*, vol. 156, pp. 727–746, 2015, doi: 10.1016/j.apenergy.2015.07.005.
[162] H. Zhai, Q. An, and L. Shi, "Analysis of the quantitative correlation between the heat source temperature and the critical temperature of the optimal pure working fluid for subcritical organic Rankine cycles," *Appl. Therm. Eng.*, vol. 99, pp. 383–391, 2016, doi: 10.1016/j.applthermaleng.2016.01.058.
[163] J. Lu, J. Zhang, S. Chen, and Y. Pu, "Analysis of organic Rankine cycles using zeotropic mixtures as working fluids under different restrictive conditions," *Energy Convers. Manag.*, vol. 126, pp. 704–716, 2016, doi: 10.1016/j.enconman.2016.08.056.
[164] E. Saloux, M. Sorin, H. Nesreddine, and A. Teyssedou, "Reconstruction procedure of the thermodynamic cycle of organic Rankine cycles (ORC) and selection of the most appropriate working fluid," *Appl. Therm. Eng.*, vol. 129, pp. 628–635, 2018, doi: 10.1016/j.applthermaleng.2017.10.077.
[165] G. Chen, Q. An, Y. Wang, J. Zhao, N. Chang, and J. Alvi, "Performance prediction and working fluids selection for organic Rankine cycle under reduced temperature," *Appl. Therm. Eng.*, vol. 153, no. February, pp. 95–103, 2019, doi: 10.1016/j.applthermaleng.2019.02.011.
[166] J. Facão, A. Palmero-Marrero, and A. C. Oliveira, "Analysis of a solar assisted micro-cogeneration ORC system," *Int. J. Low-Carbon Technol.*, vol. 3, no. 4, pp. 254–264, 2008, doi: 10.1093/ijlct/3.4.254.
[167] B. Peris, J. Navarro-esbrí, and F. Molés, "Bottoming organic Rankine cycle con fi gurations to increase Internal Combustion Engines power output from cooling water waste heat recovery," *Appl. Therm. Eng.*, vol. 61, no. 2, pp. 364–371, 2013, doi: 10.1016/j.applthermaleng.2013.08.016.
[168] M. Wang, J. Wang, Y. Zhao, P. Zhao, and Y. Dai, "Thermodynamic analysis and optimization of a solar-driven regenerative organic Rankine cycle (ORC) based on fl at-plate solar collectors," *Appl. Therm. Eng.*, vol. 50, no. 1, pp. 816–825, 2013, doi: 10.1016/j.applthermaleng.2012.08.013.
[169] M. Sadeghi, A. Nemati, and M. Yari, "Thermodynamic analysis and multi-objective optimization of various ORC (organic Rankine cycle) con fi gurations using zeotropic mixtures," *Energy*, vol. 109, pp. 791–802, 2016, doi: 10.1016/j.energy.2016.05.022.
[170] P. Klonowicz, Ł. Witanowski, Ł. Jędrzejewski, T. Suchocki, and P. Lampart, "A turbine based domestic micro ORC system," *Energy Procedia*, vol. 129, pp. 923–930, 2017, doi: 10.1016/j.egypro.2017.09.112.
[171] R. Turton, R. C. Bailie, W. B. Whiting, and D. Shaeiwitz, J. A., Bhattacharyya, *Analysis, Synthesis, and Design of Chemical Processes*, Fourth ed. Upper Saddle River, New Jersey: Pearson Education International, 2013.

[172] A. Algieri and P. Morrone, “Techno-economic analysis of biomass-fired ORC systems for single-family combined heat and power (CHP) applications,” *Energy Procedia*, vol. 45, pp. 1285–1294, 2014, doi: 10.1016/j.egypro.2014.01.134.
[173] S. Lemmens, “Cost Engineering Techniques and Their Applicability for Cost Estimation of Organic Rankine Cycle Systems,” *Energies*, 2016, doi: 10.3390/en9070485.
[174] F. Di Maria and C. Micale, “Exergetic and economic analysis of energy recovery from the exhaust air of organic waste aerobic bioconversion by organic Rankine cycle,” vol. 81, pp. 272–281, 2015, doi: 10.1016/j.egypro.2015.12.097.
[175] F. Heberle and D. Brüggemann, “Thermo-Economic Analysis of Zeotropic Mixtures and Pure Working Fluids in Organic Rankine Cycles for Waste Heat Recovery †,” 2016, doi: 10.3390/en9040226.
[176] D. Walraven, B. Laenen, and W. D’Haeseleer, “Optimum configuration of shell-and-tube heat exchangers for the use in low-temperature organic Rankine cycles,” *Energy Convers. Manag.*, vol. 83, pp. 177–187, 2014, doi: 10.1016/j.enconman.2014.03.066.
[177] E. F. Brigham and M. C. Ehrhardt, *Financial Management: Theory & Practice*, 14th ed. Cengage Learning, 2014.
[178] S. Lecompte, “Performance Evaluation of Organic Rankine Cycle Architectures: Application to Waste Heat Valorisation,” University of Gent, 2016.
[179] D. Tempesti and D. Fiaschi, “Thermo-economic assessment of a micro CHP system fuelled by geothermal and solar energy,” *Energy*, vol. 58, pp. 45–51, 2013, doi: 10.1016/j.energy.2013.01.058.
[180] K. A. Barse and M. D. Mann, “Maximizing ORC performance with optimal match of working fluid with system design,” *Appl. Therm. Eng.*, vol. 100, pp. 11–19, 2016, doi: 10.1016/j.applthermaleng.2016.01.167.
[181] J. Galindo, H. Climent, and V. Dolz, “Multi-objective optimization of a bottoming Organic Rankine Cycle (ORC) of gasoline engine using swash-plate expander,” *Energy Convers. Manag.*, vol. 126, pp. 1054–1065, 2016, doi: 10.1016/j.enconman.2016.08.053.
[182] Y. Feng, T. Hung, Y. Zhang, B. Li, J. Yang, and Y. Shi, “Performance comparison of low-grade ORCs (organic Rankine cycles) using R245fa , pentane and their mixtures based on the thermoeconomic multi-objective optimization and decision makings,” *Energy*, vol. 93, no. 2015, pp. 2018–2029, 2018, doi: 10.1016/j.energy.2015.10.065.
[183] M. Santos, J. André, E. Costa, R. Mendes, and J. Ribeiro, “Design strategy for component and working fluid selection in a domestic,” *Appl. Therm. Eng.*, vol. 169, no. December 2019, p. 114945, 2020, doi: 10.1016/j.applthermaleng.2020.114945.
[184] R. Dickes, O. Dumont, L. Guillaume, S. Quoilin, and V. Lemort, “Charge-sensitive modelling of organic Rankine cycle power systems for o ff -design performance simulation,” vol. 212, no. January, pp. 1262–1281, 2018.
[185] S. Quoilin, “Sustainable Energy Conversion Through the Use of Organic Rankine Cycles for Waste Heat Recovery and Solar Applications .,” University of Liège (Belgium), 2011.
[186] G. Manente, A. Toffolo, A. Lazzaretto, and M. Paci, “An Organic Rankine Cycle off-design model for the search of the optimal control strategy brine,” *Energy*, vol. 58, pp. 97–106, 2013, doi: 10.1016/j.energy.2012.12.035.
[187] J. Wang, Z. Yan, P. Zhao, and Y. Dai, “Off-design performance analysis of a solar-powered organic Rankine cycle,” *Energy Convers. Manag.*, vol. 80, pp. 150–157, 2014, doi: 10.1016/j.enconman.2014.01.032.
[188] M. Ibarra, A. Rovira, D. Alarcón-padilla, and J. Blanco, “Performance of a 5 kW e Organic Rankine Cycle at part-load operation,” *Appl. Energy*, vol. 120, pp. 147–158, 2014, doi: 10.1016/j.apenergy.2014.01.057.
[189] D. Hu, S. Li, Y. Zheng, J. Wang, and Y. Dai, “Preliminary design and off-design performance analysis of an Organic Rankine Cycle for geothermal sources,” *Energy Convers. Manag.*, vol. 96, pp. 175–187, 2015, doi: 10.1016/j.enconman.2015.02.078.
[190] J. Song, C. Gu, and X. Ren, “Parametric design and off-design analysis of organic Rankine cycle (ORC) system,” *Energy Convers. Manag.*, vol. 112, pp. 157–165, 2016, doi:

10.1016/j.enconman.2015.12.085.
[191] S. Bendapudi, J. E. Braun, and E. A. Groll, “A comparison of moving-boundary and finite-volume formulations for transients in centrifugal chillers Comparaison entre les formulations aux limites mobiles et ´ gimes transitoires des aux volumes finis pour les re refroidisseurs centrifuges,” *Int. J. Refrig.*, vol. 31, no. 8, pp. 1437–1452, 2008, doi: 10.1016/j.ijrefrig.2008.03.006.
[192] L. I. U. Liuchen, Z. H. U. Tong, G. A. O. Naiping, and G. A. N. Zhongxue, “A Review of Modeling Approaches and Tools for the Off-design Simulation of Organic Rankine Cycle,” vol. 27, no. 4, pp. 305–320, 2018.
[193] D. Ziviani, A. Beyene, and M. Venturini, “Advances and challenges in ORC systems modeling for low grade thermal energy recovery,” vol. 121, pp. 79–95, 2014.
[194] A. S. Wanniarachchi, U. Ratnam, B. E. Tilton, and K. Dutta-Roy, “Approximate correlations for chevron-type plate heat exchangers,” *Proc. 30th Natl. heat Transf. Conf.*, pp. 145–151, 1995.
[195] B. Thonon, “Design Method for Plate Evaporators and Condensers. 1st International Conference on Process Intensification for the Chemical Industry,” *BHR Gr. Conf. Ser. Publ.*, vol. 18, pp. 37–47, 1995.
[196] A. Maslov and L. Kovalenko, “Hydraulic resistance and heat transfer in plate heat exchangers,” *Molochn Prom-st’*, vol. 10, pp. 20–22, 1972.
[197] V. Gnielinski, “New equations for heat and mass transfer in turbulent pipe and channel flows,” *Int. Chem. Eng.*, vol. 16, no. 2, pp. 359–368, 1976.
[198] D. Han, K. Lee, and Y. Kim, “The characteristics of condensation in brazed plate heat exchangers with different chevron angles.,” *J. Korean Phys. Soc.*, vol. 43, no. 1, pp. 66–73, 2003.
[199] G. Longo, G. Righetti, and C. Zilio, “A new computational procedure for refrigerant condensation inside herring-bone-type Brazed Plate Heat Exchangers,” *Int. J. Heat Mass Transf.*, vol. 82, pp. 530–536, 2015.
[200] Y.-Y. Yan, H.-C. Lio, and T.-F. Lin, “Condensation heat transfer and pressure drop of refrigerant R-134a in a plate heat exchanger,” *Int. J. Heat Mass Transf.*, vol. 42, no. 6, pp. 993–1006, 1999, doi: 10.1016/S0017-9310(98)00217-8.
[201] M. Shah, “A general correlation for heat transfer during film condensation inside pipes,” *Int. J. Heat Mass Transf.*, vol. 22, no. 4, pp. 547–556, 1979.
[202] R. Amalfi, F. Vakili-Farahani, and J. Thome, “Flow boiling and frictional pressure gradients in plate heat exchangers. Part 2: comparison of literature methods to database and new prediction methods.,” *Int. J. Refrig.*, vol. 61, pp. 185–203, 2016.
[203] O. Calli, C. O. Colpan, and H. Gunerhan, “Thermal Modelling of a Plate-Type Heat Exchanger-Based Biomass-Fired Regenerative Organic Rankine Cycle,” in *The Role of Exergy in Energy and the Environment*, S. Nižetić and A. Papadopoulos, Eds. Springer, Cham, 2018.
[204] G. Qiu, H. Liu, and S. Riffat, “Expanders for micro-CHP systems with organic Rankine cycle,” *Appl. Therm. Eng.*, vol. 31, no. 16, pp. 3301–3307, 2011, doi: 10.1016/j.applthermaleng.2011.06.008.
[205] M. Imran, M. Usman, B. Park, and D. Lee, “Volumetric expanders for low grade heat and waste heat recovery applications,” *Renew. Sustain. Energy Rev.*, vol. 57, pp. 1090–1109, 2016, doi: 10.1016/j.rser.2015.12.139.
[206] F. Alshammari, M. Usman, and A. Pesyridis, “Expanders for Organic Rankine Cycle Technology,” in *Organic Rankine Cycle Technology for Heat Recovery*, E. Wang, Ed. Rijeka: IntechOpen, 2018.
[207] E. Winandy, C. S. O, and J. Lebrun, “Experimental analysis and simpli ® ed modelling of a hermetic scroll refrigeration compressor,” vol. 22, pp. 107–120, 2002.
[208] M. Kane, D. Larrain, D. Favrat, and Y. Allani, “Small hybrid solar power system,” vol. 28, pp. 1427–1443, 2003, doi: 10.1016/S0360-5442(03)00127-0.
[209] S. Quoilin, V. Lemort, and J. Lebrun, “Experimental study and modeling of an Organic

Rankine Cycle using scroll expander," *Appl. Energy*, vol. 87, no. 4, pp. 1260–1268, 2010, doi: 10.1016/j.apenergy.2009.06.026.
[210] R. Bracco, S. Clemente, D. Micheli, and M. Reini, "Experimental tests and modelization of a domestic-scale ORC (Organic Rankine Cycle)," *Energy*, vol. 58, pp. 107–116, 2013, doi: 10.1016/j.energy.2012.12.016.
[211] Y. Q. Zhang *et al.*, "Development and experimental study on organic Rankine cycle system with single-screw expander for waste heat recovery from exhaust of diesel engine," *Energy*, vol. 77, pp. 499–508, 2014, doi: 10.1016/j.energy.2014.09.034.
[212] A. Giuffrida, "Improving the semi-empirical modelling of a single-screw expander for small organic Rankine cycles," *Appl. Energy*, vol. 193, pp. 356–368, 2017, doi: 10.1016/j.apenergy.2017.02.015.
[213] M. Bianchi *et al.*, "Performance prediction of a reciprocating piston expander with Performance prediction of a reciprocating piston expander Cooling with semi-empirical models semi-empirical models Assessing the feasibility of using the heat demand-outdoor temperature functi," *Energy Procedia*, vol. 158, pp. 1737–1743, 2019, doi: 10.1016/j.egypro.2019.01.403.
[214] A. P. Weiss and G. Zinn, "Micro Turbine Generators For Waste Heat Recovery And Compressed Air Energy Storage," *15th Conf. Power Syst. Eng. Thermodyn. Fluid Flow - ES 2016*, pp. 1–9, 2016.
[215] S. H. Kang, "Design and experimental study of ORC (organic Rankine cycle) and radial turbine using R245fa working fl uid," *Energy*, vol. 41, no. 1, pp. 514–524, 2012, doi: 10.1016/j.energy.2012.02.035.
[216] K. Rahbar, S. Mahmoud, R. K. Al-dadah, and N. Moazami, "Modelling and optimization of organic Rankine cycle based on a small-scale radial inflow turbine," *Energy Convers. Manag.*, vol. 91, pp. 186–198, 2015, doi: 10.1016/j.enconman.2014.12.003.
[217] D. Fiaschi, G. Manfrida, and F. Maraschiello, "Design and performance prediction of radial ORC turboexpanders," *Appl. Energy*, vol. 138, pp. 517–532, 2015, doi: 10.1016/j.apenergy.2014.10.052.
[218] L. Da Lio, G. Manente, and A. Lazzaretto, "New ef fi ciency charts for the optimum design of axial fl ow turbines for organic Rankine cycles," vol. 77, pp. 447–459, 2014, doi: 10.1016/j.energy.2014.09.029.
[219] L. Talluri and G. Lombardi, "ScienceDirect ScienceDirect ScienceDirect Simulation and Design Symposium Tool for on ORC Axial Turbine Assessing the Lorenzo feasibility of using the heat demand-outdoor temperature for a demand Department function Italy forecast," *Energy Procedia*, vol. 129, pp. 277–284, 2017, doi: 10.1016/j.egypro.2017.09.154.
[220] D. Ziviani, R. Dickes, V. Lemort, J. E. Braun, and E. A. Groll, "Effects of the Working Fluid Charge in Organic Rankine Cycle Power Systems: Numerical and Experimental Analyses," in *Organic Rankine Cycle Technology for Heat Recovery*, 2018.
[221] M. Santos, J. André, R. Mendes, and J. B. Ribeiro, "Design and modelling of a small scale biomass-fueled CHP system based on Rankine technology," in *Energy Procedia*, 2017, vol. 129, doi: 10.1016/j.egypro.2017.09.143.
[222] C. C. Hiller and L. R. Glicksman, "Detailed Modeling and Computer Simulation of Reciprocating Refrigeration Compressors," *Proc. Int. Compress. Eng. Conf.*, no. 162, 1976.
[223] C. J. L. Hermes, "Refrigerant charge reduction in vapor compression refrigeration cycles via liquid-to-suction heat exchange," *Int. J. Refrig.*, vol. 52, pp. 93–99, 2015, doi: 10.1016/j.ijrefrig.2014.12.014.
[224] Y. Pan, L. Liu, and T. Zhu, "Simulation of working fluid mass distribution in small-scale Organic Rankine Cycle system under sub-critical conditions," *Appl. Therm. Eng.*, vol. 131, pp. 884–896, 2018, doi: 10.1016/j.applthermaleng.2017.12.017.
[225] R. Lockhart and R. Martinelli, "Proposed correlation data for isothermal two-phase two-component flow in pipes," *Chem. Eng. Prog.*, vol. 45, pp. 39–48, 1949.
[226] S. Zivi, "Estimation of steady-state team void-fraction by means of the principle of

minimum entropy production," *J. Heat Transfer*, vol. 86, no. 2, pp. 247–252, 1964.
[227] A. Premoli, D. Francesco, and A. Prina, "A dimensional correlation for evaluating two-phase mixture density," *La Termotec.*, vol. 25, pp. 17–26, 1971.
[228] S. Hughmark, "Effects of the Working Fluid Charge in Organic Rankine Cycle Power Systems: Numerical and Experimental Analyses," *Chem. Eng. Prog.*, 1962.
[229] D. Ziviani *et al.*, "Development and a Validation of a Charge Sensitive Organic Rankine Cycle (ORC) Simulation Tool," *Energies*, vol. 9, no. 6, pp. 1–36, 2016, doi: 10.3390/en9060389.
[230] L. Liu, T. Zhu, and J. Ma, "Working fluid charge oriented off-design modeling of a small scale Organic Rankine Cycle system," vol. 148, pp. 944–953, 2017.
[231] L. Liu, T. Zhu, T. Wang, and N. Gao, "Experimental investigation on the effect of working fl uid charge in a small-scale Organic Rankine Cycle under off-design conditions," *Energy*, vol. 174, pp. 664–677, 2019, doi: 10.1016/j.energy.2019.03.013.
[232] M. Santos, J. André, S. Francisco, R. Mendes, and J. Ribeiro, "Off-design modelling of an organic Rankine cycle micro-CHP: Modular framework, calibration and validation," *Appl. Therm. Eng.*, vol. 137, 2018, doi: 10.1016/j.applthermaleng.2018.04.009.